ABSTRACT

Title of dissertation: CLIMATE CHANGE DURING INTERVALS OF THE PAST MILLENNIUM IN THE SOUTHWESTERN TROPICAL PACIFIC

Alex Lopatka
Doctor of Philosophy, 2018

Dissertation directed by: Associate Professor Michael Evans
Department of Geology

Limited observations from the tropical Pacific over the past millennium make it difficult to assess whether different time periods had significant variations in El Niño-Southern Oscillation (ENSO) amplitude and frequency. Composited simulation results from climate models participating in the Paleoclimate Modeling Intercomparison Project suggest no difference in statistical variance and ENSO event frequency for the Medieval Climate Anomaly (MCA), Little Ice Age (LIA), and the modern Industrial Era. ENSO may not be sensitive to external radiative forcings. Unforced variability arising from the coupled ocean-atmosphere system could explain the observed past millennium results.

New coral δ^{18}O and Sr/Ca were collected from Aitutaki, southern Cook Islands in the southwestern tropical Pacific and composited with existing coral geochemical observations from Rarotonga to increase the temporal coverage of climate data over the past millennium. Forward modelling of coral δ^{18}O as a function of sea surface temperature and seawater δ^{18}O suggests this location is sensitive to interannual variations in the position of the South Pacific Convergence Zone (SPCZ) driven by ENSO activity. Analysis

of observed interannual δ^{18}O indicates interannual variations are driven primarily by sea surface salinity but also sea surface temperature forcings. More negative (positive) coral δ^{18}O results indicate warmer/wetter (cooler/dryer) conditions that occur at Aitutaki when La Niña (El Niño) events redistribute the South Pacific Convergence Zone away (towards) the equator. Spatial correlation of the coral δ^{18}O signal with regional and tropical climate variables support the interpretation that Aitutaki coral δ^{18}O varies according to changes in the SPCZ and ENSO activity. Results from modern Aitutaki coral δ^{18}O may be used to interpret coral data collected from earlier periods of time.

Paired coral δ^{18}O and Sr/Ca measurements were made on diagenetically-screened samples radiometrically dated to the Medieval Climate Anomaly. These results, used to calculate interannual $\delta^{18}O_{SW}$ anomalies, show higher statistical variance in the fossil record relative to the modern Aitutaki/Rarotonga composite record. Singular spectrum analysis shows the first ten reconstructed components explain 79-86% of the variability in the timeseries. Composited interannual frequency (2-10 year period) components show variable $\delta^{18}O_{SW}$ throughout the MCA suggesting an active ENSO period. Large variations of 0.6 permil in calculated $\delta^{18}O_{SW}$ suggest potential decadal shifts in δ^{18}O from warmer/wetter to cooler/dryer conditions. Long term trends in calculated $\delta^{18}O_{SW}$ during the earlier MCA from more negative to more positive values suggest a transition from warmer/wetter to cooler/dryer conditions. Together, the results suggest a highly variable MCA period relative to the modern period. This new data may be used in conjunction with other observations for data/model comparisons to better understand hydroclimate variability over the past millennium.

CLIMATE CHANGE DURING INTERVALS OF THE PAST MILLENNIUM IN THE SOUTHWESTERN TROPICAL PACIFIC

by

Alex Lopatka

Dissertation submitted to the Faculty of the Graduate School of the
University of Maryland, College Park in partial fulfillment
of the requirements for the degree of
Doctor of Philosophy
2018

Advisory Committee:
Associate Professor Michael Evans, Chair
Professor James Farquhar
Dr. Andrew Lorrey
Professor Raghu Murtugudde, Dean's Representative
Associate Professor Karen Prestegaard

Preface

Climate variations during intervals of the past millennium are quantified from existing data and new geochemical observations from Aitutaki, southern Cook Islands.

- Chapter 1 introduces the tropical Pacific coupled ocean-atmosphere system and how coral paleoclimatology methods may be used to infer climate variation.

- Chapter 2 reviews the current understanding of tropical Pacific climate variability over the past millennium using climate model simulation output as a null hypothesis for changes in variance. The limited amount of observations available are used to assess the extent to which interannual variability has changed over time.

- Chapter 3 uses new geochemical measurements from Aitutaki, southern Cook Islands and publicly available coral geochemical data from Rarotonga to calibrate the interpretation of coral data using contemporaneous historical climate observations. Uncertainties in coral paleoclimatology are discussed as well as the potential climate system mechanisms that may explain the observations.

- Chapter 4 uses the modern coral results of Chapter 3 to interpret newly developed fossil coral records which date to intervals of the early part of the second millennium. Data analyses of the results are used to test for changes in amplitude and frequency over time.

- Chapter 5 summarizes the major results of the dissertation and suggests future avenues of research.

Acknowledgments

I am sincerely grateful for the tremendous benefits I have received from so many people throughout my Ph.D journey. Thank you for all the support and encouragement and to those whom I may have forgotten in these acknowledgements.

Several international colleagues helped develop my dissertation project. I am thankful for the guidance and financial support of Drew Lorrey at the National Institute of Water & Atmospheric Research in Auckland, New Zealand. With his help, I collected the samples in Aitutaki, learned how to CT scan a coral, and wrote a document of best practices for quality control in coral paleoclimatology. Drew read so many drafts, providing insightful comments and constructive feedback. Perhaps the most helpful piece of advice was his admonition to "trust no one". I'd like to thank Christian Hyde for teaching me how to safely cut samples, mill thousands of powders for geochemical analyses, and was indispensable in the field with his humor and strength. Melinda Allen, of Auckland University, helped write the proposal that funded our work in Aitutaki. She and Alex Morrison offered helpful comments on some early manuscript drafts. Helen McGregor assisted with field work and provided helpful comments on chapter manuscripts.

A number of people taught me climate science, geology, statistics, teaching and more. Tracey Centorbi taught me how to teach, organize a field trip for dozens of undergraduates, and introduced me to the humor and horror of textbook publishing. Raghu Murtugudde taught me about ENSO, poked holes in many arguments, and kept me engaged during some heated seminar debates. Sumant Nigam introduced me to geophysical fluid dynamics and the coupled ocean-atmosphere system. Ross Salawitch refined my

computer programming code to be clear and concise. Tony Busalacchi taught me more earth system science in one semester than I ever expected possible and quickly made me comfortable speaking about science in front of others after a dozen presentations during my first semester. James Farquhar taught me stable isotope systems, asked interesting, difficult questions throughout my degree program, and provided some networking and career advice when I wasn't sure what to do next. Karen Prestegaard served on my committee and helped improve this work with her questions and insights. Hali Kilbourne taught me how to collect Sr/Ca measurements, identify diagenesis, how to interpret results, and graciously opened her home to me twice while working at the Chesapeake Biological Laboratory. I learned some great dinner recipes from her too.

Dorothy Brown, Suzanne Martin, Michelle Montero, and Joanna Patterson expertly and patiently navigated me through the complexities of university administration. I would like to thank Bill McDonough for checking in on me once in a while during the long, solitary work. Your recommendations, advice, and humor made me feel like a valued member of the Geology Department.

Data collection would not have been possible without Becca Plummer, the instrument expert of the Paleoclimate Co-Laboratory who taught me much about mass spectrometers and troubleshooting them. Grace Duke, Mathias Trachsel, Julian Leal, Anna Lowien, Katie Haviland, Leah Mudd, Christina Justice, Xiaomin Zeng, Kaitlyn Steele, and other members of past and present research groups were immensely helpful with the many tasks associated with collecting data from an isotope lab, and provided helpful questions and feedback during group meeting discussions and presentations. In addition to her help at UMD, Grace assisted with laboratory work in New Zealand from June-

August 2015.

Jeffrey Brainard and Tim Oleson graciously agreed to teach a graduate student scientist how to more clearly and concisely communicate science.

Thank you to my many fellow graduate students (from Geology, Atmospheric & Oceanic Science, Chemistry, and the Mathematics Departments) for the commiseration, late night fun, and good humor: Mike Antonelli, Debdeep Bhattacharya, Tom Doody, Stefan Dbozczak, Nick Esposito, Dan Goldberg, Adam Greeley, Matt Guay, Shahan Haq, Pratima Hebbar, Courtney Love, Katie Lukens, Kevin Miller, Dave New, Scott Ozog, and Allison Ring. And thank you to visiting postdoctoral researcher, Damien Huffer, for the good food, conversation, and Taiko performances.

My advisor, Mike Evans, taught me how to approach a scientific problem through critical thinking and analysis, encouraging me throughout the process to try my best to answer my own questions. I'm grateful for his support when I had to convince the department to let me pursue my wide interests in science policy and writing. Mike also taught me statistics, working safely in an isotope lab, computer programming, many topics in earth science, and manuscript writing.

Solvitur ambulando – many miles through woods and parks with Dalton kept my mind and body active. Mom, Dad, Andrew, and Julie have supported my endeavors from the beginning. A special thank you to my close friend Bryan Edwards for the many conversations over the years. My final thank you goes to Stephanie Young for the love, laughs, and food.

Table of Contents

List of Tables

List of Figures

List of Abbreviations

CMIP5	Climate Modelling Intercomparison Project 5
ENSO	El Niño-Southern Oscillation
He	Helium
IE	Industrial Era (1850-2000 C.E.)
ITCZ	Intertropical Convergence Zone
LIA	Little Ice Age
MCA	Medieval Climate Anomaly
PMIP3	Paleoclimate Modelling Intercomparison Project 3
SAM	Southern Annular Mode
SCI	southern Cook Islands
SLP	sea level pressure
SOI	Southern Oscillation Index
SPCZ	South Pacific Convergence Zone
SSS	sea surface salinity
SST	sea surface temperature
U/Th	Uranium/Thorium
V-PDB	Vienna Pee Dee Belemnite
V-SMOW	Vienna Standard Mean Ocean Water
XRD	x-ray diffraction
ZC	Zebiak-Cane

Chapter 1: Introduction

1.1 Problem Statement

How will El Niño-Southern Oscillation (ENSO) amplitude, frequency, and spatial pattern change in response to 21st century external radiative forcing? Helping to address this outstanding scientific research question is important because ENSO events cause droughts and floods, impact fisheries, and affect economic and social well-being (*Glantz et al.*, 1991; *IPCC Working Group 1 et al.*, 2013). The *IPCC Working Group 1 et al.* (2013) suggests ENSO will remain the key component of tropical Pacific interannual variability in the 21st century. But significant uncertainty in how the tropical Pacific coupled atmosphere-ocean system will respond to anthropogenic forcing limits adaptation, mitigation, and resilience strategies. A better understanding of future global change and ENSO variability can improve scientists' ability to make successful forecasts and aid policymakers in developing scientifically-grounded adaptation, mitigation, and resiliency legislation.

1.2 Hypotheses for ENSO activity in the 21st century

Scientists debate how ENSO amplitude, frequency, and spatial pattern may vary in response to 21st century external radiative forcing (*IPCC Working Group 1 et al.*, 2013).

Simulations predict more warm phase (El Niño) events, more cold phase (La Niña) events, and no discernible change in ENSO behavior (*Bellenger et al.*, 2014; *Collins et al.*, 2010; *Guilyardi et al.*, 2009; *Stevenson*, 2012; *Vecchi and Wittenberg*, 2010). Radiative and internal dynamical forcings could both affect ENSO behavior in the 21st century. The first includes total solar irradiance, explosive volcanism, and the addition of anthropogenic greenhouse gases into the atmosphere (*IPCC Working Group 1 et al.*, 2013). These are defined here (and in the literature) as external forcings because they do not arise within the climate system from geophysical fluid dynamics or the biogeochemical cycles operating within and between the major components of the Earth System (atmosphere, biosphere, cryosphere, lithosphere, and oceans).

A plausible forcing of ENSO is increased concentrations of well-mixed greenhouse gases via the response of the tropical coupled ocean-atmosphere system (*IPCC Working Group 1 et al.*, 2013). The ocean thermostat mechanism (*Clement et al.*, 1996) suggests surface warming from uniform external radiative forcing would increase the zonal sea surface temperature (SST) gradient in the tropical Pacific, favoring more cold phase (La Niña) conditions. Alternatively, a weakening of the Pacific Walker Circulation (*Vecchi*, 2008; *Vecchi et al.*, 2006) caused by differential rates of water vapor and precipitation increases in response to external radiative forcing (*Held and Soden*, 2006), would suggest weakened easterly trade winds, a reduced tropical Pacific sea level pressure (SLP) and zonal SST gradient and more warm phase (El Niño) conditions (*DiNezio et al.*, 2013). A different recent study, however, suggests precipitation and evaporation rates are not very different from the increased water vapor rates expected from external radiative forcing. These results suggest the tropical Pacific Walker Circulation has experienced a multi-

decadal strengthening since the mid-20th century (*L'Heureux et al.*, 2013).

Detecting an ENSO response to external radiative forcings, such as greenhouse gases, is difficult because of significant unforced variability of the climate system arising from the dynamics of the coupled ocean-atmosphere system (*Bellenger et al.*, 2014; *Collins et al.*, 2010) (Figure 1.1). ENSO variability has also been simulated even in the absence of external radiative forcings (*Wittenberg*, 2009; *Zebiak and Cane*, 1987). Unforced variations in the depth of the thermocline or changes in the intensity of westerly winds can cause changes in the sea surface temperature gradient of the tropical Pacific and cause an ENSO event (*Fedorov and Philander*, 2000). Combinations of different forced and unforced mechanisms may produce a range of ENSO types with different amplitudes, time evolutions, and spatial patterns (*Capotondi et al.*, 2015).

Therefore, another plausible hypothesis is that the tropical Pacific ocean-atmosphere system is capable of producing many variations in ENSO with and without external radiative forcings. Model simulations with realistic external radiative forcings have produced a wide spectrum of results predicting increased El Niño events, increased La Niña events, and no change at all in 21st century ENSO variance (*Bellenger et al.*, 2014; *Collins et al.*, 2010). Coupled ocean-atmosphere general circulation models are numerical representations of dynamical processes operating between the ocean and atmosphere that are used to make a simplified model of the climate system. The greenhouse gas radiative forcing may be small relative to the internal variability of the climate system that can produce ENSO variability even in the absence of this external forcing, and the systematic errors in models all contribute towards the uncertainty in 21st century ENSO variance (*Bellenger et al.*, 2014). In addition, there are a range of potential feedbacks that could affect the

structure of ENSO (*Collins et al.*, 2010) with little to no consistency between models (*Guilyardi et al.*, 2009). Recent research using the most up-to-date suite of available climate models from Coupled Modelling Intercomparison Project (CMIP5) (*Taylor et al.*, 2012) to compare 20th to 21st century climate change suggested no clear spatial pattern in SST but a somewhat consistent pattern of increased precipitation in the central equatorial Pacific with decreased precipitation in the western Pacific warm pool (*Power et al.*, 2013). However, *Bellenger et al.* (2014) suggests CMIP5 modeled precipitation still has high errors in its Indo-Pacific precipitation predictions as well as other ENSO metrics such as NINO3 annual cycle SST amplitude, equatorial zonal wind stress, and NINO3 net surface heat flux. Other studies show increased precipitation in the South Pacific Convergence Zone (SPCZ) of the southwestern Pacific (*Brown et al.*, 2012a,c). A different study suggests a small decrease in SPCZ rainfall (*Widlansky et al.*, 2012) that could be altered by changing atmospheric moisture levels (*Held and Soden*, 2006). Other research suggests the response of ENSO variance in the 21st century could be explained predominantly by internal variability of the climate system rather than external radiative forcing (*Ault et al.*, 2013; *Gershunov and Barnett*, 1998).

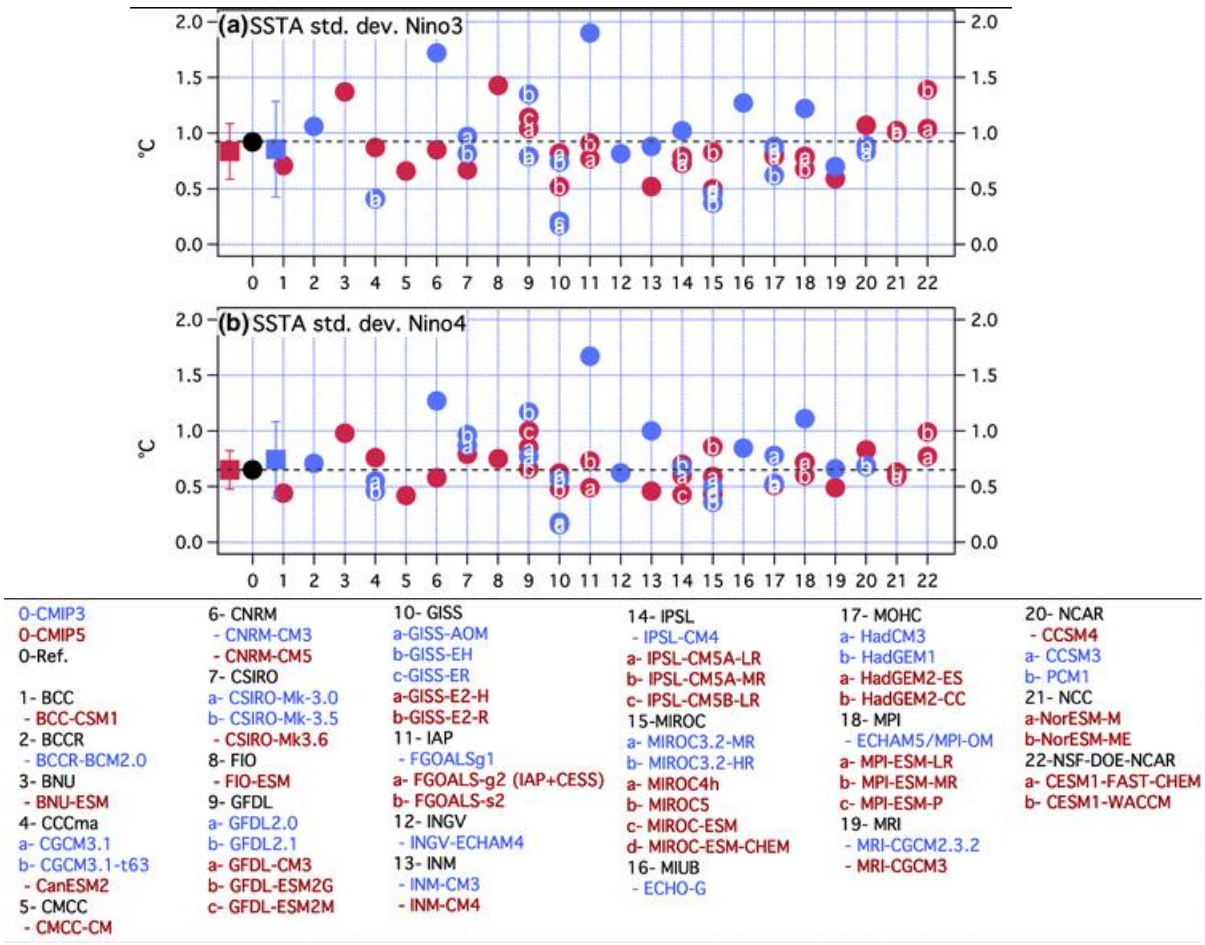

Figure 1.1: ENSO variability from preindustrial control simulations for CMIP3 (blue) and CMIP5 (red) relative to observations (black, HadISST1.1). a.) standard deviation of the sea surface temperature anomaly for the Niño3 region. b.) as in a. but for the Niño4 region. Reprinted by permission from Springer Nature: Springer Berlin Heidelberg, Climate Dynamics, *Bellenger et al.* (2014) © Copyright 2014.

Given the range of hypotheses for ENSO variability, a better diagnosis of the changing background mean climate state could improve our understanding of ENSO predictions for the 21st century. *Fedorov and Philander* (2000) suggest that a changing climate background state and internal variability in the climate system itself could be responsible for the production of different ENSO events. One ENSO warm phase mode, known as the

delayed oscillator, is produced from a deep thermocline in the eastern equatorial Pacific and strong westward winds across the ocean surface. The second mode has little to no change in thermocline depth but has winds converge just east of the central equatorial Pacific to produce high SSTs. *Fedorov and Philander* (2000) use the thermocline depth and mean easterly wind stress to model the period of the most unstable mode (Figure 1.2). Frequency analysis of ENSO-sensitive paleoclimate data may be used to assess the hypothesis of whether the mean climate state changed over time. If conditions in the past suggest increased frequency of ENSO events, for example, the mean climate state may lie somewhere closer to point E of Figure 1.2, suggesting a reduced mean thermocline depth and increased intensity of mean easterly wind stress. Modern conditions correspond to points A and B with a period somewhere in-between the two end-member modes. Estimating the period of warm phase events from paleodata can allow one to understand how the thermocline depth and mean wind stress anomaly could have varied in order to estimate the spatial pattern and mode of past ENSO compared to modern ENSO activity.

Other research has explored interdecadal variability in the tropical Pacific and its impacts to the mean climate state, such as the tropical Interdecadal Pacific Oscillation (IPO) with a period of about 30 years (*Folland et al.*, 2002). Some literature suggests the IPO is a persistent component of the larger, basin wide Pacific Decadal Oscillation (*Gershunov and Barnett*, 1998; *Mantua et al.*, 1997; *Pierce*, 2001). Research focused in the South Pacific suggests there could be an interdecadal component of IPO variability with a period of 20 years (*Linsley et al.*, 2008) as well as another mode unique to the Southern Hemisphere with a period of 10-20 years known as the Southern Hemisphere Pacific Decadal Oscillation (SHPDO) (*DeLong et al.*, 2012). Other research suggests that

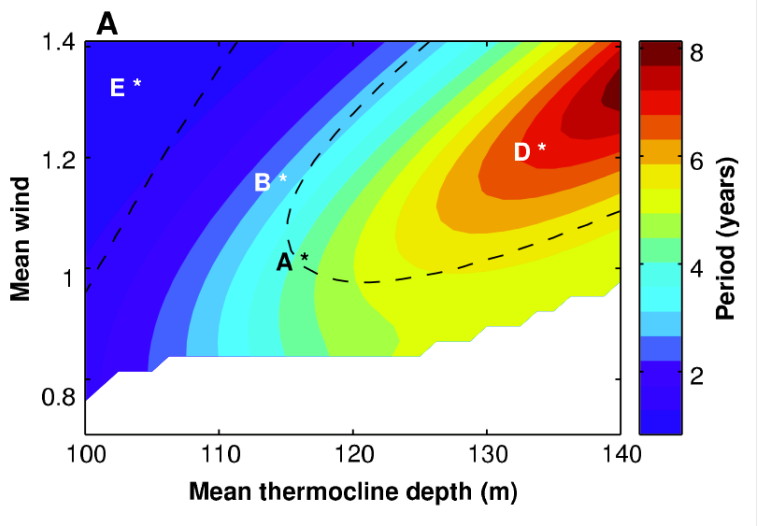

Figure 1.2: The period (in years) of ENSO, modelled as the most unstable oscillation of the coupled ocean-atmosphere system produced from changing mean easterly winds and thermocline depth. Points A and B correspond to the modern mean climate state of the tropical Pacific. From *Fedorov and Philander* (2000). Reprinted with permission from AAAS.

these different oscillations may a part of Pacific Decadal Variability (PDV) originating in the tropical Pacific (*Garreaud and Battisti*, 1999; *Hoerling et al.*, 2001) from the anomalous surface heat fluxes produced from ENSO activity (*Deser et al.*, 2010; *Evans et al.*, 2001; *Newman et al.*, 2003). Limited observations and understanding of these variations of the climate system may interact with the mean climate state and contribute towards uncertainty in 21st century projections of ENSO activity.

1.3 What can paleoclimatology contribute?

Direct observations of climate variables, such as temperature, precipitation, and wind stress, through *in-situ* and remote sensing measurements, are limited, extending only to the early 20th or mid-19th century (and the satellite era only from 1979-present)

(*Compo et al.*, 2011; *Delcroix et al.*, 2011; *Huang et al.*, 2015). Limited observations make it difficult to understand decadal and longer timescale variability of ENSO and tropical Pacific climate change due to few realizations of the phenomena (*Vecchi*, 2008; *Vecchi and Wittenberg*, 2010). Extended indirect observations of past climate can improve our understanding of how ENSO amplitude, frequency, and spatial pattern may change in the 21st century by (1) studying climate variability over a greater time range than the instrumental era (*Cobb et al.*, 2003a), and by (2) choosing from all possible model simulations those which are most consistent with the paleoclimate observations (*Braconnot et al.*, 2012). For example, climate model simulations with single and/or cumulative external radiative forcings (well-mixed greenhouse gas concentrations, volcanism, ozone, solar irradiance, and land use/land change) have been used to better understand the mechanisms of global, basin-wide, and regional sea surface temperature variations over the past 2,000 years (*McGregor et al.*, 2015).

The past millennium particularly interesting because the Medieval Climate Anomaly (MCA, 800-1300 C.E.) and Little Ice Age (LIA, 1300-1800 C.E.) are periods when North America and Eurasia may have experienced an anomalously warm/wet period followed by a cold/dry period (*Bradley et al.*, 2003; *Cook et al.*, 2004; *Lamb*, 1965), respectively, driven by tropical Pacific climate forcings (*Braconnot et al.*, 2012; *Diaz et al.*, 2011; *Schmidt et al.*, 2011). The role of unforced variability during these periods may be assessed in comparison to the external radiative forcings (*Ammann et al.*, 2007; *Diaz et al.*, 2011; *Gao et al.*, 2008; *Jungclaus et al.*, 2010; *Schmidt*, 2010). While a number of observations and simulations from these periods have been collected, there are still few consistent results (*Cobb et al.*, 2013; *Graham et al.*, 2011; *Phipps et al.*, 2013) and even

fewer paleoclimate records are available during the MCA that are sensitive to variations in hydroclimate (*Smerdon et al.*, 2017). Global temperature patterns for these time periods are uncertain and could depend on the method of multiproxy reconstruction (*Wang et al.*, 2014), parameterization of model physics (*Graham et al.*, 2011), the external radiative forcings during the MCA, or all of these factors (*Phipps et al.*, 2013). Therefore, additional paleoclimate observations from the tropical Pacific during the MCA may help address these outstanding questions and uncertainties.

Paleoclimate observations show real changes to the climate and model simulations show relationships between mechanisms and the modeled climate. By identifying the subset of simulations most consistent with observations, we may say that a particular climate pattern was produced from a particular climate mechanism (*Braconnot et al.*, 2012; *Schmidt*, 2010). Additional MCA observations may allow for further insight into how this time period compares to the modern era. Previous literature suggests orbital and solar forcings were negligible (*Ammann et al.*, 2007) and anthropogenic influences to the climate only extend to 1850, leaving hundreds of years of observations of "natural" climate variability (*Schmidt*, 2010). Furthermore, *Bellenger et al.* (2014) and others (*Wittenberg*, 2009) argue 300-500 years of data are required to accurately evaluate ENSO frequency variability from spectral analysis. The large range of ENSO variance observed and simulated could provide a better understanding of how ENSO activity responded to past external and internal forcings, making the MCA (and LIA) a natural laboratory whose results could be used towards improving 21st century ENSO predictions.

Despite the benefits of the paleodata-model inter-comparison approach, it must be used with caution because there are large uncertainties, some of which are only poorly

characterized (*Jones et al.*, 2009). Uncertainty exists in the observations: scientific understanding of the model relating the paleodata to a climate variable (*Phipps et al.*, 2013), the ability of one location to reliably predict measurements at other locations where paleodata are absent (*Thompson et al.*, 2011), the lack of replicated paleoclimate data (*DeLong et al.*, 2013), and age model error (*Comboul et al.*, 2015). Even the most up-to-date climate model simulations (CMIP5; (*Taylor et al.*, 2012)) remain inconsistent with observations in their reproduction of the mean climate state and key ENSO metrics (*Bellenger et al.*, 2014). Additional caution must be exercised when interpreting data as hydroclimatological indicators given the spatially diffuse signals, low replication of results, spectral reddening, and the sometimes low signal to noise ratios given the large unforced variability of the climate system during the MCA and LIA periods (*Smerdon et al.*, 2017).

1.4 Interpretational Framework

Observations from a few ENSO-sensitive locations in the tropical Pacific, though limited in space and time, may be used to infer the large-scale, well-characterized patterns of climate variation (*Evans et al.*, 1999, 2000, 2002; *Kaplan et al.*, 1998; *Wallace*, 1996b). Comparison of observations can determine if they are consistent with our prior knowledge of how climate patterns arise and are expressed in the tropical Pacific (*Evans et al.*, 2000, 2002). This approach can also be applied to midlatitude regions that have ENSO teleconnections (*Cook et al.*, 1994, 1999, 2000; *Li et al.*, 2011, 2013). In other words, if ENSO activity causes characteristic, consistent climate variations in a remote location, those observations can be used to infer the state of tropical Pacific climate and whether there was any ENSO-like activity.

1.4.1 The tropical Pacific mean climate state

The general circulation of the atmosphere and ocean may be described in terms of their zonal (east-west) and meridional (north-south) motion driven ultimately by solar irradiance as well as heat transfer between these Earth System components (*Holton and Hakim*, 2013; *Philander*, 1990; *Vallis*, 2006). Sea surface temperatures are warm in the western equatorial Pacific and cool in the eastern equatorial Pacific. The eastern cold tongue is the result of Ekman divergence along the equator and the coast of Peru. The thermocline – the interface between well-mixed warm surface layer and colder intermediate ocean – is deep (150-200 m) in the western Pacific warm pool and surfaces offshore of South America in the eastern equatorial Pacific. Significant latent and sensible heat exchange between the atmosphere and the warm, moist western Pacific warm pool water coupled with easterly trade winds result in rising atmospheric motion. Elsewhere, in the central and eastern equatorial Pacific, the zonal asymmetry in wind forcing balances the rising atmospheric motion in the west with weak subsidence of atmospheric mass after moving through the upper troposphere. In the tropical Pacific, this zonal (east to west) motion is known as the Pacific Walker Circulation. In the atmosphere, equatorial trade winds sustain a convergence of heat and moisture to a narrow roughly zonal band across the equator. This Intertropical Convergence Zone transports heat from the surface to the upper troposphere via adiabatic cooling in large, narrow, cumulonimbus clouds. The ITCZ is the convective maxima in the tropical Pacific and is usually located a few degrees north of the equator, causing significant rainfall in a narrow zonal band. The position of the ITCZ is dependent on ocean-driven heat transport from the Southern to the Northern

Hemisphere (*Marshall et al.*, 2014; *Schneider et al.*, 2014).

The southern hemisphere equivalent to the ITCZ is the South Pacific Convergence Zone (SPCZ), which extends diagonally from Indonesia southeastwards towards the Cook Islands. The position of these convergence zones changes based on the annual cycle of solar irradiance and the asymmetry of the meridional atmospheric Hadley cells. The Hadley circulation consists of thermally direct cells where warm tropical air rises in the convergence zones. Once aloft, the air mass travels poleward, losing moisture along the way as rain and losing heat via radiative cooling and sinks at around 30^o latitude before traveling equatorward along the sea surface towards lower pressure tropical convergence regions.

Zonally, rising motion in the west and sinking motion in the east tend to produce lower sea level pressures (SLP) in the western equatorial Pacific and higher SLP in the eastern equatorial Pacific supporting zonal advection of warm surface water from east to west. This SLP pattern in the mean state of the atmosphere is known as the Southern Oscillation, first systematically observed by Sir Gilbert Walker in the early 20th century. The Southern Oscillation Index is the normalized sea level pressure difference between Tahiti and Darwin, which can be used to infer El Niño or La Niña activity.

1.4.2 The tropical Pacific annual cycle

During the annual cycle, the net incoming solar radiation in the northern tropics is greatest in June-August (Northern Hemisphere, NH summer) and greatest in the southern tropics during December-February (NH winter). Tropical SSTs vary in phase with net incoming solar radiation, with regions of warm SSTs causing a deepening of the thermo-

cline and cooler SSTs causing a shoaling of the thermocline. The net outgoing longwave radiation in the northern tropics is greater in NH winter and greater in the southern tropics during NH summer (*Philander*, 1990). Zonal SLP differences in the tropical Pacific are small in March/April and large during August/September, which corresponds to a weaker and stronger Pacific Walker Circulation, respectively. The ITCZ moves furthest north (about 12^{o}N) in August/September where SSTs are warmer and southeast trades are greater than the northeast and just north of the equator in March/April when equatorial ocean temperatures and atmospheric wind patterns are reversed. Rainfall seasonal variations are in phase with ITCZ movements which are affected by SST seasonal variations. Associated with these changes in the ITCZ are changes in zonal winds with the northeasterly trade winds smaller and the southeasterly trades greater in August/September with reversed conditions in March/April (*Philander*, 1990). The meridional component of the atmosphere's general circulation, the Hadley cell is greater in the winter hemisphere due to the larger latitudinal thermal gradient and subdued in the summer hemisphere from a smaller latitudinal thermal gradient.

In the southwest tropical Pacific, the position of the SPCZ is constrained primarily from the sea surface temperature gradients (*Folland et al.*, 2002; *Kiladis et al.*, 1989; *Widlansky et al.*, 2012). East-to-west variations in the surface ocean temperature cause coincident atmospheric pressure variations, which drive winds towards the low pressure zones and results in moisture convergence (*Vincent*, 1994). In the eastern portion of the SPCZ where the convergence band is more diagonal, its position is controlled by the interaction of storms moving from the tropics to the midlatitudes with atmospheric regions of low pressure known as troughs (*Folland et al.*, 2002; *Vincent*, 1994).

1.4.3 ENSO and interannual variations in tropical Pacific climate

ENSO is a coupled atmosphere-ocean phenomenon with a periodicity of 2-8 years that originates in the tropical Pacific (*Jin*, 1997) (Figure 1.3). The redistribution of warm water eastward across the Pacific leads to a shallowing of the thermocline in the western Pacific, a deepening of it in the eastern Pacific, a reduction in the zonal SLP gradient, and eastward movement of the Pacific Walker Circulation. The combined changes to the atmosphere and ocean described above are known as a warm-phase or El Niño event. An enhancement of more typical conditions described in the previous sections is known as a cold-phase or La Niña event.

Jin (1997) synthesized many of the earlier ENSO dynamics results into a conceptual recharge oscillator model of ENSO that is still the predominant paradigm used to understand ENSO physics. *Bjerknes* (1969), described a positive feedback between the coupled ocean-atmosphere that is the primary mechanism sustaining warm or cold phase ENSO events. In the Bjerknes feedback loop, SST anomalies induce easterly trade wind anomalies and affect the upwelling of cold water in the eastern equatorial Pacific. *Wyrtki* (1975) used the Bjerknes feedback loop and an understanding of the seasonal cycle to describe the recharge-discharge hypothesis. Strong persistent easterly trade winds could lead to a buildup of warm water in the western Pacific with an increased zonal sea surface slope and thermocline. After about 18 months (about two winters and a summer season), the western Pacific warm pool water discharged eastward in conjunction with weakened easterly trade winds during northern hemisphere spring. Using their ENSO model of intermediate complexity (ZC), *Cane and Zebiak* (1985) determined the "memory" of the

tropical Pacific Ocean was important for ENSO dynamics by suggesting the Bjerknes feedback loop could only sustain warm (cold) events when the tropical Pacific ocean heat content was larger (smaller) than typical conditions.

Suarez and Schopf (1988) developed a delayed oscillator non-linear ENSO model in response to the results of *Cane and Zebiak* (1985) which suggested the periodicity of ENSO events depended on the transit times of oceanic Rossby waves westward and Kelvin waves eastward carrying warm water important for development of the coupled ocean-atmosphere (i.e. Bjerknes) feedback loop. *Battisti and Hirst* (1989) developed a ZC-type model focusing on the growth rate, magnitude, and lag of wave processes to study how the mean state and ocean basin geometry affected tropical coupled ocean-atmosphere variability, and their results suggested only the Pacific Ocean had a sufficient width of 13,000 km to generate ENSO and that the mean state was crucial for determining the growth rate of ENSO events. *Jin and Neelin* (1993) refined the understanding of unstable ocean dynamical modes by determining that there was a fast SST and fast wave limit which merge continuously in model space to produce a range of results in the coupled atmosphere-ocean models (*Jin*, 1997). In the SST limit case, the timescale of SST variability is faster than ocean dynamics meaning that SST is a function of subsurface feedback processes; in the fast wave limit case, ocean dynamics timescales are faster than SST variability, so SST change is dominated by surface layer processes which are in equilibrium with the subsurface ocean dynamics (*Jin*, 1997).

The recharge oscillator ENSO model of *Jin* (1997) incorporates tropical atmosphere-ocean coupling as the growth mechanism and the recharge-discharge of equatorial heat content as the mechanism for phase changes (Figure 1.3). First, there is a positive sea

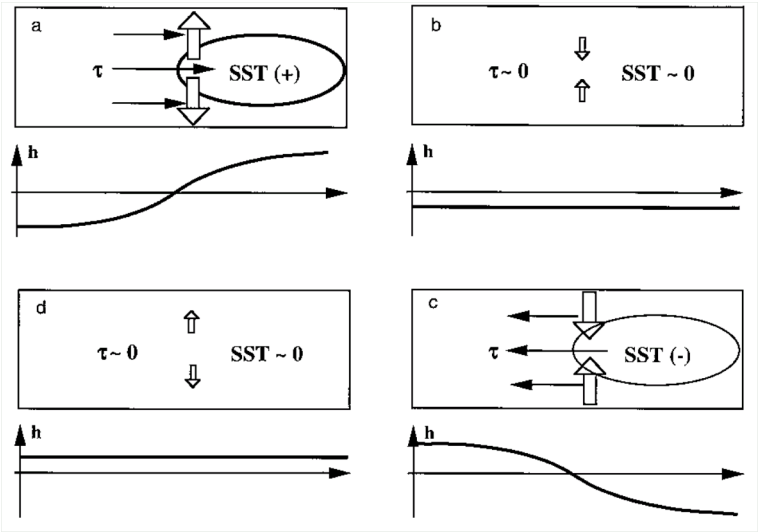

Figure 1.3: Schematic model illustrating the onset, propagation, and termination of El Niño or warm phase events in the tropical Pacific, from *Jin* (1997). Dark thin arrows (τ) are zonal wind stress, large white arrows are meridional heat transport, and h is depth of thermocline. Reproduced from the © American Meteorological Society. Used with permission.

surface temperature (SST) anomaly in the eastern Pacific, which causes a westerly wind anomaly. This results in a decrease in thermocline slope, becoming deeper in the eastern Pacific and shallower in the western Pacific, and there is a warm phase or El-Niño event (1.3a). The Hadley cell transports heat out of the tropics, reducing the thermocline and the positive SST anomaly in the eastern equatorial Pacific. As the positive SST anomaly approaches zero, the westerly wind stress also decreases. The thermocline is anomalously shallow across the basin due to the heat loss (1.3b). The shallow thermocline in the eastern Pacific enables upwelling of cold water via Ekman pumping to the surface layer, resulting in a negative SST anomaly in the east and an increase in easterly wind stress. The thermocline then becomes shallower in the eastern Pacific and deepens in the western Pacific as warm water builds in this region, leading to cold phase or La-Niña conditions

(1.3c). The strengthened easterly trade winds move towards the equator (deflected to the right in the Northern and to the left in the Southern Hemisphere from the Coriolis force), bringing surface ocean water which gathers heat during this journey. The influx of heat into the equatorial tropics makes the thermocline anomalously deep across the Pacific, dampening the SST and wind stress anomalies (1.3d).

On interannual timescales, the El Niño-Southern Oscillation has a significant impact on the position of the South Pacific Convergence Zone. Changes in zonal (east-to-west) and meridional (north-to-south) atmospheric circulation driven by changing sea surface temperature gradients during El Niño events change the location of moisture convergence from its usual mean position in the southwestern tropical Pacific towards the central equatorial region (*Folland et al.*, 2002; *Lorrey et al.*, 2012; *Philander*, 1990; *Salinger et al.*, 1995; *Widlansky et al.*, 2012). Anomalous advection of tropical oceanic currents also affect the position of the South Pacific Convergence Zone by altering the location of the warmest sea surface temperatures that are needed to sustain the tropical convergence zones (*Gouriou and Delcroix*, 2002; *Hasson et al.*, 2013; *Picaut et al.*, 1996).

1.5 Coral paleoclimatology

The proxy system model paradigm from (*Evans et al.*, 2013) provides a means by which to interpret paleoclimate observations: an *archive* is the medium in which a *sensor* imprints a response to *environmental forcing*, and from which we make *observations*. The coral proxy system model is a simplification of the relationship between climate and the δ^{18}O measurements of the aragonitic skeleton (*Thompson et al.*, 2011). A sensor's (*Porites* reef coral, for example) growth is affected by "environmental forcings". A

"sensor" can record these environmental forcing variations in an "archive" (such as the aragonitic skeleton of a coral). "Measurements" taken from the archive (coral skeleton δ^{18}O) may then be modeled as a climate indicator within quantifiable uncertainty.

Geochemical measurements of coral archives may be interpreted as indirect observations of the major atmospheric and oceanic mechanisms producing the near surface tropical Pacific climate described via different variables in the preceding sections. Stable isotope and trace element measurements of the aragonitic skeleton of stony reef corals may be used to record changes in tropical Pacific climate because colonies are long-lived (decades to hundreds of years) (*Lough*, 2010), grow continuously throughout the year in tropical latitudes (*Knutson et al.*, 1972), live in the surface ocean (*Dunbar and Cole*, 1996), respond to thermal and hydrologic forcings, and records within or between different corals can be replicated to improve the overall signal to noise ratio (*DeLong et al.*, 2013; *Jones et al.*, 2009). Microatoll *Porites* coral live in shallow, knee-deep water, initially grow upwards towards the sea surface before growing laterally outward in a circular geometry, and have been validated as a reliable source of climate information from previous research (*McGregor et al.*, 2011).

1.5.1 Coral sensors

The controls on ^{18}O in coral aragonite are sea surface temperature (*Epstein et al.*, 1951, 1953; *McCrea*, 1950; *Weber and Woodhead*, 1972), the oxygen isotope composition of seawater (*Bradley*, 1999; *Cole et al.*, 2000; *Le Bec et al.*, 2000), light levels (*Lough*, 2010), evaporation-precipitation balance (*Cole and Fairbanks*, 1990; *Linsley et al.*, 1994), photosynthesis (*Lough*, 2010), and metabolic ("vital") effects (*Grottoli and Eakin*, 2007;

McConnaughey, 1989a,b). These controls yield coral oxygen isotope ratios that are not in equilibrium with seawater (*Kim and O'Neil*, 1997; *McConnaughey*, 1989a,b). However, *McConnaughey* (1989a) argues that if growth-related isotopic effects are constant and well characterized, the residual isotopic variations can be used to to constrain environmental variation. Given the controls on the ^{18}O of coral aragonite, the oxygen isotope composition of coral may be modeled approximately linearly as a bivariate function of calcification temperature and seawater δ^{18}O (*Dee et al.*, 2015; *Evans et al.*, 2013; *Smerdon et al.*, 2017; *Thompson et al.*, 2011). This observation is measured using delta notation, δ^{18}O, relative to an international reference standard (commonly V-SMOW, Vienna Standard Mean Ocean Water).

1.5.2 Coral δ^{18}O forward model

Coral δ^{18}O paleoclimate observations may also be forward modeled via the proxy system model paradigm (*Dee et al.*, 2015; *Evans et al.*, 2013; *Thompson et al.*, 2011). Calcification temperature may be approximated by sea surface temperature because the water in the pore space of the aragonite skeleton is in contact with open ocean water surrounding it in the reef (*Corrége*, 2006; *Grottoli and Eakin*, 2007; *Kim and O'Neil*, 1997). Sea surface salinity may be substituted for seawater δ^{18}O because of their linear empirical relationship: both change predictably with precipitation (more ^{18}O in ocean, less saline) and evaporation (less ^{18}O in ocean, more saline) processes in the tropical latitudes (*LeGrande and Schmidt*, 2006; *McGregor et al.*, 2011; *Thompson et al.*, 2011). With these simplifications, inputs of SST and SSS anomalies into the *Thompson et al.* (2011) coral δ^{18}O anomaly forward model produce coral δ^{18}O anomaly outputs (**Equation 1**, where

a_1 relates the ‰ change in coral δ^{18}O to SST, while a_2 does the same but for SSS).

$$\delta^{18}O_{coral} \approx a_1 * SST + a_2 * SSS \quad \textbf{[Eq. 1]}$$

1.5.3 Coral Sr/Ca

The coral Sr/Ca ratio measurement may also be used to record climate variation in the coupled atmosphere-ocean system (*Corrége*, 2006; *De Villiers et al.*, 1994; *Lough*, 2010). Light levels, and calcification chemistry variation (*Corrége*, 2006; *Lough*, 2010) can affect Sr/Ca values, but unlike the coral δ^{18}O, the Sr/Ca ratio in reef coral is not sensitive to the seawater δ^{18}O (*Evans et al.*, 1999). The variation in the Sr/Ca ratio of seawater has been studied and shown to cause variations in reconstructed sea surface temperature of 0.2^{o}C or less (*De Villiers et al.*, 1994). While photosynthetic algae also cause variations in skeletal Sr/Ca values unrelated to sea surface temperature (*Cohen et al.*, 2001), interannual Sr/Ca dataseries (calculated by removing the annual mean) show high correlation with sea surface temperature datasets in the southwest tropical Pacific (*Kilbourne et al.*, 2004; *Linsley et al.*, 2000, 2006). Thus, calcification temperature may be approximated with sea surface temperature in an inverse linear regression coral Sr/Ca model as done previously in the literature (*Corrége*, 2006; *Linsley et al.*, 2000, 2004; *Ren et al.*, 2002).

1.5.4 Coral $\delta^{18}O_{SW}$

Coral δ^{18}O and Sr/Ca measurements are independent of each other and can be used to deconvolve the SST contribution from the seawater δ^{18}O contribution in the coral δ^{18}O measurement (*McCulloch et al.*, 1994). With aliquot measurements of coral δ^{18}O and

Sr/Ca, the coral $\delta^{18}O_{SW}$ may be calculated as in **Equation 2**. The a_1 coefficient, as in **Equation 1**, relates the ‰ change in coral δ^{18}O to temperature ($\alpha = -0.22 + / - 0.02$) (*Evans et al.*, 2000; *Lough*, 2004; *Thompson et al.*, 2011), while a_2 in this equation is the empirically derived coefficient (mmol/mol per ^{o}/C) of the linear regression of Sr/Ca measurements onto SST observations ($\rho = 0.0725 + / - 0.0095$) (*Corrége*, 2006; *Linsley et al.*, 2000, 2004; *Ren et al.*, 2002). Measured δ^{18}O and Sr/Ca have analytical uncertainty (0.1‰, 0.011 mmol/mol, respectively) and the empirically derived coefficients also have error. Propagation of error modeled as the summation of each fractional uncertainty (*Taylor*, 1997). Measured δ^{18}O and Sr/Ca fractional uncertainty was calculated as the standard error of analytical precision divided by the root mean square error of the total respective dataseries. This error propagation analysis resulted in an error estimate for calculated coral $\delta^{18}O_{SW}$ of 36% of the measured geochemical value (i.e., uncertainty of about third the value, 0.6 ± 0.2 permil).

$$\delta^{18}O_{SW} \approx \delta^{18}O_{coral} - \rho * Sr/Ca \quad \textbf{[Eq. 2]}$$

1.5.5 Chronology development

The age of coral samples may be determined through absolute and relative dating methods. A combination of dating methods may be applied to paleoclimate observations to better transform a coral dataseries of depth into a dataseries in time.

An absolute date provides a precise data point in time at some specific depth of the coral record. For modern coral samples, the date at which the samples were acquired marks an absolute youngest age for a coral sample. For fossil corals, U/Th radiomet-

ric dating methods provide a precise and absolute date on a particular location on the coral sample (*Cobb et al.*, 2003b; *Edwards et al.*, 1987). ^{238}U is a radioactive, naturally-occurring isotope which emits alpha radiation (a helium nucleus) leading to spontaneous decay to ^{234}U, ^{230}Th, ^{232}Th, and the stable ^{206}Pb. U and Th isotopes can be measured using isotope-dilution mass spectrometry (*Edwards et al.*, 1987). The extreme fractionation of U from Th in seawater and the observation that ^{230}Th does not fractionate greatly from ^{238}U in coral growth (*Edwards et al.*, 1987) provides initial radioactive conditions to develop an equation describing the radioactivity of the U/Th system. Thus, an accurate, precise age can be determined by solving **Equation 3** for time (T) provided the aragonite does not mix U and Th with the environment (closed system); that the decay constants (λ) of ^{238}U, ^{234}U, and ^{232}Th are known accurately and precisely; that U has an isotopic composition not affected by isotope fractionation; that non-radiogenic Th isotope concentrations are known (*Cobb et al.*, 2003b); and that analytical errors are well-characterized and quantified (*Edwards et al.*, 1987).

$$1 - \left[\frac{^{230}Th}{^{238}U}\right] = e^{-\lambda_{230}T} - \left[\frac{\delta^{234}U(0)}{1000}\right]\left[\frac{\lambda_{230}}{\lambda_{230} - \lambda_{234}}\right] * (1 - e^{(\lambda_{234} - \lambda_{230})T}) \quad \textbf{[Eq. 3]}$$

Relative dating methods for coral may be determined by counting the annual density bands and annual isotopic variations controlled by the annual cycle (*Knutson et al.*, 1972; *Lough*, 2010). This banded age model accounts for error by considering uncertainty as arising from doubly counted bands and missing annual banding within a sample (*Comboul et al.*, 2015). Relative dating may also be accomplished by counting the annual variations in a coral geochemical dataseries. In coral proxy system modeling, it is assumed that SST and SSS covary inversely to one another (i.e. it is either warm and/or wet or cold

and/or dry) based on the coral δ^{18}O anomaly forward model (Eqn. 1) (*Thompson et al.*, 2011) and our understanding of the annual cycle described earlier. It is further assumed that δ^{18}O is most negative when SST is highest, and SSS is lowest, while δ^{18}O is most positive when SST is lowest and SSS is highest (*Corrége*, 2006; *Lough*, 2010).

With these assumptions, understanding of the annual cycle, and one absolute date, a relative chronology may be produced for the entire coral specimen (*Dunbar and Cole*, 1996). Absolute and relative dating methods may be combined with each other to produce a modern coral timeseries with an absolutely known collection date and a relative model for each counted band. For fossil timeseries, at least one radiometric date combined with counted bands may produce a "floating" chronology during a particular time period whose error constitutes the uncertainty in the absolute radiometric age and the error in relative dating associated with the banded age model (*Comboul et al.*, 2015).

1.5.6 Diagenesis

In corals, diagenesis is defined as the precipitation of secondary aragonite or calcite within the skeleton, and/or the replacement of primary skeletal aragonite predominantly with calcite (*Allison et al.*, 2007; *McGregor and Gagan*, 2003). More recent research suggests diagenesis can occur in corals that are only 30 years old (*Sayani et al.*, 2011). Subaerial and submarine post depositional processes, such as weathering, erosion, fluid flow, and compaction, can cause re-crystallization of the aragonitic skeleton. The destruction of primary aragonite removes any δ^{18}O variations in the skeleton that would have been associated with climate variations and can cause a several degree offset in reconstructed temperature values (*Allison et al.*, 2007; *McGregor et al.*, 2011; *Sayani et al.*,

2011). Given the potential for significant biases arising from unrecognized diagenetic alteration of samples, multiple quality control protocols should be used to ensure measured coral δ^{18}O and Sr/Ca values are representative of climate processes. X-ray diffractometry (XRD), thin section analysis, and secondary ion mass spectrometry techniques have been developed to detect and quantify the levels of primary aragonite, calcite and secondary aragonite, calcite in fossil coral samples (*Allison et al.*, 2007; *DeLong et al.*, 2013; *McGregor et al.*, 2011; *McGregor and Gagan*, 2003; *Sayani et al.*, 2011).

1.5.7 Using coral paleoclimatology to understand ENSO activity

Coral δ^{18}O and Sr/Ca values reflect the oceanic and atmospheric components of surface climate variation. Tropical Pacific interannual climate variations are sensitive to ENSO activity, so coral paleoclimatology may be used to reconstruct climate variation associated with ENSO activity via anomalous sea surface temperature and rainfall variations (*Cobb et al.*, 2003a; *Cole and Fairbanks*, 1990; *Evans et al.*, 1999; *Hereid et al.*, 2013; *Kilbourne et al.*, 2004; *McCulloch et al.*, 1994; *McGregor and Gagan*, 2004). Provided that fossil materials are well-preserved, coral paleoclimate observations may also reconstruct ENSO activity over a longer period of time than the instrumental era (late 19th to 21st century) (*Jones et al.*, 2009).

This dissertation will present new coral geochemistry results with existing paleoclimate observations to better understand variations in ENSO during intervals of the past millennium. Chapter 2 will use climate model simulations as a null hypothesis to test whether existing paleoclimate observations can be used to identify periods of different ENSO activity in the past relative to the present day conditions. Simple event counts of

ENSO activity will be used to assess changes in ENSO frequency. Chapter 3 will introduce new modern coral results calibrated and tested via the proxy system model paradigm and validated through comparisons with climate timeseries and existing paleoclimate observations. Spatial and pattern correlations will be used to assess the sensitivity of different locations across the tropical Pacific to ENSO activity. Spectral analysis will be used to filter the signals of different time resolution to better understand interannual ENSO and lower frequency Pacific decadal variability. Chapter 4 will apply the interpretation developed in Chapter 3 on fossil coral samples. Amplitude and frequency analyses described here will be used to assess the degree to which ENSO has varied during intervals of the past millennium relative to modern, present day conditions. Chapter 5 will summarize the results and suggest additional analyses and future avenues of research.

Chapter 2: Last millennium observations and simulations suggest limited change in ENSO variance

2.1 Tropical Pacific climate variability over the past millennium

Observations from a few locations in the tropical Pacific, though spatially and temporally limited, can be used to infer the large-scale, well-characterized patterns of climate variation provided the processes that drive the variations are spatiotemporally stable within the tropical region (*Comboul et al.*, 2015; *Evans et al.*, 1998, 2000, 2002; *Wallace*, 1996a,b).

The "Medieval Climate Anomaly" (MCA, 800-1300 C.E.) and the "Little Ice Age" (LIA, 1300-1800 C.E.) are periods when North America and Eurasia may have experienced a climate characterized by anomalously warmer/wetter and colder/drier surface temperatures conditions respectively. (*Bradley et al.*, 2003; *Cook et al.*, 2004; *Diaz et al.*, 2011; *Lamb*, 1965; *Mann et al.*, 2009). However, the tropical Pacific climate may have experienced colder/drier conditions in the MCA followed by warmer/wetter conditions in the LIA (*Allen*, 2006; *Cobb et al.*, 2003a; *Hendy et al.*, 2002; *Yan et al.*, 2011b). *Henke et al.* (2015) inferred a transition from ENSO warm phase to cold phase from the MCA to LIA in a reconstruction of hydrological changes, and no significant difference in ENSO phase from a reconstruction of temperature changes.

If there were changes in climate between these periods, mechanisms originating in the tropical Pacific (*Emile-Geay et al.*, 2013b; *Graham et al.*, 2007; *Vecchi and Wittenberg*, 2010) such as the El Niño-Southern Oscillation, the largest source of interannual climate variability (*Wallace and Hobbs*, 2006) may be part of the forcing which caused a response in the climate system. External radiative forcings for the tropical Pacific (solar, volcanism, land use/land change, well-mixed greenhouse gas (GHG) concentrations) are relatively small over the past millennium (*Schmidt et al.*, 2011) compared to the unforced variability which arises from the coupled ocean-atmosphere dynamics of the climate system (*Ault et al.*, 2013; *Deser et al.*, 2010; *Fedorov and Philander*, 2000).

But, determining the mean climate of the MCA and LIA, and whether there were distinct interannual variations in ENSO during these periods remains significantly uncertain because of limited high-resolution tropical Pacific observations (*Emile-Geay et al.*, 2013b; *Neukom and Gergis*, 2011), the likely large unforced variability in the climate system (*Ault et al.*, 2013), the sensitivity of climate reconstructions to the methodology (*Phipps et al.*, 2013; *Wang et al.*, 2014), limitations in coupled general circulation models (*Graham et al.*, 2011; *Phipps et al.*, 2013), the forcings applied to these models (*Schmidt et al.*, 2014), or perhaps most likely, some combination of all these factors.

Previous syntheses of tropical Pacific climate variability over the past millennium have not definitively determined if the climate system did or did not change during the MCA and LIA. Some syntheses have used different observations in each time period based on the availability of records (*Li et al.*, 2011, 2013; *Mann et al.*, 2009; *Tierney et al.*, 2015), have focused primarily on observations without comparison to simulations (*Li et al.*, 2011, 2013), and some have not had a sufficiently high temporal resolution to

study ENSO (*McGregor et al.*, 2015).

2.1.1 A cold phase MCA followed by a warm phase LIA

Several reconstructions of past climate from temperature and hydrological observations in the central tropical Pacific suggest more warm phase-like (El Niño) mean conditions in the LIA relative to the MCA. The movement of the Intertropical Pacific Convergence Zones (ITCZ) produces anomalously high temperature and rainfall at Palmyra and Kiritimati Islands with anomalous aridity at the more northward located Washington Island (*Cobb et al.*, 2003a). *Cobb et al.* (2003a) reconstructed coral δ^{18}O from Palmyra Island over intervals of the last millennium. More negative δ^{18}O anomalies in the LIA (1300-1450 A.D., 1550-1650 A.D.) suggests warm/wet conditions indicative of warm phase (El Niño) conditions. More positive δ^{18}O anomalies in the MCA (950-1250 A.D.) suggests cool/dry conditions indicative of cold phase (La Niña) conditions. *Sachs et al.* (2009) used microbiological sensors stored in lake sediment archives and measured their to infer rainfall amount and vertical mixing in tropical lakes. Washington and Kiritimati Island results showed cool/dry and warm/wet conditions, respectively, which suggests the northward Washington Island received less rainfall during the LIA while the southward Kiritimati Island received anomalously high rainfall. The sediment core-based observations from Washington Island extending into the MCA (beginning at 950 A.D.) suggest wetter conditions, implying a northward-displaced ITCZ. Together, these central tropical Pacific results suggests a more cold phase-like MCA and a more warm phase-like LIA.

Some reconstructions from multiple observations also support a cold phase-like MCA. *Graham et al.* (2007) suggests that there were cooler eastern Pacific SSTs in the

MCA relative to the MCA-LIA transition based on data from *Cobb et al.* (2003a) in addition to other marine and terrestrial records from ENSO-sensitive regions around the globe. *Graham et al.* (2011) took these observations and compared them to a coupled climate simulation, which suggested an increase in the zonal Pacific SST gradient in the MCA with coordinated NH atmospheric circulation patterns, indicative of cold phase conditions. *Henke et al.* (2015) selected observations from the Pacific rim, separated them as precipitation or temperature sensitive, and then conducted a weighted EOF analysis to estimate the ENSO phase over time. Their results, which suggest ENSO cold phase conditions in the MCA followed by ENSO warm phase conditions in the LIA is informed from the precipitation-based reconstruction, whereas the temperature reconstruction shows no significant ENSO phase over time.

During modern ENSO warm phase events, the South Pacific Convergence Zone (SPCZ) shifts northeastward of its mean position, reorganizing in the central equatorial Pacific (*Folland et al.*, 2002; *Picaut et al.*, 1996; *Vincent*, 1994). Therefore, if results from the central tropical Pacific indicate more rainfall during the LIA and are suggestive of warm phase ENSO conditions, reduced rainfall conditions would be expected along the mean climatological position of the SPCZ. *Linsley et al.* (2006) collected coral from Rarotonga in the southern Cook Islands and Fiji that date from 1600 A.D. – present. The ocean surrounding these two southwestern tropical Pacific islands experience interannual variations in freshwater input and subsurface temperature associated with the SPCZ from the movement of western Pacific warm pool water towards the central equatorial Pacific during ENSO warm phase events (*Picaut et al.*, 1996; *Ramesh and Murtugudde*, 2012). Using measurements of coral δ^{18}O to reconstruct interannual hydrological varia-

tions, *Linsley et al.* (2006, 2008) suggested the southwestern tropical Pacific experienced drier (and perhaps cooler) conditions in the late LIA (1600-1850 A.D.) relative to the 20th century, a pattern consistent with modern ENSO warm phase conditions (*Clarke*, 2014; *Gouriou and Delcroix*, 2002; *Singh and Delcroix*, 2011). *Lorrey et al.* (2014) reconstructed geopotential height anomalies during the LIA using paleoequilibrium lines of 22 glaciers in New Zealand. The geopotential height is a vertical coordinate used to describe energetic large-scale atmospheric motion (*Wallace and Hobbs*, 2006). Results suggested negative 1000 hPa geopotential height anomalies in the southwestern Pacific, which could mean there was reduced subsidence (i.e., reduced downward air flow) in the South Pacific Anticyclone region and a reduction in east-to-west surface air flow. These inferences further suggest the SPCZ could have shifted northeastwards during the months of December-February because of changing surface flow from the South Pacific Anticyclone. This means the LIA may have experienced more warm phase conditions (*Lorrey et al.*, 2014). *Goodwin et al.* (2014) reconstructed and analyzed sea level pressure (SLP) variations during the MCA and the MCA-LIA transition using a synoptic climate analogue approach (*Graham et al.*, 2007) with paleoclimate data and a coupled atmosphere-ocean global climate model simulation.

In the southwest Pacific, the Southern Annual Mode is an atmospheric pressure gradient between the mid and high latitudes whose positive (negative) phase consists of a positive (negative) mid-latitude pressure anomaly coincident with a high-latitude negative (positive) pressure anomaly (*Gomez et al.*, 2011). These observations suggest a transition from a persistently positive phase of the Southern Annular Mode during the MCA to a more negative phase during the MCA-LIA transition. These conditions, the authors

conclude, would have been more favorable for the development of ENSO warm phase events because previous research suggests ENSO atmospheric teleconnections to the mid- and high-latitudes of the South Pacific is dependent, in part, on the phase of the Southern Annular Mode (*Fogt and Bromwich*, 2006). This interpretation assumes the interaction between ENSO and the Southern Annular Mode has remained consistent over time, but some research suggests this is not the case (*Gomez et al.*, 2011).

2.1.2 Or a warm phase MCA followed by a cold phase LIA

Hereid et al. (2013) measured coral δ^{18}O and Sr/Ca values from samples collected in Papua New Guinea during the 15th to 17th century (233 years). A negative median shift in coral δ^{18}O suggests a transition from cooler/drier to warmer/wetter conditions in the western tropical Pacific. δ^{18}O values below a threshold value were concluded to be the result of warm phase conditions. These results suggest a reduced number of warm phase events in the fossil record from about 1550-1650 CE, or more cold phase-like conditions during the LIA. However, the results of *Hereid et al.* (2013) are not consistent with those of *Linsley et al.* (2006), which suggested generally positive δ^{18}O anomalies for the late 16th to early 17th century and more ENSO warm phase conditions during the LIA.

Yan et al. (2011b) used two reconstructions of tropical Pacific hydrological variability (one from the eastern (*Conroy et al.*, 2009) and one from the western (*Oppo et al.*, 2009) tropical Pacific) to reconstruct a 'pseudo-SOI' (Southern Oscillation Index) index. The SOI is calculated as the normalized difference in sea level pressure anomaly between Tahiti and Darwin, which has been shown to be a reasonable indicator of the phase and magnitude of ENSO (*Trenberth*, 1984). Results from this reconstruction suggest a Pacific-

wide enhancement of the zonal (east to west) Walker Circulation during the LIA period compared to the MCA. A strengthening of this circulation suggests a stronger zonal equatorial SLP gradient, which typically occurs during cold phase events.

2.1.3 Summarized past millennium paleoclimate evidence

While a debate exists in the literature about the mean climate state of the tropical Pacific and its variability during the MCA, LIA, and the transition period, more literature supports a cold phase MCA followed by a warm phase transition period and LIA (Figure 2.1). Paleo-records covering the MCA (*Cobb et al.*, 2003a; *Conroy et al.*, 2009; *Li et al.*, 2011, 2013; *Oppo et al.*, 2009; *Sachs et al.*, 2009) suggests more warm phase conditions in the LIA relative to the MCA. Results which suggest the South Pacific Convergence Zone shifted eastward of its present position (*Linsley et al.*, 2006; *Lorrey et al.*, 2014) in the southwestern tropical Pacific supports this interpretation. However, results from the western tropical Pacific (*Hereid et al.*, 2013) and a hydrological reconstruction of ENSO (*Yan et al.*, 2011b) suggests there could have been an enhanced Pacific Walker Circulation during the LIA, which would suggest more ENSO cold phase conditions.

A new synthesis of the available tropical Pacific paleoclimate observations and its comparison to realistically forced climate model simulations may provide mechanism-based inferences from changes to the mean climate state. In section 2, we describe the data inputs and our synthesis approach. In Sections 3 and 4, results are presented and compared to existing, independent estimates of tropical Pacific mean climate and variation. Finally, Section 5 summarizes this work and suggests future avenues of research.

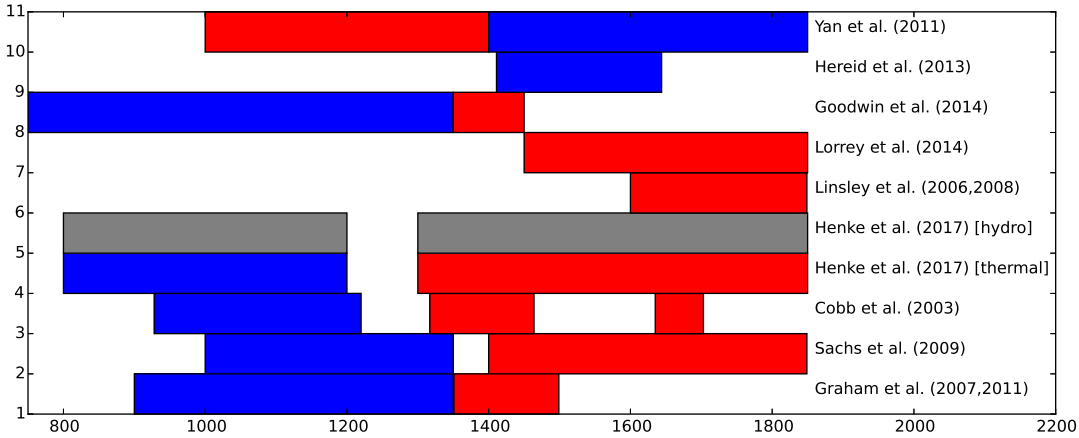

Figure 2.1: Summary schematic of reviewed literature. ENSO interpretation for intervals of the past millennium as El Niño (red), La Niña (blue), or equivocal (grey) for the cited literature. The position on the y-axis does not denote the amplitude of ENSO phase.

2.2 Experimental Design & Data

2.2.1 Using Climate Model Output as a Null Hypothesis

Estimates of the simulated mean climates were determined for the MCA (1000-1250 C.E.), LIA (1600-1850 C.E.) and the Present Day (1850-2005 CE) (Figures 2.2,2.3). The Coupled Modelling Intercomparison Project 5 / Paleoclimate Modelling Intercomparison Project 3 (CMIP5/PMIP3) is a suite of climate model simulations of the past 1,000 years driven with realistic external solar, volcanic, land use, and greenhouse gas radiative forcings (*Braconnot et al.*, 2012; *Taylor et al.*, 2012). This study used the "past1000" experiment and sea surface temperature (SST, denoted "tos" in the CMIP5/PMIP3 archive) and sea surface salinity (SSS, denoted "sos") variables and estimated the mean climate and the multi-model average interannual variation (Figures 2.2,2.3). Four models were used: CCSM4, GISS, MPI, and HadCM3.

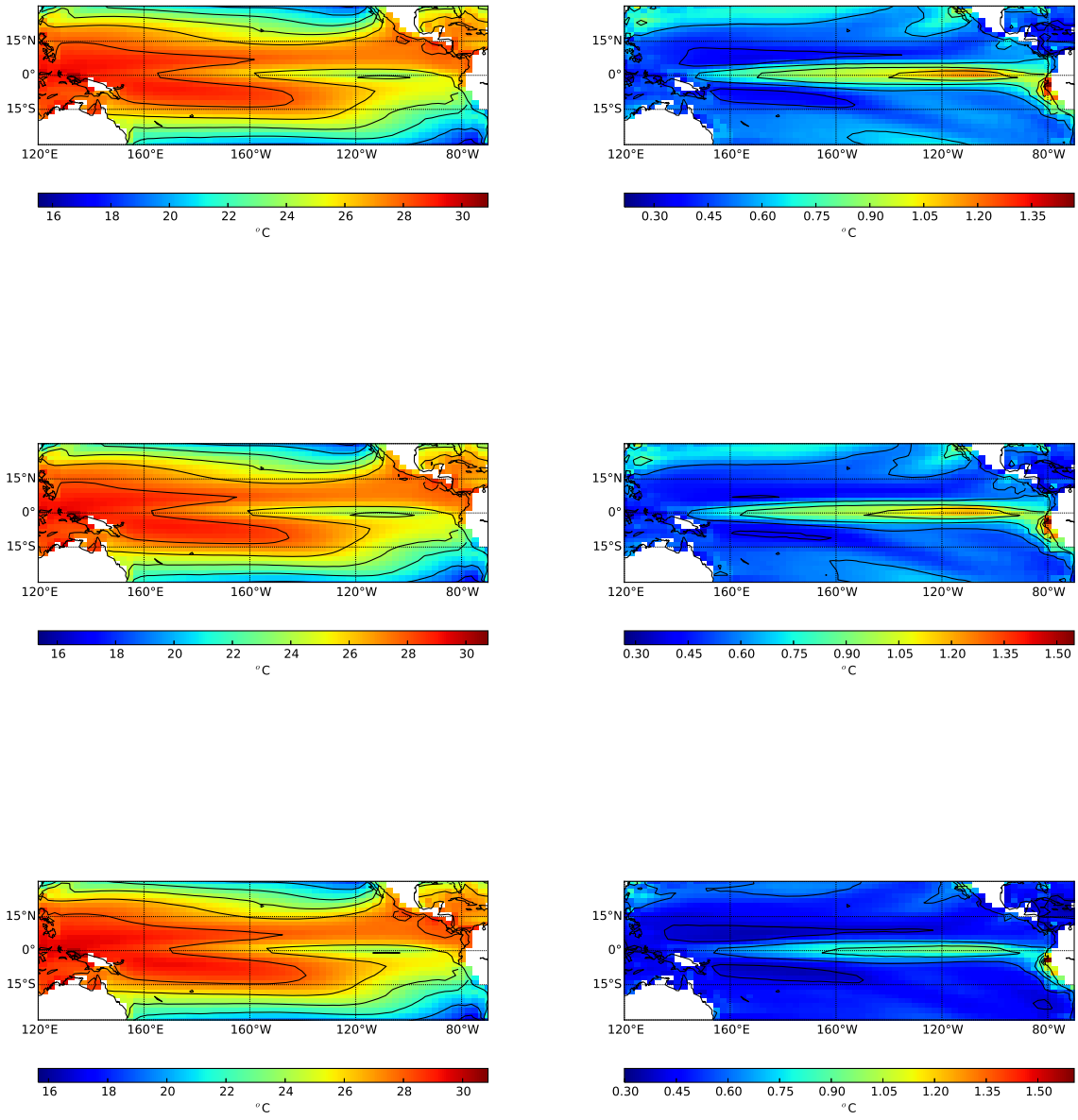

Figure 2.2: Multi-model composite of mean surface temperature (left column) and multi-model average standard deviation (right column) for the MCA (first row), LIA (second row), and 20th century (third row) time periods

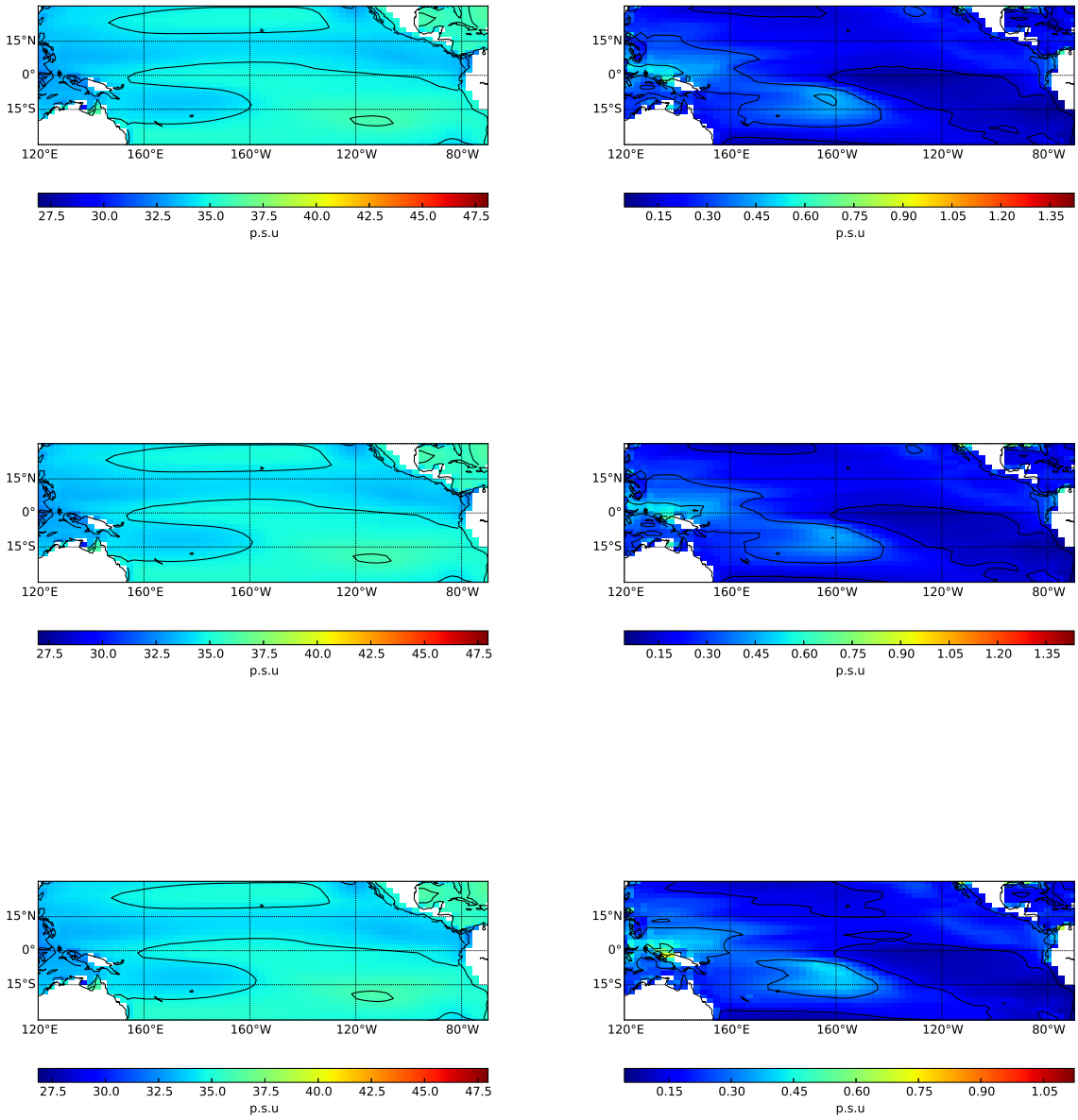

Figure 2.3: Multi-model composite of mean surface salinity (left column) and standard deviation (right column) for the MCA (first row), LIA (second row), and 20th century (third row) time periods

2.2.2 Paleoclimate Observations and Proxy System Modelling

Paleoclimate data are not direct observations of climatological variables such as temperature or salinity (Figures 2.2,2.3). But, these quantities can be inferred from measurements made on an archive, such as a coral or tree (*Evans et al.*, 2013). Climate variables may also be used as inputs in a mechanistic proxy system model (*Evans et al.*, 2013) to compare actual and simulated paleoclimate observations (*Dee et al.*, 2015; *Evans et al.*, 2013; *Phipps et al.*, 2013; *Thompson et al.*, 2011).

The strength of the forward modelling approach is that the climate variable (temperature, for example) does not have to be inferred through inversion of a linear regression (*Cook and Evans*, 1999; *Mann et al.*, 2009; *Smerdon*, 2012), and the experiment does not have to assume stationarity of this regression over time, which some research has now called into question (*Phipps et al.*, 2013), but this approach does assume stationarity of the proxy system model over time. Paleoclimate observations may be directly compared to paleoclimate simulations through a large-scale comparison using the principal components of variation in the paleoclimate observations and simulations, masking for locations where paleoclimate observations do not exist *Evans et al.* (1999); *Li et al.* (2011, 2013). A comparison between the full-field and sparse-field results can be used to assess how the observational network itself may bias the results (*Smerdon*, 2012; *Smerdon et al.*, 2011; *Wang et al.*, 2014), and to determine which locations are best suited for recording changes in ENSO amplitude and frequency.

2.2.3 Observational Data

Precisely-dated and highly-resolved paleoclimate observations from locations sensitive to significant variations in basin-scale tropical Pacific variability (as described previously) were obtained from the U.S. National Climatic Data Center for Paleoclimatology for this study. Based on the chosen criteria, the available data for this synthesis yielded 7 records of many temporal resolutions – 1 coral sensor, 1 ocean core sensor, 4 lake sensors, and 1 ice core sensor. The relaxed selection criteria yielded 16 records, whose data covers the LIA and 20th century but not the MCA. Of the 16 records, most are ocean-based (10, of which 9 are coral sensors), and are located predominantly in the western Pacific (9), with some records in the central (3) and eastern (4) tropical Pacific. There are 4 northern and 12 southern hemisphere records, but 9 are within 15 degrees of the equator. The authors for 5 (4) of the data sources describe the environmental forcing as sea surface temperature (salinity/rainfall) only. 7 records are described in the literature as a combined temperature/salinity environmental forcing. Individual records and their metadata are summarized in Table 2.1.

ENSO-Sensitive Paleoclimate Metadata

Lat, Lon	Location	Time	Observation	Sensor	Archive	Environmental Forcing	Reference
22^{o}S, 166^{o}E	New Caledonia	1657-1992	δ^{18}O	coral	colony	SST	Quinn et al. (1998)
11^{o}S, 153^{o}E	Papua New Guinea	1411-1644	δ^{18}O, Sr/Ca	coral	colony	SST, SSS	Hereid et al. (2013)
25^{o}S, 166^{o}E	New Caledonia	1650-2000	Sr/Ca	coral	colony	SST	DeLong et al. (2012)
4^{o}S, 119^{o}E	Makassar Strait	250BCE-2000	δ^{18}O, Mg/Ca	oceans	sediments	SST, SSS	Oppo et al. (2009)
18^{o}S, 146^{o}E	Great Barrier Reef	1612-1985	luminescence	coral	colony	rainfall	Hendy et al. (2003)
18^{o}S, 146^{o}E	Great Barrier Reef	1565-20th c.	δ^{18}O, Sr/Ca	coral	colony	SST, SSS	Hendy et al. (2002)
22-3^{o}S, 152-3^{o}E	Great Barrier Reef	1635 - 1989	δ^{18}O, δ^{13}C	coral	colony	SST, SSS	Druffel & Griffin (1993; 1999)

16^{o}S, 179^{o}E	Fiji	1620-20th c.	δ^{18}O, Sr/Ca	coral	colony	SST, SSS	Linsley et al. (2006)
6^{o}N, 162^{o}W	Palymyra island	930-2000*	δ^{18}O	coral	colony	SST, rainfall	Cobb et al. (2003)
4^{o}N, 160^{o}W	Washington island	800-2000		lake	sediments	SSS, rainfall	Sachs et al. (2009)
7^{o}N, 134^{o}E	Mecherchar island	1500-2000		lake	sediments	SSS, rainfall	Sachs et al. (2009)
1^{o}S, 90^{o}W	El Junco Lake	7000BCE-2000	grain size	lake	sediments	SST	Conroy et al. (2008)
1^{o}S, 90^{o}W	El Junco Lake	730-2000	diatom ratio	lake	sediments	SST	Conroy et al. (2009)
1^{o}S, 92^{o}W	Galápagos	1600-1992	δ^{18}O	coral	colony	SST	Dunbar (1994)
13^{o}S, 70^{o}W	Quelccaya ice cap	200 - 2000	δ^{18}O	ice sheet	ice core	SST, rainfall	Thompson et al. (2013)
16^{o}N, 112^{o}E	Dongdao island	1000-2000	grain size	lake	sediments	rainfall	Yan et al. (2011b)

Table 2.1: SST = sea surface temperature, SSS = sea surface salinity. Time is reported in C.E. (i.e., A.D.). Isotopic measurements are reported in permil (‰), geochemical analyses are reported in concentrations. An asterisk (*) notes a discontinuous record. See "Methods" for the criteria used to select records. Paleoclimate metadata are organized according to the proxy system model convention (*Evans et al.*, 2013).

2.2.4 Synthesizing ENSO-Sensitive Paleoclimate Observations

To develop a simple, quantitative estimate of climate variability during the MCA and LIA relative to the Present Day, the statistical variance in the paleoclimate observations records was computed for the MCA and LIA relative to the variance in the same timeseries of the 20th century. Records were selected according to the following criteria:

1. Some records chosen were discontinuous, but records have data from the MCA ($\sim$900-1300 C.E.), the LIA ($\sim$1300-1850 C.E.), and the 20th century ($\sim$1850-present) for a present day modern reference for the paleoclimate observations. This criterion is a compromise between the length of records required to observe changes in ENSO amplitude and frequency (*Russon et al.*, 2014, 2015; *Wittenberg*, 2009), and the available paleoclimate observations within these time periods. Many other studies (*Henke et al.*, 2015; *Mann et al.*, 2009) have used all available paleoclimate observations, but this experiment sought to eliminate the influence of the number of available records on the result at the expense of having even fewer available records (*Evans et al.*, 2002). The potential effect of a limited observational network impacting the results was explicitly tested through a comparison of the sparse field to the full field model-derived results.

2. Chosen records are located in the tropical Pacific basin (110^oE-70^oW, 35^oN-35^oS), where ENSO events originate, evolve, mature, and decay often in phase with the annual cycle (*Clarke*, 2014; *Philander*, 1990). Some previous studies (*Cook et al.*, 2004; *Li et al.*, 2011, 2013; *Mann et al.*, 2009) have used networks of records outside the tropics and have undertaken extensive calibration and validation exercises

to better understand the teleconnection between ENSO and remote, mid-latitude locations. In this experiment, tropical locations are used and the results are compared to some of the previous ENSO reconstructions whose data are independent from this synthesis.

3. Chosen records are sensitive to ENSO amplitude or frequency changes. Here, we rely upon validated local or remote calibrations and mechanistic studies completed by the original references in the peer-reviewed literature to assess the skill of the record in reconstructing ENSO behavior.

Records from different places with different units of measurement, proxy system models, chronological resolution, and uncertainty estimates are difficult to objectively synthesize together (*McGregor et al.*, 2015). In order to produce composited variance estimates for the MCA and LIA relative to the present day, the data was processed as follows:

1. Records were binned into a high resolution group (at least annually resolved) and a low resolution group (of the same temporal resolution were composited together, yielding a high resolution ensemble of records (annual) and a low resolution ensemble (interannual-decadal).

2. Variance from each observations for each of the three temporal bins was calculated. Past variance in the MCA and LIA were normalized relative to 20th century variance. Each unique observations is assumed to represent an independent estimate of the true variance of ENSO. Box-and-whisker plots were constructed to assess the distribution of variance across the ensemble of records.

2.2.5 Frequency analysis

In order to better understand the frequency of tropical Pacific interannual variability from a small set of observations, the interannual timeseries from Figures 2.2 & 2.3 were binned according to their amplitude into one of three terciles: warm, neutral, and cold phase events after separately subtracting the mean from the timeseries for each period and model simulation. This event frequency analysis for the CMIP5/PMIP3 simulations can serve as a frequency null hypothesis to compare to paleoclimate observations. The same analysis was repeated for the paleoclimate observations.

2.3 Results

The event frequency analysis for SST, SSS, and δ^{18}O shows approximately the same number of median events across variables and time period but differences across ENSO phase (Figure 2.4). With the exception of cold phase synthetic δ^{18}O the present day results show more variability in event counts than the MCA and LIA periods. Comparing phases shows the most number of events are neutral phase (36-8) followed by warm (32-4) and cold (28-32) phase (Figure 2.4). The event frequency analysis also indicates the median (red line of each boxplot) is often not a good indicator of the central tendency of the samples (n=5, four models listed previously in addition to MIROC).

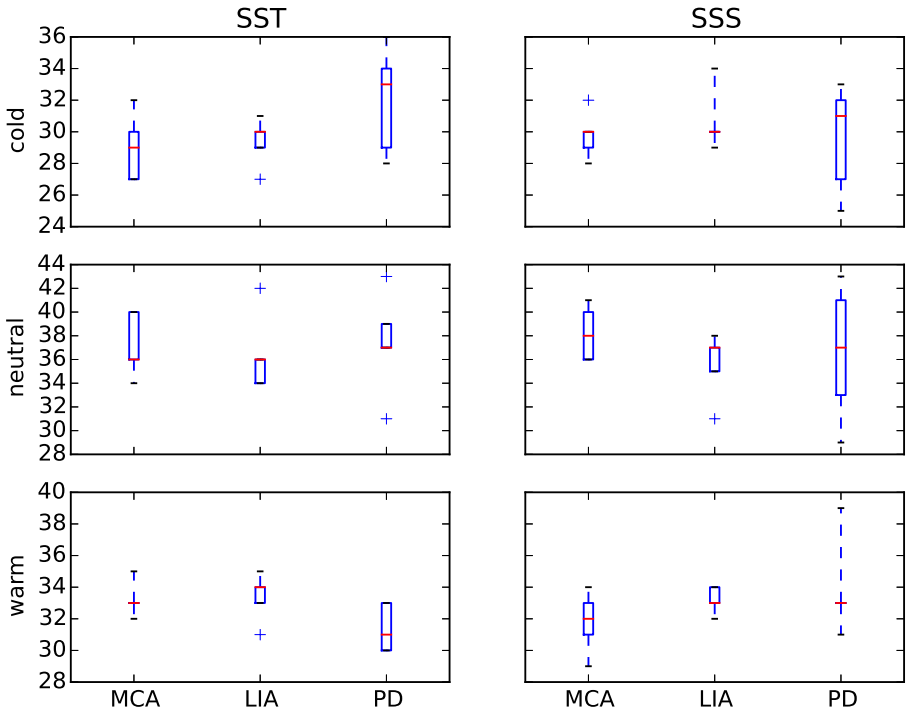

Figure 2.4: ENSO event counts. The number of 20^{o}N-20^{o}S, April-March averages of climatological SST and SSS anomalies (columns left to right) that fall below (between, above) the 33rd (33rd-66th, 67th) percentiles (rows top to bottom) for 850-2000 CE, for the Medieval Climate Anomaly (MCA, 1000-1250), Little Ice Age (LIA, 1600-1850) and the Present Day (PD, 1850-2000). Original data from CMIP5/PMIP3 participating models described in the Methods. Below 33rd (between 33rd and 66th, above 67th) percentiles interpreted as cold, (neutral, warm phase) conditions, respectively. Data series have been filtered with an 11-year smoother to focus on interannual variations. After *Duke* (2015).

2.3.1 CMIP5/PMIP3 SST, SSS variance

For mean sea surface temperature, all models show an expected temperature gradient from the tropics to the poles with the greatest values in the western tropical Pacific

as well as a east-to-west spatial pattern of high SSTs corresponding to the Pacific's Intertropical and South Pacific Convergence Zones.

For the standard deviation of monthly SST anomalies, all models, to varying amplitudes, show eastern equatorial variability. This is expected given that the thermocline is usually near the surface allowing for the upwelling of cold water. During anomalous periods, warm phase ENSO events depress the thermocline when warm water travels eastward, resulting in unusually warm SSTs off the coast of South America, extending into the central equatorial Pacific.

For the mean sea surface salinity maps, model results show the lowest salinity values in the western tropical Pacific, which corresponds to the warmest SSTs. This large body of warm water generates cumulonimbus convection and strong vertical velocities, which generate substantial rainfall. A band of low salinity can be seen across the tropical Pacific north of the equator and a smaller low salinity band south of the equator, corresponding to the ITCZ and SPCZ, although some models clearly show a "double ITCZ" bias where the SPCZ extends parallel to the equator, rather than its observed diagonal pattern northwest to southeast.

For the standard deviation of monthly SSS anomalies, only some models, GISS and HadCM3 primarily, show a high salinity anomaly in the western Pacific. This pattern follows from the movement of warm water eastward during anomalous climate (i.e., ENSO warm phase events) which leads to a shift of the tropical convergence zones eastward and towards the equator and a zonal shift of the Pacific Walker Circulation.

2.3.2 Comparison of MCA-to-LIA observations

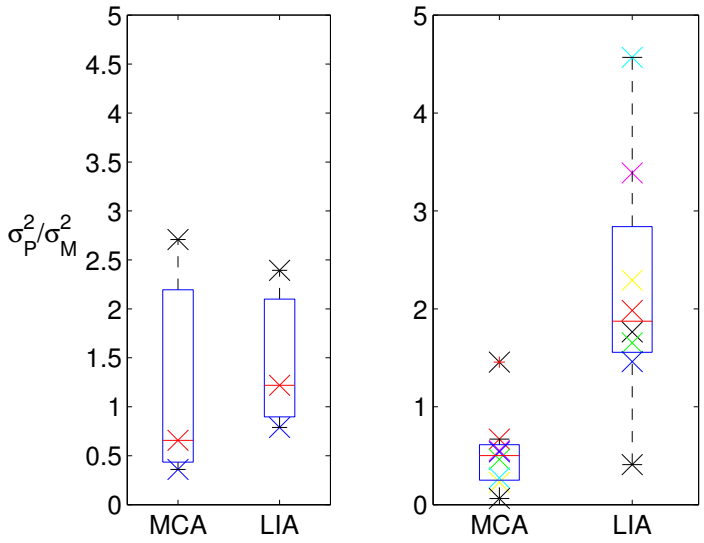

Figure 2.5: Variance changes from the "Medieval Climate Anomaly" (800-1300 C.E.) to the "Little Ice Age" (1300-1800 C.E.) (x-axis) relative to the 20th century for select proxy records of the past millennium. The y-axis shows the ratio of variance (past:present period) where a value of 1 is defined as equal variance between past and present. The high-resolution (annual) left panel uses records from *Cobb et al.* (2003a), *Thompson et al.* (2013b), and *Oppo et al.* (2009), while the lower resolution (decadal) right panel uses records from *Yan et al.* (2011a), *Conroy et al.* (2009), and *Conroy et al.* (2008).

The change in variance from the MCA to LIA, expressed as a ratio of past to present variance, using only the observations from the strict selection criteria, is shown to the left in Figure 2.5, and the results from the observations selected with more relaxed selection criteria are shown to the right in Figure 2.5. A variance ratio of 1 indicates no change in variance between the past and present period, whereas values higher or lower than 1

indicate increased or decreased variance in the past relative to the present period, respectively.

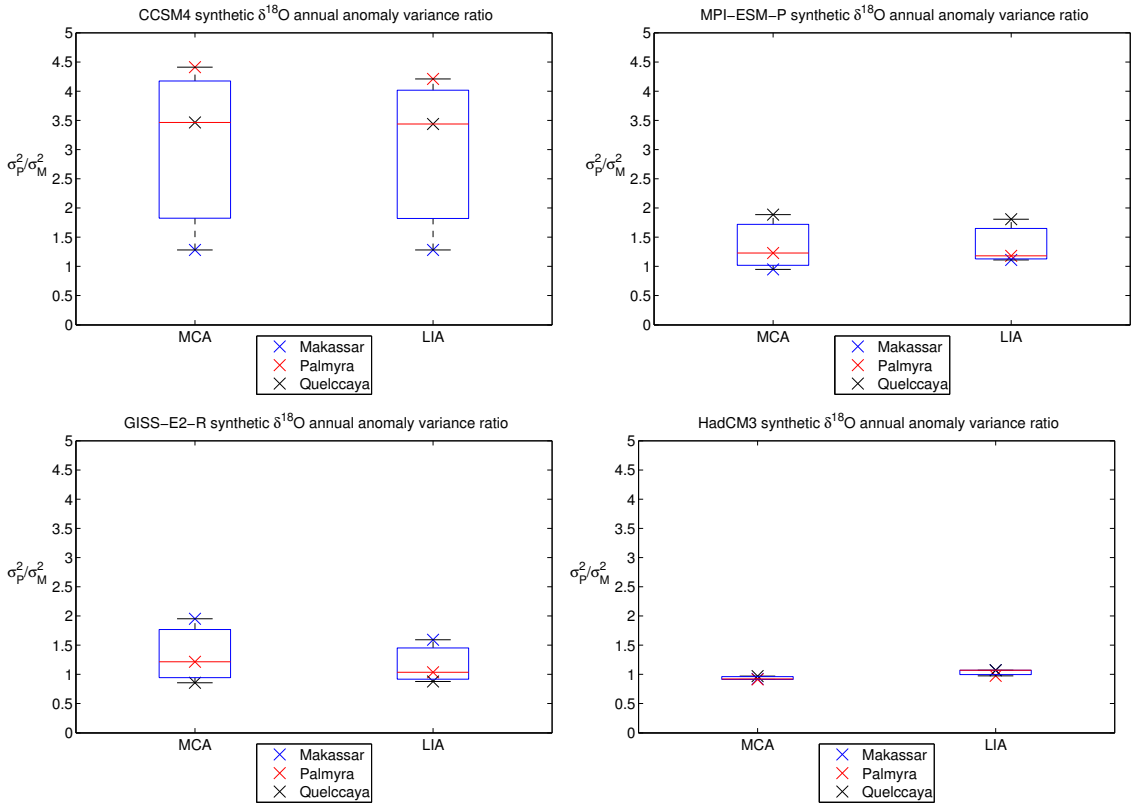

Figure 2.6: Same as Figure 2.5 but variance of high resolution (annual) synthetic δ^{18}O using the forward model approach with inputs of SST and SSS from CMIP5/PMIP3 participating models. Location-limited based on the available high-resolution observations. No low resolution result is shown here.

The same analysis that was done for the observations was also done for the four PMIP3/CMPI5 climate model simulations which had available sea surface temperature (termed "tos") and salinity (termed "sos") data for their "historical" and "past1000" experiments. The results, which are only based on model simulation results from locations where actual observations exist for the past millennium, are shown in Figure 2.6. The results for the full field model results are shown in Figure 2.10.

In order to determine how well the paleoclimate observations and model simulations capture ENSO behavior, the same analysis was done for the NINO3.4 region, where an indexed measure of sea surface temperature anomalies is used to indicate the phase and intensity of ENSO. Only two of the observations synthesized in this work are located within the NINO3.4 region. However, Figure 2.7 shows the model-derived variance ratio results for the MCA- and LIA-era relative to the 20th century using the NINO3.4 definition (5^{o}N-5^{o}S, 120^{o}W-170^{o}W) from *Trenberth* (1997).

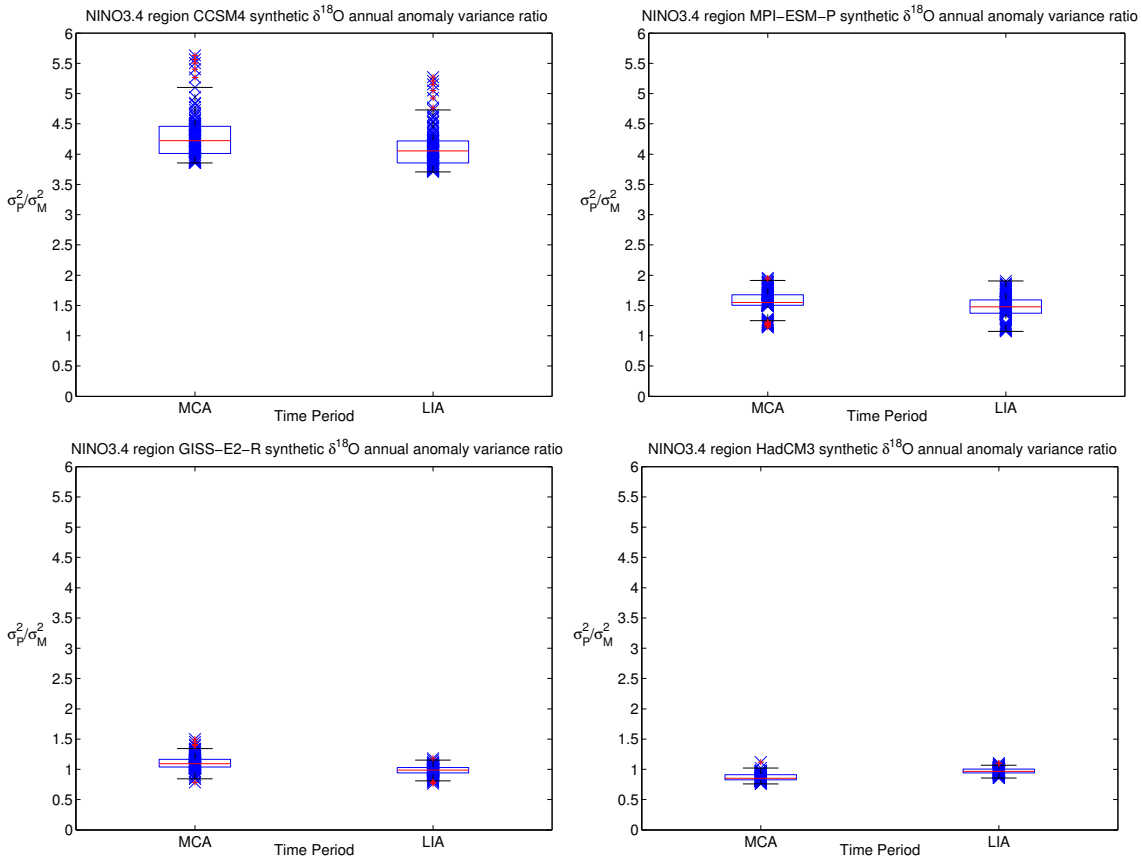

Figure 2.7: Same as Figure 2.10 but only for the NINO3.4 region (5^{o}N-5^{o}S, 120^{o}W-170^{o}W) (*Trenberth*, 1997).

In order to assess ENSO frequency and analyze a potential for event counts to change over time, anomalies of at least annually resolved data were binned into terciles

and assigned as cold, neutral, and warm phase events for the MCA, LIA, and PD time periods as done in Table 2.4. The number of events for each time period are shown in Figure 2.8.

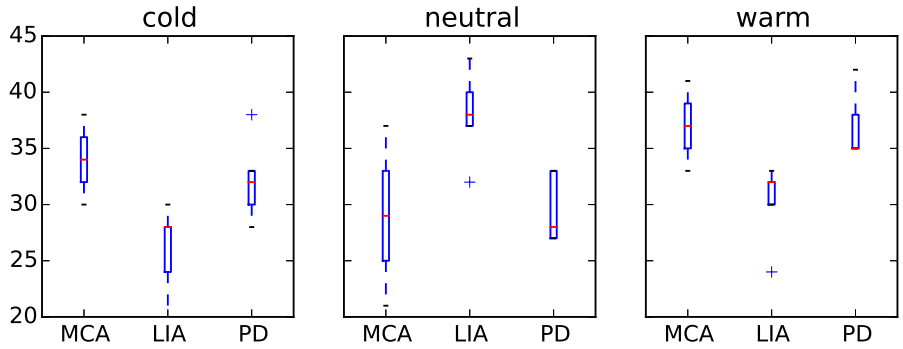

Figure 2.8: ENSO event counts from observations. The number of ENSO events from paleoclimate observations that fall below (between, above) the 33rd (33rd-66th, 67th) percentiles of the corresponding data series (*Cobb et al.*, 2003a; *DeLong et al.*, 2012; *Druffel and Griffin*, 1999; *Dunbar et al.*, 1994; *Thompson et al.*, 2013b) for 850-2000 CE, for the Medieval Climate Anomaly (MCA), Little Ice Age (LIA) and Present Day (PD). Below 33rd (between 33rd and 66th, above 67th) percentiles interpreted as cold, (neutral, warm phase) conditions, respectively. Results for δ^{18}O above 33rd (between 33rd and 66th, below 67th) percentiles interpreted as cold, (neutral, warm phase) conditions, respectively. After *Duke* (2015).

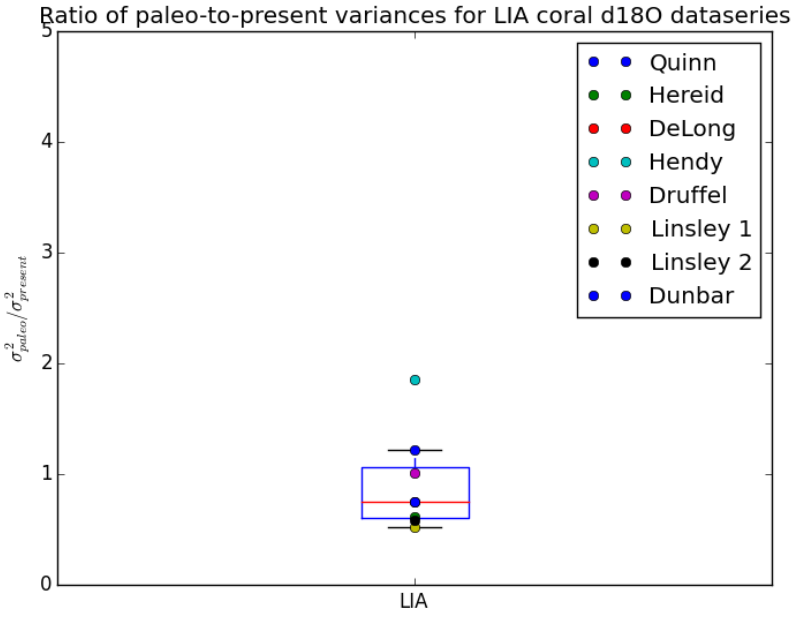

Figure 2.9: Same as Figure 2.5, but only the coral δ^{18}O dataseries of Table 2.1 are used here to calculate the ratio of variances. The *Cobb et al.* (2003a) coral δ^{18}O data is excluded here in order to have independent results to compare with that of Figure 2.5, which includes that data.

2.4 Discussion

The low number of available observations and model simulations used in these analyses prevents the use of statistical tests which rely on higher N values. Therefore, the results will be interpreted qualitatively instead of through quantitative statistical testing.

Model results have uncertainties arising from structural uncertainty associated with the simplified representation of earth system processes (*Collins et al.*, 2010; *Guilyardi et al.*, 2009), our limited understanding of the external radiative forcings to the system (*Schmidt et al.*, 2011, 2012), and the difficulty in separating forced and unforced variability in the climate system which can arise from the dynamics of the coupled ocean-

atmosphere system (*Ault et al.*, 2013; *Wittenberg*, 2009), and non-climatic systematic bias. But model simulations continue to better represent the climate system and simple robust metrics of model skill have been developed to determine which models best represent reality (*Bellenger et al.*, 2014; *Russon et al.*, 2014, 2015; *Schmidt et al.*, 2014).

Paleoclimate observations often have uncertain age models (*Comboul et al.*, 2014), simplified or parameterized proxy system models (*Dee et al.*, 2015; *Evans et al.*, 2013), tend to preferentially filter low frequency signals (*Emile-Geay et al.*, 2013a; *Evans et al.*, 2002), and have data in limited time periods and spatial locations with often few replicated results (*Comboul et al.*, 2015; *Jones et al.*, 2009; *Mann et al.*, 2009; *Neukom and Gergis*, 2011). Without having a perfect understanding of the ENSO phenomenon being studied, many records from a variety of locations can be used to develop coarse but robust estimates of variance with uncertainty measurements (as done in (*McGregor et al.*, 2015).

Despite the many sources of uncertainty in both observations and simulations, these sources are predominantly independent. Therefore, if data-model comparison results display consistency, the mechanisms responsible for the results could be better understood, within the uncertainty.

2.4.1 Observations

Results from Figure 2.5 are qualitatively similar to one another. The annually resolved records show the same variance ratio in the MCA and LIA, The additional coral δ^{18}O data selected with the more relaxed criteria (Figure 2.9) shows qualitatively similar variance from the LIA to the present (the median value is nearly 1, and the 25th and 75th percentiles are very close to 1).

Other literature showing a highly variable climate (*Cobb et al.*, 2013; *Emile-Geay et al.*, 2013b) and ENSO activity (*Li et al.*, 2011, 2013) over the past millennium suggests the mean tropical Pacific climate and ENSO may be insensitive to external radiative forcings (*DiNezio et al.*, 2009, 2013), and that variability may arise from unforced, internal variability of the climate system (*Otto-Bliesner et al.*, 2016).

Records with less than one sample per year show a small change from decreased variance in the MCA to increased variance in the LIA. The records used in this analysis come from the reconstructed Southern Oscillation Index of *Yan et al.* (2011a) using data from the western (*Oppo et al.*, 2009) and the eastern (*Conroy et al.*, 2009) Pacific, so it is not independent from the other plotted data. The low resolution records (*Conroy et al.*, 2009) all come from the Galapagos island in the eastern Pacific, making the available low frequency data locationally-constrained. With additional locations, the sampled variance for the time period may appear more similar to the MCA for this time resolution. The qualitative difference in variance between the MCA and LIA relative to the present day for the less than annually resolved records may also arise from lower frequency (decadal to multi-decadal) temporal variability, but the limited temporal coverage makes it difficult to further assess this possibility.

Only two records *Cobb et al.* (2003a); *Thompson et al.* (2013b) included MCA data, but the event count analysis (Figure 2.8) suggests the observations record approximately the same number of events compared to the PMIP3/CMIP5 forward model δ^{18}O event frequency analysis (Figure 2.4). Additional data which covers the LIA and Present Day show differences in the number of cold, neutral, and warm phase events in the LIA relative to the present day (Figure 2.8). The results also show a decrease in the number of cold

and warm phase events in the LIA relative to the MCA, with a consequent increase in neutral phase events. However, this result suffers from a lack of observations with annual resolution in the period of interest (n=2 in MCA). One large outlier in the LIA data for the neutral and warm phase categories could skew these interpretations, given the low number of observations (n=5 for LIA, PD periods)

2.4.2 Comparison of paleoclimate observations to simulations

The paleoclimate observations are in modest qualitative agreement with the PMIP3 past1000 experiment simulations (Figure 2.5,2.6). Variance ratios from model simulation results location-limited to the Niño3.4 region do not show qualitative differences across the MCA and LIA with respect to present day variance estimates (Figure 2.7) and show similar ratios to the analysis limited to locations where observations are present (Figure 2.6).

In order to assess how only a few paleoclimate observations affect the results, the same analysis was done for the full-field of the tropical Pacific (i.e., at every grid point). Figure 2.10 shows that the CCSM4 model displays a large range of variability in variance during the MCA and LIA relative to the present day from 1.5 - 8.5. However, the MPI-ESM-P and HadCM3 models (50% of model simulations) show a slightly elevated variance in the past compared to present (ratio values of 1-1.5). The GISS-E2-R model shows slightly decreased variance in the MCA relative to present day – 0.5-1, while the LIA has approximately equal variance relative to present day (a ratio value of 1). Most models show higher median variance in the MCA and LIA relative to the present day, which is qualitatively similar to observations (Figure 2.6). Collectively, these two analy-

ses suggest the number of available locations to include does not significantly impact the results.

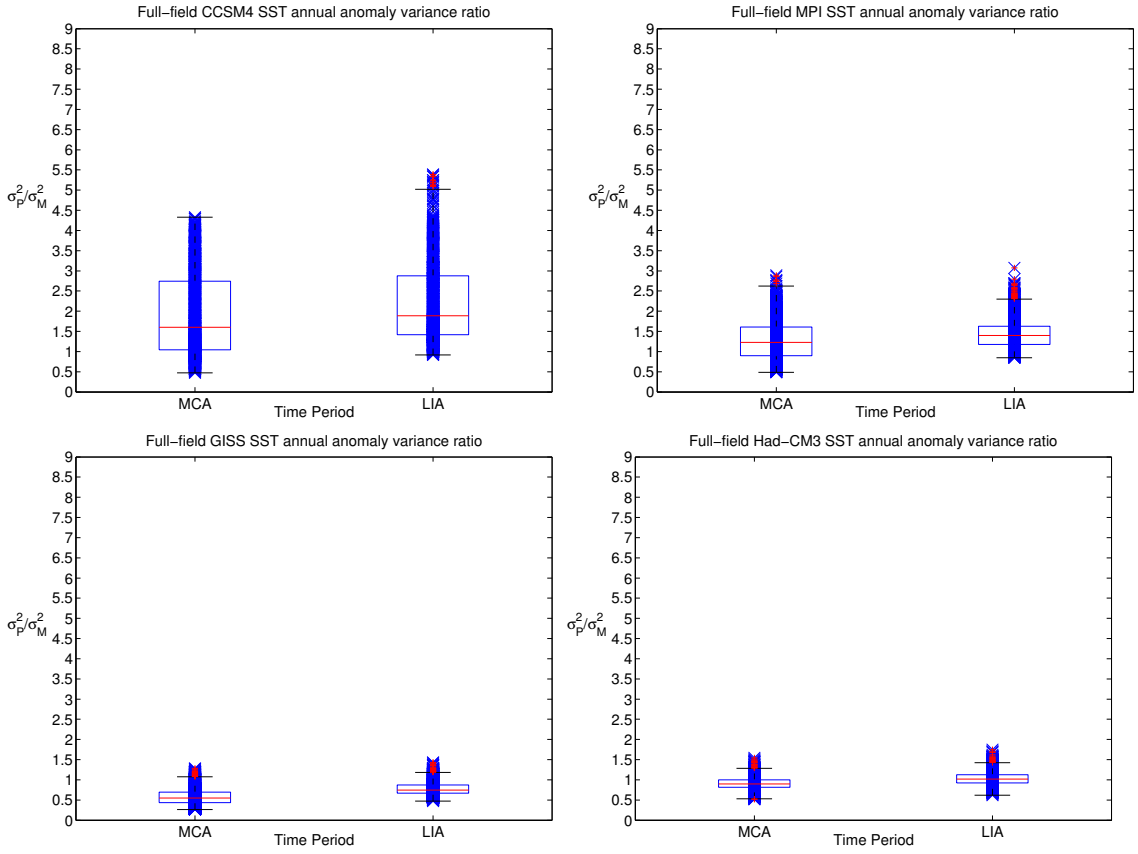

Figure 2.10: Same as Figure 2.6 but SST annual average anomaly data for the full tropical Pacific (35^{o}N-35^{o}S, 110^{o}E-70^{o}W) spatial field. Here each data point is a ratio of grid cells at different time windows.

The effect of an incorrect age model was tested by changing the time periods of the MCA to 800-1300 CE and the LIA to 1300-1800 CE. The results (not shown) did not differ from the earlier-used definitions. The proxy system models do have their own sets of uncertainties; however, they do avoid the issues of which can impact other regression-based reconstruction methods (*Dee et al.*, 2015; *Evans et al.*, 2013; *Thompson et al.*, 2011). The data for this study was annually resolved and used to look at interannual

anomalies, limiting the filtering effect.

2.4.3 Forced & unforced ENSO over the last millennium

The qualitative agreement between model simulations and the limited number of paleoclimate observations available for this experiment suggest that ENSO (being the dominant driver of tropical Pacific interannual variability) is not particularly sensitive to external radiative forcings. External radiative forcings for the present day are dominated by anthropogenic increases in greenhouse gas concentrations in the atmosphere (*IPCC Working Group 1 et al.*, 2013), yet Figures 2.6 and 2.10 show the past time periods have larger variance (the only exception being the GISS-E2-R full-field). These results suggest the response of interannual climate variability to external radiative forcing over the past millennium is small relative to the unforced, internal variability. The response could be small given the small magnitude of the external radiative forcings over the past millennium (*Schmidt et al.*, 2011, 2012). But some recent paleoclimate reconstructions suggest that the dominant external radiative forcings over the past millennium prior to the Present Day (1850-present) was increased volcanism in the LIA (*McGregor et al.*, 2015; *Tierney et al.*, 2015).

Rather than external radiatively-forced variability, dynamic (unforced) variability in the climate system that arises from the coupled dynamics of the ocean-atmosphere system (*Deser et al.*, 2010; *Fedorov and Philander*, 2000) may explain a large component of the observed interannual variability during intervals of the past millennium. *Emile-Geay et al.* (2013a,b) used two validated statistical methods to reconstruct central equatorial Pacific SST variability over the past millennium and found substantial interannual vari-

ability in the tropical Pacific climate system as well no evidence to support a systematic change in Nino 3.4 SST between the MCA and LIA time periods. *Otto-Bliesner et al.* (2016) conducted a last millennium experiment with the same model conditions except for small changes to the initial surface air temperature, and their results showed a range of interannual variability.

A second reason why ENSO does not seem to respond to external radiative forcings could be because the coupled ocean-atmosphere system has dynamical adjustments and feedbacks which limit the timing of ENSO phase (*Clarke*, 2014; *Collins et al.*, 2010; *Deser et al.*, 2010; *Guilyardi et al.*, 2009). The forcings for the CMIP5 20th-21st century results differ in magnitude to the past millennium forcings, so they may be able to be used to better understand how the forcings impact ENSO variability. However, 21st century simulations from CMIP5 participating models do not agree whether ENSO will become more warm phase-like, cold phase-like, or remain similar to modern conditions (*Collins et al.*, 2010; *Thompson et al.*, 2011). Increased GHG forcing increases sea surface temperatures across all CGCMs (*Collins et al.*, 2010). One result of this forcing could be a weakening of the trade winds, a flattening the equatorial thermocline, and a reduction in upwelling of cold, eastern Pacific water – this is the Bjerknes feedback (*Bjerknes*, 1969; *Ramesh and Murtugudde*, 2012). This mechanistic response is supported by some model results (*Vecchi et al.*, 2006; *Yeh et al.*, 2009), but another feature of this result is a shoaling of the thermocline depth because of decreased zonal trade winds relative to meridional circulation (*Yeh et al.*, 2009). A decrease in the thermocline depth suggests higher eastern Pacific SSTs. Thus, the ocean-atmosphere system employs its own dynamical adjustments in response to GHG forcing which make it difficult to assess whether ENSO will

have more El Niño or La Niña in the future. Significant decadal and centennial scale variability in ENSO is supported by observational studies over the past millennium (*Li et al.*, 2011, 2013) and further back into the Holocene (*Cobb et al.*, 2013).

Increased GHG forcing has also been suggested to cause differential rates of sea surface temperature increases (*Clement et al.*, 1996) resulting in an increasing SST asymmetry in the tropical Pacific. This ocean dynamical thermostat mechanism, as it is called, would result in increased trade winds, an intensification of zonal atmospheric circulation, increased upwelling, and potentially decreased ENSO warm phase activity. Some CMIP5-era model support this interpretation, but some also show a stronger Bjerknes feedback (*Bellenger et al.*, 2014; *Collins et al.*, 2010; *Phipps et al.*, 2013). Thus, 21st century climate model simulations with strong GHG forcing are equivocal.

In order to move forward, replicated, composited, and precisely-dated paleoclimate observations and careful comparisons between records from different locations in the tropical Pacific are needed, both in the early millennium as well as the modern era (*Emile-Geay et al.*, 2013b) to better understand interannual climate variability and decadal to centennial variability in particular. Observational coverage of the Southern Hemisphere remains poor, and global or hemispheric composites or reconstructions of climate field variables in strategically targeted locations could benefit from additional records.

Attribution of specific climate mechanisms responsible for the observed climate can be determined by choosing the climate simulations of the past millennium most consistent with the paleoclimate observations (*Braconnot et al.*, 2012; *Schmidt*, 2010; *Schmidt et al.*, 2014; *Smerdon et al.*, 2017). However, there is still debate in the literature about how to quantitatively and consistently do this (*Phipps et al.*, 2013; *Smerdon et al.*, 2017).

Furthermore, an open area of research that should continue is developing methods to rank model outputs (*Bellenger et al.*, 2014) based on their consistency and accuracy to actual observations, and to develop techniques that are better suited for hydrological reconstructions (*Smerdon et al.*, 2017).

2.5 Conclusions

In order to better understand tropical Pacific interannual variability, a new synthesis of existing paleoclimate observations was completed and compared to climate model output over intervals of the past millennium. Restricting the synthesis to annually-resolved observations with data in the MCA, LIA, and present day with at least 100 years in the tropical Pacific resulted in a small number of paleoclimate observations available for the synthesis. Analysis of interannual variance ratio results suggested no qualitative difference between interannual variance in the climate of the MCA and LIA relative to the present day. Analysis of additional observations with less than annually resolved resolution showed a small qualitative increase in variance during the LIA relative to the MCA with respect to present day variance measurements. The number of ENSO events per 100 years was not qualitatively different between the MCA, LIA, and present day.

These observations were also compared to CMIP5/PMIP3 model simulation results of sea surface temperature and salinity. Results from the Niño 3.4 region as well as the full-field, showed no difference in interannual variance of MCA and LIA climate relative to the present day. Interestingly, the CCSM4 model was the only one which showed a higher ratio of variances in the observation-limited, Niño 3.4 region, and full-field cases. Comparison of the paleoclimate observations and simulations showed qualitative agree-

ment and was insensitive to changing the boundaries of the time periods studied. Results suggest that ENSO activity may not be particularly sensitive to external radiative forcings over the past millennium. The impact of unforced, internal variability on the coupled ocean-atmosphere climate system may be large relative to the magnitude of external radiative forcings.

Chapter 3: Detecting ENSO from modern southern Cook Island corals

3.1 Introduction

The El Niño-Southern Oscillation (ENSO) is a coupled ocean-atmosphere phenomenon of the climate system that originates in the tropical Pacific and impacts global climate (*Clarke*, 2014). ENSO showed significant variations in amplitude between events (*Capotondi et al.*, 2015) and differences in the incidence of eastern versus central Pacific events (*Ashok et al.*, 2007; *Yeh et al.*, 2009) in the 20th century. The most recent synthesis of climate change literature suggests ENSO will continue to cause dramatic interannual variations in Earth's climate in the 21st century (*IPCC Working Group 1 et al.*, 2013).

Despite ENSO's importance, uncertainty remains in how its amplitude and spatial pattern will change in the 21st century. Model simulations using a range of external radiative forcings scenarios (*Braconnot et al.*, 2012; *Taylor et al.*, 2012) disagree on whether ENSO, under the influence of anthropogenic climate change, will transition to a La Niña (cold phase) state via the ocean dynamical thermostat (*Clement et al.*, 1996; *DiNezio et al.*, 2013), or to a more El Niño (warm phase) state driven by a weakened Walker Circulation (*L'Heureux et al.*, 2013; *Vecchi*, 2008; *Vecchi et al.*, 2006), or not experience any significant change from present conditions (*Bellenger et al.*, 2014; *Collins et al.*, 2010; *Guilyardi et al.*, 2009). The few tropical paleoclimate data available before the 19th cen-

tury (*McGregor et al.*, 2015; *Tierney et al.*, 2015) make it difficult to assess how ENSO varied over the past millennium (Chapter 2).

Observations of past climate, or paleoclimatology, provide a means to study ENSO variability over a time range greater than that of the instrumental era (*Cobb et al.*, 2003a) and under different external radiative forcings (*Braconnot et al.*, 2012; *Schmidt*, 2010). Paleoclimate observations have contributed towards improving the scientific understanding of low frequency modes of climate variability, such as ENSO (*Evans et al.*, 1999), and the Interdecadal Pacific Oscillation (*Linsley et al.*, 2008). However, in order to best understand the amplitude, frequency, and spatial pattern of these modes of climate variability, hundreds of years of data are required (*Wittenberg*, 2009). Yet few high-resolution, tropical paleoclimate data are available before the "Little Ice Age" (1400 - 1800 C.E.) (*Smerdon et al.*, 2017; *Tierney et al.*, 2015). Paleoclimate data can also be used to test which climate model simulations of past climate have the most agreement with the observations (*Braconnot et al.*, 2012; *Smerdon et al.*, 2017). These experiments may increase our confidence in the forecasts of future climate provided by these models.

Many publications in the literature thus far have focused on clear and easily detectable changes in air or sea surface temperature variability (*McGregor et al.*, 2015; *Tierney et al.*, 2015). However, hydrological variability also has significant impacts to the climate system, leading to more research in this field (*Smerdon et al.*, 2017). This study aims to contribute to the emerging literature of hydroclimatological variability, specifically in the southwestern tropical Pacific. In this region, hydrological change results primarily from changes in the position and strength of the South Pacific Convergence Zone (SPCZ) (*Delcroix et al.*, 2011; *Gouriou and Delcroix*, 2002; *Vincent*, 1994). In-

terannual variations in SPCZ position and strength are associated with El Niño-Southern Oscillations (ENSO) warm and cold phase activity because of changes in zonal and meridional atmospheric circulation (*Folland et al.*, 2002; *Lorrey et al.*, 2012; *Philander*, 1990; *Salinger et al.*, 1995; *Widlansky et al.*, 2012) and the anomalous advection of tropical oceanic currents (*Gouriou and Delcroix*, 2002; *Hasson et al.*, 2013; *Picaut et al.*, 1996).

The emerging literature of southwestern tropical Pacific hydroclimate (*Brown et al.*, 2012a; *Power et al.*, 2013; *Widlansky et al.*, 2012) has not yet definitively answered how the SPCZ will change in response to 21st century external radiative forcings (*IPCC Working Group 1 et al.*, 2013). Therefore, increased observations in time and space would improve our understanding of the SPCZ and its potential drivers of change, particularly ENSO by providing additional realizations of events. Observations from different locations, when combined together into a network, may improve our characterizations of large regional modes of climate variability, such as ENSO (*Comboul et al.*, 2015; *Evans et al.*, 1999, 2002).

Detecting an ENSO-related hydroclimatological signal may be accomplished by calculating $\delta^{18}O_{SW}$ using coral paleoclimatology techniques (*Cobb et al.*, 2003a; *Hereid et al.*, 2013; *Kilbourne et al.*, 2004; *Linsley et al.*, 2006). Paired coral $\delta^{18}O$ and Sr/Ca observations may be used to record sea surface temperature (*Lough and Barnes*, 2000; *Weber and Woodhead*, 1972) and $\delta^{18}O_{SW}$ variations (*Ren et al.*, 2002) over time in the tropical Pacific via geochemical measurements made on their aragonite skeleton (*Dunbar and Cole*, 1996). Variations in the oxygen isotope composition ($\delta^{18}O$) of coral material are approximately linearly dependent on the calcification temperature and the oxygen isotope composition of seawater (*Dee et al.*, 2015; *Epstein et al.*, 1951; *Evans et al.*, 2013;

Thompson et al., 2011). We approximate the calcification temperature with the sea surface temperature (*Stevenson et al.*, 2013) where the corals grow throughout the year (*Knutson et al.*, 1972). In the southwest tropical Pacific, seawater δ^{18}O is affected primarily by the precipitation-evaporation-advection balance of the surface water determined primarily by the position and strength of the South Pacific Convergence Zone (*Delcroix et al.*, 2011; *Folland et al.*, 2002; *Salinger et al.*, 2001). We approximate seawater δ^{18}O using sea surface salinity measurements (*Thompson et al.*, 2011). But, the δ^{18}O/SSS slope used is not site-specific but rather a best estimate for the south Pacific region in general (*Conroy et al.*, 2017; *LeGrande and Schmidt*, 2006; *Stevenson et al.*, 2013; *Thompson et al.*, 2013a). Therefore, we test this approximation by using paired Sr/Ca data to help resolve coral $\delta^{18}O_{SW}$ directly, given observational uncertainty. The Sr/Ca measurements of coral do not vary with seawater δ^{18}O, but are related linearly to temperature (*Corrége*, 2006; *DeLong et al.*, 2007b; *Shen et al.*, 1996). Therefore, these two measurements together may be used to distinguish the SST contribution from the seawater δ^{18}O contribution (Figure 3.2) in the coral δ^{18}O measurement (*Beck et al.*, 1992; *Evans et al.*, 2013; *McCulloch et al.*, 1994). We may then interpret the differences in these data as an estimate of seawater δ^{18}O plus uncertainty to better understand the precipitation-evaporation-advection balance, the SPCZ, and ENSO.

A critical step in the use of paleoclimate data is to develop an unambiguous interpretation of the climate signal within the data. A common approach in the paleoclimatology literature is to use a portion of the data in a calibration analysis in order to determine the relationship between the paleoclimate data and the climate variable (*Cook et al.*, 2004; *Mann et al.*, 2009). Then, this calibration is tested through a validation exercise with

independent data (*Emile-Geay et al.*, 2013a; *Jones et al.*, 2009). Here, we use modern paleoclimate data from corals and compare those results to direct observations of climate using a coral forward modeling approach (*Evans et al.*, 2013; *Phipps et al.*, 2013; *Thompson et al.*, 2011) to develop an interpretation.

Aitutaki, located in the southern Cook Islands group, was selected as a field site given its suitability for measuring ENSO activity (Figure 3.1). Located in the southwestern tropical Pacific, Aitutaki is at the mean position of the SPCZ (*Stoddart and Gibbs*, 1975; *Thompson*, 1986). During ENSO warm phase (El Niño) events, the SPCZ band shifts northeastward towards the equator, which would suggest higher sea surface salinity at Aitutaki and a increased δ^{18}O value. Conversely, during ENSO cold phase (La Niña) events, the SPCZ band shifts southwestward away from the equator, resulting in decreased SSS at Aitutaki and decreased δ^{18}O values (*Delcroix et al.*, 2011; *Folland et al.*, 2002). Figure 3.1 also highlights how the regional hydroclimatological impact of the SPCZ results in large (small) interannual SSS (SST) measurements (*Linsley et al.*, 2006).

A strong and significant spatial correlation of the sea surface salinity (SSS) field with the NINO 3.4 and Southern Oscillation Index, two common metrics of ENSO, suggests that ENSO-related variability may be detectable in the δ^{18}O signal at Aitutaki (Figure 3.2). The nearby island of Rarotonga from which there is already existing coral δ^{18}O and Sr/Ca observations from 1727 CE to the modern era suggests this location may be sensitive to variations in the position of the SPCZ (*Linsley et al.*, 2006). Therefore, we hypothesize that a composited interannual δ^{18}O timeseries from new Aitutaki corals and existing Rarotonga corals (*Linsley et al.*, 2006) will record changes in the position of the SPCZ brought about by ENSO variability.

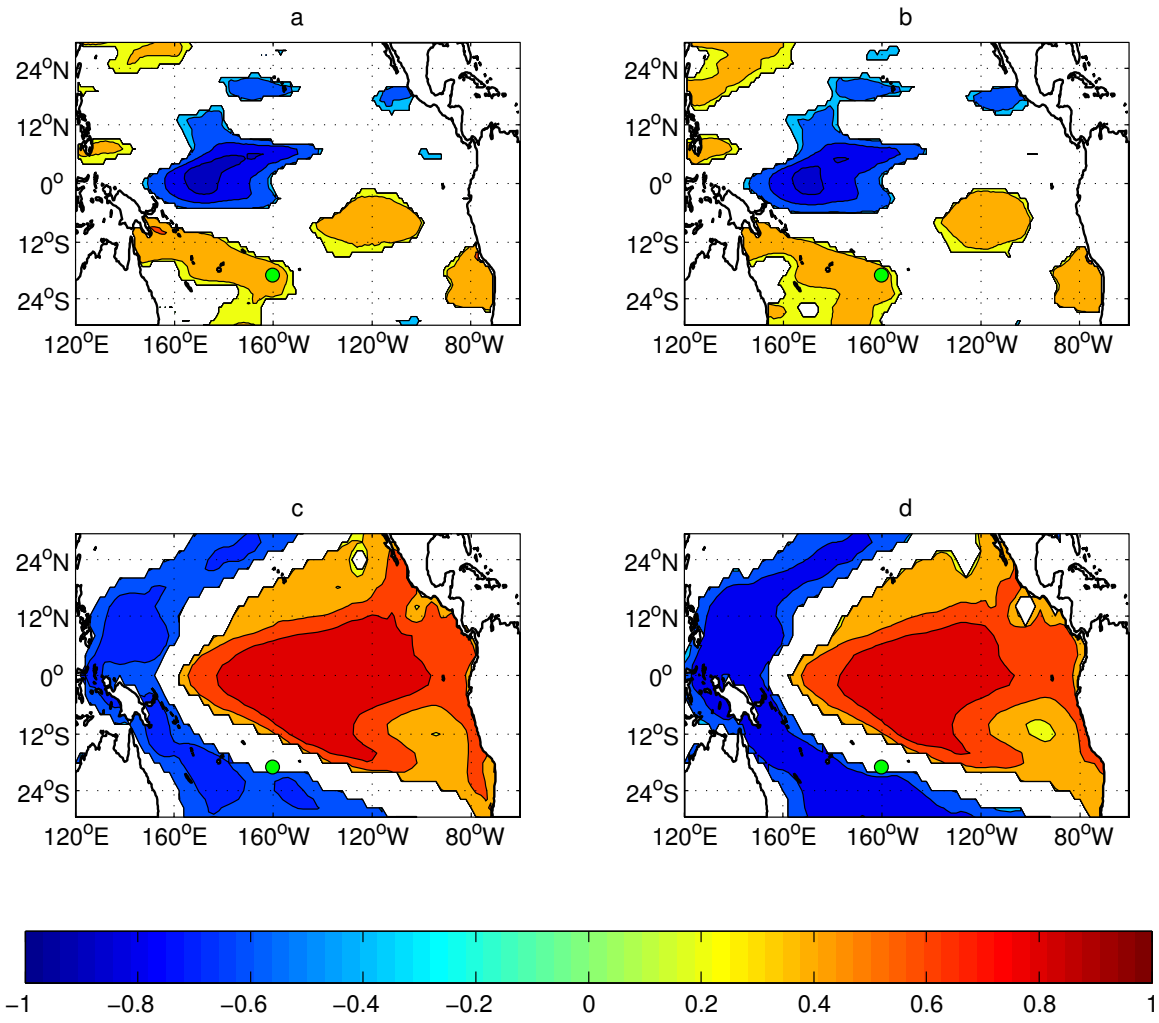

Figure 3.1: a.) correlation of the NINO 3.4 monthly SST anomaly ((*NOAA*, 2018a)) with monthly SSS anomaly field, 1975-2009 (df=34, $p<0.05$) (*Delcroix et al.*, 2011). Location of Aitutaki is indicated with a green filled circle, and correlations with $p>0.05$ have been masked. b.) as in a., but NINO 3.4 is correlated with the monthly SOI anomaly multiplied by -1 for comparison to a. ((*NOAA*, 2018b)). c.) as in a., but NINO3.4 is correlated to the SST anomaly field. d.) as in b., but SOI is correlated with the SST anomaly field.

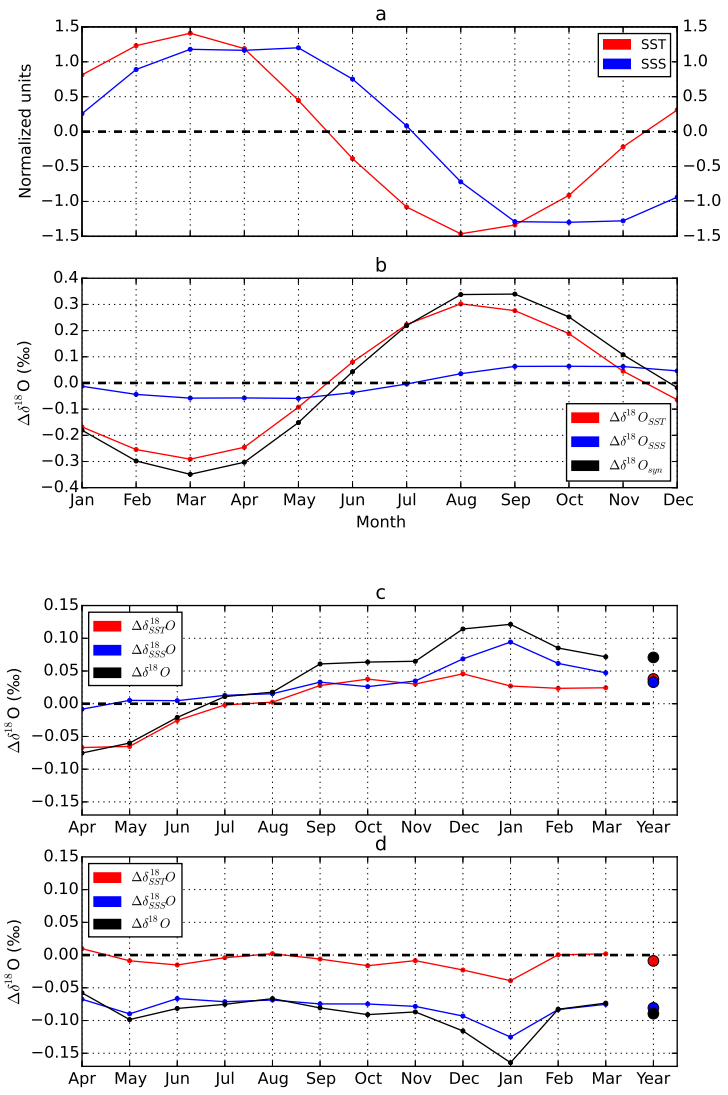

Figure 3.2: a.) SSS (blue) (*Delcroix et al.*, 2011) multiplied by -1 and SST (red) (*Huang et al.*, 2015) monthly standardized climatology (annual mean removed) for Aitutaki grid point (1975-2009 CE). b.) *Thompson et al.* (2011) coral δ^{18}O forward model with total δ^{18}O(black), $\delta^{18}O_{SSS}$ (blue), and $\delta^{18}O_{SST}$ SST (red). c.) Mean monthly and Apr-Mar average synthetic δ^{18}O anomaly for warm phase events (n=9, 1982-3, 1986-7, 1987-8, 1991-2, 1994-5, 1997-8, 2002-3, 2004-5, 2006-7) identified as the upper 75th percentile of NINO3.4 Apr-Mar annually averaged SSTA. d.) same as c., but for cold phase events (n=8, 1975-6, 1984-5, 1985-6, 1988-9, 1998-9, 1999-2000, 2000-1, 2007-8) identified as the lower 25th percentile of NINO3.4 Apr-Mar annually averaged SSTA.

3.2 Data & Methods

3.2.1 Coral δ^{18}O and Sr/Ca analysis

One live (ATC13100) coral was selected for analysis from the Aitutaki coral archive curated at the National Institute of Water & Atmospheric Research in Auckland, NZ. Samples were collected within 100 meters of the fringing reef surrounding the island where daily wave action from the open ocean continually flushes the shallower lagoon area that suggests conditions reflective of the open ocean (*McGregor et al.*, 2011). The Aitutaki coral samples display a microatoll morphology – growing radially outward and upward towards the water surface, remaining covered during high tide and often subaerially exposed during low tide. Aitutaki corals selected for analysis had no extensive bioerosion features.

Each coral sample analyzed underwent a series of quality control protocols. First, samples were rinsed with freshwater in the field after collection. The largest and most well-preserved samples were cut into 7 mm slices, and cleaned three times in deionized water using an ultrasonic probe. Slices were visually inspected under ultraviolet light for evidence of diagenetic alteration of the primary aragonite skeleton. One off-center sample slice was used for diagenesis testing via x-ray diffraction analyses conducted at the University of Auckland Department of Geology. The center sample slice was scanned using x-ray computed tomography (CT) to produce a digital image of the coral's alternating low and high density banding structure, which has been determined to reflect continuous and annual growth (*Knutson et al.*, 1972).

After these quality-control protocols, samples were micromilled continuously along

the maximum growth axis identified in the scans at 1 mm intervals using a mechanical, human-guided drill press at the University of Maryland Department of Geology and a computer-guided automated micromill at the National Institute of Water & Atmospheric Research (NIWA) in Auckland, New Zealand. Several hundred μg of coral carbonate powder were recovered at each interval.

Stable isotope measurements were made on aliquots of the coral samples at the Paleoclimate Co-Laboratory, University of Maryland following the *Evans et al.* (2016) experimental protocol. Samples and laboratory standards with a mass of $100 \pm 10\mu$g reacted with $\approx 100\mu$L of phosphoric acid (density = 1.92 g/mL) on a 65^{o}C autosampler rack for a minimum of 1 hour. The CO_2 product gas was analyzed for δ^{18}O and δ^{13}C simultaneously in a continuous-flow isotope ratio mass spectrometer system with a He carrier gas. Craig corrections were applied to the raw data. Then, a correction algorithm (*Evans et al.*, 2016) was applied to the data to correct for scale compression, run time drift, and signal amplitude. Results are reported relative to the V-SMOW and V-PDB international reference materials. External precision of individual measurements is $0.1‰$.

Trace element Sr/Ca measurements were made on aliquots of the coral samples at the University of Maryland Center for Environmental Science using an inductively coupled plasma optical emissions spectrometer. Samples of $88 - 240$ μg were dissolved in a 1.5-4.5 mL solution of 2% trace metal grade nitric acid. Elemental Sr/Ca ratio data were collected and corrected following the rapid, high-precision *Schrag* (1999) method. An independent coral standard run with the samples ($N = 136$) had a precision of 0.011 mmol/mol (0.12% rsd, 1σ). A gravimetric matrix matched standard run with the samples ($N = 104$) had a precision of 0.011 mmol/mol (0.12% rsd, 1σ).

In order to reconstruct SST from Sr/Ca, average of the linear regressions developed in *Linsley et al.* (2000, 2004) for Rarotonga was applied to this data. This reconstruction technique assumes a stationary relationship between the paleoclimate data and the climate variable (*Evans et al.*, 2013). While linearity must also be assumed in this model, previous research into inorganic aragonite precipitation suggests this relationship is valid (*Beck et al.*, 1992; *Corrége*, 2006; *Epstein et al.*, 1951, 1953).

3.2.2 Age Modeling

Establishing time in the dataseries was accomplished using cyclical variations in the δ^{18}O data, as done successfully in other southwest tropical Pacific studies (*Kilbourne et al.*, 2004; *Linsley et al.*, 2000, 2006). Local maxima and minima δ^{18}O values were assigned to September and April when mean sea surface temperature is highest and lowest at Aitutaki, respectively (Figure 3.2) (*Stoddart and Gibbs*, 1975; *Thompson*, 1986). The timeseries was developed by linearly interpolating to a uniform 12 samples/year resolution. To test whether the annual Apr-Mar mean δ^{18}O was affected by the extension rate, the different numbers of points in each band were retained after the interpolation. The results showed no difference in annual mean δ^{18}O (not shown).

But, error in placing tie-points would propagate over the length of the dataseries and introduce uncertainty. The modern Aitutaki coral, ATC13100, was collected live in June 2013 and x-rays showed well-defined density banding. The error in the tie-point age model of this coral was testable because results from ATC13100 were replicated because of the opportunity to drill two sampling tracks on this coral. An age model was developed for each sampling tract separately using the density banding, tie-point

method, and the June 2013 collection date. These two dataseries were then composited into a single timeseries. The layer counted chronology method for corals, particularly fossilized specimens, may be explicitly tested further through application of the banded age model, which considers the error in age as a function of miscounted and/or missing layers (*Comboul et al.*, 2014).

3.2.3 Data analysis

We used the *Thompson et al.* (2011) forward model to simulate δ^{18}O using inputs of SST (*Huang et al.*, 2015) and SSS (*Delcroix et al.*, 2011). This model provides a framework through which to interpret the composted Aitutaki/Rarotonga record. To assess the timing of Aitutaki interannual variations, mean monthly synthetic δ^{18}O was subtracted from corresponding δ^{18}O values and binned into ENSO warm (upper 75th), neutral (25th-75th), or cold (lower 25th) phase according to NINO3.4 index quartiles. Statistical tests were used to assess which data were significantly different from each other and a zero anomaly value. Synthetic δ^{18}O was also separated into its components as a function of SST, $\delta^{18}O_{SST}$, and SSS, $\delta^{18}O_{SSS}$, to better understand the relative contributions of each to total δ^{18}O.

Two sampling tracts were milled for ATC13100, and the results shown are a composite of those two dataseries from the same individual coral but from different growth surfaces. Each individual dataseries mean was shifted relative to the long term mean coral δ^{18}O of the 3-coral composite results from *Linsley et al.* (2006). Rarotonga Sr/Ca data from *Linsley et al.* (2006) was used to shift the mean of ATC13100 to have the same mean Sr/Ca value. Only one sampling from ATC13100 was used for the Sr/Ca analysis. While

this dataseries extends beyond 1850 to 1727 CE, only the modern 1850-2000 CE data is used in this study in order to focus on modern, industrial era climate variations and their associated external radiative forcings (*Diaz et al.*, 2011; *Taylor et al.*, 2012) and not the "Little Ice Age" period (1400-1800 CE).

The climatological mean for the δ^{18}O and Sr/Ca analyses was removed and each timeseries was detrended to interpret interannual anomalies. Annual average anomalies were calculated after interpolating all data to a uniform 8 samples per year. The observations were compared with the synthetic δ^{18}O produced by the coral forward model (*Thompson et al.*, 2011). The composited Aitutaki/Rarotonga timeseries was correlated with SST (*Huang et al.*, 2015) and SSS (*Delcroix et al.*, 2011) as done in Figure 3.1 with synthetic δ^{18}O. The oxygen isotope composition of seawater, $\delta^{18}O_{SW}$, was calculated using 3.1 to remove the temperature-based contribution to coral δ^{18}O (*McCulloch et al.*, 1994; *Stevenson et al.*, 2013; *Thompson et al.*, 2011).

$$\delta^{18}\mathrm{O}_{SW} \approx \delta^{18}\mathrm{O}_{coral} - a_1 * \beta Sr/Ca] \tag{3.1}$$

The a_1 term is the coefficient ($‰/^oC$) estimating the dependence of the oxygen isotope composition on temperature (*Epstein et al.*, 1951; *Grossman and Ku*, 1986; *Kinsman and Holland*, 1969), and β is the empirically-derived coefficient (mmol/mol/^{o}C) of the linear regression of Sr/Ca on sea surface temperature at Rarotonga (*Linsley et al.*, 2000, 2004). A scatter plot of annual, Apr-Mar, averages was used to assess to what extent coral δ^{18}O data are explained by $\delta^{18}O_{SW}$. Singular spectrum analysis was applied to the data to separate variability in the timeseries with different frequencies followed by the

multitaper spectral estimation method (*Thomson et al.*, 2000) to isolate the interannual variability. Singular spectrum analysis is particularly useful for climate time series which can be short, nonlinear, and include some chaotic behavior (*Ghil et al.*, 2002; *Vautard et al.*, 1992). An embedding dimension of m=30 was chosen to capture variability in the annual to low-frequency (>10 year period) range. Additional analysis with a smaller (20) and larger (40) embedding dimension changed the total variance explained from 90-93% to 95-98% (m=20) and 87-88% (m=40). The interpretation of the ninth and tenth reconstructed component did vary between annual and interannual (2-10 year period) frequency, but this change only affected the percent of explained variance by 4% at the most (results not shown).

3.3 Results

Annual variation of the sea surface temperature and salinity observations at Aitutaki show a distinct cycle (Figure 3.2a). Maximum (minimum) values of SST (SSS) occur in April of each year, while minimum (maximum) values of SST (SSS) occur in September of each year. Variations over the calendar year show that simulated δ^{18}O as a function of temperature only has an amplitude three times that of simulated δ^{18}O as a function of salinity only, explaining most of the variation (Figure 3.2b) (*Linsley et al.*, 2006). Interannual variations, in contrast to the annual variability, show that simulated δ^{18}O as a function of salinity only at Aitutaki is approximately three times larger in amplitude than simulated δ^{18}O as a function of temperature only for portions of the year (Figure 3.2c,d).

Differences between warm and cold phase treatments were significant for September, October, December, and January ($p<0.05$, df=21). October cold phase, December

warm phase, and January cold & warm phase results were significantly different from zero (Figure 3.2). Annual (Apr-Mar) average anomalies for warm and cold phase were also statistically significant from each other ($p<0.05$, df=15). Only cold phase annual (Apr-Mar) average synthetic δ^{18}O anomaly was significantly different from a mean of zero ($p<0.1$).

The $\delta^{18}O_{SSS}$ variation had a larger amplitude in both warm and cold phases (n=9,8) for all months except April, May, and June warm phase treatment (Figure 3.2). In the warm phase treatment (Figure 3.2c), April and May $\delta^{18}O_{SST}$ were significantly different from zero ($p<0.1$), while September, December, and January $\delta^{18}O_{SSS}$ were significantly different from zero ($p<0.1$). In the cold phase treatment (Figure 3.2d), April, May, September, December, and January $\delta^{18}O_{SSS}$ were significantly different from zero ($p<0.1$). Annual (Apr-Mar) average anomalies of synthetic $\delta^{18}O_{SSS}$ for warm and cold phase were also statistically significant from each other ($p<0.02$, df=15), but not synthetic $\delta^{18}O_{SST}$. Warm and cold phase annual (Apr-Mar) average synthetic $\delta^{18}O_{SSS}$ was statistically significant from a mean of zero ($p<0.1$, $p<0.05$, respectively).

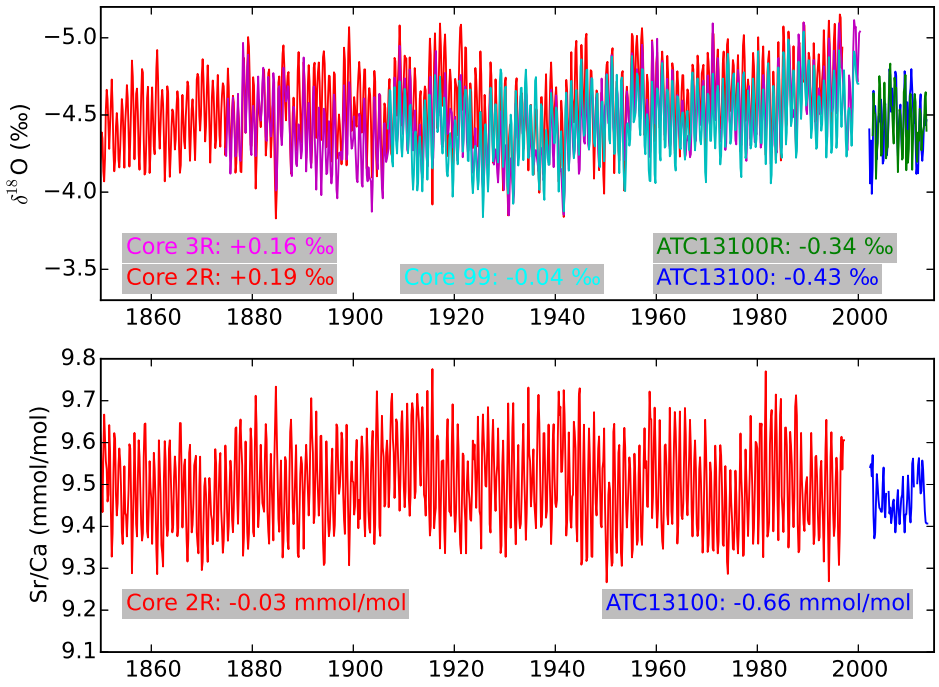

Figure 3.3: Top: Rarotonga (Core 2R, 3R, 99) and Aitutaki (ATC13100, ATC13100R) coral δ^{18}O data for the Industrial Era (8 samples/year). Correlations between Rarotonga records is reported in *Linsley et al.* (2006); r(ATC13100,ATC13100)= 0.61, p<0.001. Bottom: as in Top, but Rarotonga Core 2R and Aitutaki ATC13100 Sr/Ca.

Coral δ^{18}O and Sr/Ca results show agreement over time and in their serial correlation (Aitutaki, r=0.61, Rarotonga, (*Linsley et al.*, 2006)), suggesting these dataseries may be composited together (Figure 3.3, 3.3). Inter-colony δ^{18}O reproducibility of -0.43 to +0.19 ‰ is comparable to previous studies (*Cobb et al.*, 2003a; *Felis et al.*, 2003; *Linsley et al.*, 1999). The ATC1300 Sr/Ca offset of -0.66 mmol/mol is considered further in the Discussion. The composited coral geochemistry results from Aitutaki and previously published Rarotonga data (*Linsley et al.*, 2006) show interannual (2-10 year period) and

lower frequency (>10 year period) variability, explaining portions of the total variation of the δ^{18}O (20%, 31%, respectively) and Sr/Ca (14%, 9%, respectively) dataseries (Figure 3.4, 3.4). The calculated trendline for the composited anomaly timeseries was significant but the linear model only explained 4% of total variance (not shown).

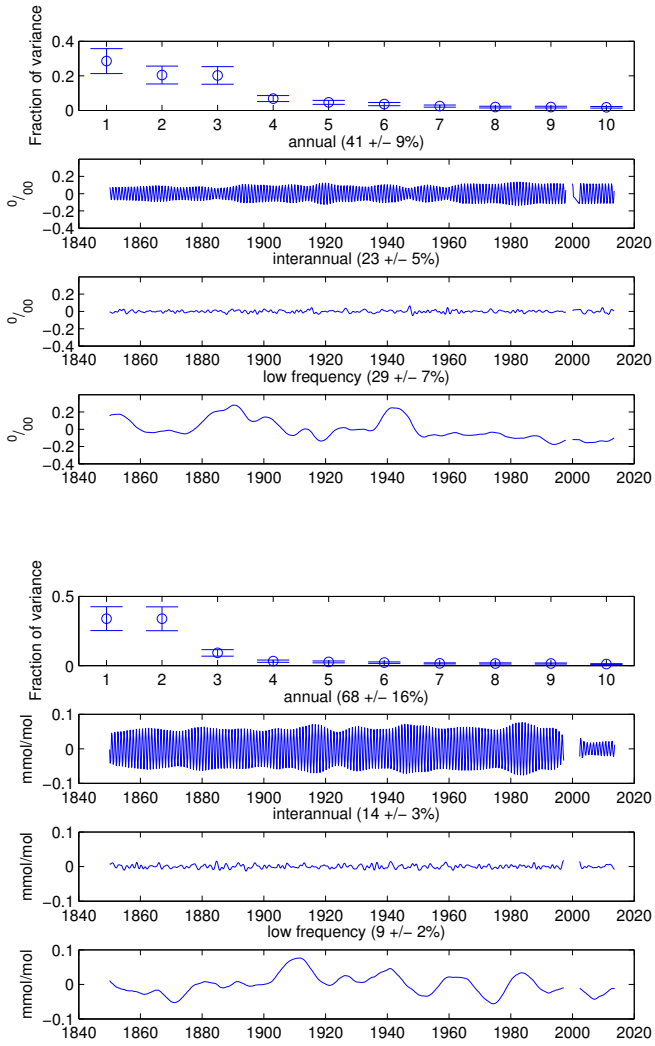

Figure 3.4: Singular spectrum analysis. Top: Eigenvalues of singular spectrum analysis for coral δ^{18}O (3.1 with embedding dimension of 5 years. Uncertainty estimates were calculated using Equation 3.1a,b (*Ghil and Mo*, 1991). Shown are composited reconstructed components identified in the annual (1 year period), interannual (2-10 year period), and low frequency (>10 year period) frequency bands through analysis of spectral power from a multitaper power spectral density figure (not shown). Explained variance for each composite is shown in parentheses. Bottom: same as Top, but Sr/Ca.

The oxygen isotope composition of seawater anomaly, $\delta^{18}O_{SW}$, calculated using

3.1, explains 71+/-4% (r=0.84, p<0.001) of coral δ^{18}O variation (Figure 3.5). Propagation of coral δ^{18}O and Sr/Ca analytical error and the uncertainty in the empirically derived coefficients in 3.1 resulted in a fractional uncertainty (*Taylor*, 1997) in calculated $\delta^{18}O_{SW}$ of 45%. The $\delta^{18}O_{SST}$ component explains 14+/-4% (r=0.37, p<0.001). Linear regression of $\delta^{18}O_{SW}$ and $\delta^{18}O_{SST}$ on δ^{18}O produced slopes (with standard error) of 1.59+/-0.08 and 0.18+/-0.04, respectively. Singular spectrum analysis of the calculated $\delta^{18}O_{SW}$ timeseries shows 49% of variation may be attributed to the interannual frequency band, 27% to low frequency (>10 year period) variability, and 6% to annual variation (Figure 3.6).

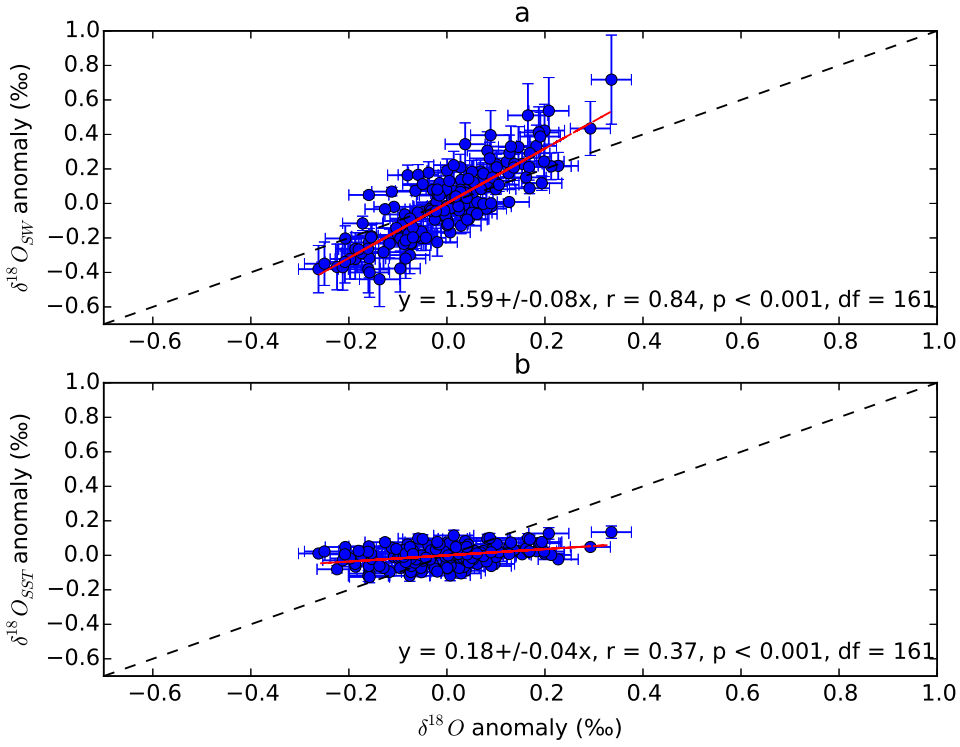

Figure 3.5: a.) The oxygen isotope composition of seawater, $\delta^{18}O_{SW}$ (3.1) versus the coral $\delta^{18}O$ timeseries, Apr-Mar annual average anomalies. The ordinary least squares regression (red) is shown with linear equation and statistics. The 1:1 line is shown in black. Error bars show the calculated fractional percent uncertainty following propagation of errors (*Taylor*, 1997) in 3.1 b.) same as a.), but for $\delta^{18}O_{SST}$ component.

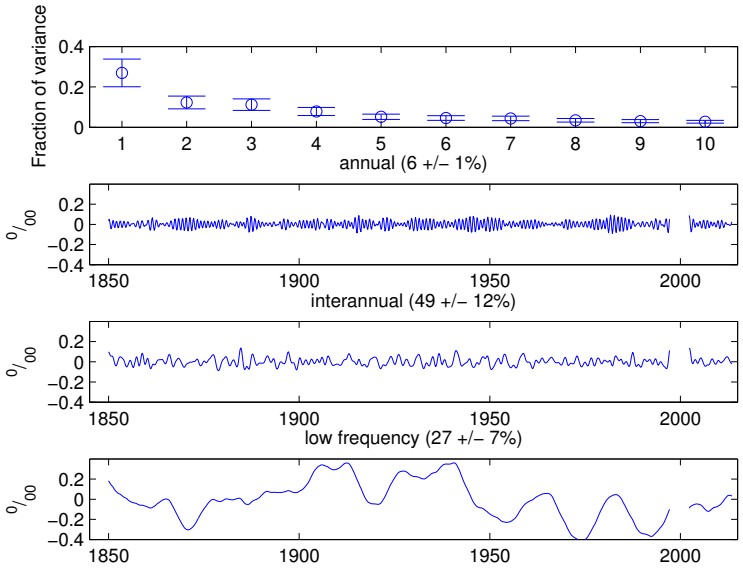

Figure 3.6: Singular spectrum analysis. As in Figure 3.4, but for calculated $\delta^{18}O_{SW}$ data.

3.4 Discussion

3.4.1 Coral geochemical modeling

Modeling of the annual cycle in synthetic $\delta^{18}O$ predicted that climatological SST was the more important determinant of variation. However, interannual variability in observed SST is small, so synthetic $\delta^{18}O$ is primarily caused by seawater $\delta^{18}O$ variations associated with SSS variations (Figure 3.2), themselves a part of the larger scale pattern associated with ENSO activity (Figure 3.1). Statistical analysis showed synthetic $\delta^{18}O$ anomalies were most significant in amplitude during the boreal winter season of December, January, February (DJF) (Figure 3.2). The DJF season also corresponds to the mature stage of ENSO events (*Philander*, 1990).

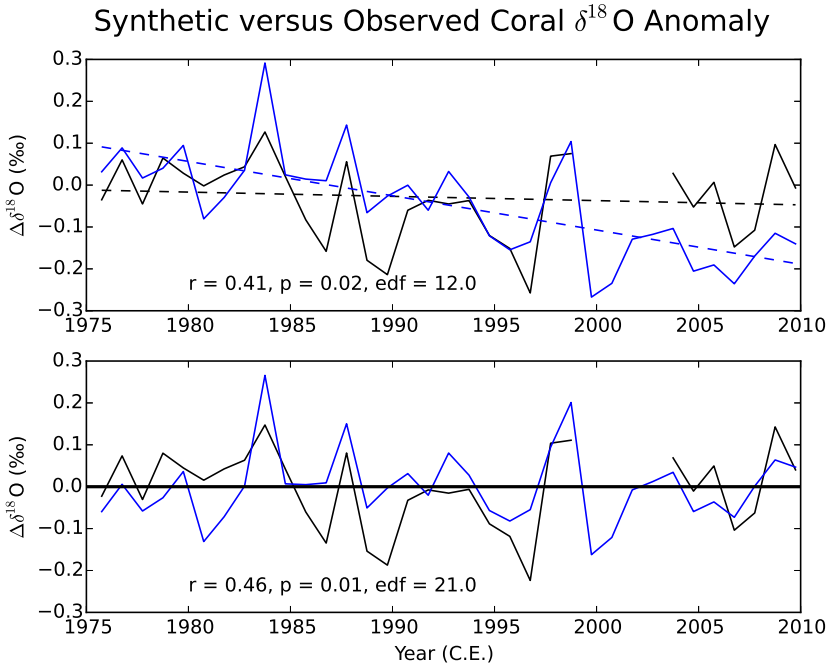

Figure 3.7: Top: Annual Apr-Mar synthetic δ^{18}O anomaly (blue) computed using the *Thompson et al.* (2011) proxy system model with SST (*Kennedy et al.*, 2011) and SSS (*Delcroix et al.*, 2011) inputs is compared to observations (black): a 3-sample composite coral δ^{18}O record (1975-1998 C.E.) from Rarotonga (*Linsley et al.*, 2006) and a 2-track line composite coral δ^{18}O record (2002-2009 C.E.) from Aitutaki, southern Cook Islands. Dashed lines show linear, long term trends in the data. Effective degrees of freedom, edf, is calculated using *Wilks* (2006) eq. 5.12. Bottom: as in Top, but the timeseries have been detrended to emphasize the impact of interannual variability.

The similarity between the new composited southern Cook Islands coral δ^{18}O record and synthetic δ^{18}O constructed from SST and SSS inputs (Figure 3.7) suggests the coral forward model may be used to explain the variance in δ^{18}O observations as a function of SST and SSS variability. In the modern period, we can examine how well the synthetic and observed timeseries captured ENSO events. Both the observed and synthetic δ^{18}O

data show a positive δ^{18}O excursion for the 1982 and the 1997 El Niño events, the two largest of the century at this location.

A positive δ^{18}O anomaly is suggestive of cooler and/or dryer conditions (*Folland et al.*, 2002). Given Aitutaki's position within the South Pacific Convergence Zone, cooler and/or dryer conditions would imply that the SPCZ has shifted towards the equator as a result of a shifted Pacific Walker Circulation and eastward displacement of warm Western Pacific surface water from ENSO warm phase events (*Widlansky et al.*, 2011; *Yan et al.*, 2011a). The smaller 1986-1987 event also shows a positive δ^{18}O anomaly in the data. Other warm phase events of the late-twentieth and early twenty-first century do not appear detectable in the data (1991-1994, 2006). But, no one site can be a perfect recorder of ENSO because of paleoclimate observational uncertainty and differences in the amplitude, timing, and spatial structure of individual ENSO events.

Offsets of individual coral δ^{18}O and Sr/Ca records from the Rarotonga 2R 1960-1990 average are variable. The Core 99 offset of -0.04 ‰ is less than analytical uncertainty of 0.1 ‰, while Core 2R and 3R are approximately twice that of analytical uncertainty (0.16, 0.19 ‰, respectively). These offsets are similar to that of other coral paleocliate studies (*Cobb et al.*, 2003a; *Hereid et al.*, 2013). But the Aitutaki records, ATC13100 and ATC13100R, show δ^{18}O offsets of -0.34 and -0.43 ‰. Coral δ^{18}O is primarily influenced by temperature at annual time resolutions, and these offsets correspond to sea surface temperature differences of 1.5-2.0^{o}C. ATC13100 had a Sr/Ca offset of -0.66 mmol/mol, which would correspond to a SST difference of 9^{o}C. Previous studies have reported δ^{18}O offsets of 0.4 ‰ elsewhere in the tropical Pacific (*Linsley et al.*, 1999), suggesting these differences arise from variations extension rate (*Felis et al.*, 2003) and

in local environmental conditions (*Cobb et al.*, 2003a; *Linsley et al.*, 2006) yet insensitive to coral age (*Linsley et al.*, 1999). The Aitutaki record, ATC13100, was a microatoll coral collected within an inlet flushed with ocean water approximately 100 meters from the outer fringing reef. Previous research has suggested these microatoll environments reflect open ocean conditions (*McGregor et al.*, 2011), but their offsets may be larger due to the local water depth, light availability, and nutrient levels (*Cobb et al.*, 2003a) that may impact the Aiutaki lagoon environment (*Stoddart and Gibbs*, 1975; *Vazey*, 2008).

3.4.2 Seawater δ^{18}O variability

The agreement between synthetic δ^{18}O and Aitutaki/Rarotonga coral δ^{18}O observations suggests we can use the linear bivariate *Thompson et al.* (2011) coral sensor model to interpret the observations. Calculation of $\delta^{18}O_{sw}$ and $\delta^{18}O_{SST}$ using the coral δ^{18}O and Sr/Ca measurements shows interannual variability comes from both components of variability and a larger magnitude from the $\delta^{18}O_{SW}$ component (Figure 3.5). These results were predicted by the proxy system model results (Figure 3.2). These analyses suggest that interannual variability at Aitutaki/Rarotonga stems from changes in the position of the SPCZ driven primarily by $\delta^{18}O_{SW}$. As a major convergence center, the SPCZ region has higher sea surface temperatures and increased seawater δ^{18}O values from increased precipitation. During ENSO warm phase events, shifts in the SPCZ towards the central equatorial Pacific leave Aitutaki/Rarotonga cooler/dryer (increased δ^{18}O values), while during ENSO cold phase events, poleward shifts in the SPCZ produce warmer/wetter (decreased δ^{18}O values) conditions at Aitutaki/Rarotonga. Analysis of each component of δ^{18}O variability supports this conclusion because the data can be reasonably approximated

by the 1:1 line (Figure 3.5).

3.4.3 Southwestern tropical Pacific variability

The spatial correlation of SSS and SST in Figure 3.8 show similar spatial structure as Figure 3.1 with correlation in the southwest Pacific with the SSS anomaly field and correlation in the western Pacific with SST anomaly field. To first order, this is to be expected given that the synthetic δ^{18}O is calculated with SST and SSS inputs. The similarity to Figure 3.1 also suggests ENSO could be the driver of coral δ^{18}O variations in this region where SSS variations are significant. While the correlation of the coral δ^{18}O with SST does not have a significant correlation with the central Pacific as in Figure 3.1, there still is a similar horseshoe negative correlation pattern in the western Pacific, which suggests even SST variations in the southwest Pacific are at least, in part, influenced by ENSO events (*Jochum and Murtugudde*, 2004). This provides further evidence that Aitutaki δ^{18}O can be used to infer basin-scale ENSO phase over time.

3.4.4 Interpretational uncertainties

Observational uncertainty can limit the interpretations which can be concluded from coral paleoclimate data. The proxy system model is mechanistically-derived with empirically determined coefficients whose representation of interannual coral δ^{18}O variability does not account for biological effects (*Dee et al.*, 2015; *Evans et al.*, 2013; *Smerdon et al.*, 2017; *Thompson et al.*, 2011). Local anomalous surface temperature and salinity anomalies are not a response entirely from regional or Pacific-wide interannual ENSO variation. A single record from one location cannot record all ENSO events given ob-

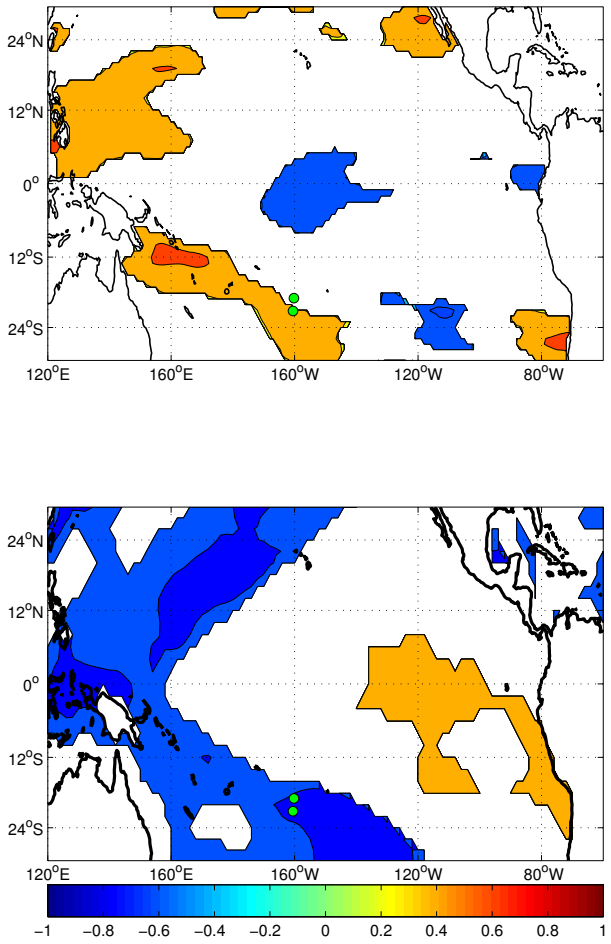

Figure 3.8: Top: Apr-Mar average annual coral δ^{18}O anomaly using data from *Linsley et al.* (2006) (1975-1995 C.E.) and this study (2002-2012 C.E.) correlated to the SSS anomaly field (*Delcroix et al.*, 2011). Grid cells with a p-value $>$0.05 have been removed. Bottom: same as Top, but for the SST anomaly field (*Huang et al.*, 2015)

servational error (*Comboul et al.*, 2015; *Evans et al.*, 2013; *Lough*, 2010), but replication of results can improve reconstructions. Age model error can limit our ability to pinpoint specific events of the past, but within error, the timeseries can provide information about past variability within a specified period.

A second source of uncertainty is the understanding of the physics of ENSO with some evidence suggesting it is a weakly chaotic dynamical system (*Jochum and Murtugudde*, 2004), while other research represents ENSO as a quasi-periodic oscillation of the coupled ocean-atmosphere system (*Bjerknes*, 1969; *Wyrtki*, 1975). This variation of ENSO itself produces a spectrum of events with differences in space (*Ashok et al.*, 2007; *Yeh et al.*, 2009), frequency (*Fedorov and Philander*, 2000), timing (*Ramesh and Murtugudde*, 2012), and amplitude (*Jin*, 1997).

The synthetic δ^{18}O analyses suggest a statistically significant response during boreal winter (DJF), when ENSO amplitude is largest (*Philander*, 1990). Events may be identified in this season, yet modern events are detectable in the 20th century annual (Apr-Mar) average anomaly results too (Figure 3.7). Implicit in this interpretation of the data is the assumption of uniformity in the relationship between coral δ^{18}O and the SPCZ and ENSO behavior. If this relationship was not stationary over time (*Evans et al.*, 2013; *Phipps et al.*, 2013), the isotope data may be indicative of some other climate phenomena. While there are uncertainties to consider when interpreting coral δ^{18}O as an ENSO indicator, these preliminary results suggest that some ENSO activity may be identified in coral geochemical data from the southern Cook Islands through analysis of signal amplitude and separation of the signal into its different frequency domains. Given these modern results and assuming a similar relationship between regional SPCZ dynamics and ENSO activity, fossil corals from Aitutaki may be able to be used for reconstructing changes in the position of the SPCZ and ENSO variability in the past.

3.5 Conclusions

A combination of new and existing paired coral δ^{18}O and Sr/Ca observations from Aitutaki and Rarotonga, southern Cook Islands, were used to construct estimates of the regional southwestern tropical Pacific response of $\delta^{18}O_{SW}$ to ENSO activity. Analysis of observed interannual δ^{18}O indicates interannual variations are primarily from the coral $\delta^{18}O_{SW}$ component. These results suggests that hydrological variation, measured as coral $\delta^{18}O_{SW}$, is the primary driver in explaining interannual δ^{18}O changes. Observed interannual $\delta^{18}O_{SW}$ variation is interpreted to reflect changes in the position of the South Pacific Convergence Zone. The response of interannual $\delta^{18}O_{SW}$ amplitude is most significant in the DJF boreal winter season when ENSO events are strongest, perhaps redistributing the heat and moisture of the mean SPCZ. Strong modern ENSO events are detectable in this record at this location, suggesting stability in the relationship between the SPCZ and ENSO, at least over the latter 20th century. The interpretation of modern coral geochemical results as ENSO sensitive may permit the reconstruction of SPCZ and ENSO variability during intervals of the past millennium.

Chapter 4: Variable ENSO recorded in early millennium Aitutaki corals

4.1 Introduction

A key question yet unanswered in the literature is how the El Niño-Southern Oscillation (ENSO) amplitude, frequency, and spatial pattern will respond to 21st century external radiative forcings (*IPCC Working Group 1 et al.*, 2013). ENSO is a significant source of global interannual climate variability (*Glantz et al.*, 1991; *IPCC Working Group 1 et al.*, 2013; *Philander*, 1990), which originates in the tropical Pacific when easterly trade winds weaken and water from the western Pacific warm pool travels eastward, redistributing heat and moisture across the tropical Pacific (*Bjerknes*, 1969; *Clarke*, 2014; *Wyrtki*, 1975). Teleconnected regions such as South Africa, North America, and Australia experience anomalous temperature and rainfall as a result of ENSO activity.

There is little agreement as to how ENSO will change in response to external radiative forcings. Theoretical studies used to model ENSO predict both increased and decreased amplitude of ENSO events (*Clement et al.*, 1996; *Collins et al.*, 2010; *Guilyardi et al.*, 2009; *Vecchi et al.*, 2006) due to changes in greenhouse gas concentrations, volcanism, solar irradiance, and land use/land change. ENSO events have a typical frequency of 2-8 years, so modern instrumental observing networks do not have enough realizations to adequately capture its variability on interannual, decadal, and multidecadal timescales

(*Wittenberg*, 2009). Observations are equivocal at this point because of the limited data available.

Coral paleoclimatology can assist in the effort to better understand ENSO and hydroclimate variability of the tropical Pacific by providing paleoclimate observations of ENSO activity during intervals of the past millennium (*Dunbar and Cole*, 1996; *Jones et al.*, 2009; *Lough*, 2010). Variations in coral geochemistry reflect changes in environmental forcings (*Evans et al.*, 2013; *McGregor et al.*, 2011). Provided that the corals are well-preserved, long-lived, and that their growth is well characterized, paired δ^{18}O and Sr/Ca measurements made on the aragonite skeleton can be used to infer surface ocean temperature and seawater δ^{18}O (*Evans et al.*, 2013; *Lopatka et al.*, in prep.; *Lough and Barnes*, 1997; *Stevenson et al.*, 2013; *Thompson et al.*, 2011). Because corals have lived far beyond the 20th century instrumental era, results from fossil corals may be used to interpret past ENSO variability, decadal to multidecadal variability, and what past forcings may be responsible for these observations (*Cobb et al.*, 2003a; *Cole and Fairbanks*, 1990; *Evans et al.*, 1999; *Hereid et al.*, 2013; *Kilbourne et al.*, 2004; *Woodroffe and Gagan*, 2000).

During an earlier phase of the Past Global Changes (PAGES) Ocean2k project, sea surface temperature of the tropical oceans over the past four centuries were reconstructed from dozens of coral archives (*Tierney et al.*, 2015). A key finding was that neither anthropogenic nor natural forcings altered ENSO-related variance in SST. In the next phase, the new PAGES CoralHydro2k group aims to reconstruct hydroclimatological trends in new and existing coral data in order to produce reconstructions of hydroclimate variability from estimates of coral seawater δ^{18}O. In the southwestern tropical Pacific,

hydrological variations arise from the precipitation, evaporation, runoff, and advection balance controlled primarily by the frequency and intensity of rainfall from the persistent South Pacific Convergence Zone (SPCZ) (*Delcroix et al.*, 2011; *Gouriou and Delcroix*, 2002; *Hasson et al.*, 2013; *Lopatka et al.*, in prep.; *Lorrey et al.*, 2012; *Picaut et al.*, 1996; *Vincent*, 1994; *Widlansky et al.*, 2012).

In the southwest tropical Pacific, variations in coral δ^{18}O data may indicate changes in sea surface salinity on interannual timescales, because the redistribution of warm water eastward during a ENSO warm phase event shifts the SPCZ equatorward, leaving the southwestern tropical Pacific surface water more saline relative to ENSO neutral or cold phase conditions (*Folland et al.*, 2002; *Salinger et al.*, 2001, 1995). Previous work has also indicated changes in the position of the salinity front of the SPCZ during times of significant ENSO activity (*Goodwin et al.*, 2014; *Kilbourne et al.*, 2004; *Linsley et al.*, 2006; *Lorrey et al.*, 2012).

In this study, we develop monthly-resolved records of southwestern tropical Pacific coral δ^{18}O and Sr/Ca from approximately 1,000 years ago, during a time period many describe as the "Medieval Climate Anomaly" (MCA) or the "Medieval Warm Period" (*Lamb*, 1965; *Mann et al.*, 2009) when Earth's climate may have been warmer/wetter relative to present day. The MCA is thought to have anthropogenic external radiative forcings significantly lower than the Industrial Era (*Schmidt et al.*, 2014). An ensemble of model simulations using the same external radiative forcings but perturbed with slightly different beginning surface air temperatures suggests that unforced variation arising from the coupled ocean-atmosphere system may be significant in producing the observed climate (*Otto-Bliesner et al.*, 2016). Therefore, paleoclimate observations during the MCA

may help improve our understanding of unforced variation in tropical Pacific climate and the response of ENSO to those climate forcings. A better understanding of the amplitude and frequency response of ENSO to hydrological change during the MCA may help improve predictions of 21st century hydroclimatological changes in ENSO activity (*Braconnot et al.*, 2012; *Taylor et al.*, 2012).

4.2 Methods

4.2.1 Study Site

A total of 101 *Porites* reef coral samples were collected from Aitutaki, southern Cook Islands, a volcanically produced atoll with a carbonate fringing reef surrounding a shallow water lagoon (*Stoddart and Gibbs*, 1975), during a field expedition in June-July 2013. Subaerial, storm-washed coral heads beached on shore were collected, as in *Cobb et al.* (2003a); *Hereid et al.* (2013), within about 100 meters of the fringing reef reflective of open-ocean climate conditions given the daily tidal flows on the windward side of Aitutaki (Figure 4.1). Live corals collected for comparison were *Porites* with microatoll morphology, which live in shallow, knee-deep water and grow upwards toward the sea surface and extend laterally outward and have been validated as a reliable source of paleoclimate data (*McGregor et al.*, 2011).

Figure 4.1: Locations along the windward, fringing reef of Aitutaki from which *Porites* storm-washed coral heads and in-situ microatoll samples were collected during the June-July 2013 field expedition. Yellow star indicates the site of fossil samples ATC13075,76,96.

4.2.2 Diagenetic Testing

The corals used for this study are curated at the National Institute of Water and Atmospheric Research in Auckland, NZ. Individual cores selected for this study were cleaned with an ultrasonic probe and cut into three 7mm wide slabs (Figure 4.2. All cores used for this study were viewed under UV light for qualitative examination of diagenesis. To quantitatively estimate potential diagenetic alteration of the coral's aragonite skeleton, bulk powdered samples of about 1 mg were taken from the surface of one of three slabs cut from ATC13096 that was not used for micromilling samples for geochemical analyses. A second XRD preparation technique of grinding the powder and smearing it onto

a glass slide, was done for ATC13096 in addition to a replication of the bulk powdered sample method. Analyses for ATC13075 and ATC13076 were collected using the XRD "smear" method and replicated twice. All XRD work was done at the Department of Geology, University of Auckland with an X-ray diffractometer with a Cu K-alpha radiation source following *Lopatka et al.* (2015) and as done in *Sayani et al.* (2011). Previous research studying the geochemical impacts of diagenesis may be used to qualitatively analyze the new observations in this study. Subaerially exposed corals that have been diagenetically altered show depleted δ^{18}O and Sr/Ca values (*McGregor and Gagan*, 2003; *Sayani et al.*, 2011). Submarine corals and corals that display dissolution features suggestive of secondary aragonite tend to show enriched δ^{18}O and Sr/Ca values (*Allison et al.*, 2007; *Enmar et al.*, 2000; *Hendy et al.*, 2007; *Sayani et al.*, 2011).

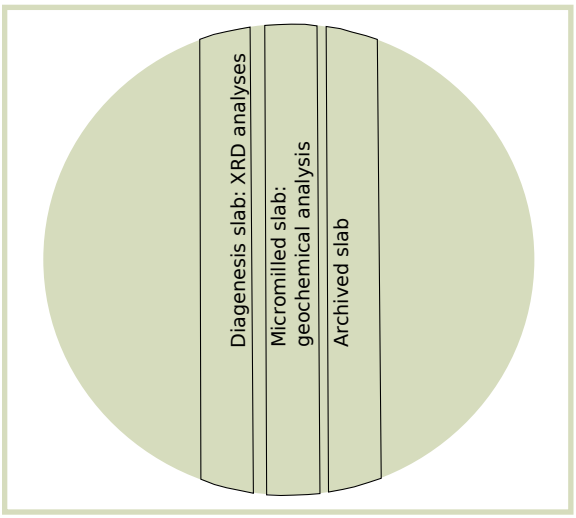

Figure 4.2: Coral core cuts. Schematic diagram view down the length of the core showing the three slabs cut from each coral core, with exaggerated spacing between slabs with text describing their use for geochemical analyses, XRD analyses, or archived material.

4.2.3 X-Ray CT Scanning

X-ray computed tomography (CT) images for each coral were obtained from the Ascot Hospital Radiology Department in Auckland, New Zealand to identify annual density banding and the maximum growth axis in support of the chronology development (*Lough*, 2010) and determination of the micromilling sampling resolution. Image editing software was used to identify the annual growth bands, defined as a pair of darker and lighter bands (*Knutson et al.*, 1972). The location of the maximum growth axis, perpendicular to the annual growth bands and parallel to growth features (*DeLong et al.*, 2013), was identified and marked on the sample.

4.2.4 Chronology development

From the corals which passed diagenetic screening, U/Th decay series radiometric dating (*Cobb et al.*, 2003b; *Edwards et al.*, 1987) identified three corals with ages of approximately 1,000 years ago (Table 4.1) during the time period known as the Medieval Climate Anomaly (*Cobb et al.*, 2003a; *Lamb*, 1965; *Mann et al.*, 2009). Coral age models were developed by using the U/Th date as an absolute age estimate with error and the relative dating method of tying local maxima and minima of the geochemical dataseries to the annual cycle. Dataseries were linearly interpolated to a uniform 12 samples per year of growth. To test whether the annual Apr-Mar mean δ^{18}O was affected by the extension rate, the different numbers of points in each band were retained after the interpolation. The results showed no difference in annual mean δ^{18}O (not shown).

Name	Age (C.E.)	Error (yr)	Depth (mm)	Range (C.E.)
ATC13075	948	5	237	942-1007
ATC13096	1034	6	315	1007-1058
ATC13076	1133	5	65	1120-1166

Table 4.1: U/Th radiometric age, error, sample location as a function of depth down core for each individual coral, and the age-modeled range of time of each individual coral.

The layer counted chronology method used for these fossilized coral specimens, was explicitly tested using the PRYSM (*Dee et al.*, 2015) application of the banded age model, which propagated error in age as a function of miscounted and/or missing layers (*Comboul et al.*, 2014) to the chronology using a rate of 5% for each (*DeLong et al.*, 2013).

4.2.5 Geochemical Analyses

After these quality-control protocols, samples were micromilled continuously along the maximum growth axis identified in the scans at 1 mm intervals using a computer-guided automated micromill at the National Institute of Water & Atmospheric Research (NIWA) in Auckland, New Zealand. Several hundred μg of coral carbonate powder were recovered at each interval.

Stable isotope measurements were made on aliquots of the coral samples at the Paleoclimate Co-Laboratory, University of Maryland following the *Evans et al.* (2016)

experimental protocol. Samples and laboratory standards with a mass of $100 \pm 10\mu$g reacted with $\approx 100\mu$L of phosphoric acid (density = 1.92 g/mL) on a 65^{o}C autosampler rack for a minimum of 1 hour. The CO_2 product gas was analyzed for δ^{18}O and δ^{13}C simultaneously in a continuous-flow isotope ratio mass spectrometer system with a He carrier gas. Craig corrections were applied to the raw data to remove the interference effect of ^{17}O on the δ^{18}O and δ^{13}C of the CO_2 product gas (*Craig*, 1957). Then, a correction algorithm (*Evans et al.*, 2016) was applied to the data to correct for scale compression, run time drift, and signal amplitude. Results are reported relative to the V-SMOW and V-PDB international reference materials. External precision of individual measurements is $0.1‰$.

Trace element Sr/Ca measurements were made on aliquots of the coral samples at the University of Maryland Center for Environmental Science using an inductively coupled plasma optical emissions spectrometer. Samples of $88 - 240$ μg were dissolved in a 1.5-4.5 mL solution of 2% trace metal grade nitric acid. Elemental Sr/Ca ratio data were collected and corrected following the rapid, high-precision *Schrag* (1999) method. An independent coral standard run with the samples ($N = 136$) had a precision of 0.011 mmol/mol (0.12% rsd, 1σ). A gravimetric matrix matched standard run with the samples ($N = 104$) had a precision of 0.011 mmol/mol (0.12% rsd, 1σ).

4.2.6 Data Analyses

Age model uncertainty was estimated by using the PRYSM implementation (*Dee et al.*, 2015) of the banded age model (*Comboul et al.*, 2014). Designed for coral archives, this method calculates an ensemble of possible ages by quantifying the annually banded

effect of missing and doubly counted years in the dataseries. A 5% error rate for both missing and doubly counted years was used as in *Comboul et al.* (2014), which is more conservative than other error estimations (*DeLong et al.*, 2013). Figure 3.2 shows a synthetic δ^{18}O maximum between August and September over the 1975-2009 interval, while the synthetic δ^{18}O minimum occurs in March. Estimating uncertainty in accurately identifying the maximum of half a month yields an error rate of 4.2% per year which is similar to the 5% error rate described earlier. A 5% error rate also corresponds to misidentifying one ENSO event per 100 years, which assumes an average period of 5 years or 20 events per 100 years.

Paired δ^{18}O and Sr/Ca analyses, re-interpolated to a lowest common temporal resolution of 6 samples per year, were used in conjunction to calculate estimates of $\delta^{18}O_{SW}$ (Equation 1, (*Lopatka et al.*, in prep.)). Linear regression of annual, Apr-Mar, data averages was used to assess to what extent coral δ^{18}O data are explained by $\delta^{18}O_{SW}$ and $\delta^{18}O_{SST}$. A statistical test was used to analyze whether for equality of variance between the Medieval Climate Anomaly and the modern period. The F-test equality of variances tests the null hypothesis that samples from two normal populations have equal variances, where the F-statistic is the ratio of variances. Histograms of the data were used to qualitatively assess the normality of the distribution of data as well as probability plots.

Singular spectrum analysis was applied to the data to separate variability in the timeseries with different frequencies followed by the multitaper spectral estimation method (*Thomson et al.*, 2000) to isolate the interannual variability. Singular spectrum analysis is particularly useful for climate time series which can be short, nonlinear, and include some chaotic behavior (*Ghil et al.*, 2002; *Vautard et al.*, 1992). An embedding dimension of

m=30 was chosen to capture variability in the annual to low-frequency (>10 year period) range. An additional singular spectrum analysis was performed on the shortest individual record, ATC13096, to test for sensitivity of the results to timeseries length.

Calculated variance of interannual fossil coral data were compared to modern coral variance results from the same location (*Lopatka et al.*, in prep.) to assess the extent to which observed interannual variance changed over time. Event recurrence interval estimates were calculated using percentage thresholds of the data to analyze changes in event frequency over time.

4.3 Results

4.3.1 Diagenetic analyses

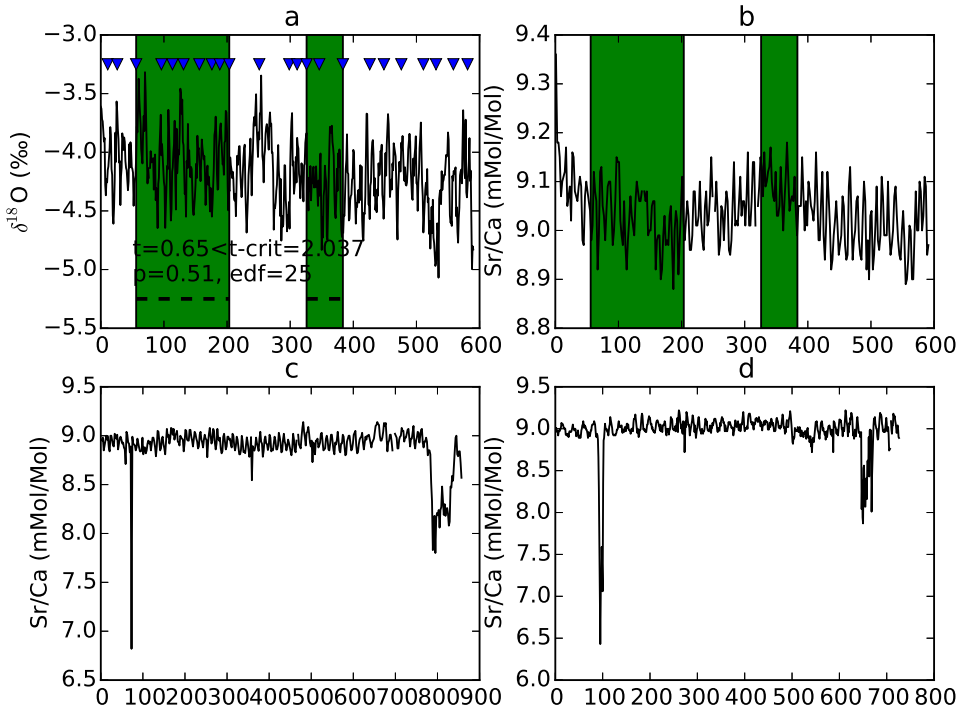

Figure 4.3: a.)Aitutaki coral ATC13096 δ^{18}O determinations as a function of depth (mm). Triangles indicate locations where XRD samples were taken from the slab interfacing with the slab used for micromilling powders for geochemical analyses. Green shading (black dashed line) indicates where the first (second) XRD analysis indicated secondary calcite in excess of 1%. T-test of independent samples between altered and pristine material failed to reject the null hypothesis. Estimated degrees of freedom calculated using equation 5.12 (*Wilks*, 2006) b.) as in a., but Sr/Ca. c.) as in b., but ATC13075 measurements. d.) as in c., but ATC13076 measurements

The first XRD analysis of ATC13096 powders showed some localized evidence for secondary calcite but no characteristic depletion in δ^{18}O and Sr/Ca values (Figure 4.3). Samples greater than 1% calcite had a mean of 2.9% across a range from 1.2-7%. Replication of this first analysis (black dashed lines, Figure 4.3) was equivocal with a mean percent difference in aragonite and calcite of (0.2, 0.01%, respectively). Two additional XRD analyses using the "smear method" for ATC13096 failed to replicate these initial results, showing no evidence of diagenetic alteration (*Lorrey*, 2018). XRD analyses for ATC13075 and ATC13076 had no samples greater than 1% calcite (*Lorrey*, 2018).

While the δ^{18}O dataseries did not show obvious changes, the ATC13075 and ATC13076 dataseries showed substantial localized lower Sr/Ca values suggestive of diagenetic alteration (Figure 4.3). Both corals were subaerially exposed, which can produce diagenetic alterations with depleted Sr/Ca values (*McGregor and Gagan*, 2003; *Sayani et al.*, 2011). We therefore have removed the values less than 8.5 mmol/mol from the Sr/Ca dataseries as well as the corresponding δ^{18}O aliquots and make no interpretation of climate from them.

4.3.2 Singular spectrum analysis

Singular spectrum analysis results of calculated $\delta^{18}O_{SW}$ is shown in Figure 4.4. With an embedding dimension of m=30, the first ten reconstructed components explain 82 and 83% of the variance in the modern and MCA timeseries, respectively. Choosing a smaller (m=20) and larger (m=40) embedding dimensions increases (92, 91%) and decreases (75, 77%) the total explained variance of the first ten reconstructed compo-

nents of the modern and MCA timeseries, respectively. Applying the singular spectrum analysis to the shortest MCA record, ATC13096, yields the same percent of explained variance for the first ten eigenvalues and the same percent of explained variance for the composited eigenvalues of each grouping (annual, interannual, and low frequency) within uncertainty (results not shown). Fractional uncertainty of the total variance explained (using an embedding dimension of m=30), which was calculated as the sum of uncertainty for each eigenvalue, is $\pm$10%, and the fractional uncertainty for each frequency group of composited reconstructed components is shown in Figure 4.4.

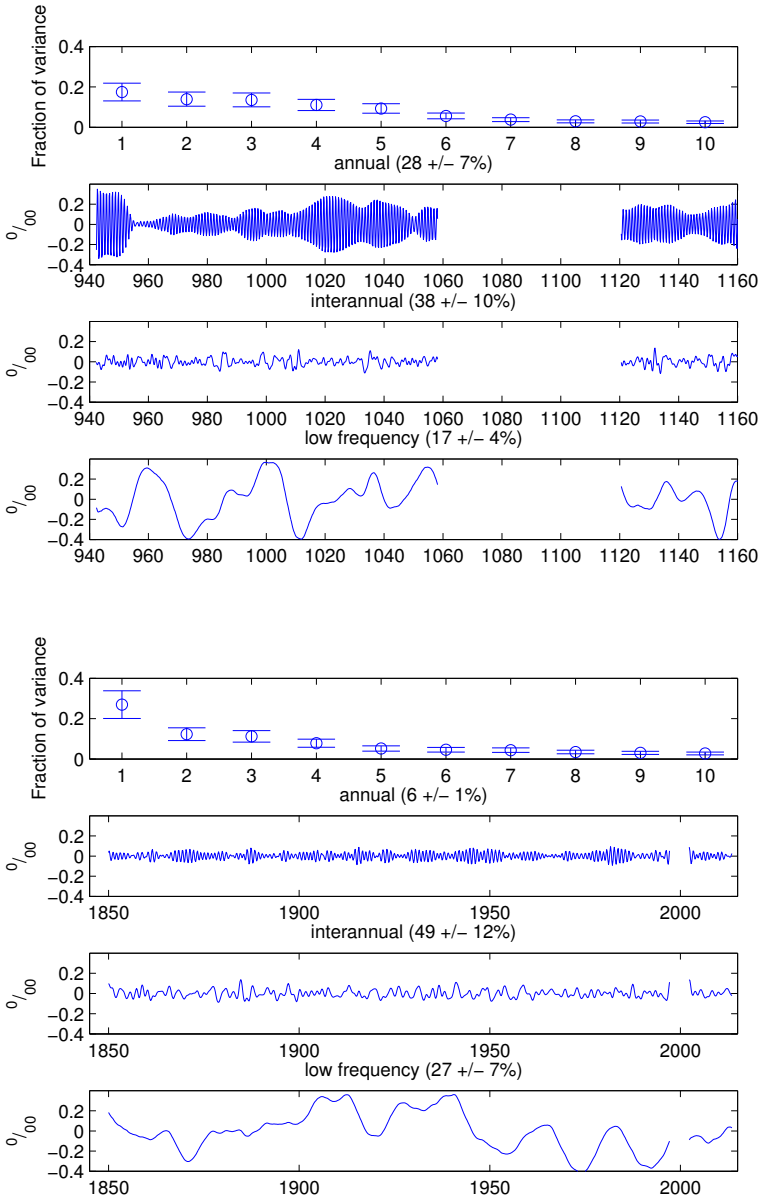

Figure 4.4: Singular spectrum analysis of modern and fossil data. Top: fraction of variance explained for individual eigenvalues of $\delta^{18}O_{SW}$ timeseries with embedding dimension of 5 years. Uncertainty estimates were calculated using Equation 3.1a,b (*Ghil and Mo*, 1991). Composited RC's of the analysis identified in the annual, interannual, and low frequency band using the multitape power spectral density (*Thomson et al.*, 2000) with explained variance in parentheses. Bottom: as in Top, but modern $\delta^{18}O_{SW}$.

4.3.3 Variance analysis results

Initial geochemical results (Figure 4.5) show similar mean offsets to modern results (Figure 3.3). ATC13075 and ATC13096, as plotted, do overlap by 1 year (1007 CE), but the uncertainty in U/Th radiometric ages (Table 4.1) is 5-6 years.

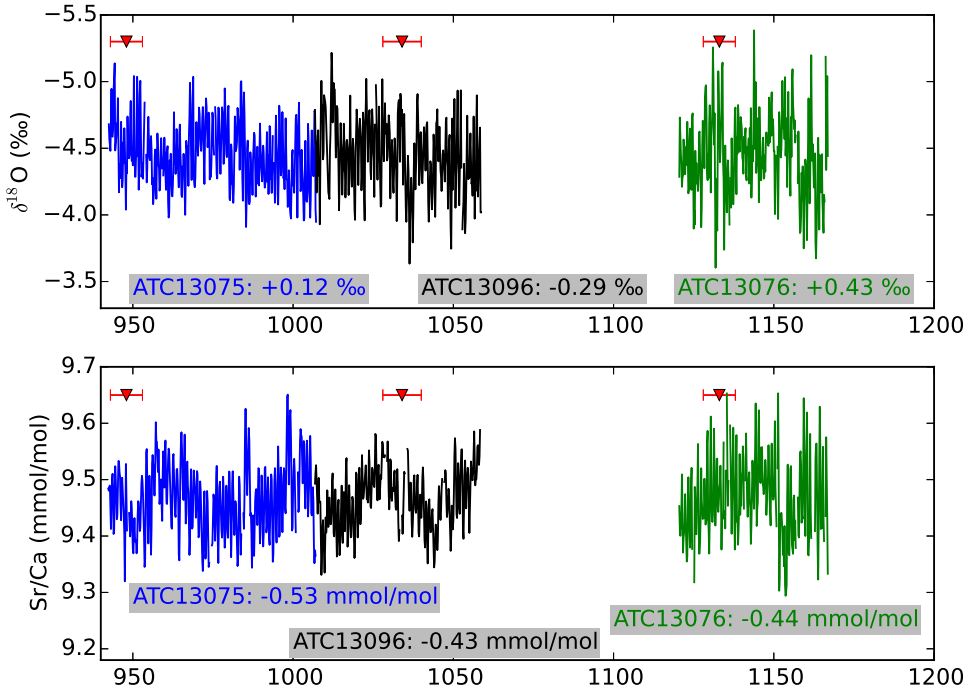

Figure 4.5: Top: Aitutaki coral δ^{18}O data (ATC13075, ATC13096, ATC13076) for the Medieval Climate Anomaly (6 samples/year) Red triangles denote U/Th dates with error (Table 4.1). ATC13075 and ATC13096 do overlap by 1 year (1007 CE) but U/Th uncertainty is greater (Table 4.1). Bottom: as in Top, but corresponding Sr/Ca data.

Fossil coral geochemical results suggests increased variability in the Medieval Climate Anomaly relative to the modern period using a common resolution of 6 samples

per year (Figure 4.6, Table 4.2). The variance of the composited interannual, detrended composited coral δ^{18}O anomaly for the MCA period (0.07‰^{2}) is higher than modern (0.024‰^{2}) (Table 4.2. This result was not sensitive to the length of timeseries after doing an F-test for the shortest individual δ^{18}O record, ATC13096 (Table 4.2).

Calculated coral $\delta^{18}O_{SW}$ also shows higher variance in the MCA relative to the modern period (Table 4.2). This results is not sensitive to averaging of individual records: interannual coral δ^{18}O timeseries have variances of 0.03, 0.03, 0.02, and 0.01‰^{2} for Rarotonga 2R (147 yr), 3R (125 yr), 99 (93 yr), and ATC13100 (11 years), respectively (blue dashed lines, Figure 4.6). The null hypothesis of equal variance in detrended, interannual, composited Sr/Ca could not be rejected (Table 4.2).

Data	**F-statistic**	**p value**	**edf**
δ^{18}O	1.37	< 0.001	41
ATC13096 δ^{18}O	1.60	< 0.001	41
δ^{18}O Composited RC's	2.22	0.001	41
$\delta^{18}O_{SW}$	1.69	< 0.001	42
$\delta^{18}O_{SW}$ Composited RC's	1.23	0.0007	42
Sr/Ca Composited RC's	0.78	0.9999	47

Table 4.2: Statistical test results: F-test for equality of variance. Comparison of variance for detrended, interannual composite of original data and reconstructed components identified in the singular spectrum analysis of calculated $\delta^{18}O_{SW}$ for the MCA (940-1160) and modern (1850-2013) periods. Effective degrees of freedom, edf, calculated using *Wilks* (2006) equation 5.12.

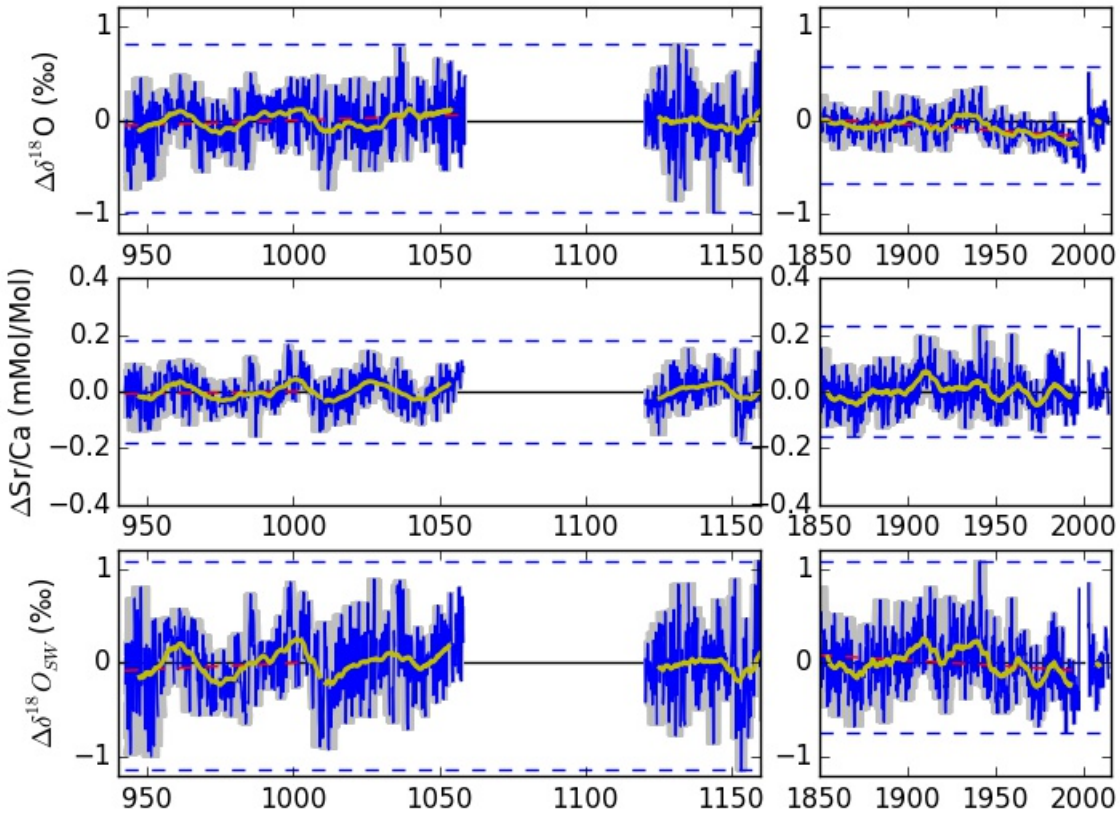

Figure 4.6: Top: Aitutaki and Rarotonga interannual coral δ^{18}O anomaly (blue) and 5-yr running mean (yellow). Records were interpolated to a common 6 points/yr and corrected for mean δ^{18}O offset using the Rarotonga 2R 1960-1990 mean. Individual coral, ATC13075, ATC13096, and ATC13075 – radiometric dates are 948±5, 1034±6, and 1133±5 C.E., respectively. Trend lines (red dashed) significant at p<0.05 or better. Maximum and minimum δ^{18}O values of individual dataseries (blue dashed horizontal lines) effect of compositing individual records. Age model uncertainty estimated using the PRYSM implementation (*Dee et al.*, 2015) of the banded age model (*Comboul et al.*, 2014) (grey shading). Middle: as in Top, but aliquot Sr/Ca measurements. Bottom: calculated $\delta^{18}O_{sw}$ from δ^{18}O and Sr/Ca data using **Equation 2**.

4.3.4 Frequency analysis results

The number of ENSO warm, neutral, and cold phase events were calculated by grouping dataseries into the lower 25th, 25th-75th, and upper 25th percentiles of the interannual frequency reconstructed component composite. Results showed similar frequencies of cold, neutral, and warm phase events in the MCA relative to the modern period (Table 4.3). The results (not shown) of the ratio of event types across time periods were insensitive to the choice of percentile cutoff (lower and upper 33rd; lower and upper 10th).

Time	**CP**	**NP**	**WP**
Medieval Climate Anomaly	28	48	24
Modern Era	22	57	22

Table 4.3: ENSO cold (CP), neutral (NP), and warm (WP) phase event counts scaled per 100 years for the Medieval Climate Anomaly (MCA) and modern (1850-present) periods calculated as the upper and lower 25th percentiles of the interannual frequency reconstructed component composite from the singular spectrum analysis.

Power spectra for each reconstructed component estimated from the multitaper method (*Thomson et al.*, 2000) and stacked according to annual, interannual, and low frequency grouping and time period are shown in Figure 4.7. Repetition of the singular spectrum analysis repeated for different embedding dimensions changed the interpretation of frequency for some individual reconstructed components. Additional analysis with a smaller (20) and larger (40) embedding dimension changed the total variance explained

Time Period	low frequency	interannual	annual
MCA	23, 17, 15	33, 38, 36	35, 28, 26
PD	33, 27, 24	46, 49, 48	13, 6, 3

Table 4.4: Range of percent explained variance for each time period (MCA, modern period) and frequency grouping (low frequency, >10 year period, interannual, 2-10 year period, annual, 1 year period) for embedding dimension choice, m=20,30,40, respectively.

from 90-93% to 95-98% (m=20) and 87-88% (m=40). The interpretation of the ninth and tenth reconstructed component did vary between annual and interannual (2-10 year period) frequency, but this change only affected the percent of explained variance by 4% at the most (results not shown). The uncertainty in explained variance for each grouping due to the choice of embedding dimension is show in Table 4.4.

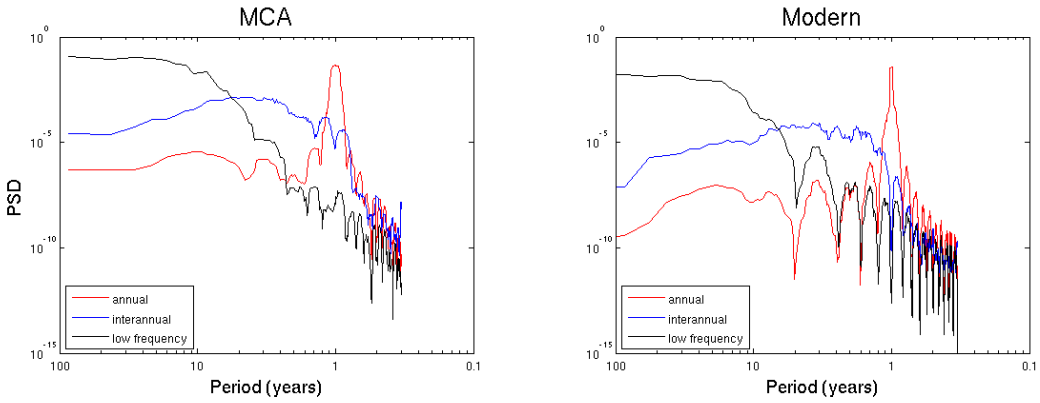

Figure 4.7: Stacked power spectral density of reconstructed components of calculated $\delta^{18}O_{SW}$ for the MCA and modern time periods using embedding dimension m=30.

4.4 Discussion

4.4.1 Diagenesis analyses

Despite some evidence of diagenesis in ATC13096 (Figure 4.3), no statistically significant mean difference between the altered and pristine geochemical data from ATC13096 was observed (Figure 4.3). If diagenesis were present, even small amounts, secondary calcite would replace the original geochemical signature of the primary aragonite, but the δ^{18}O and Sr/Ca dataseries show clear cycles in the data suggestive of the annual cycle (Figure 4.3). Neither the ATC13096 δ^{18}O nor Sr/Ca dataseries showed characteristic lower geochemical concentrations that would indicate diagenesis. In addition, the results from the "smear" method ATC13096 XRD analyses showed no evidence of diagenetic alteration. The different results between the bulk powdered samples and the "smear" method may be due to analytical differences or localized diagenetic alteration of the coral slab used for bulk powdered XRD analysis not used for the "smear" method XRD and geochemical analyses. As in *Lopatka et al.* (in prep.), the 1960-1990 Rarotonga coral Core 2R mean δ^{18}O was used to correct for individual coral offsets. ATC13096 had an offset of 0.28‰, which is of comparable magnitude to other tropical Pacific corals with no observable diagenetic alteration (*Cobb et al.*, 2003a; *Linsley et al.*, 2006) and of less magnitude than other data used in this study: the modern ATC13100 coral offsets were -0.42, -0.34‰ for the left- and right-side milled tracks, respectively (*Lopatka et al.*, in prep.).

But results for ATC13075 and ATC13076 showed localized lower Sr/Ca values from expected values of approximately 9 mmol/mol to values of 8 mmol/mol and as

low as 6.5 mmol/mol. Previous literature has shown that subaerial diagenesis can lower Sr/Ca values due to dissolution and precipitation processes within an open system, which redistribute trace metals in the coral archive (*McGregor and Gagan*, 2003; *Sayani et al.*, 2011). Using the average of the calibration slopes produced for Rarotonga (*Linsley et al.*, 2000, 2004), observed depletions of 1 to 3.5 mmol/mol in Aitutaki Sr/Ca data would result in SST values of +14-48^{o}C – clearly unrealistic temperature variations. We have therefore removed these values from all dataseries before any further data analyses or interpretation. Given these geochemical results and the current understanding of diagenesis in corals, we feel confident that the variations in the dataseries analyzed here are interpretable as climate-driven rather than diagenetic alteration.

Individual corals also show inter-colony variability (*McGregor et al.*, 2011). Previously reported Rarotonga data had inter-colony variability in Sr/Ca of 0.08 to 0.1 mmol/mol (± 0.11 mmol/mol) (*Linsley et al.*, 2006). The mean inter-colony variability in Sr/Ca between Aitutaki corals (including the live, modern ATC13100 sample) was 0.089 mmol/mmol ($1\sigma = 0.13$). These standard deviations calibrated to temperature correspond to 1.5-1.8^{o}C. Aitutaki corals were centered to the Rarotonga 2R 1960-1990 mean, and had a mean offset of 0.514 mmol/mmol ($1\sigma = 0.089$, or 1.8^{o}C). Aitutaki coral δ^{18}O had a mean offset of -0.21‰($1\sigma = 0.31$), which is similar to variation in individual coral δ^{18}O reported previously in the literature of 0.1-0.4‰ (*Cobb et al.*, 2003a; *Guilderson and Schrag*, 1999; *Hereid et al.*, 2013; *Linsley et al.*, 2006; *McGregor et al.*, 2011). Given the similarity of our results to previous studies and the similarity in the magnitude of offsets between fossilized and live, modern samples, it appears these Aitutaki corals are not impacted by diagenesis.

4.4.2 Age Modeling

The PRYSM implementation (*Dee et al.*, 2015) of the banded age model (*Comboul et al.*, 2014) using 1,000 estimates of the age model error of the dataseries showed age model uncertainty for modern results of less than one year, but this uncertainty estimate increased back in time to an error as high as a few years for an individual geochemical measurement (Figure 4.6). A single U/Th radiometric sample was measured for each coral record, but additional measurements for each coral could reduce this age model uncertainty (*Cobb et al.*, 2003a; *DeLong et al.*, 2012; *Hereid et al.*, 2013). The period known as the Medieval Climate Anomaly has different estimates for its beginning and end (*Cook et al.*, 2004; *Diaz et al.*, 2011; *Goodwin et al.*, 2014; *Graham et al.*, 2011; *Lamb*, 1965; *Mann et al.*, 2009). But the reconstructed coral paleoclimate observations fall well within this range.

4.4.3 Frequency analysis

No long term trend was found in the singular spectrum analysis of fossil coral δ^{18}O and Sr/Ca (Figure 4.4). Small magnitude trends found in the δ^{18}O and Sr/Ca anomaly results were not identified in the singular spectrum analysis, but composited low frequency ($>$10 year period) components show periodic fluctuations well approximated by a five-year running mean (Figure 4.6, 4.4). The highly variable δ^{18}O and Sr/Ca results suggests that Aitutaki during the Medieval Climate Anomaly was characterized by changing periods of warmer/wetter and cooler/dryer conditions.

Composited interannual $\delta^{18}O_{SW}$ reconstructed components from the analysis show

reductions in amplitude in the mid 900s C.E. and the mid 1100s C.E. (Figure 4.4). A similar feature in the mid 900s C.E. of the reconstructed Sr/Ca components is seen too (Figure 4.4). This suggests a perhaps wetter period in the mid 1100s C.E. and a possibly warmer/wetter period in the mid 900s compared to the preceding and following decades. But, these variations in $\delta^{18}O_{SW}$ amplitude are not entirely resolvable from each other given the fractional uncertainty of 36% per data point.

Singular spectrum analysis of modern δ^{18}O show some differences than their MCA counterparts (Figure 4.4). The modern δ^{18}O low frequency component shows a trend from cooler/dryer to warmer/wetter conditions, which agrees, in sign, with anthropogenic warming trends of sea surface temperature over the Industrial Era (*Deser et al.*, 2010; *McGregor et al.*, 2015). Interannual δ^{18}O explains less variance in the modern (23%) relative to the fossil (34%) period. The component of δ^{18}O associated with annual frequency (<2 year period) are not much different between the modern (41%) and fossil (42%) periods.

The unexplained variance in the singular spectrum analysis of 9-21% has been explained in previous literature as a biological effects of the coral organism not related to climate (*Evans et al.*, 1999; *Linsley et al.*, 2000). Explained variance changed by 1-8 percentage points when choosing an embedding dimension smaller (20) and larger (40) than the results reported using an embedding dimension, m=30 (Table 4.4). Interpretation of the seventh, eighth, ninth and tenth RC as representing annual or interannual variation did change depending upon the choice of embedding dimension. The rank of the low frequency reconstructed component varied from the first to the third component depending on embedding dimension. These differences are sufficient to explain the changes in total and partially (annual, interannual, low frequency) explained variance. Given the observa-

tional uncertainty in calculated $\delta^{18}O_{SW}$ of 36% as well as the simplifying assumptions of the coral proxy system model (*Lopatka et al.*, in prep.; *Thompson et al.*, 2011), it would be unexpected to explain all variance in the dataseries from climate.

4.4.4 Past SPCZ, ENSO variability

Aitutaki and Rarotonga experience interannual climate variations associated with hydroclimatological variability in the south Pacific driven by changes in the position of the South Pacific Convergence Zone and the phase of the El Niño-Southern Oscillation (*Delcroix et al.*, 2011; *Folland et al.*, 2002; *Gouriou and Delcroix*, 2002; *Hasson et al.*, 2013; *Lopatka et al.*, in prep.; *Lorrey et al.*, 2012; *Picaut et al.*, 1996; *Salinger et al.*, 2001, 1995; *Vincent*, 1994; *Widlansky et al.*, 2012). Therefore, analysis of Aitutaki $\Delta\delta^{18}O_{SW}$ timeseries, calculated using aliquots of coral δ^{18}O and Sr/Ca and the methodology from *Lopatka et al.* (in prep.); *Ren et al.* (2002); *Thompson et al.* (2011) are interpreted as arising from changes in the position of the SPCZ and phase of ENSO. Results from the intervals of the Medieval Climate Anomaly show that $\Delta\delta^{18}O_{SW}$ from this location explains 74% of the variation in the coral δ^{18}O timeseries (Figure 4.8). The regression slope for the $\Delta\delta^{18}O_{SW}$ data of 1.24±0.06 suggests larger amplitude variations than the coral δ^{18}O data that would plot on the 1:1 line (dashed black, Figure 4.8). The regression slope of 0.24±0.06 for the $\Delta\delta^{18}O_{SST}$ suggests the SST signal may have some destructive interference with the $\delta^{18}O_{SW}$ signal. Modelling of interannual δ^{18}O as a function of SST and SSS (Figure 3.2) does show a difference in sign between $\delta^{18}O_{SSS}$ and $\delta^{18}O_{SST}$ over results of composited April, May, and part of June (1975-2009 CE) data. Future analyses of the oxygen isotope composition of surface seawater samples may also help further test

the validity of the proxy system model as an approximately linear, bivariate representation of Aitutaki coral δ^{18}O (*Thompson et al.*, 2011).

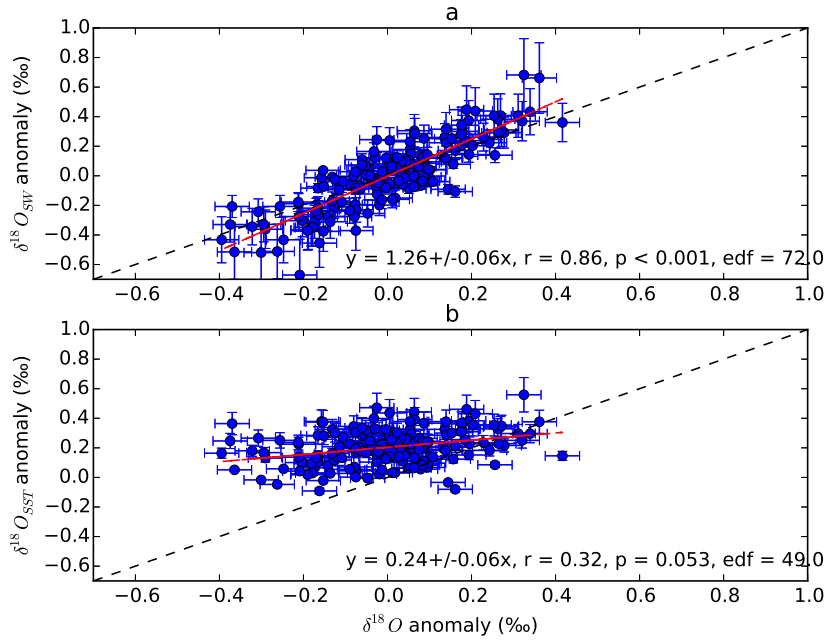

Figure 4.8: a.) The oxygen isotope composition of seawater, $\delta^{18}O_{SW}$ (3.1) versus the coral δ^{18}O timeseries, Apr-Mar annual average and detrended anomalies. The ordinary least squares regression (red) is shown with linear equation and statistics. The 1:1 line is shown in black. Error bars show the calculated fractional percent uncertainty following propagation of errors (*Taylor*, 1997) in 3.1. Effective degrees of freedom, edf, is calulated using *Wilks* (2006) eq. 5.12. b.) same as a.), but for $\delta^{18}O_{SST}$ component.

The $\delta^{18}O_{SW}$ timeseries shows periodic decadal fluctuations of 0.2-0.3‰ (thick yellow line, Figure 4.6) in addition to large interannual variations of almost 1‰. A significant long term trend in the earlier interval (942-1058 C.E.) suggests a change in mean state from warmer/wetter to cooler/dryer conditions. Calculated variance in the MCA period ($0.13‰^2$) is significantly larger than the modern period ($0.08‰^2$) and not sensitive

to the number of available observations (Figure 4.6). This suggests ENSO behavior with periodic warm and cold phase events which may impact climate in the south Pacific based on changes in the amplitude of $\delta^{18}O_{SW}$ over time (Figure 4.6). During the MCA, with most of the variation in the interannual coral $\delta^{18}O$ timeseries explained by seawater $\delta^{18}O$ variation (Figure 4.8), we interpret the variability in the interannual coral $\delta^{18}O$ data from the fossil period to reflect changes in SPCZ position. Periodic decadal fluctuations of coral $\delta^{18}O$ (Figure 4.4) suggests a decadal component to changes in the SPCZ position *Linsley et al.* (2008).

While calculated coral $\delta^{18}O_{SW}$ interannual measurements explain the majority of the variance, some variation is from the $\delta^{18}O_{SST}$ component (Figure 4.8), in agreement with modern Aitutaki/Rarotonga results (*Lopatka et al.*, in prep.). Changes in the position of the SPCZ could produce a change in sea surface temperature in addition to seawater $\delta^{18}O$ so these differences could perhaps result from a long term displacement in the mean position of the SPCZ (*Linsley et al.*, 2006, 2008). Modelling of SPCZ dynamics with 21st century forcings suggests two mechanisms: on one hand, warming of mean SSTs may increase atmospheric moisture and produce an enhanced hydrological cycle ("wet gets wetter" hypothesis) (*Widlansky et al.*, 2012). On the other hand, if SSTs increase more in localized regions, atmospheric moisture may have focused convergence over these areas and produce a "warmest gets wetter" dynamic response to 21st century forcing (*Widlansky et al.*, 2012). If the mean SPCZ position moved equatorward sometime after the MCA, Aitutaki would be cooler/dryer, supporting the "warmest gets wetter" hypothesis, whereas the larger impact of $\delta^{18}O_{SW}$ in the MCA resulted from Aitutaki being centered along the mean SPCZ position.

Spectral analysis of calculated $\delta^{18}O_{SW}$ shows results with different percentages of explained variance relative to the $\delta^{18}O$ and Sr/Ca singular spectrum analyses (Figure 4.4, 4.4). Interestingly, the amount of variance explained by the interannual composite is higher in the modern period (49%) relative to the MCA (38%). More variance is explained by a low frequency reconstructed component in the modern (27%) relative to the MCA (17%).

The annual variations only explain 6% in the modern timeseries but 28% in the MCA timeseries. Large increases in annual cycle amplitude are observed in the mid 900's C.E. and early-mid 1000s C.E.. Such variations could indicate periods of enhanced precipitation or dryness with decreased and increased $\delta^{18}O_{SW}$ values, which could stem from an intensification or weakening of the South Pacific Convergence Zone over time. But the power spectra of each composited reconstructed components frequency group shows some power "leaking" into other frequency domains Figure (4.7). Together with fractional uncertainty of 36% for the calculated $\delta^{18}O_{SW}$ timeseries, these sources of observational uncertainty make it difficult to fully evaluate the causes of potential changes in annual cycle amplitude over time and the fraction of variance explained by each reconstructed component of the singular spectrum analysis.

4.4.5 Hypotheses of Medieval Climate Anomaly variability

The available information for external radiative forcing during the MCA shows volcanic eruptions with smaller magnitude forcing (*Gao et al.*, 2008; *Jungclaus et al.*, 2010; *Sigl et al.*, 2015) relative to the Little Ice Age period following the MCA, small and stable well-mixed greenhouse gas concentrations relative to modern (*Schmidt et al.*,

2011), and solar irradiance similar to modern observations (*Ammann et al.*, 2007).

Volcanic research has shown large, tropical eruptions can produce a strong ENSO warm phase response (*Emile-Geay et al.*, 2008; *Stevenson et al.*, 2016), although some model simulations suggest a cold phase response (*McGregor and Timmermann*, 2011). Climate model simulations forced with a doubling of carbon dioxide concentrations resulted in a reduction of the Walker Circulation, and a weakening of ocean dynamical cooling throughout the equatorial Pacific that produces conditions more similar to ENSO cold phase conditions (*DiNezio et al.*, 2009). But the presence of aerosols and unforced variation of the climate system resulted in a dampened sensitivity of the Walker Circulation to external radiative forcing such as increased greenhouse gases (*DiNezio et al.*, 2013).

The null hypothesis of equal variance in coral geochemical data between modern and past periods from Aitutaki and Rarotonga of the southwestern tropical Pacific was rejected based on evidence from statistical tests for equal variances between samples of the same population (Table 4.2). This result is not in agreement with event count frequency analysis which suggests reasonably similar frequencies of El Niño and La Niña) events in the MCA relative to the modern period (Table 4.3). This ENSO-related interannual variance difference between the MCA and modern period is a result not sensitive to data treatment and specific to the interannual variability that was calibrated for interpretation (Chapter 3).

Given the relatively weak external radiative forcings of the MCA relative to the modern period, a simple explanation for significant interannual variability in the MCA relative to the modern period is an unforced climate system producing significant varia-

tion because of dynamics of the coupled ocean-atmosphere system (*Fernández-Donado et al.*, 2013; *Otto-Bliesner et al.*, 2016; *Schurer et al.*, 2013). The limited reconstructions of land use during the MCA, however, is a source of uncertainty, that one study suggests has increased the incidence of warm phase ENSO conditions in the 20th century (*Stevenson et al.*, 2017). Observational uncertainty of this analysis includes the error in calculated $\delta^{18}O_{SW}$ measurements (Figure 4.8), in the eigenvalues of the singular spectrum analysis (Figure 4.4), the leakage of spectral power across frequency groupings (Figure 4.7), and the uncertainty in interpreting results for the tropical Pacific from a single coral paleoclimate record (*DeLong et al.*, 2007a).

4.5 Conclusions

New paired $\delta^{18}O$ and Sr/Ca measurements were made on diagenetically screened corals collected from Aitutaki, southern Cook Islands of the southwestern tropical Pacific radiometrically dated to the Medieval Climate Anomaly. Variance of interannual $\delta^{18}O$ and calculated $\delta^{18}O_{SW}$ anomalies was increased relative to the modern Rarotonga (*Linsley et al.*, 2006) and Aitutaki composited record. Singular spectrum analysis of the timeseries shows a large component of the total variance can be explained by the first 10 reconstructed components of the $\delta^{18}O_{SW}$ timeseries, with significant variance explained by the composited interannual and low frequency components. Reductions in amplitude during intervals in the MCA suggest reduced ENSO activity and stability in the position of the SPCZ. But, large changes in interannual $\delta^{18}O_{SW}$ throughout the period studied suggests periods of warmer/wetter and cooler/dryer conditions. Decadal timescale periods of warmer/wetter and cooler/dryer climate as well as a long term trend toward cooler/dryer

conditions from an earlier warmer/wetter period suggests a MCA more variable relative to the modern period, which may result from large unforced variations of the coupled ocean-atmosphere climate system.

Chapter 5: Conclusion

5.1 Chapter 2 summary

Analysis of available oceanographic paleoclimate records spanning intervals of the MCA, LIA, and PD suggests no difference in interannual variance between time periods. Analysis of multi-model composites in the locations where observations are available, the NINO3.4 region, and the full-field tropical Pacific agree with observations and suggest no difference in interannual variance between the MCA, LIA, and PD. Counting ENSO events using percentile binning of observation and model data show little variation in the number of warm, neutral, and cold phase events throughout the last 1,000 years.

The less than annual resolution subset of the observations used in this analysis showed an increase in variance from the MCA to the LIA. However, this subset uses data from just three locations. The CCSM4 model shows increased variance in the MCA and LIA relative to the PD, a pattern not found in the other model results. Additional observations from only the LIA show no substantial difference in variance relative to the PD.

The results from observations and models suggest ENSO is not particularly sensitive to the changing external radiative forcings over the past millennium. The results may be explained by the dynamic, unforced, internal variability of the coupled ocean-

atmosphere climate system. Improvements may be possible with additional observations spanning key periods of the past millennium, especially for the MCA and the Southern Hemisphere.

5.2 Chapter 3 summary

New coral geochemistry measurements were collected for a modern Aitutaki coral that was composited with existing coral geochemical measurements from another southern Cook Island – Rarotonga. Interannual coral δ^{18}O results agreed with calculated synthetic interannual δ^{18}O results, which suggests observations are primarily a function of sea surface temperature and the oxygen isotope composition of seawater. Modelling of synthetic δ^{18}O showed that most of the total variation of interannual coral δ^{18}O in the southern Cook Islands could be explained by the $\delta^{18}O_{SW}$ component, calculated from paired coral δ^{18}O and Sr/Ca measurements.

These modern period results suggest interannual coral δ^{18}O measurements from the southwestern Pacific are sensitive to changes in the position of the South Pacific Convergence Zone. On interannual timescales, this convergence zone redistributes heat and moisture towards the equator during the warm phase of the El Niño-Southern Oscillation and towards the South Pole during the cold phase. Spatial correlation of anomalies for Aitutaki climate variables with synthetic δ^{18}O and coral δ^{18}O resemble the spatial pattern of sea surface temperature and salinity during ENSO warm and cold phase, which suggests this location may be sufficient to identify ENSO variability in the past before the instrumental era.

5.3 Chapter 4 summary

New fossil coral geochemistry measurements were collected from three diagenetically-screened Aitutaki samples radiometrically dated to the early millennium in the Medieval Climate Anomaly time period. Variance of calculated interannual $\delta^{18}O_{SW}$ was greater during the MCA relative to the modern period. This result was not sensitive to selected removals of portions of the dataseries, the number of individual records, and specific to the interannual variation in the timeseries identified as ENSO-related in Chapter 3. A five-year running mean of the data showed decadal variations suggesting prolonged periods of warmer/wetter and cooler/dryer conditions. Interannual coral $\delta^{18}O$ and Sr/Ca results for the earlier MCA period had a small but statistically significant trend over the length of the time series from warmer/wetter to cooler/dryer conditions. Calculated $\delta^{18}O_{SW}$ showed similar results, suggesting the interannual ENSO-related signal at Aitutaki is driven primarily from hydrological variations related to changes in the position of the South Pacific Convergence Zone.

Singular spectrum analysis of the data suggested a large component of the total variability came from the interannual (2-10 year period) frequency band. Pairs of eigenvalues which explained similar amount of variance for different dataseries suggest quasi-periodic oscillatory behavior not unlike the El Niño-Southern Oscillation. No long term trends were detected in the data, which may be due to the fact that no trends were observed in the late MCA which was included with the early MCA data in the analysis.

Given the results from Chapter 3, the fossil coral results suggest a variable early millennium climate with no long term trends but significant interannual and decadal vari-

ability. Modern and fossil results show $\delta^{18}O_{SW}$ as a significant source of variation, which can be interpreted as a response to changes in the position of the South Pacific Convergence Zone driven, at least in part, by ENSO warm and cold phase activity over time. The few MCA records available for comparison also conclude that this time period was marked by significant interannual and decadal variability with a potential slow transition from warmer/wetter to cooler/dryer conditions *Cobb et al.* (2003a); *Li et al.* (2011); *Oppo et al.* (2009); *Sachs et al.* (2009); *Thompson et al.* (2013b)

5.4 ENSO in the 21st century

The motivating question for this project has been how El Niño-Southern Oscillation amplitude and frequency may change in response to 21st century external radiative forcing. The model simulation results from Chapter 2 suggested no difference in interannual variance between different time periods of the past millennium which had similar external radiative forcing from solar irradiation, greenhouse gas concentration, volcanism, and land use. But, the small number of available paleoclimate records is a significant source of uncertainty in this interpretation. Compositing different records of climate variation from locations with different sensitivities to ENSO or in the magnitude of their response to ENSO may limit the interpretations which can be drawn from the results. Model biases (*Phipps et al.*, 2013), particularly for SPCZ position (*Brown et al.*, 2012b; *Widlansky et al.*, 2012) also contribute uncertainty in the analyses of Chapter 2. The influence of well-mixed greenhouse gases, one of the most plausible forcing mechanisms of the 21st century, is difficult to test in a paleoclimate context because that forcing was small over the past millennium (*Schmidt et al.*, 2011).

Additional observations made from new measurements of Aitutaki coral dated to the Medieval Climate Anomaly from Chapter 4 suggest increased variance in calculated interannual coral $\delta^{18}O_{SW}$ relative to the modern time period with no observable difference in frequency as inferred from an event count analysis and the similar percentage of variance explained, within uncertainty, by composited interannual frequency (2-10 year period). The interpretation from these results would suggest that ENSO activity changed the position, and perhaps the intensity, of the South Pacific Convergence Zone. Uncertainty arises from the unreplicated coral archive, the limited length of the record, the possibility of spectral leakage between frequency groups, the large uncertainty in calculated $\delta^{18}O_{SW}$ arising from the propagation of errors, and the difficulty of capturing an ENSO signal from a single point location in the tropical Pacific.

ENSO frequency changes, inferred from paleoclimate records, may be used to better understand the mean climate state of the tropical Pacific and the external radiative forcings operating on that system (*Fedorov and Philander*, 2000). In this interpretational framework, the frequency of ENSO warm phase may vary as a function of the delayed oscillator model. The first state in this framework is produced from a deep thermocline in the eastern equatorial Pacific and strong westerly winds (what the literature refers to as "canonical" El Niño). The second state of the tropical Pacific described has wind convergence east of the central equatorial Pacific with little to no change in the eastern equatorial Pacific thermocline (known as El Niño "Modoki").

The frequency of ENSO results in Chapter 2 and Chapter 4 (which is compared to Chapter 3) shows little to no change in the number of warm phase events per 100 years, suggesting a stable frequency of ENSO activity over time. Within the delayed oscillator

model framework, the paleoclimate results suggest a relatively stable background state despite the changing external radiative forcings. The variation in calculated interannual, ENSO-related Aitutaki $\delta^{18}O_{SW}$ observations may arise from unforced variation of the coupled ocean-atmosphere climate system. This interpretation, however, is limited by uncertainty from the simplification of the climate state into an intermediate complexity (delayed oscillator) model, the few paleoclimate records available through which to test this hypothesis, the error in the coral paleoclimate observations, and the error in the past millennium forcings themselves.

5.5 Future research

Additional corals from the southern Cook Islands would allow for replication of results and provide more than one realization of coral $\delta^{18}O$ during intervals of the past millennium. Such efforts would reduce the observational uncertainties described in Chapters 2-4. The coral archive curated at the National Institute of Atmospheric Research has several additional coral "candidates" that could be in good condition and may date to periods of interest in the past millennium.

More quality control testing of corals has been proposed in the literature *Sayani et al.* (2011). Supplementing the best practices described here with a more systematic analysis of thin section mapping would benefit coral paleoclimatology (*Lopatka et al.*, 2015). Drilling of coral cores is a common method to extract a relevant portion of in-situ or beached coral boulders, followed by cutting of the core into slabs suitable for geochemical analyses and quality control analyses. Rather than selecting just a few locations along the slab interface, thin sections should be collected along the entire slab which mirrors

the slab used in geochemical analyses. Continuous thin sectioning of this kind would allow for localized assessment of diagenetic alteration at a higher precision than the current standard practice.

Additional local field site data collection may improve coral paleoclimatology-based climate reconstruction efforts. The standard techniques used often compare a modern-aged coral with estimates of local climate variables obtained from satellite, or gridded data products with at best 1^o precision but sometimes even coarser resolution. Improved calibration of coral geochemical measurements to local and regional climate could be realized with additional data collected during field expeditions. Given the interest of the PAGES2k community to produce better reconstructions of hydroclimate variability, water samples, wind measurements, as well as biological and environmental data may improve our understanding of coral growth. Water samples, for example, would enable the comparison of coral δ^{18}O directly to seawater δ^{18}O . Data logger instruments without much upkeep can be deployed at the beginning of a field season for in-situ data collection (*Pereira et al.*, 2017). The collection of δ^{13}C, for example, is now common practice during acquisition of δ^{18}O measurements and a rich archive of data awaits one who wishes to better understand the relationship between coral δ^{13}C and climate. Similarly, developing routine collection of local environmental data with corals can result in improved results and a better understanding of the uncertainties in coral paleoclimatology techniques.

Another research trend has been in the comparison of data with results from model simulations. Significant advances in temperature reconstructions of the past 2,000 years have been due, in part, to data model comparisons. The techniques applied to temperature, however, do not translate well for reconstructions hydroclimate. Best practices for com-

paring data and models to better understand hydroclimate are emerging (*Smerdon et al.*, 2017). Using outputs of simulations to drive the coral proxy system model and comparing these results to actual observations across a network of sites may yield new insights into the spatial extent and time-varying character of hydroclimate over the tropical Pacific. A study focused on southwestern tropical Pacific coral sites in conjunction with appropriate model output may provide new understanding of ITCZ and SPCZ variability.

Additional research comparing the relative contributions of forced and unforced variability may help better answer how ENSO responds to these different mechanisms. Models of intermediate complexity, such as the *Zebiak and Cane* (1987) model or the delayed oscillator used in *Fedorov and Philander* (2000) should be compared to coupled general circulation models drive with realistic external radiative forcings, such as those from the Modelling Intercomparison Project. The sixth and fourth phase of the historical and paleoclimate intercomparison project simulations will be completed soon and could advance the representation of climate phenomena such as ENSO and decadal to centennial scale tropical Pacific variability.

Appendix A: Data

A.1 ATC13100

ATC13100				
depth (mm)	$\delta^{18}O$	$\delta^{13}C$	r/Ca (mmol/mo	age_model
002	-4.90	-2.54	NaN	2002.17
004	-4.90	-2.29	NaN	2002.2
005	-4.90	-2.24	8.75	2002.23
006	-4.83	-1.61	NaN	2002.26
007	-4.93	-2.29	NaN	2002.29
008	-4.99	-2.09	NaN	2002.32
009	-4.92	-2.32	NaN	2002.35
010	-4.88	-1.84	8.76	2002.38
011	-4.77	-1.45	NaN	2002.41
012	-4.58	-1.89	NaN	2002.44
013	-4.61	-2.36	NaN	2002.47
013	-4.64	-2.46	NaN	2002.5
015	-4.61	-1.92	8.92	2002.54
016	-4.60	-1.95	NaN	2002.57
017	-4.66	-2.27	NaN	2002.6
018	-4.75	-2.67	NaN	2002.63
020	-4.86	-2.28	NaN	2002.66
021	-4.72	-2.14	8.82	2002.69
022	-5.08	-2.48	NaN	2002.72
022	-5.02	-2.48	NaN	2002.75
023	-5.20	-2.61	NaN	2002.77
024	-5.06	-1.56	NaN	2002.8
025	-4.97	-0.9	8.83	2002.82
025	-4.76	-1.27	NaN	2002.85
026	-4.80	-2.05	NaN	2002.87
026	-4.86	-1.86	NaN	2002.89
027	-4.73	-1.98	NaN	2002.92
028	-4.74	-1.82	8.91	2002.94
028	-4.65	-1.64	NaN	2002.96
029	-4.54	-1.6	NaN	2002.99
029	-4.65	-1.38	NaN	2003.01
030	-4.47	-1.48	NaN	2003.04
030	-4.54	-1.75	8.89	2003.06
031	-4.64	-1.97	NaN	2003.08
032	-4.55	-2.11	NaN	2003.11
032	-4.81	-2.16	NaN	2003.13
033	-4.55	-2.21	NaN	2003.16
033	-4.63	-2.33	8.81	2003.18
034	-4.86	-2.38	NaN	2003.2
034	-4.67	-2.55	NaN	2003.23
035	-5.01	-2.53	NaN	2003.25
036	-5.11	-2.36	NaN	2003.29
036	-5.08	-2.12	NaN	2003.33
037	-4.92	-1.77	NaN	2003.37
037	-5.00	-2	NaN	2003.4
038	-4.97	-2.1	NaN	2003.44
038	-4.91	-2.17	NaN	2003.48

039	-5.06	-2.04	8.78	2003.52
040	-5.03	-1.76	NaN	2003.56
041	-4.95	-1.7	NaN	2003.6
041	-4.82	-1.45	NaN	2003.63
042	-4.90	-2.05	NaN	2003.67
042	-5.06	-2.2	8.85	2003.71
043	-4.98	-2.37	NaN	2003.75
043	-5.09	-1.96	NaN	2003.79
043	-5.00	-1.92	NaN	2003.82
044	-4.86	-2.23	NaN	2003.86
044	-5.02	-2.59	8.91	2003.89
045	-4.48	-1.66	NaN	2003.93
045	-5.20	-2.34	NaN	2003.96
046	-5.11	-2.75	NaN	2004
046	-4.89	-2.44	NaN	2004.04
047	-4.73	-2.24	8.89	2004.07
048	-4.79	-2.43	NaN	2004.11
048	-5.23	-2.79	NaN	2004.14
049	-5.19	-2.43	NaN	2004.18
049	-5.09	-2.11	NaN	2004.21
050	-5.04	-2.14	8.76	2004.25
050	-5.11	-1.78	NaN	2004.28
051	-5.21	-1.82	NaN	2004.31
051	-5.30	-2.21	NaN	2004.34
052	-5.22	-2.11	NaN	2004.37
052	-5.02	-1.84	8.75	2004.4
053	-4.99	-1.7	NaN	2004.43
053	-4.91	-1.36	NaN	2004.46
054	-4.89	-1.71	NaN	2004.49
054	-4.93	-1.52	NaN	2004.51
055	-4.55	-1.64	8.82	2004.54
055	-4.89	-1.91	NaN	2004.57
056	-4.65	-1.79	NaN	2004.6
056	-4.69	-1.8	NaN	2004.63
057	-4.56	-2.15	NaN	2004.66
057	-4.78	-2.5	8.88	2004.69
058	-5.02	-2.73	NaN	2004.72
059	-4.60	-2.17	NaN	2004.75
059	-4.92	-2.47	NaN	2004.77
060	-4.78	-2.61	NaN	2004.79
061	-4.79	-2.46	8.77	2004.82
061	-5.19	-2.46	NaN	2004.84
062	-4.88	-2.46	NaN	2004.86
062	-5.19	-2.21	NaN	2004.88
063	-5.16	-2.14	NaN	2004.9
063	-5.23	-1.77	8.79	2004.92
064	-5.34	-1.89	NaN	2004.95
064	-4.99	-1.89	NaN	2004.97
065	-5.33	-1.58	NaN	2004.99

065	-5.01	-1.86	NaN	2005.01
066	-4.79	-1.82	8.73	2005.03
066	-4.96	-1.93	NaN	2005.05
067	-4.97	-1.66	NaN	2005.08
067	-4.90	-1.63	NaN	2005.1
068	-4.90	-1.69	NaN	2005.12
068	-4.93	-1.74	8.77	2005.14
069	-4.80	-1.61	NaN	2005.16
069	-4.81	-1.9	NaN	2005.19
070	-4.76	-1.47	NaN	2005.21
070	-4.60	-1.49	NaN	2005.23
071	-4.58	-1.64	8.87	2005.25
071	-4.75	-2	NaN	2005.28
072	-4.68	-2.1	NaN	2005.3
072	-4.67	-2.26	NaN	2005.33
073	-4.70	-1.96	NaN	2005.36
073	-4.75	-1.99	8.81	2005.38
074	-4.81	-2.24	NaN	2005.41
074	-4.79	-2.45	NaN	2005.43
075	-4.89	-2.26	NaN	2005.46
075	-4.89	-2.26	NaN	2005.49
076	-4.97	-2.53	8.81	2005.51
076	-5.01	-2.31	NaN	2005.54
077	-5.02	-2.27	NaN	2005.57
077	-5.01	-2.29	NaN	2005.59
078	-4.95	-1.98	NaN	2005.62
078	-4.94	-2.01	8.75	2005.64
079	-4.93	-1.69	NaN	2005.67
079	-5.00	-1.7	NaN	2005.7
080	-5.05	-1.56	NaN	2005.72
080	-5.00	-1.79	NaN	2005.75
081	-4.86	-1.51	8.75	2005.79
081	-4.87	-1.69	NaN	2005.83
082	-4.89	-2.02	NaN	2005.87
082	-4.91	-1.88	NaN	2005.9
083	-4.69	-2.05	NaN	2005.94
083	-5.03	-1.8	8.79	2005.98
084	-4.80	-2.26	NaN	2006.02
084	-4.65	-1.94	NaN	2006.06
085	-4.76	-2.28	NaN	2006.1
085	-4.70	-2.09	NaN	2006.13
086	-4.58	-2.31	8.84	2006.17
086	-4.80	-2.27	NaN	2006.21
087	-4.97	-2.2	NaN	2006.25
087	-4.78	-2.37	NaN	2006.28
087	-4.85	-2.46	NaN	2006.31
088	-4.65	-2.56	8.8	2006.33
088	-4.83	-2.54	NaN	2006.36
089	-4.87	-2.53	NaN	2006.39

089	-5.11	-2.46	NaN	2006.42
090	-5.27	-2.44	NaN	2006.44
090	-5.10	-2.82	8.76	2006.47
091	-5.18	-3.16	NaN	2006.5
091	-5.05	-2.01	NaN	2006.53
092	-5.24	-2.11	NaN	2006.56
092	-5.24	-2.23	NaN	2006.58
093	-5.08	-2.36	8.72	2006.61
093	-5.14	-2.22	NaN	2006.64
094	-5.27	-1.86	NaN	2006.67
094	-5.40	-1.58	NaN	2006.69
095	-5.21	-1.65	NaN	2006.72
095	-5.04	-1.45	8.75	2006.75
096	-5.01	-1.81	NaN	2006.78
096	-4.98	-1.68	NaN	2006.81
097	-4.97	-1.98	NaN	2006.84
097	-4.81	-1.77	NaN	2006.88
098	-4.91	-1.52	8.8	2006.91
098	-4.89	-1.64	NaN	2006.94
099	-4.98	-2	NaN	2006.97
099	-4.79	-1.65	NaN	2007
100	-4.84	-1.83	NaN	2007.03
100	-5.02	-2.17	8.82	2007.06
101	-5.00	-2.22	NaN	2007.09
101	-4.92	-2.12	NaN	2007.13
102	-4.73	-2.08	NaN	2007.16
102	-4.99	-2.14	NaN	2007.19
103	-5.07	-2.16	8.78	2007.22
104	-5.11	-2.32	NaN	2007.25
104	-4.89	-2.56	NaN	2007.28
104	-4.88	-2.63	NaN	2007.31
105	-4.94	-2.53	NaN	2007.34
105	-5.07	-2.76	8.76	2007.37
106	-4.98	-2.65	NaN	2007.4
106	-4.95	-1.93	NaN	2007.43
107	-5.35	-1.73	NaN	2007.46
107	-5.37	-1.9	NaN	2007.49
108	-5.34	-2.09	8.75	2007.51
108	-5.01	-1.69	NaN	2007.54
109	-5.28	-1.67	NaN	2007.57
109	-5.19	-1.75	NaN	2007.6
110	-5.23	-1.69	NaN	2007.63
110	-5.12	-1.44	8.79	2007.66
110	-5.52	-0.97	NaN	2007.69
111	-5.37	-1.41	NaN	2007.72
111	-5.24	-1.49	NaN	2007.75
112	-5.20	-0.88	NaN	2007.78
112	-5.02	-1.28	8.77	2007.81
113	-5.36	-1.44	NaN	2007.84

113	-4.91	-1.94	NaN	2007.87
114	-4.90	-1.42	NaN	2007.9
115	-4.85	-1.59	NaN	2007.93
115	-4.75	-2.05	8.83	2007.96
116	-4.80	-1.53	NaN	2007.99
116	-4.75	-1.91	NaN	2008.01
117	-4.61	-1.5	NaN	2008.04
117	-4.59	-1.68	NaN	2008.07
118	-4.62	-1.92	#VALUE!	2008.1
118	-4.62	-1.83	NaN	2008.13
119	-4.68	-1.74	NaN	2008.16
119	-4.65	-1.81	NaN	2008.19
120	-4.83	-1.99	NaN	2008.22
120	-4.69	-1.75	8.85	2008.25
121	-4.72	-1.96	NaN	2008.29
121	-4.59	-1.71	NaN	2008.33
122	-4.72	-1.63	NaN	2008.37
122	-4.83	-1.61	NaN	2008.4
123	-4.88	-1.38	8.83	2008.44
123	-5.02	-1.83	NaN	2008.48
124	-4.86	-1.7	NaN	2008.52
124	-5.12	-1.26	NaN	2008.56
125	-5.02	-1.43	NaN	2008.6
125	-5.01	-1.47	8.77	2008.63
126	-5.06	-1.37	NaN	2008.67
126	-4.97	-1.06	NaN	2008.71
127	-5.18	-1.3	NaN	2008.75
127	-4.88	-1.32	NaN	2008.79
128	-5.08	-1.21	8.76	2008.82
128	-4.89	-1.31	NaN	2008.86
129	-4.98	-1.14	NaN	2008.89
129	-4.92	-0.93	NaN	2008.93
130	-4.90	-1.25	NaN	2008.96
130	-4.58	-1.21	8.8	2009
131	-4.69	-1.51	NaN	2009.04
131	-5.02	-1.39	NaN	2009.07
132	-4.82	-1.13	NaN	2009.11
132	-4.77	-1.26	NaN	2009.14
133	-4.51	-1.3	8.88	2009.18
133	-4.80	-1.49	NaN	2009.21
134	-4.65	-1.64	NaN	2009.25
134	-4.58	-1.87	NaN	2009.29
135	-4.67	-1.97	NaN	2009.33
135	-4.45	-1.94	8.9	2009.38
136	-4.60	-1.85	NaN	2009.42
136	-4.61	-2.06	NaN	2009.46
137	-4.68	-1.87	NaN	2009.5
137	-4.71	-1.74	NaN	2009.54
138	-4.96	-1.72	8.84	2009.58

138	-4.57	-1.97	NaN	2009.63
139	-4.86	-1.97	NaN	2009.67
139	-4.85	-2.03	NaN	2009.71
140	-4.95	-2.03	NaN	2009.75
140	-5.07	-1.83	8.78	2009.8
141	-5.09	-1.71	NaN	2009.84
141	-5.10	-1.68	NaN	2009.89
142	-5.12	-1.74	NaN	2009.93
142	-5.06	-1.71	NaN	2009.98
143	-5.01	-1.52	8.77	2010.02
143	-5.10	-2.06	NaN	2010.07
144	-5.08	-1.1	NaN	2010.11
144	-5.08	-1.26	NaN	2010.16
145	-5.15	-0.95	NaN	2010.2
145	-4.84	-0.65	8.79	2010.25
146	-5.12	-1.23	NaN	2010.29
146	-5.07	-1.29	NaN	2010.33
147	-5.27	-1.28	NaN	2010.38
147	-5.14	-1.19	NaN	2010.42
148	-4.92	-0.9	8.78	2010.46
148	-4.99	-0.97	NaN	2010.5
149	-4.85	-1.26	NaN	2010.54
149	-4.73	-1.05	NaN	2010.58
150	-5.00	-1.54	NaN	2010.63
150	-4.92	-1.26	8.8	2010.67
151	-4.87	-1.1	NaN	2010.71
151	-4.95	-1.21	NaN	2010.75
152	-4.75	-1.07	NaN	2010.78
152	-4.75	-1.07	NaN	2010.81
153	-4.86	-1.28	8.82	2010.84
153	-4.68	-1.27	NaN	2010.87
154	-4.62	-1.24	NaN	2010.9
154	-4.81	-1.56	NaN	2010.93
155	-4.64	-1.51	NaN	2010.96
155	-4.70	-1.58	8.89	2010.99
156	-4.89	-1.39	NaN	2011.01
156	-4.72	-1.84	NaN	2011.04
157	-4.75	-1.76	NaN	2011.07
157	-5.02	-2.13	NaN	2011.1
158	-4.83	-1.54	8.81	2011.13
158	-4.99	-1.74	NaN	2011.16
159	-4.98	-1.9	NaN	2011.19
159	-5.00	-1.78	NaN	2011.22
160	-4.91	-1.96	NaN	2011.25
160	-5.08	-1.73	8.73	2011.3
161	-5.02	-1.58	NaN	2011.35
161	-4.90	-1.84	NaN	2011.4
162	-4.96	-1.58	NaN	2011.45
162	-4.96	-1.39	NaN	2011.5

163	-4.99	-1.39	8.71	2011.55
163	-5.03	-1.6	NaN	2011.6
164	-4.93	-1.5	NaN	2011.65
164	-4.95	-1.26	NaN	2011.7
165	-4.94	-1.32	NaN	2011.75
165	-5.11	-1.95	8.76	2011.8
166	-5.07	-1.28	NaN	2011.84
166	-4.95	-0.95	NaN	2011.89
167	-4.82	-1.78	NaN	2011.93
167	-4.82	-1.32	NaN	2011.98
168	-4.85	-1.23	8.78	2012.02
168	-4.76	-1.59	NaN	2012.07
169	-4.60	-1.26	NaN	2012.11
169	-4.57	-1.34	NaN	2012.16
170	-4.57	-1.45	NaN	2012.2
170	-4.36	-1.72	8.93	2012.25
171	-4.29	-1.56	NaN	2012.3
171	-4.42	-1.46	NaN	2012.34
172	-4.45	-1.6	NaN	2012.39
172	-4.41	-1.76	NaN	2012.43
173	-4.45	-1.95	8.86	2012.48
173	-4.35	-2.21	NaN	2012.52
174	-4.58	-2.02	NaN	2012.57
174	-4.46	-1.47	NaN	2012.61
175	-4.80	-1.91	NaN	2012.66
175	-4.59	-1.79	8.89	2012.7
176	-4.63	-1.92	NaN	2012.75
176	-4.47	-1.83	NaN	2012.88
177	-4.30	-1.52	NaN	2013
177	-4.55	-1.67	NaN	2013.13
178	-4.44	-1.23	8.91	2013.25
178	-4.41	-1.77	NaN	2013.3
179	-4.61	-1.49	NaN	2013.35
179	-4.40	-1.61	NaN	2013.4
180	-4.62	-1.56	NaN	2013.45
180	-4.84	-1.58	8.84	2013.5

A.2 ATC13100R

ATC13100R			
depth (mm)	$\delta^{18}O$	$\delta^{13}C$	age_model
001	-4.74	-2.36	2002.75
001	-4.80	-2.60	2002.77
002	-4.83	-2.52	2002.78
002	-4.90	-2.33	2002.80
003	-5.16	-2.31	2002.82
003	-5.13	-2.33	2002.83
004	-4.99	-1.91	2002.85
004	-4.99	-1.67	2002.87
005	-5.00	-1.65	2002.88
005	-5.05	-1.44	2002.90
006	-5.10	-1.40	2002.92
006	-4.89	-2.06	2002.93
007	-5.08	-2.23	2002.95
007	-5.10	-2.34	2002.97
008	-5.14	-2.25	2002.98
008	-4.97	-2.37	2003.00
009	-4.77	-2.24	2003.02
009	-4.83	-1.50	2003.03
010	-4.80	-1.51	2003.05
010	-4.98	-2.07	2003.07
011	-4.69	-1.77	2003.08
011	-4.78	-2.75	2003.10
012	-4.74	-2.42	2003.12
012	-4.48	-2.18	2003.13
013	-4.48	-2.03	2003.15
013	-4.53	-1.57	2003.17
014	-4.70	-2.25	2003.18
014	-4.70	-1.94	2003.20
015	-4.64	-2.73	2003.22
015	-4.49	-2.70	2003.23
016	-4.72	-2.62	2003.25
016	-4.55	-2.37	2003.29
017	-4.61	-2.27	2003.32
017	-4.62	-2.47	2003.36
018	-4.84	-2.89	2003.39
018	-4.84	-2.75	2003.43
019	-4.71	-2.66	2003.46
019	-4.86	-2.69	2003.50
020	-4.91	-2.82	2003.54
020	-4.84	-2.59	2003.57
021	-4.77	-2.48	2003.61
021	-4.79	-2.52	2003.64
022	-5.11	-2.45	2003.68
022	-5.08	-2.14	2003.71
023	-4.81	-1.55	2003.75
023	-4.96	-1.80	2003.79
024	-4.84	-2.26	2003.82

024	-4.94	-1.82	2003.86
025	-4.72	-1.97	2003.89
025	-4.67	-1.93	2003.93
026	-4.68	-2.26	2003.96
026	-4.68	-1.89	2004.00
027	-4.52	-1.90	2004.04
027	-4.78	-2.03	2004.07
028	-4.86	-1.99	2004.11
028	-4.60	-1.65	2004.14
029	-4.13	-2.07	2004.18
029	-4.42	-1.77	2004.21
030	-4.53	-1.64	2004.25
030	-4.57	-1.99	2004.28
031	-4.49	-2.18	2004.30
031	-4.56	-2.02	2004.33
032	-4.68	-2.27	2004.35
032	-4.52	-2.17	2004.38
033	-4.61	-2.12	2004.40
033	-4.57	-2.37	2004.43
034	-4.83	-2.44	2004.45
034	-4.73	-2.51	2004.48
035	-4.88	-2.22	2004.50
035	-4.95	-2.82	2004.53
036	-4.91	-2.58	2004.55
036	-5.13	-2.32	2004.58
037	-4.84	-2.17	2004.60
037	-4.91	-2.06	2004.63
038	-4.81	-1.50	2004.65
038	-5.00	-1.70	2004.68
039	-4.91	-1.89	2004.70
039	-4.75	-1.83	2004.73
040	-4.75	-1.80	2004.75
040	-4.90	-1.72	2004.80
041	-4.82	-1.67	2004.84
041	-4.79	-1.54	2004.89
042	-4.81	-1.93	2004.93
042	-4.92	-1.70	2004.98
043	-4.91	-1.48	2005.02
043	-5.05	-1.81	2005.07
044	-4.56	-1.52	2005.11
044	-4.82	-2.03	2005.16
045	-4.74	-2.30	2005.20
045	-4.69	-1.93	2005.25
046	-4.67	-1.69	2005.28
046	-5.17	-1.99	2005.31
047	-4.59	-2.32	2005.34
047	-4.62	-2.59	2005.38
048	-4.39	-2.19	2005.41
048	-4.65	-2.07	2005.44

049	-4.55	-2.37	2005.47
049	-4.46	-2.53	2005.50
050	-4.49	-2.20	2005.53
050	-4.57	-2.01	2005.56
051	-4.76	-2.28	2005.59
051	-4.81	-2.21	2005.63
052	-4.86	-2.26	2005.66
052	-4.90	-1.97	2005.69
053	-4.96	-1.71	2005.72
053	-4.98	-1.67	2005.75
054	-4.97	-1.73	2005.78
054	-5.02	-1.54	2005.81
055	-4.84	-2.21	2005.84
055	-4.91	-2.00	2005.87
056	-4.74	-1.64	2005.90
056	-4.78	-1.81	2005.93
057	-4.71	-1.40	2005.96
057	-4.54	-0.98	2005.99
058	-4.57	-1.30	2006.01
058	-4.53	-1.63	2006.04
059	-4.54	-1.94	2006.07
059	-4.49	-1.99	2006.10
060	-4.44	-1.82	2006.13
060	-4.45	-1.79	2006.16
061	-4.48	-2.05	2006.19
061	-4.80	-2.03	2006.22
062	-4.74	-2.52	2006.25
062	-4.91	-2.65	2006.28
063	-4.74	-2.60	2006.31
063	-4.71	-2.42	2006.34
064	-4.50	-2.09	2006.37
064	-4.47	-2.19	2006.40
065	-4.47	-2.26	2006.43
065	-4.68	-2.33	2006.46
066	-4.77	-2.31	2006.49
066	-4.79	-2.07	2006.51
067	-5.12	-2.21	2006.54
067	-5.03	-2.16	2006.57
068	-5.06	-2.01	2006.60
068	-5.12	-1.74	2006.63
069	-4.91	-1.81	2006.66
069	-5.02	-1.36	2006.69
070	-5.02	-2.03	2006.72
070	-5.11	-1.47	2006.75
071	-5.14	-1.39	2006.78
071	-5.01	-1.22	2006.81
072	-4.78	-1.44	2006.84
072	-4.99	-1.14	2006.88
073	-4.78	-1.51	2006.91

073	-4.72	-1.57	2006.94
074	-4.67	-1.42	2006.97
074	-4.49	-1.53	2007.00
075	-4.57	-1.84	2007.03
075	-4.55	-1.53	2007.06
076	-4.48	-2.16	2007.09
076	-4.41	-2.11	2007.13
077	-4.45	-2.30	2007.16
077	-4.67	-1.97	2007.19
078	-4.45	-2.26	2007.22
078	-4.48	-2.56	2007.25
079	-4.55	-2.23	2007.28
079	-4.58	-2.10	2007.31
080	-4.62	-2.44	2007.34
080	-4.88	-2.39	2007.38
081	-4.79	-2.81	2007.41
081	-4.73	-2.40	2007.44
082	-4.74	-2.37	2007.47
082	-4.76	-1.80	2007.50
083	-4.93	-1.93	2007.53
083	-4.92	-1.62	2007.56
084	-5.04	-1.47	2007.59
084	-4.89	-1.38	2007.63
085	-4.84	-1.64	2007.66
085	-4.89	-1.77	2007.69
086	-4.85	-1.92	2007.72
086	-4.67	-2.04	2007.75
087	-4.94	-2.09	2007.78
087	-4.70	-2.02	2007.80
088	-4.60	-1.76	2007.83
088	-4.69	-2.18	2007.86
089	-4.67	-2.21	2007.88
089	-4.55	-1.97	2007.91
090	-4.62	-1.86	2007.93
090	-4.63	-1.93	2007.96
091	-4.56	-1.96	2007.99
091	-4.74	-1.89	2008.01
092	-4.42	-1.83	2008.04
092	-4.46	-2.31	2008.07
093	-4.48	-2.26	2008.09
093	-4.37	-2.45	2008.12
094	-4.57	-2.48	2008.14
094	-4.81	-2.47	2008.17
095	-4.67	-2.16	2008.20
095	-4.83	-2.27	2008.22
096	-4.93	-2.38	2008.25
096	-4.93	-2.45	2008.28
097	-5.00	-2.43	2008.32
097	-5.02	-2.23	2008.35

098	-4.88	-2.32	2008.38
098	-4.85	-1.86	2008.42
099	-5.05	-1.72	2008.45
099	-5.10	-1.97	2008.48
100	-4.93	-1.71	2008.52
100	-5.18	-1.93	2008.55
101	-5.13	-2.03	2008.58
101	-5.25	-1.69	2008.62
102	-5.10	-1.48	2008.65
102	-5.06	-1.68	2008.68
103	-5.10	-1.50	2008.72
103	-4.90	-1.54	2008.75
104	-4.92	-1.66	2008.78
104	-4.83	-1.86	2008.81
105	-4.79	-1.82	2008.84
105	-4.66	-2.07	2008.88
106	-4.68	-2.26	2008.91
106	-4.93	-2.29	2008.94
107	-4.99	-2.07	2008.97
107	-4.77	-1.90	2009.00
108	-4.85	-2.44	2009.03
108	-4.59	-2.04	2009.06
109	-4.60	-2.25	2009.09
109	-4.59	-2.34	2009.13
110	-4.99	-2.53	2009.16
110	-5.04	-2.27	2009.19
111	-4.87	-2.29	2009.22
111	-4.88	-2.41	2009.25
112	-4.88	-2.26	2009.28
112	-4.85	-2.31	2009.31
113	-4.75	-2.30	2009.34
113	-4.90	-2.43	2009.37
114	-4.90	-2.39	2009.40
114	-4.97	-2.34	2009.43
115	-4.98	-2.09	2009.46
115	-5.21	-1.79	2009.49
116	-5.22	-2.02	2009.51
116	-5.18	-1.90	2009.54
117	-5.17	-1.73	2009.57
117	-5.22	-1.58	2009.60
118	-5.29	-1.13	2009.63
118	-5.26	-1.72	2009.66
119	-5.32	-1.52	2009.69
119	-5.08	-1.39	2009.72
120	-5.38	-1.20	2009.75
120	-5.02	-1.21	2009.80
121	-5.12	-1.35	2009.84
121	-5.11	-1.09	2009.89
122	-4.87	-1.74	2009.93

122	-4.97	-1.25	2009.98
123	-4.91	-1.83	2010.02
123	-4.79	-2.04	2010.07
124	-5.16	-2.07	2010.11
124	-4.88	-2.28	2010.16
125	-4.59	-1.80	2010.20
125	-4.86	-2.18	2010.25
126	-4.53	-2.29	2010.30
126	-4.54	-2.13	2010.34
127	-4.58	-2.77	2010.39
127	-4.74	-2.81	2010.43
128	-4.56	-2.67	2010.48
128	-4.80	-2.17	2010.52
129	-4.77	-2.11	2010.57
129	-4.78	-2.27	2010.61
130	-4.49	-2.27	2010.66
130	-4.56	-2.21	2010.70
131	-4.79	-2.45	2010.75
131	-5.08	-2.43	2010.77
132	-4.98	-2.48	2010.79
132	-5.22	-2.47	2010.81
133	-4.90	-2.16	2010.83
133	-4.80	-1.75	2010.85
134	-5.14	-1.93	2010.87
134	-5.39	-2.29	2010.89
135	-5.25	-1.78	2010.91
135	-5.02	-1.99	2010.93
136	-4.94	-1.60	2010.95
136	-4.92	-1.25	2010.97
137	-4.85	-1.15	2010.99
137	-4.82	-0.78	2011.01
138	-5.05	-0.78	2011.03
138	-5.26	-0.82	2011.05
139	-4.80	-1.10	2011.07
139	-4.56	-1.65	2011.09
140	-4.40	-1.40	2011.11
140	-4.51	-1.77	2011.13
141	-4.53	-1.57	2011.15
141	-4.63	-1.38	2011.17
142	-4.51	-1.46	2011.19
142	-4.55	-1.43	2011.21
143	-4.58	-1.35	2011.23
143	-4.55	-1.46	2011.25
144	-4.62	-1.56	2011.29
144	-4.55	-1.51	2011.32
145	-4.58	-1.40	2011.36
145	-4.70	-1.69	2011.39
146	-4.74	-1.78	2011.43
146	-4.89	-1.78	2011.46

147	-5.23	-1.94	2011.50
147	-5.13	-2.09	2011.54
148	-4.98	-1.99	2011.57
148	-5.03	-1.98	2011.61
149	-5.08	-1.67	2011.64
149	-5.03	-1.39	2011.68
150	-5.14	-1.37	2011.71
150	-5.04	-1.00	2011.75
151	-5.05	-1.31	2011.78
151	-5.19	-1.09	2011.82
152	-5.07	-1.16	2011.85
152	-5.06	-0.93	2011.88
153	-4.98	-1.08	2011.92
153	-4.86	-1.42	2011.95
154	-4.93	-1.14	2011.98
154	-4.90	-1.18	2012.02
155	-4.67	-1.19	2012.05
155	-4.68	-1.30	2012.08
156	-4.65	-1.27	2012.12
156	-4.72	-1.42	2012.15
157	-4.47	-1.57	2012.18
157	-4.47	-1.51	2012.22
158	-4.58	-1.58	2012.25
158	-4.65	-1.90	2012.28
159	-4.73	-1.88	2012.30
159	-4.52	-2.02	2012.33
160	-4.72	-1.77	2012.36
160	-4.43	-1.90	2012.38
161	-4.86	-1.90	2012.41
161	-4.75	-1.96	2012.43
162	-4.79	-1.92	2012.46
162	-4.81	-1.88	2012.49
163	-4.87	-1.79	2012.51
163	-4.70	-1.63	2012.54
164	-4.95	-1.86	2012.57
164	-4.70	-1.78	2012.59
165	-4.90	-1.88	2012.62
165	-4.93	-1.77	2012.64
166	-4.86	-1.63	2012.67
166	-4.87	-1.67	2012.70
167	-5.01	-1.67	2012.72
167	-5.02	-1.75	2012.75
168	-4.88	-1.35	2012.79
168	-4.92	-1.42	2012.82
169	-4.83	-1.59	2012.86
169	-5.22	-1.21	2012.89
170	-5.31	-1.41	2012.93
170	-5.12	-0.98	2012.96
171	-4.94	-1.10	2013.00

171	-4.99	-1.23	2013.04
172	-5.01	-1.24	2013.07
172	-4.85	-1.17	2013.11
173	-4.84	-1.27	2013.14
173	-4.78	-1.25	2013.18
174	-4.75	-1.46	2013.21
174	-4.91	-1.18	2013.25
175	-4.70	-1.68	2013.28
175	-4.65	-1.69	2013.31
176	-4.70	-1.43	2013.33
176	-4.71	-1.54	2013.36
177	-4.50	-1.57	2013.39
177	-4.66	-1.58	2013.42
178	-4.48	-1.58	2013.44
178	-4.54	-1.69	2013.47
179	-4.42	-1.45	2013.50

A.3 ATC13096

depth (mm)	$\delta^{18}O$	$\delta^{13}C$	age_model	Sr/Ca (mmol/mol)	age_model
001	-3.61	-0.07	1058.58	9.18	1058.42
002	-3.63	0.11	1058.50	9.13	1058.25
003	-3.72	0.09	1058.41	9.09	1058.08
004	-3.74	0.25	1058.32	9.11	1057.92
005	-3.81	0.34	1058.23	9.12	1057.75
006	-3.91	-0.15	1058.15	9.15	1057.58
007	-3.88	-0.04	1058.06	9.11	1057.42
008	-4.28	-0.27	1057.97	9.06	1057.25
009	-4.37	-1.43	1057.88	9.08	1057.08
010	-4.23	-0.70	1057.80	9.07	1056.92
011	-4.26	-1.21	1057.71	9.05	1056.75
012	-4.15	-1.04	1057.62	9.16	1056.58
013	-4.12	-0.41	1057.53	9.15	1056.42
014	-4.05	-0.10	1057.44	9.09	1056.25
015	-3.96	0.16	1057.36	9.07	1056.08
016	-3.79	0.12	1057.27	9.06	1055.92
017	-3.85	-0.08	1057.18	9.08	1055.75
018	-4.14	-0.23	1057.09	9.10	1055.58
019	-4.19	-0.20	1057.01	9.10	1055.42
020	-4.54	-0.54	1056.92	9.07	1055.25
021	-4.61	-0.56	1056.83	8.98	1055.08
022	-4.47	-0.62	1056.74	8.97	1054.92
023	-4.24	-1.24	1056.66	9.06	1054.75
024	-3.83	-0.49	1056.57	9.09	1054.58
025	-4.08	-0.50	1056.48	9.09	1054.42
026	-3.57	0.31	1056.39	9.07	1054.25
027	-3.65	0.12	1056.31	9.04	1054.08
028	-3.80	-0.54	1056.22	8.99	1053.92
029	-3.89	-0.59	1056.13	9.12	1053.75
030	-4.09	-1.06	1056.04	9.09	1053.58
031	-4.07	-1.11	1055.96	9.07	1053.42
032	-4.45	-1.24	1055.87	8.98	1053.25
033	-4.20	-1.35	1055.78	8.95	1053.08
034	-4.13	-0.92	1055.69	9.02	1052.92
035	-3.84	-1.06	1055.61	9.12	1052.75
036	-3.88	-1.00	1055.52	9.13	1052.58
037	-3.98	-1.07	1055.43	9.12	1052.42
038	-3.87	-1.27	1055.34	9.07	1052.25
039	-3.91	-1.02	1055.26	9.04	1052.08
040	-4.08	-1.36	1055.17	8.98	1051.92
041	-4.13	-1.23	1055.08	9.06	1051.75
042	-4.15	-0.80	1054.99	9.10	1051.58

043	-4.23	-0.44	1054.91	9.10	1051.42
044	-4.32	-0.52	1054.82	9.02	1051.25
045	-4.25	-0.47	1054.73	8.99	1051.08
046	-3.93	-0.28	1054.64	9.03	1050.92
047	-4.13	-0.29	1054.56	9.11	1050.75
048	-3.91	-0.46	1054.47	9.14	1050.58
049	-3.98	-0.77	1054.38	9.14	1050.42
050	-4.13	-1.06	1054.29	9.08	1050.25
051	-4.14	-1.14	1054.20	9.01	1050.08
052	-4.17	-1.25	1054.12	8.99	1049.92
053	-4.46	-1.43	1054.03	8.98	1049.75
054	-4.27	-1.34	1053.94	9.05	1049.58
055	-4.24	-1.30	1053.85	8.99	1049.42
056	-4.20	-1.38	1053.77	8.94	1049.25
057	-4.04	-1.49	1053.68	8.94	1049.08
058	-3.78	-1.08	1053.59	8.99	1048.92
059	-3.83	-0.42	1053.50	9.02	1048.75
060	-3.64	-0.46	1053.42	9.06	1048.58
061	-3.37	-0.93	1053.33	9.04	1048.42
062	-3.55	-0.91	1053.24	9.02	1048.25
063	-3.67	-0.98	1053.15	9.00	1048.08
064	-3.76	-1.07	1053.07	9.00	1047.92
065	-3.97	-1.28	1052.98	9.06	1047.75
066	-4.03	-1.58	1052.89	9.10	1047.58
067	-4.10	-1.43	1052.80	9.07	1047.42
068	-3.83	-1.02	1052.72	9.06	1047.25
069	-3.69	-0.74	1052.63	9.07	1047.08
070	-3.82	-0.43	1052.54	nan	1046.92
071	-3.32	0.15	1052.45	nan	1046.75
072	-3.49	0.06	1052.37	9.07	1046.58
073	-3.79	-0.18	1052.28	9.07	1046.42
074	-4.05	-0.47	1052.19	9.03	1046.25
075	-4.27	-1.11	1052.10	9.00	1046.08
076	-4.13	-1.21	1052.02	9.00	1045.92
077	-4.22	-1.00	1051.93	9.03	1045.75
078	-1.27	-0.26	1051.84	9.06	1045.58
079	-4.13	-0.78	1051.75	9.06	1045.42
080	-3.99	-0.71	1051.67	8.99	1045.25
081	-4.09	-0.67	1051.58	8.93	1045.08
082	-4.08	-0.65	1051.49	8.96	1044.92
083	-4.07	-0.80	1051.40	8.98	1044.75
084	-4.05	-1.28	1051.31	8.99	1044.58
085	-4.32	-1.45	1051.23	8.99	1044.42

086	-4.10	-1.64	1051.14	8.94	1044.25
087	-4.02	-1.01	1051.05	8.91	1044.08
088	-4.41	-0.67	1050.96	8.92	1043.92
089	-4.31	-0.87	1050.88	8.97	1043.75
090	-4.41	-0.96	1050.79	9.00	1043.58
091	-4.65	-1.06	1050.70	9.03	1043.42
092	-4.27	-1.17	1050.61	8.99	1043.25
093	-4.22	-0.57	1050.53	8.97	1043.08
094	-3.96	-0.21	1050.44	8.98	1042.92
095	-3.83	0.12	1050.35	8.97	1042.75
096	-3.68	0.13	1050.26	9.02	1042.58
097	-4.03	-0.26	1050.18	9.04	1042.42
098	-3.93	-0.59	1050.09	9.01	1042.25
099	-4.03	-1.04	1050.00	8.94	1042.08
100	-4.15	-1.18	1049.91	8.90	1041.92
101	-4.25	-1.11	1049.83	9.00	1041.75
102	-4.29	-1.06	1049.74	9.03	1041.58
103	-4.65	-0.87	1049.65	9.03	1041.42
104	-4.45	-0.95	1049.56	8.96	1041.25
105	-4.20	-0.36	1049.48	8.93	1041.08
106	-4.12	-0.19	1049.39	8.99	1040.92
107	-4.14	0.45	1049.30	9.05	1040.75
108	-3.64	0.90	1049.21	9.08	1040.58
109	-3.80	0.74	1049.13	9.10	1040.42
110	-3.99	0.15	1049.04	9.05	1040.25
111	-4.38	-0.24	1048.95	9.00	1040.08
112	-4.58	-0.83	1048.86	9.00	1039.92
113	-4.49	-1.16	1048.78	9.05	1039.75
114	-4.17	-0.35	1048.69	9.04	1039.58
115	-4.13	0.18	1048.60	8.98	1039.42
116	-4.00	0.24	1048.51	8.96	1039.25
117	-3.93	0.21	1048.43	8.99	1039.08
118	-3.73	0.09	1048.34	9.07	1038.92
119	-4.22	-0.63	1048.25	9.08	1038.75
120	-4.49	-0.95	1048.16	9.03	1038.58
121	-3.80	-1.03	1048.07	9.01	1038.42
122	-4.18	-0.99	1047.99	9.01	1038.25
123	-4.07	-0.94	1047.90	9.02	1038.08
124	-3.99	-1.04	1047.81	9.05	1037.92
125	-4.02	-0.75	1047.72	9.10	1037.75
126	-3.82	-0.72	1047.64	9.04	1037.58
127	-3.46	0.34	1047.55	9.00	1037.42
128	-3.50	-0.19	1047.46	8.97	1037.25

129	-3.67	-0.03	1047.37	8.96	1037.08
130	-3.55	-0.40	1047.29	9.03	1036.92
131	-3.91	-0.85	1047.20	9.07	1036.75
132	-3.94	-0.67	1047.11	9.06	1036.58
133	-4.12	-0.54	1047.02	9.01	1036.42
134	-4.35	-0.68	1046.94	9.02	1036.25
135	-4.30	-0.57	1046.85	9.05	1036.08
136	-4.55	-0.78	1046.76	9.09	1035.92
137	-4.07	-0.66	1046.67	9.15	1035.75
138	-4.14	-1.16	1046.59	9.10	1035.58
139	-3.76	-1.55	1046.50	6.71	1035.42
140	-4.13	-0.99	1046.41	2.00	1035.25
141	-3.98	-0.71	1046.32	6.69	1035.08
142	-4.13	-0.43	1046.24	9.06	1034.92
143	-4.21	-0.29	1046.15	9.10	1034.75
144	-4.13	-0.32	1046.06	9.07	1034.58
145	-4.14	-1.39	1045.97	9.03	1034.42
146	-4.30	-1.49	1045.89	8.98	1034.25
147	-4.50	-1.36	1045.80	8.97	1034.08
148	-4.53	-1.37	1045.71	9.04	1033.92
149	-4.46	-1.24	1045.62	nan	1033.75
150	-4.38	-1.21	1045.54	nan	1033.58
151	-4.28	-0.70	1045.45	nan	1033.42
152	-4.10	-0.95	1045.36	9.00	1033.25
153	-4.22	-0.84	1045.27	8.95	1033.08
154	-3.86	-1.06	1045.19	8.97	1032.92
155	-3.99	-1.60	1045.10	9.02	1032.75
156	-3.96	-1.33	1045.01	9.10	1032.58
157	-4.08	-1.50	1044.92	9.07	1032.42
158	-4.13	-1.30	1044.83	9.02	1032.25
159	-4.25	-1.08	1044.75	9.02	1032.08
160	-4.05	-0.60	1044.66	9.02	1031.92
161	-3.89	0.06	1044.57	9.06	1031.75
162	-3.96	0.24	1044.48	9.11	1031.58
163	-4.01	0.13	1044.40	9.05	1031.42
164	-4.06	-0.26	1044.31	9.05	1031.25
165	-4.03	-1.00	1044.22	9.06	1031.08
166	-4.17	-0.75	1044.13	9.05	1030.92
167	-4.45	-1.01	1044.05	9.02	1030.75
168	-4.32	-0.59	1043.96	9.07	1030.58
169	-4.18	-0.13	1043.87	9.14	1030.42
170	-4.11	0.47	1043.78	9.07	1030.25
171	-4.28	-0.02	1043.70	9.01	1030.08

172	-4.21	-0.57	1043.61	9.02	1029.92
173	-4.30	-0.93	1043.52	9.07	1029.75
174	-4.50	-0.69	1043.43	9.13	1029.58
175	-4.30	-0.55	1043.35	9.14	1029.42
176	-4.41	-0.41	1043.26	9.06	1029.25
177	-4.55	-0.41	1043.17	nan	1029.08
178	-4.43	-0.04	1043.08	nan	1028.92
179	-4.27	0.27	1043.00	9.13	1028.75
180	-4.14	-0.09	1042.91	9.09	1028.58
181	-3.85	-0.35	1042.82	9.12	1028.42
182	-3.82	0.05	1042.73	9.10	1028.25
183	-3.70	-0.13	1042.65	9.12	1028.08
184	-3.88	-0.74	1042.56	9.14	1027.92
185	-4.19	-1.17	1042.47	9.13	1027.75
186	-4.32	-1.01	1042.38	9.07	1027.58
187	-4.31	-0.56	1042.30	9.07	1027.42
188	-3.96	0.21	1042.21	9.09	1027.25
189	-3.89	0.40	1042.12	9.03	1027.08
190	-3.79	0.23	1042.03	9.04	1026.92
191	-3.75	-0.24	1041.94	9.08	1026.75
192	-3.89	-0.76	1041.86	9.11	1026.58
193	-4.00	-0.99	1041.77	9.05	1026.42
194	-4.10	-1.25	1041.68	9.01	1026.25
195	-4.08	-1.12	1041.59	9.07	1026.08
196	-4.19	-0.25	1041.51	9.11	1025.92
197	-3.92	0.37	1041.42	9.18	1025.75
198	-3.91	0.43	1041.33	9.12	1025.58
199	-3.65	0.67	1041.24	9.06	1025.42
200	-3.66	0.29	1041.16	9.05	1025.25
201	-3.82	0.04	1041.07	9.07	1025.08
202	-4.29	-0.48	1040.98	9.06	1024.92
203	-4.50	-0.96	1040.89	9.11	1024.75
204	-4.32	-0.39	1040.81	9.07	1024.58
205	-4.33	0.41	1040.72	9.03	1024.42
206	-4.04	0.26	1040.63	9.00	1024.25
207	-4.11	0.26	1040.54	9.04	1024.08
208	-4.15	-0.55	1040.46	9.05	1023.92
209	-4.22	-0.81	1040.37	9.15	1023.75
210	-4.17	-0.85	1040.28	9.09	1023.58
211	-4.23	-0.89	1040.19	9.03	1023.42
212	-4.39	-0.99	1040.11	9.03	1023.25
213	-4.41	-1.06	1040.02	9.04	1023.08
214	-4.35	-0.63	1039.93	9.03	1022.92

215	-4.55	-0.26	1039.84	9.10	1022.75
216	-4.29	-0.10	1039.76	9.09	1022.58
217	-4.03	0.25	1039.67	9.08	1022.42
218	-4.11	0.29	1039.58	9.06	1022.25
219	-4.02	0.17	1039.49	9.04	1022.08
220	-3.95	-0.38	1039.41	9.03	1021.92
221	-3.95	-0.53	1039.32	9.04	1021.75
222	-4.17	-0.62	1039.23	9.11	1021.58
223	-4.30	-0.68	1039.14	9.11	1021.42
224	-4.38	-0.72	1039.06	9.02	1021.25
225	-4.30	0.08	1038.97	8.98	1021.08
226	-4.17	-0.16	1038.88	9.00	1020.92
227	-4.04	0.52	1038.79	9.07	1020.75
228	-3.96	0.65	1038.70	9.12	1020.58
229	-3.94	0.27	1038.62	9.02	1020.42
230	-4.32	-0.39	1038.53	8.96	1020.25
231	-4.53	-0.95	1038.44	8.97	1020.08
232	-4.68	-1.04	1038.35	9.05	1019.92
233	-4.55	-1.02	1038.27	9.11	1019.75
234	-4.40	-0.65	1038.18	9.06	1019.58
235	-4.20	0.30	1038.09	9.00	1019.42
236	-4.10	0.61	1038.00	8.92	1019.25
237	-4.03	0.68	1037.92	8.94	1019.08
238	-3.88	0.01	1037.83	8.98	1018.92
239	-4.09	-0.60	1037.74	9.01	1018.75
240	-4.37	-0.96	1037.65	9.05	1018.58
241	-4.13	-1.00	1037.57	9.03	1018.42
242	-3.98	-0.08	1037.48	8.98	1018.25
243	-3.76	0.64	1037.39	8.96	1018.08
244	-3.70	0.58	1037.30	8.98	1017.92
245	-3.77	0.23	1037.22	9.00	1017.75
246	-3.65	0.05	1037.13	9.06	1017.58
247	-3.51	0.01	1037.04	9.05	1017.42
248	-3.78	-0.16	1036.95	9.00	1017.25
249	-3.92	-0.56	1036.87	8.95	1017.08
250	-4.04	-0.47	1036.78	8.95	1016.92
251	-3.83	0.47	1036.69	9.09	1016.75
252	-3.89	0.07	1036.60	9.12	1016.58
253	-3.67	0.69	1036.52	9.07	1016.42
254	-3.67	0.81	1036.43	8.98	1016.25
255	-3.35	0.82	1036.34	8.97	1016.08
256	-3.72	-0.06	1036.25	9.02	1015.92
257	-4.03	-0.32	1036.17	9.07	1015.75

258	-4.08	-0.65	1036.08	8.97	1015.58
259	-4.26	-1.05	1035.99	8.94	1015.42
260	-4.03	-0.07	1035.90	9.03	1015.25
261	-3.99	0.27	1035.81	9.09	1015.08
262	-3.84	0.67	1035.73	8.97	1014.92
263	-3.78	0.71	1035.64	8.98	1014.75
264	-3.76	0.30	1035.55	8.93	1014.58
265	-3.80	-0.26	1035.46	8.94	1014.42
266	-3.90	-0.54	1035.38	9.03	1014.25
267	-3.98	-0.70	1035.29	9.04	1014.08
268	-3.73	0.38	1035.20	9.00	1013.92
269	-3.66	0.68	1035.11	8.92	1013.75
270	-3.77	0.57	1035.03	8.95	1013.58
271	-3.76	0.10	1034.94	8.99	1013.42
272	-4.00	-0.23	1034.85	9.05	1013.25
273	-4.00	-0.30	1034.76	9.05	1013.08
274	-4.17	-0.58	1034.68	8.98	1012.92
275	-4.66	-1.18	1034.59	8.96	1012.75
276	-4.47	-0.61	1034.50	8.99	1012.58
277	-4.48	-0.62	1034.41	9.07	1012.42
278	-4.43	-0.76	1034.33	9.09	1012.25
279	-4.33	-0.44	1034.24	9.04	1012.08
280	-4.28	0.20	1034.15	8.99	1011.92
281	-4.08	0.20	1034.06	8.99	1011.75
282	-3.94	-0.06	1033.98	8.99	1011.58
283	-4.16	-0.65	1033.89	9.01	1011.42
284	-4.24	-0.73	1033.80	9.07	1011.25
285	-4.54	-1.43	1033.71	9.00	1011.08
286	-4.23	-1.19	1033.63	8.97	1010.92
287	-4.75	-0.85	1033.54	9.07	1010.75
288	-4.54	-0.71	1033.45	9.03	1010.58
289	-4.64	-0.71	1033.36	8.95	1010.42
290	-4.62	-0.71	1033.28	9.00	1010.25
291	-4.42	0.01	1033.19	9.00	1010.08
292	-4.11	0.10	1033.10	8.91	1009.92
293	-4.11	-0.23	1033.01	8.90	1009.75
294	-4.40	-1.24	1032.93	8.93	1009.58
295	-4.50	-1.53	1032.84	8.99	1009.42
296	-4.67	-1.27	1032.75	9.00	1009.25
297	-4.54	-0.95	1032.66	8.96	1009.08
298	-4.63	-0.78	1032.57	8.90	1008.92
299	-4.42	-0.78	1032.49	8.90	1008.75
300	-4.65	-0.70	1032.40	9.00	1008.58

301	-4.12	-0.50	1032.31	9.06	1008.42
302	-3.89	-0.38	1032.22	9.00	1008.25
303	-3.74	0.10	1032.14	9.06	1008.08
304	-3.67	0.58	1032.05	9.08	1007.92
305	-4.11	-0.14	1031.96	9.00	1007.75
306	-4.08	-0.57	1031.87	9.02	1007.58
307	-4.35	-0.79	1031.79	9.04	1007.42
308	-4.29	-0.33	1031.70	9.09	1007.25
309	-4.24	0.07	1031.61	9.10	1007.08
310	-4.04	-0.63	1031.52	9.06	1006.92
311	-4.26	0.03	1031.44		
312	-3.88	0.25	1031.35		
313	-3.94	0.15	1031.26		
314	-3.97	-0.07	1031.17		
315	-4.19	-0.37	1031.09		
316	-4.23	-0.29	1031.00		
317	-4.39	-0.91	1030.91		
318	-4.27	-0.91	1030.82		
319	-4.09	-0.39	1030.74		
320	-4.18	-0.41	1030.65		
321	-4.24	-0.19	1030.56		
322	-4.42	-0.15	1030.47		
323	-4.11	0.19	1030.39		
324	-4.10	-0.03	1030.30		
325	-3.92	0.02	1030.21		
326	-3.87	-0.50	1030.12		
327	-3.84	-0.20	1030.04		
328	-4.41	-0.69	1029.95		
329	-4.41	-0.38	1029.86		
330	-4.50	-0.87	1029.77		
331	-4.22	-0.73	1029.69		
332	-4.33	-0.38	1029.60		
333	-4.12	-0.34	1029.51		
334	-4.41	-0.23	1029.42		
335	-4.26	-0.33	1029.33		
336	-4.26	-0.07	1029.25		
337	-4.15	-0.26	1029.16		
338	-4.12	-0.84	1029.07		
339	-4.30	-1.36	1028.98		
340	-4.26	-1.45	1028.90		
341	-4.30	-1.47	1028.81		
342	-4.12	-0.97	1028.72		
343	-4.26	-0.43	1028.63		

344	-4.31	-0.16	1028.55
345	-4.46	-0.27	1028.46
346	-4.24	-0.11	1028.37
347	-4.37	0.75	1028.28
348	-4.15	1.01	1028.20
349	-4.01	-0.05	1028.11
350	-4.45	-0.45	1028.02
351	-4.83	-0.82	1027.93
352	-4.55	-0.66	1027.85
353	-4.73	-0.32	1027.76
354	-4.37	-0.45	1027.67
355	-4.31	0.06	1027.58
356	-4.11	0.56	1027.50
357	-4.20	0.43	1027.41
358	-4.25	0.16	1027.32
359	-4.72	-0.47	1027.23
360	-4.75	-0.22	1027.15
361	-4.46	-0.40	1027.06
362	-4.16	-0.80	1026.97
363	-3.97	-0.47	1026.88
364	-3.78	0.16	1026.80
365	-3.79	0.12	1026.71
366	-3.83	-0.25	1026.62
367	-3.77	-0.54	1026.53
368	-3.91	-1.21	1026.44
369	-3.96	-1.16	1026.36
370	-4.03	-0.92	1026.27
371	-4.35	-1.13	1026.18
372	-4.52	-0.79	1026.09
373	-4.56	-0.79	1026.01
374	-4.41	-1.18	1025.92
375	-4.14	-1.05	1025.83
376	-4.33	-0.59	1025.74
377	-4.01	-0.20	1025.66
378	-4.12	-0.48	1025.57
379	-3.98	-0.44	1025.48
380	-4.05	-1.15	1025.39
381	-4.48	-1.30	1025.31
382	-4.66	-1.25	1025.22
383	-4.72	-1.07	1025.13
384	NaN	NaN	1025.04
385	-4.68	-1.00	1024.96
386	-4.53	-0.76	1024.87

387	-4.54	-0.50	1024.78
388	-4.35	-0.19	1024.69
389	-4.14	0.09	1024.61
390	-4.07	0.24	1024.52
391	-3.85	0.22	1024.43
392	-4.17	-0.49	1024.34
393	-4.18	-0.91	1024.26
394	-4.58	-1.26	1024.17
395	-4.57	-1.45	1024.08
396	-4.41	-1.19	1023.99
397	-4.37	-0.92	1023.91
398	-4.36	-0.86	1023.82
399	-4.23	0.18	1023.73
400	-4.22	0.32	1023.64
401	-3.98	0.27	1023.56
402	-4.00	-0.70	1023.47
403	-4.26	-0.92	1023.38
404	-4.41	-0.96	1023.29
405	-4.61	-0.64	1023.20
406	-4.43	-0.43	1023.12
407	-4.47	-0.63	1023.03
408	-4.36	-0.70	1022.94
409	-4.32	-0.83	1022.85
410	-4.43	-0.60	1022.77
411	-4.35	-0.18	1022.68
412	-4.11	0.00	1022.59
413	-4.41	0.30	1022.50
414	-4.12	-0.08	1022.42
415	-4.57	-0.51	1022.33
416	-4.72	-0.46	1022.24
417	-4.75	-0.63	1022.15
418	-4.52	-1.44	1022.07
419	-4.53	-0.48	1021.98
420	-4.37	-0.32	1021.89
421	-3.98	-0.11	1021.80
422	-3.67	0.22	1021.72
423	-3.67	0.03	1021.63
424	-4.04	-0.45	1021.54
425	-4.45	-0.59	1021.45
426	-4.44	-0.68	1021.37
427	-4.57	-0.88	1021.28
428	-4.29	-0.38	1021.19
429	-4.25	-0.11	1021.10

430	-4.01	0.09	1021.02
431	-3.91	0.16	1020.93
432	-3.90	0.17	1020.84
433	-4.02	-0.27	1020.75
434	-4.37	-0.71	1020.67
435	-4.22	-0.58	1020.58
436	-4.49	-0.40	1020.49
437	-4.42	-0.35	1020.40
438	-4.51	-0.31	1020.31
439	-4.32	-0.40	1020.23
440	-4.37	-0.36	1020.14
441	-4.09	-0.27	1020.05
442	-4.20	-0.30	1019.96
443	-4.18	-0.31	1019.88
444	-3.99	-0.23	1019.79
445	-4.00	-0.40	1019.70
446	-3.94	-0.53	1019.61
447	-4.36	-0.54	1019.53
448	-4.42	-0.64	1019.44
449	-4.57	-0.93	1019.35
450	-4.45	-0.84	1019.26
451	-4.17	-0.67	1019.18
452	-4.01	-0.29	1019.09
453	-4.20	-0.39	1019.00
454	-3.93	-0.07	1018.91
455	-3.80	0.13	1018.83
456	-3.67	0.28	1018.74
457	-3.76	0.33	1018.65
458	-4.01	-0.31	1018.56
459	-4.38	-0.76	1018.48
460	-4.30	-1.28	1018.39
461	-4.23	-1.06	1018.30
462	-4.32	-0.84	1018.21
463	-4.10	-0.32	1018.13
464	-4.15	-0.15	1018.04
465	-3.92	0.25	1017.95
466	-3.96	-0.07	1017.86
467	-3.99	-0.04	1017.78
468	-4.04	-0.20	1017.69
469	-4.24	-0.37	1017.60
470	-4.58	-0.96	1017.51
471	-4.74	-0.95	1017.43
472	-4.33	-0.55	1017.34

473	-4.21	-1.06	1017.25
474	-4.08	-0.83	1017.16
475	-4.16	-0.34	1017.07
476	-4.16	-0.40	1016.99
477	-3.92	-0.56	1016.90
478	-3.98	-1.01	1016.81
479	-3.86	-0.81	1016.72
480	-4.05	-0.64	1016.64
481	-4.18	-0.82	1016.55
482	-4.24	-0.49	1016.46
483	-4.13	-0.08	1016.37
484	-4.27	-0.68	1016.29
485	-4.28	-0.41	1016.20
486	-4.26	-0.40	1016.11
487	-4.15	-0.53	1016.02
488	-3.97	-0.67	1015.94
489	-3.91	-0.24	1015.85
490	-3.84	-0.09	1015.76
491	-3.91	-0.18	1015.67
492	-4.14	-0.91	1015.59
493	-4.25	-1.06	1015.50
494	-4.39	-0.08	1015.41
495	-4.41	-0.35	1015.32
496	-4.05	-0.24	1015.24
497	-4.20	0.17	1015.15
498	-4.03	0.17	1015.06
499	-3.97	-0.11	1014.97
500	-3.86	-0.38	1014.89
501	-4.27	-0.99	1014.80
502	-4.27	-1.20	1014.71
503	-4.50	-0.85	1014.62
504	-4.26	-0.26	1014.54
505	-4.17	-0.55	1014.45
506	-3.96	-0.19	1014.36
507	-3.88	0.69	1014.27
508	-3.75	0.92	1014.19
509	-4.03	0.54	1014.10
510	-4.27	0.07	1014.01
511	-4.38	-0.34	1013.92
512	-4.68	-0.27	1013.83
513	-4.56	0.13	1013.75
514	-4.41	0.09	1013.66
515	-4.32	-0.29	1013.57

516	-4.26	0.10	1013.48
517	-4.36	0.06	1013.40
518	-4.14	0.17	1013.31
519	-4.43	-0.48	1013.22
520	-4.39	-0.43	1013.13
521	-4.70	-1.01	1013.05
522	-4.59	-0.47	1012.96
523	-4.82	-0.62	1012.87
524	-4.67	-0.21	1012.78
525	-4.47	0.04	1012.70
526	-4.69	0.21	1012.61
527	-4.41	-0.07	1012.52
528	-4.73	-0.46	1012.43
529	-4.77	-0.43	1012.35
530	-4.87	-0.68	1012.26
531	-4.97	-0.56	1012.17
532	-4.94	-0.44	1012.08
533	-4.83	-0.38	1012.00
534	-4.61	-0.35	1011.91
535	-4.67	-0.51	1011.82
536	-5.07	-0.32	1011.73
537	-4.40	-0.02	1011.65
538	-4.34	0.07	1011.56
539	-4.32	0.01	1011.47
540	-4.44	-0.34	1011.38
541	-4.16	-0.73	1011.30
542	-4.32	-1.07	1011.21
543	-4.25	-1.12	1011.12
544	-4.24	-0.85	1011.03
545	-4.19	-0.67	1010.94
546	-4.20	-0.27	1010.86
547	-4.10	0.23	1010.77
548	-4.02	0.65	1010.68
549	-4.04	0.55	1010.59
550	-4.02	0.43	1010.51
551	-3.83	0.32	1010.42
552	-3.89	0.22	1010.33
553	-4.23	-0.24	1010.24
554	-4.54	-0.10	1010.16
555	-4.60	-0.19	1010.07
556	-4.58	-0.64	1009.98
557	-4.63	-0.61	1009.89
558	-4.20	-0.03	1009.81

559	-4.24	0.64	1009.72
560	-4.16	0.78	1009.63
561	-4.18	0.71	1009.54
562	-4.16	0.66	1009.46
563	-4.13	0.63	1009.37
564	-4.55	-0.05	1009.28
565	-4.47	-0.19	1009.19
566	-4.68	0.10	1009.11
567	-4.77	-0.02	1009.02
568	-4.56	-0.32	1008.93
569	-4.47	0.07	1008.84
570	-4.20	0.41	1008.76
571	-4.16	0.54	1008.67
572	-4.15	0.23	1008.58
573	-4.26	0.31	1008.49
574	-3.91	1.16	1008.41
575	-3.64	1.09	1008.32
576	-3.84	0.10	1008.23
577	-4.17	-0.83	1008.14
578	-4.22	-1.06	1008.06
579	-3.72	-0.05	1007.97
580	-4.34	-0.73	1007.88
581	-4.38	-0.64	1007.79
582	-4.28	0.16	1007.70
583	-4.18	0.69	1007.62
584	-4.08	0.97	1007.53
585	-3.88	0.98	1007.44
586	-4.24	0.36	1007.35
587	-4.16	0.17	1007.27
588	-4.56	-0.33	1007.18
589	-5.00	-0.58	1007.09
590	-4.80	-0.84	1007.00
591	-4.83	0.11	1006.92

A.4 ATC13075

atc13075_backup

depth (mm)	$\delta^{18}O$	$\delta^{13}C$	age_model	depth (mm)	Sr/Ca (mmol/mol)
001	NaN	NaN	942.25	002	8.96
002	-4.77	-1.38	942.33	004	8.95
003	-4.81	-1.12	942.42	006	8.98
004	-4.63	-0.91	942.50	008	8.85
005	-4.64	-0.73	942.58	010	8.90
006	-4.59	-0.46	942.67	012	8.96
007	-4.85	-0.71	942.75	014	9.00
008	-5.06	-1.20	942.83	016	8.96
009	-5.03	-1.23	942.92	018	8.99
010	-4.88	-1.49	943.00	020	8.88
011	-4.77	-1.72	943.08	022	8.84
012	-4.71	-1.92	943.17	024	9.00
013	-4.63	-1.78	943.25	026	9.00
014	-4.75	-1.43	943.33	028	8.95
015	-4.63	-1.22	943.42	030	8.90
016	-4.70	-0.69	943.50	032	8.89
017	-4.65	0.02	943.58	034	9.02
018	-4.56	-0.04	943.67	036	9.00
019	-5.01	-0.41	943.75	038	8.97
020	-5.16	-0.74	943.84	040	9.01
021	-5.26	-1.31	943.92	042	8.86
022	-5.11	-1.67	944.00	044	8.91
023	-4.74	-1.26	944.09	046	8.97
024	-4.57	-0.81	944.17	048	8.99
025	-4.64	-0.72	944.25	050	8.96
026	-4.67	-0.38	944.34	052	8.92
027	-4.68	-0.42	944.42	054	8.93
028	-4.59	-0.18	944.50	056	8.88
029	-4.60	0.18	944.59	058	8.86
030	-4.83	-0.31	944.67	060	8.71
031	-4.75	-0.79	944.75	062	9.04
032	-5.01	-0.96	944.84	064	9.01
033	-4.61	-0.99	944.92	066	8.93
034	-4.56	-0.76	945.00	068	8.92
035	-4.26	-0.47	945.09	070	8.83
036	-4.33	-0.27	945.17	072	8.89
037	-4.49	-0.32	945.25	074	6.82
038	-4.69	-0.41	945.34	076	8.99
039	-4.38	-0.21	945.42	078	8.92
040	-4.33	-0.08	945.50	080	8.91
041	-4.44	-0.16	945.59	082	8.90
042	-4.51	-0.44	945.67	084	8.85

043	-4.84	-0.57	945.75	086	8.88
044	-4.57	-0.81	945.84	088	8.97
045	-4.64	-0.75	945.92	090	8.92
046	-4.35	-0.53	946.00	092	8.88
047	-4.18	-0.82	946.09	094	8.84
048	-4.34	-0.75	946.17	096	8.84
049	-4.56	-0.67	946.25	098	8.85
050	-4.62	-0.75	946.34	100	8.98
051	-4.71	-0.76	946.42	102	8.81
052	-4.61	-0.53	946.50	104	8.88
053	-4.46	-0.25	946.59	106	8.88
054	-4.50	-0.45	946.67	108	8.82
055	-4.81	-0.84	946.76	110	8.85
056	-4.58	-0.87	946.84	112	8.92
057	-4.79	-1.05	946.92	114	8.95
058	-4.62	-1.48	947.01	116	8.92
059	-4.83	-1.45	947.09	118	8.94
060	-4.74	-1.47	947.17	120	8.85
061	-4.28	-0.96	947.26	122	8.91
062	-4.07	-0.79	947.34	124	8.98
063	-4.17	-0.76	947.42	126	8.98
064	-4.14	-0.67	947.51	128	8.94
065	-4.31	-0.90	947.59	130	8.88
066	-4.72	-0.67	947.67	132	8.79
067	-4.70	-0.54	947.76	134	8.89
068	-4.33	-0.47	947.84	136	9.05
069	-4.72	-0.70	947.92	138	9.04
070	-4.87	-0.93	948.01	140	8.95
071	-4.88	-1.48	948.09	142	8.85
072	-4.91	-1.63	948.17	144	8.87
073	-4.68	-1.34	948.26	146	8.97
074	-4.46	-1.08	948.34	148	8.99
075	-4.46	-0.94	948.42	150	8.91
076	-4.43	-0.65	948.51	152	8.87
077	-4.66	-0.67	948.59	154	8.81
078	-4.39	-0.65	948.67	156	8.94
079	-4.57	-0.62	948.76	158	9.07
080	-4.27	-0.49	948.84	160	8.99
081	-4.76	-0.24	948.92	162	9.01
082	-4.80	-0.94	949.01	164	8.92
083	-4.89	-0.90	949.09	166	8.97
084	-5.02	-1.22	949.17	168	9.08
085	-4.73	-1.00	949.26	170	9.07

086	-4.59	-1.13	949.34	172	9.01
087	-4.62	-0.99	949.43	174	9.07
088	-4.72	-0.82	949.51	176	8.96
089	-4.58	-0.66	949.59	178	9.01
090	-4.48	-0.54	949.68	180	9.02
091	-4.47	-0.34	949.76	182	9.05
092	-4.64	-0.64	949.84	184	8.94
093	-4.38	-0.56	949.93	186	8.93
094	-4.84	-0.50	950.01	188	8.90
095	-4.71	-0.59	950.09	190	9.00
096	-5.22	-0.98	950.18	192	8.98
097	-4.99	-1.17	950.26	194	8.97
098	-4.71	-0.96	950.34	196	8.96
099	-4.44	-0.85	950.43	198	8.84
100	-4.42	-0.88	950.51	200	8.92
101	-4.22	-0.86	950.59	202	9.06
102	-4.43	-0.63	950.68	204	9.05
103	-4.68	-0.37	950.76	206	8.96
104	-4.49	-0.40	950.84	208	8.95
105	-4.52	-0.17	950.93	210	8.95
106	-4.63	-0.38	951.01	212	9.06
107	-5.32	-0.73	951.09	214	9.06
108	-4.87	-1.07	951.18	216	8.99
109	-4.88	-1.53	951.26	218	8.95
110	-4.96	-1.43	951.34	220	8.89
111	-5.04	-1.71	951.43	222	8.96
112	-4.94	-1.24	951.51	224	9.04
113	-4.54	-0.80	951.59	226	9.02
114	-4.55	-0.75	951.68	228	8.97
115	-4.76	-0.60	951.76	230	8.94
116	-4.71	-0.64	951.84	232	8.87
117	-4.31	-0.53	951.93	234	8.89
118	-4.29	-0.23	952.01	236	9.01
119	-5.03	-0.38	952.09	238	9.04
120	-5.16	-1.26	952.18	240	8.96
121	-4.89	-1.19	952.26	242	8.93
122	-4.75	-1.18	952.35	244	8.88
123	-4.47	-1.17	952.43	246	8.96
124	-4.40	-1.11	952.51	248	9.01
125	-4.32	-0.81	952.60	250	8.97
126	-4.51	-0.76	952.68	252	8.96
127	-4.50	-0.51	952.76	254	8.78
128	-4.38	-0.38	952.85	256	8.93

129	-4.52	-0.60	952.93	258	9.02
130	-4.78	-0.23	953.01	260	9.08
131	-4.78	-0.38	953.10	262	8.99
132	-5.20	-1.00	953.18	264	8.92
133	NaN	NaN	953.26	266	8.95
134	-4.78	-1.10	953.35	268	9.07
135	-4.67	-1.09	953.43	270	9.05
136	-4.49	-0.81	953.51	272	8.93
137	-4.33	-0.34	953.60	274	8.86
138	-4.44	-0.72	953.68	276	8.92
139	-4.49	-0.55	953.76	278	9.07
140	-4.38	-0.16	953.85	280	8.97
141	-4.74	-0.05	953.93	282	8.95
142	-4.93	-0.23	954.01	284	8.98
143	-4.82	-0.65	954.10	286	8.87
144	-4.74	-0.94	954.18	288	8.82
145	-4.51	-1.07	954.26	290	8.84
146	-4.57	-0.74	954.35	292	8.99
147	-4.52	-0.67	954.43	294	9.02
148	-4.52	-0.48	954.51	296	8.93
149	-4.68	-0.20	954.60	298	8.86
150	-4.60	0.01	954.68	300	8.89
151	-4.57	0.04	954.76	302	8.99
152	-4.68	-0.27	954.85	304	8.99
153	-4.73	-0.59	954.93	306	8.96
154	-4.76	-0.86	955.01	308	8.97
155	-4.58	-0.66	955.10	310	8.91
156	-4.23	-0.93	955.18	312	8.88
157	-4.41	-0.77	955.27	314	9.02
158	-4.41	-0.56	955.35	316	9.00
159	-4.36	-0.58	955.43	318	8.90
160	-4.12	-0.27	955.52	320	8.85
161	-4.48	-0.40	955.60	322	8.90
162	-4.11	-0.25	955.68	324	8.99
163	-4.20	0.00	955.77	326	8.96
164	-4.66	-0.51	955.85	328	8.88
165	-4.52	-0.54	955.93	330	8.81
166	-4.65	-0.89	956.02	332	8.81
167	-4.50	-0.94	956.10	334	8.85
168	-4.32	-0.64	956.18	336	9.00
169	-4.17	-0.61	956.27	338	8.94
170	-4.38	-0.30	956.35	340	8.83
171	-4.49	-0.24	956.43	342	8.84

172	-4.60	-0.27	956.52	344	8.82
173	-4.37	-0.05	956.60	346	8.91
174	-4.33	-0.05	956.68	348	8.98
175	-4.88	-0.50	956.77	350	8.93
176	-4.95	-0.95	956.85	352	8.87
177	-4.51	-1.08	956.93	354	8.78
178	-4.45	-1.25	957.02	356	8.84
179	-4.61	-0.92	957.10	358	8.99
180	-4.36	-0.63	957.18	360	8.54
181	-4.28	-0.46	957.27	362	8.89
182	-4.31	-0.46	957.35	364	8.86
183	-4.32	-0.37	957.43	366	8.85
184	-4.36	-0.26	957.52	368	8.89
185	-4.58	0.08	957.60	370	8.98
186	-4.58	-0.17	957.68	372	8.92
187	-4.78	-0.76	957.77	374	8.89
188	-4.67	-0.75	957.85	376	8.84
189	-4.69	-1.09	957.93	378	8.97
190	-4.52	-0.88	958.02	380	9.04
191	-4.43	-0.52	958.10	382	8.94
192	-4.50	-0.50	958.19	384	8.92
193	-3.03	-0.33	958.27	386	8.78
194	-4.34	-0.53	958.35	388	8.85
195	-4.42	-0.15	958.44	390	8.96
196	-4.47	0.24	958.52	392	8.99
197	-4.49	0.05	958.60	394	8.92
198	-4.77	-0.66	958.69	396	8.91
199	-4.71	-0.46	958.77	398	8.85
200	-4.58	-0.75	958.85	400	8.89
201	-4.55	-0.94	958.94	402	9.01
202	-4.57	-0.83	959.02	404	8.98
203	-4.40	-0.27	959.10	406	8.84
204	-4.36	-0.01	959.19	408	8.86
205	-4.26	-0.13	959.27	410	8.85
206	-4.34	-0.08	959.35	412	8.92
207	-4.35	-0.02	959.44	414	8.99
208	-4.65	-0.28	959.52	416	8.95
209	-4.71	-0.45	959.60	418	8.86
210	-4.61	-0.77	959.69	420	8.86
211	-4.57	-0.91	959.77	422	8.90
212	-4.84	-0.80	959.85	424	9.03
213	-4.11	-0.64	959.94	426	8.99
214	-4.07	-0.63	960.02	428	8.93

215	-4.24	-0.53	960.10	430	8.83
216	-4.60	-0.40	960.19	432	8.84
217	-4.59	-0.39	960.27	434	8.96
218	-4.23	-0.35	960.35	436	9.02
219	-4.25	0.06	960.44	438	8.94
220	-4.59	-0.68	960.52	440	8.91
221	-4.72	-0.73	960.60	442	8.85
222	-4.38	-0.84	960.69	444	8.89
223	-4.28	-1.14	960.77	446	8.96
224	-4.16	-1.07	960.86	448	8.93
225	-4.45	-0.75	960.94	450	8.88
226	-4.31	-0.48	961.02	452	8.84
227	-4.30	-0.49	961.11	454	8.80
228	-4.61	-0.32	961.19	456	8.88
229	-4.65	-0.24	961.27	458	9.02
230	-4.48	-0.02	961.36	460	8.96
231	-5.00	-0.21	961.44	462	8.85
232	-4.88	-0.52	961.52	464	8.83
233	-4.86	-0.74	961.61	466	8.95
234	-4.75	-0.93	961.69	468	
235	-4.71	-0.72	961.77	470	9.01
236	-4.46	-0.56	961.86	472	8.91
237	-4.57	-0.74	961.94	474	8.89
238	-4.59	-0.37	962.02	476	8.87
239	-4.48	-0.23	962.11	478	8.99
240	-4.50	-0.07	962.19	480	9.08
241	-4.40	-0.27	962.27	482	9.14
242	-4.37	0.04	962.36	484	9.04
243	-4.59	-0.36	962.44	486	8.98
244	-4.80	-0.77	962.52	488	8.90
245	-4.75	-0.77	962.61	490	9.03
246	-4.56	-0.79	962.69	492	9.04
247	-4.53	-1.07	962.77	494	9.09
248	-4.45	-0.82	962.86	496	9.02
249	-4.55	-0.50	962.94	498	8.93
250	-4.39	-0.41	963.02	500	8.89
251	-4.39	-0.12	963.11	502	8.95
252	-4.21	0.08	963.19	504	8.73
253	-4.75	-0.08	963.27	506	8.93
254	-4.74	-0.34	963.36	508	8.91
255	-4.87	-0.55	963.44	510	8.81
256	-4.47	-0.67	963.52	512	8.95
257	-4.54	-0.61	963.61	514	8.95

258	-4.33	-0.64	963.69	516	8.97
259	-4.22	-0.54	963.78	518	8.88
260	-4.20	-0.39	963.86	520	8.90
261	-4.46	-0.11	963.94	522	8.93
262	-4.49	-0.13	964.03	524	9.02
263	-4.30	0.32	964.11	526	9.03
264	-4.60	-0.07	964.19	528	8.93
265	-4.56	-0.32	964.28	530	8.85
266	-4.45	-0.70	964.36	532	8.86
267	-4.38	-0.51	964.44	534	8.87
268	-4.18	-0.55	964.53	536	8.97
269	-4.07	-0.34	964.61	538	9.00
270	-4.23	-0.76	964.69	540	8.95
271	-4.50	-0.70	964.78	542	8.86
272	-4.70	-0.27	964.86	544	8.85
273	-4.67	-0.23	964.94	546	8.92
274	-4.58	-0.31	965.03	548	9.01
275	-4.65	-0.39	965.11	550	9.01
276	-4.56	-0.47	965.19	552	8.92
277	-4.72	-0.62	965.28	554	8.85
278	-4.52	-0.45	965.36	556	8.81
279	-4.01	0.03	965.44	558	8.93
280	-4.49	-0.68	965.53	560	8.91
281	-4.79	-0.80	965.61	562	8.96
282	-4.72	-0.72	965.69	564	9.04
283	-4.77	-0.89	965.78	566	8.95
284	-4.67	-1.37	965.86	568	8.85
285	-4.84	-1.09	965.94	570	8.83
286	-4.77	-0.54	966.03	572	8.92
287	-4.79	-0.42	966.11	574	8.92
288	-4.94	-0.30	966.19	576	9.01
289	-5.12	-0.55	966.28	578	8.99
290	-5.10	-0.69	966.36	580	8.90
291	-5.02	-0.56	966.44	582	8.80
292	-4.58	-0.45	966.53	584	8.81
293	-4.56	-0.53	966.61	586	8.94
294	-4.33	-0.19	966.70	588	8.97
295	-4.38	0.03	966.78	590	9.00
296	-4.56	-0.05	966.86	592	9.00
297	-4.86	-0.31	966.95	594	8.92
298	-4.93	-0.44	967.03	596	8.85
299	-5.24	-1.04	967.11	598	8.86
300	-5.23	-1.15	967.20	600	8.92

301	-4.50	-0.62	967.28	602	9.01
302	-4.38	-0.68	967.36	604	9.03
303	-4.35	-0.83	967.45	606	9.05
304	-4.33	-0.66	967.53	608	8.90
305	-4.28	-0.36	967.61	610	8.82
306	-4.40	-0.13	967.70	612	8.83
307	-4.36	0.28	967.78	614	8.91
308	-4.42	0.19	967.86	616	8.96
309	-4.51	0.11	967.95	618	8.98
310	-4.63	-0.27	968.03	620	8.99
311	-4.91	-1.04	968.11	622	9.03
312	-4.77	-1.08	968.20	624	8.93
313	-4.61	-0.86	968.28	626	8.86
314	-4.67	-0.81	968.36	628	8.93
315	-4.63	-0.54	968.45	630	8.99
316	-4.48	-0.30	968.53	632	8.96
317	-4.71	-0.45	968.61	634	9.00
318	-4.76	-0.39	968.70	636	9.00
319	-4.90	-0.51	968.78	638	9.01
320	-4.92	-0.53	968.86	640	8.97
321	-4.94	-0.61	968.95	642	8.93
322	-4.84	-1.03	969.03	644	8.88
323	-4.72	-0.92	969.11	646	8.93
324	-4.62	-0.45	969.20	648	8.95
325	-4.64	-0.27	969.28	650	8.97
326	-4.55	-0.38	969.36	652	9.04
327	-4.71	-0.37	969.45	654	9.10
328	-4.67	-0.18	969.53	656	9.11
329	-4.81	-0.55	969.62	658	9.14
330	-4.95	-0.41	969.70	660	9.12
331	-4.95	-0.51	969.78	662	9.11
332	-4.85	-0.59	969.87	664	9.00
333	-4.91	-1.17	969.95	666	8.95
334	-4.62	-1.24	970.03	668	8.95
335	-4.55	-0.96	970.12	670	8.98
336	-4.38	-0.50	970.20	672	9.04
337	-4.31	-0.54	970.28	674	9.13
338	-4.37	-0.43	970.37	676	9.10
339	-4.57	-0.39	970.45	678	9.13
340	-4.80	-0.82	970.53	680	8.99
341	-4.77	-0.53	970.62	682	8.84
342	-4.82	-0.73	970.70	684	8.93
343	-5.00	-1.16	970.78	686	8.95

344	-4.99	-0.92	970.87	688	9.01
345	-4.98	-1.38	970.95	690	9.01
346	-4.78	-1.27	971.03	692	8.94
347	-4.73	-1.18	971.12	694	8.85
348	-4.52	-0.94	971.20	696	
349	-4.71	-0.96	971.28	698	
350	-4.67	-0.79	971.37	700	9.02
351	-4.65	-0.46	971.45	702	9.00
352	-4.87	-0.34	971.53	704	8.98
353	-4.91	-0.19	971.62	706	8.87
354	-4.82	-0.52	971.70	708	8.87
355	-5.03	-0.66	971.78	710	8.96
356	-4.84	-0.55	971.87	712	8.99
357	-4.53	-0.28	971.95	714	9.00
358	-4.27	-0.54	972.03	716	9.08
359	-4.50	-0.38	972.12	718	9.05
360	-4.51	-0.15	972.20	720	9.05
361	-4.31	-0.36	972.29	722	8.94
362	-4.56	-0.56	972.37	724	8.98
363	-4.45	-0.20	972.45	726	8.98
364	-4.59	-0.33	972.54	728	9.02
365	-4.92	-0.75	972.62	730	9.06
366	-4.87	-0.75	972.70	732	9.07
367	-4.88	-0.83	972.79	734	8.98
368	-4.74	-0.80	972.87	736	8.89
369	-4.59	-0.58	972.95	738	8.97
370	-4.54	-0.53	973.04	740	8.97
371	-4.60	-0.55	973.12	742	9.03
372	-4.74	-0.28	973.20	744	9.10
373	NaN	NaN	973.29	746	8.92
374	-4.86	-0.51	973.37	748	8.87
375	-4.94	-0.85	973.45	750	8.95
376	-5.01	-0.95	973.54	752	8.98
377	-4.71	-0.62	973.62	754	9.04
378	-4.52	-0.69	973.70	756	9.03
379	-4.40	-0.42	973.79	758	8.93
380	-4.25	-0.34	973.87	760	9.00
381	-4.54	-0.51	973.95	762	9.06
382	-4.57	-0.47	974.04	764	9.07
383	-4.63	-0.46	974.12	766	8.93
384	-4.72	-0.23	974.20	768	8.88
385	-4.77	-0.26	974.29	770	8.94
386	-4.95	-0.66	974.37	772	8.94

387	-4.96	-0.85	974.45	774	8.98
388	-5.00	-1.03	974.54	776	8.94
389	-4.80	-0.93	974.62	778	8.80
390	-4.64	-0.77	974.70	780	8.85
391	-4.37	-0.58	974.79	782	8.85
392	-4.45	-0.37	974.87	784	8.81
393	-4.56	-0.35	974.95	786	8.52
394	-4.61	-0.15	975.04	788	8.33
395	-4.57	-0.27	975.12	790	7.83
396	-4.63	-0.47	975.21	792	8.17
397	-4.93	-0.93	975.29	794	8.18
398	-4.92	-1.02	975.37	796	7.80
399	-4.86	-1.13	975.46	798	8.16
400	-4.92	-1.01	975.54	800	8.21
401	-4.58	-0.81	975.62	802	8.19
402	-4.45	-0.84	975.71	804	8.24
403	-4.50	-0.78	975.79	806	8.06
404	-4.51	-0.57	975.87	808	8.24
405	-4.54	-0.48	975.96	810	8.27
406	-4.88	-0.62	976.04	812	8.48
407	-4.73	-0.40	976.12	814	8.33
408	-5.00	-0.86	976.21	816	8.19
409	-5.07	-0.95	976.29	818	8.30
410	-5.08	-1.16	976.37	820	8.18
411	-5.28	-1.05	976.46	822	8.25
412	-4.69	-0.71	976.54	824	8.26
413	-4.72	-0.55	976.62	826	8.20
414	-4.54	-0.55	976.71	828	8.08
415	-4.49	-0.49	976.79	830	8.12
416	-4.75	-0.46	976.87	832	8.48
417	-4.70	-0.46	976.96	834	8.47
418	-4.75	-0.31	977.04	836	8.59
419	-5.22	-0.72	977.12	838	8.54
420	-4.94	-0.83	977.21	840	8.71
421	-4.64	-0.85	977.29	842	8.84
422	-4.58	-1.25	977.37	844	8.98
423	-4.31	-0.90	977.46	846	9.00
424	-4.20	-0.69	977.54	848	8.81
425	-4.24	-0.54	977.62	850	8.79
426	-4.20	-0.36	977.71	852	8.84
427	-4.24	-0.37	977.79	854	8.84
428	-4.15	-0.27	977.87	856	8.72
429	-4.61	-0.59	977.96	858	8.57

430	-4.68	-0.64	978.04
431	-4.60	-0.81	978.13
432	-4.65	-0.92	978.21
433	-4.55	-0.93	978.29
434	-4.26	-1.01	978.38
435	-4.38	-0.73	978.46
436	-4.12	-0.63	978.54
437	-4.32	-0.15	978.63
438	-4.31	-0.14	978.71
439	-4.31	-0.16	978.79
440	-4.53	-0.42	978.88
441	-5.04	-0.57	978.96
442	-4.80	-0.77	979.04
443	-4.78	-1.26	979.13
444	-4.79	-1.39	979.21
445	-4.70	-0.98	979.29
446	-4.46	-0.85	979.38
447	-4.75	-0.72	979.46
448	-4.56	-1.02	979.54
449	-4.59	-0.90	979.63
450	-4.56	-0.66	979.71
451	-4.80	-0.86	979.79
452	-4.69	-0.70	979.88
453	-4.98	-0.99	979.96
454	-4.80	-1.17	980.04
455	-4.89	-0.94	980.13
456	-4.84	-0.90	980.21
457	-4.77	-1.06	980.29
458	-4.34	-0.66	980.38
459	-4.54	-0.53	980.46
460	-4.69	-0.39	980.54
461	-4.47	-0.50	980.63
462	-4.79	-0.34	980.71
463	-5.09	-0.36	980.79
464	-5.06	-0.43	980.88
465	-5.22	-0.74	980.96
466	-4.99	-0.39	981.05
467	-4.44	-0.40	981.13
468	-4.09	-1.15	981.21
469	-4.37	-1.51	981.30
470	-4.82	-1.43	981.38
471	-4.88	-1.43	981.46
472	-4.96	-1.42	981.55

473	-5.01	-1.35	981.63
474	-5.02	-1.16	981.71
475	-5.15	-1.14	981.80
476	-4.80	-0.75	981.88
477	-4.72	-0.60	981.96
478	-4.43	-0.21	982.05
479	-4.71	-0.15	982.13
480	-4.39	-0.39	982.21
481	-4.05	-0.57	982.30
482	-3.99	-0.88	982.38
483	-4.08	-1.49	982.46
484	-4.20	-1.37	982.55
485	-4.45	-1.59	982.63
486	-4.65	-1.57	982.71
487	-4.70	-1.14	982.80
488	-4.65	-0.52	982.88
489	-4.39	-0.23	982.96
490	-4.15	0.22	983.05
491	-4.14	0.02	983.13
492	-4.30	-0.22	983.21
493	-4.14	-0.73	983.30
494	-4.16	-0.75	983.38
495	-4.26	-1.22	983.46
496	-4.31	-1.41	983.55
497	-4.47	-1.45	983.63
498	-4.58	-1.23	983.71
499	-4.67	-1.19	983.80
500	-4.70	-0.87	983.88
501	-4.36	-0.13	983.97
502	-4.34	-0.11	984.05
503	-4.52	-0.45	984.13
504	-4.19	-0.46	984.22
505	-4.31	-0.54	984.30
506	-4.55	-1.02	984.38
507	-4.50	-1.39	984.47
508	-4.52	-1.77	984.55
509	-4.66	-1.47	984.63
510	-4.74	-0.84	984.72
511	-4.72	-0.42	984.80
512	-4.19	0.07	984.88
513	-4.29	-0.16	984.97
514	-4.42	-0.18	985.05
515	-4.28	-0.28	985.13

516	-4.31	-0.51	985.22
517	-4.53	-0.70	985.30
518	-4.74	-0.97	985.38
519	-4.64	-0.67	985.47
520	-4.47	-0.49	985.55
521	-4.28	-0.19	985.63
522	-4.40	-0.72	985.72
523	-4.41	-0.89	985.80
524	-4.39	-1.03	985.88
525	-4.24	-0.93	985.97
526	-4.47	-1.07	986.05
527	-4.49	-1.55	986.13
528	-4.67	-1.74	986.22
529	-4.76	-1.43	986.30
530	-4.82	-1.34	986.38
531	-4.84	-1.03	986.47
532	-4.64	-0.36	986.55
533	-4.34	-0.16	986.64
534	-4.51	-0.57	986.72
535	-4.51	-0.87	986.80
536	-4.36	-0.70	986.89
537	-4.45	-0.75	986.97
538	-4.32	-0.89	987.05
539	-4.41	-1.67	987.14
540	-4.64	-1.49	987.22
541	-4.54	-1.28	987.30
542	-4.66	-1.06	987.39
543	-4.68	-0.87	987.47
544	-4.33	-0.24	987.55
545	-4.31	-0.33	987.64
546	-4.48	-0.85	987.72
547	-4.34	-0.83	987.80
548	-4.44	-0.67	987.89
549	-4.29	-0.94	987.97
550	-4.26	-0.90	988.05
551	-4.41	-1.02	988.14
552	-4.46	-1.42	988.22
553	-4.78	-1.70	988.30
554	-4.88	-1.33	988.39
555	-4.78	-1.13	988.47
556	-4.70	-1.24	988.55
557	-4.56	-0.55	988.64
558	-4.27	-0.26	988.72

559	-4.40	-0.66	988.80
560	-4.71	-0.85	988.89
561	-4.47	-0.78	988.97
562	-4.65	-0.83	989.05
563	-4.39	-1.01	989.14
564	-4.21	-1.03	989.22
565	-4.26	-1.14	989.30
566	-4.47	-1.71	989.39
567	-4.67	-1.32	989.47
568	-4.80	-1.38	989.56
569	-4.85	-1.63	989.64
570	-4.81	-0.97	989.72
571	-4.58	-0.51	989.81
572	-4.35	-0.28	989.89
573	-4.31	-0.70	989.97
574	-4.40	-0.95	990.06
575	-4.43	-0.86	990.14
576	-4.18	-1.08	990.22
577	-4.43	-1.24	990.31
578	-4.49	-1.10	990.39
579	-4.57	-1.17	990.47
580	-4.70	-1.44	990.56
581	-4.85	-1.56	990.64
582	NaN	NaN	990.72
583	-4.79	-0.89	990.81
584	-4.45	-0.30	990.89
585	-4.38	-0.45	990.97
586	-4.30	-1.27	991.06
587	-4.57	-0.78	991.14
588	-3.91	-0.51	991.22
589	-4.56	-0.91	991.31
590	-4.49	-1.25	991.39
591	-4.64	-1.24	991.47
592	-4.80	-1.57	991.56
593	-4.75	-1.44	991.64
594	-4.70	-1.39	991.72
595	-4.87	-1.41	991.81
596	-4.96	-1.48	991.89
597	-4.96	-0.87	991.97
598	-4.52	-0.28	992.06
599	-4.61	-0.58	992.14
600	-4.56	-0.46	992.22
601	-4.27	-0.77	992.31

602	-4.28	-0.61	992.39
603	-4.15	-1.07	992.48
604	-4.23	-1.31	992.56
605	-4.27	-1.39	992.64
606	-4.41	-1.38	992.73
607	-4.62	-1.85	992.81
608	-4.87	-1.50	992.89
609	-4.98	-1.42	992.98
610	-5.09	-1.68	993.06
611	-4.89	-1.00	993.14
612	-4.97	-0.46	993.23
613	-4.73	-0.34	993.31
614	-4.61	-0.39	993.39
615	-4.67	-0.71	993.48
616	-4.42	-0.81	993.56
617	-4.53	-0.77	993.64
618	-4.39	-0.99	993.73
619	-4.47	-1.10	993.81
620	-4.43	-1.22	993.89
621	-4.44	-1.07	993.98
622	-4.36	-1.14	994.06
623	-4.66	-1.35	994.14
624	-4.71	-1.49	994.23
625	-4.87	-1.53	994.31
626	-4.96	-1.43	994.39
627	-4.81	-0.93	994.48
628	-4.58	-0.81	994.56
629	-4.46	-0.99	994.64
630	-4.39	-1.26	994.73
631	-4.50	-1.31	994.81
632	-4.25	-1.49	994.89
633	-4.50	-1.45	994.98
634	-4.41	-1.37	995.06
635	-4.33	-1.21	995.14
636	-4.31	-1.32	995.23
637	-4.24	-1.38	995.31
638	-4.41	-1.65	995.40
639	-4.62	-1.99	995.48
640	-4.60	-2.29	995.56
641	-4.62	-2.24	995.65
642	-4.67	-1.71	995.73
643	-4.85	-1.60	995.81
644	-4.76	-1.66	995.90

645	-4.85	-1.58	995.98
646	-4.73	-1.38	996.06
647	-4.61	-1.34	996.15
648	-4.38	-1.25	996.23
649	-4.53	-1.50	996.31
650	-4.41	-1.49	996.40
651	-4.40	-1.16	996.48
652	-4.32	-1.07	996.56
653	-4.42	-1.27	996.65
654	-4.43	-1.26	996.73
655	-4.35	-1.20	996.81
656	-4.42	-1.15	996.90
657	-4.26	-1.36	996.98
658	-4.23	-1.27	997.06
659	-4.19	-1.37	997.15
660	-4.27	-1.27	997.23
661	-4.09	-1.26	997.31
662	-4.17	-1.42	997.40
663	-4.19	-1.31	997.48
664	-4.33	-1.27	997.56
665	-4.38	-1.17	997.65
666	-4.47	-1.15	997.73
667	-4.56	-1.10	997.81
668	-4.39	-0.63	997.90
669	-4.35	-0.36	997.98
670	-4.18	-0.38	998.07
671	-4.18	-0.68	998.15
672	-4.19	-0.78	998.23
673	-4.13	-0.77	998.32
674	-4.09	-0.57	998.40
675	-4.15	-0.84	998.48
676	-4.10	-1.21	998.57
677	-4.11	-1.38	998.65
678	-4.07	-1.47	998.73
679	-4.17	-1.40	998.82
680	-4.52	-1.42	998.90
681	-4.53	-1.07	998.98
682	-4.68	-0.90	999.07
683	-4.62	-0.74	999.15
684	-4.34	-0.23	999.23
685	-4.33	-0.57	999.32
686	-4.39	-0.66	999.40
687	-4.42	-0.47	999.48

688	-4.24	-0.48	999.57
689	-4.38	-0.98	999.65
690	-4.40	-0.79	999.73
691	-4.66	-1.52	999.82
692	-4.66	-1.94	999.90
693	-4.81	-1.94	999.98
694	-4.88	-1.62	1000.07
695	-4.82	-0.93	1000.15
696	-4.00	-0.19	1000.23
697	-4.08	-0.72	1000.32
698	-4.45	-0.63	1000.40
699	-4.61	-1.21	1000.48
700	-4.52	-1.63	1000.57
701	-4.58	-1.66	1000.65
702	-4.61	-1.99	1000.73
703	-4.72	-1.99	1000.82
704	-4.64	-1.83	1000.90
705	-5.02	-1.87	1000.99
706	-4.98	-1.93	1001.07
707	-4.97	-1.67	1001.15
708	-4.83	-1.50	1001.24
709	-4.81	-0.95	1001.32
710	-4.41	-0.23	1001.40
711	-4.45	-0.65	1001.49
712	-4.64	-0.64	1001.57
713	-4.52	-0.62	1001.65
714	-4.44	-0.85	1001.74
715	-4.38	-0.92	1001.82
716	-4.27	-1.05	1001.90
717	-4.27	-1.26	1001.99
718	-4.36	-1.41	1002.07
719	-4.61	-1.70	1002.15
720	-4.60	-1.58	1002.24
721	-4.38	-1.47	1002.32
722	-4.38	-1.06	1002.40
723	-4.39	-0.73	1002.49
724	-4.14	-0.68	1002.57
725	-4.02	-0.32	1002.65
726	-4.12	-0.56	1002.74
727	-4.34	-1.08	1002.82
728	-4.22	-0.89	1002.90
729	-4.08	-1.12	1002.99
730	-4.14	-1.01	1003.07

731	-4.04	-0.93	1003.15
732	-4.16	-1.24	1003.24
733	-4.38	-1.53	1003.32
734	-4.46	-1.59	1003.40
735	-4.72	-1.59	1003.49
736	-4.81	-1.38	1003.57
737	-4.57	-0.80	1003.65
738	-4.18	-0.22	1003.74
739	-4.23	-0.56	1003.82
740	-4.18	-0.66	1003.91
741	-4.42	-1.02	1003.99
742	-4.42	-0.71	1004.07
743	-4.27	-0.77	1004.16
744	-4.30	-1.09	1004.24
745	-4.45	-1.56	1004.32
746	-4.72	-1.60	1004.41
747	-4.98	-1.29	1004.49
748	-4.98	-1.33	1004.57
749	-4.84	-0.85	1004.66
750	-4.55	-0.32	1004.74
751	-4.54	-0.73	1004.82
752	-4.37	-0.83	1004.91
753	-4.43	-0.63	1004.99
754	-4.18	-0.95	1005.07
755	-4.16	-1.26	1005.16
756	-4.07	-1.54	1005.24
757	-4.44	-1.40	1005.32
758	-4.64	-0.90	1005.41
759	-4.48	-0.65	1005.49
760	-4.01	-0.35	1005.57
761	-4.02	-0.38	1005.66
762	-4.11	-0.90	1005.74
763	-4.23	-1.04	1005.82
764	-4.08	-1.06	1005.91
765	-4.41	-1.51	1005.99
766	-4.57	-1.38	1006.07
767	-4.53	-1.40	1006.16
768	-4.80	-1.23	1006.24
769	-4.77	-1.20	1006.32
770	-4.41	-0.79	1006.41
771	-4.51	-0.79	1006.49
772	-4.48	-0.78	1006.57
773	-4.47	-0.69	1006.66

774	-4.40	-1.03	1006.74
775	-4.42	-1.19	1006.83
776	-4.60	-1.41	1006.91
777	-4.69	-1.75	1006.99
778	-4.90	-1.11	1007.08
779	-5.09	-0.76	1007.16
780	-4.82	-0.78	1007.24
781	-4.15	-0.07	1007.33
782	-4.17	-0.55	1007.41
783	-3.98	-0.45	1007.49
784	-4.02	-0.65	1007.58
785	-3.94	-0.85	1007.66
786	-4.27	-1.05	1007.74
787	-4.24	-1.22	1007.83
788	-4.59	-1.49	1007.91
789	-4.70	-1.43	1007.99
790	-4.61	-1.05	1008.08
791	-4.16	-0.54	1008.16
792	-4.08	-0.50	1008.24
793	-4.40	-0.81	1008.33
794	-4.24	-0.66	1008.41
795	-4.19	-0.72	1008.49
796	-4.20	-1.03	1008.58
797	-4.18	-0.94	1008.66
798	-4.29	-1.06	1008.74
799	-4.54	-1.21	1008.83
800	-4.57	-1.13	1008.91
801	-4.56	-0.68	1008.99
802	-4.78	-1.32	1009.08
803	-4.36	-0.57	1009.16
804	-4.27	-0.67	1009.24
805	-4.27	-0.67	1009.33
806	-4.09	-0.64	1009.41
807	-4.22	-0.76	1009.50
808	-4.22	-1.03	1009.58
809	-4.19	-0.81	1009.66
810	-4.48	-1.09	1009.75
811	-4.38	-0.76	1009.83
812	-4.54	-0.93	1009.91
813	-4.44	-1.07	1010.00
814	-4.20	-0.46	1010.08
815	-4.06	-0.71	1010.16
816	-4.19	-0.80	1010.25

817	-4.27	-1.01	1010.33
818	-4.17	-1.05	1010.41
819	-4.07	-1.26	1010.50
820	-4.17	-1.35	1010.58
821	-4.22	-1.25	1010.66
822	-4.29	-1.31	1010.75
823	-4.66	-1.59	1010.83
824	-4.78	-1.53	1010.91
825	-4.84	-1.04	1011.00
826	-4.90	-1.02	1011.08
827	-4.62	-0.86	1011.16
828	-4.49	-0.45	1011.25
829	-4.50	-1.03	1011.33
830	-4.63	-1.14	1011.41
831	-4.54	-1.06	1011.50
832	-4.45	-1.13	1011.58
833	-4.53	-1.34	1011.66
834	-4.73	-1.74	1011.75
835	-4.70	-1.80	1011.83
836	-4.71	-1.80	1011.91
837	-4.96	-1.96	1012.00
838	-4.74	-1.72	1012.08
839	-4.92	-1.55	1012.16
840	-4.82	-1.38	1012.25
841	-4.60	-1.33	1012.33
842	-4.37	-0.72	1012.42
843	-4.05	-0.66	1012.50
844	-3.94	-0.50	1012.58
845	-4.13	-0.94	1012.67
846	-4.36	-1.01	1012.75
847	-4.73	-0.71	1012.83
848	-4.89	-0.59	1012.92
849	-4.65	-0.30	1013.00
850	-4.40	-0.09	1013.08
851	-4.44	-0.17	1013.17
852	-4.34	-0.62	1013.25
853	-4.52	-1.04	1013.33
854	-4.51	-1.59	1013.42
855	-4.56	-1.11	1013.50
856	-4.65	-1.04	1013.58
857	-4.74	-1.19	1013.67
858	-4.63	-0.98	1013.75

A.5 ATC13076

atc13076

depth (mm)	$\delta^{13}C$	$\delta^{18}O$	Sr/Ca (mmol/mol)	age_model
001	-2.03	-4.72	9.01	1120.50
002	-2.21	-4.53	9.01	1120.56
003	-2.23	-4.44	8.98	1120.63
004	-2.93	-5.78	8.97	1120.69
005	-2.69	-4.80	8.92	1120.75
006	-2.95	-4.82	8.95	1120.82
007	-3.11	-5.15	8.97	1120.88
008	-3.29	-5.04	8.98	1120.95
009	-3.06	-4.72	8.97	1121.01
010	-3.51	-4.88	8.99	1121.07
011	-3.67	-5.07	9.00	1121.14
012	-3.52	-4.73	9.01	1121.20
013	-3.39	-4.81	9.03	1121.26
014	-3.40	-4.63	9.07	1121.33
015	-3.23	-4.63	9.06	1121.39
016	-2.83	-4.65	9.02	1121.46
017	-2.64	-4.56	9.00	1121.52
018	-2.79	-4.72	8.93	1121.58
019	-2.74	-4.61	8.93	1121.65
020	-2.63	-4.80	8.93	1121.71
021	-2.43	-4.70	8.92	1121.77
022	-2.32	-4.66	8.96	1121.84
023	-2.28	-4.77	8.97	1121.90
024	-2.16	-4.96	8.97	1121.97
025	-1.73	-4.75	8.96	1122.03
026	-1.65	-4.67	8.96	1122.09
027	-1.97	-4.79	8.98	1122.16
028	-2.03	-4.68	9.00	1122.22
029	-2.66	-4.89	9.03	1122.28
030	-2.98	-5.08	9.03	1122.35
031	-3.00	-4.86	8.99	1122.41
032	-3.25	-4.89	9.00	1122.47
033	-3.30	-4.96	8.95	1122.54
034	-3.24	-4.76	8.93	1122.60
035	-3.29	-4.78	8.95	1122.67
036	-3.19	-4.68	8.90	1122.73
037	-2.91	-4.66	8.90	1122.79
038	-2.47	-4.77	8.92	1122.86
039	-2.21	-4.73	8.90	1122.92
040	-2.34	-4.73	8.91	1122.98
041	-2.42	-4.78	8.96	1123.05
042	-2.26	-4.79	8.99	1123.11
043	-2.07	-4.86	9.02	1123.18
044	-2.27	-5.23	9.05	1123.24
045	-2.36	-4.99	9.07	1123.30
046	-2.37	-5.21	9.05	1123.37
047	-2.57	-5.19	9.02	1123.43
048	-2.40	-4.70	9.03	1123.49

049	-2.49	-4.97	9.01	1123.56
050	-2.63	-5.01	8.99	1123.62
051	-2.83	-5.18	8.95	1123.69
052	-2.91	-5.05	8.90	1123.75
053	-2.94	-4.75	8.94	1123.81
054	-3.06	-5.14	8.92	1123.88
055	-3.12	-5.04	8.92	1123.94
056	-3.35	-5.47	8.97	1124.00
057	-3.41	-4.93	8.99	1124.07
058	-3.40	-4.73	9.04	1124.13
059	-3.02	-4.51	9.05	1124.19
060	-2.97	-4.65	9.05	1124.26
061	-2.76	-4.60	9.09	1124.32
062	-2.36	-4.50	9.05	1124.39
063	-2.13	-4.67	8.91	1124.45
064	-2.29	-4.60	8.94	1124.51
065	-2.32	-4.72	nan	1124.58
066	-2.24	-4.82	nan	1124.64
067	-2.19	-5.09	nan	1124.70
068	-2.35	-4.91	nan	1124.77
069	-2.42	-4.97	nan	1124.83
070	-2.20	-4.99	nan	1124.90
071	-2.07	-4.84	nan	1124.96
072	-2.40	-5.16	nan	1125.02
073	-2.62	-5.35	nan	1125.09
074	-2.91	-5.21	8.87	1125.15
075	-3.18	-5.06	8.91	1125.21
076	-3.25	-4.98	8.99	1125.28
077	-3.33	-4.92	9.05	1125.34
078	-3.38	-4.88	9.00	1125.41
079	-3.16	-4.58	8.99	1125.47
080	-3.06	-4.55	9.00	1125.53
081	-2.89	-4.71	8.97	1125.60
082	-2.73	-4.81	8.97	1125.66
083	-2.09	-4.56	8.94	1125.72
084	-2.43	-4.60	8.94	1125.79
085	-2.44	-4.61	8.97	1125.85
086	-2.20	-4.84	9.00	1125.91
087	-2.11	-5.06	9.01	1125.98
088	-2.31	-5.06	9.03	1126.04
089	-2.47	-5.22	9.04	1126.11
090	-2.59	-4.97	9.05	1126.17
091	-2.61	-4.82	9.08	1126.23
092	-2.67	-5.24	9.12	1126.30
093	-2.76	-5.27	9.12	1126.36
094	-3.02	-5.08	9.09	1126.42
095	-3.38	-5.17	9.03	1126.49
096	-3.42	-5.18	8.96	1126.55
097	-3.39	-4.84	8.93	1126.62

098	-3.31	-4.77	8.93	1126.68
099	-3.19	-4.55	8.92	1126.74
100	-3.14	-4.46	8.93	1126.81
101	-3.00	-4.32	8.92	1126.87
102	-2.52	-4.11	8.94	1126.93
103	-2.47	-4.41	8.95	1127.00
104	-2.35	-4.57	8.99	1127.06
105	-1.89	-4.49	8.99	1127.13
106	-2.10	-4.35	9.00	1127.19
107	-2.09	-4.32	9.05	1127.25
108	-2.14	-4.70	9.09	1127.32
109	-2.10	-5.15	9.06	1127.38
110	-2.22	-4.74	9.02	1127.44
111	-2.31	-4.72	9.02	1127.51
112	-2.57	-4.66	9.03	1127.57
113	-2.61	-4.81	9.04	1127.63
114	-2.82	-4.83	8.97	1127.70
115	-2.96	-4.60	8.96	1127.76
116	-3.25	-4.68	8.99	1127.83
117	-3.29	-4.70	8.97	1127.89
118	-2.80	-4.44	8.97	1127.95
119	-2.54	-4.67	9.01	1128.02
120	-2.24	-4.56	9.01	1128.08
121	-2.35	-4.83	8.99	1128.14
122	-2.31	-5.00	8.98	1128.21
123	-2.28	-5.11	9.03	1128.27
124	-2.58	-5.14	9.06	1128.34
125	-2.20	-4.90	9.05	1128.40
126	-2.06	-5.06	9.03	1128.46
127	-2.12	-5.12	9.00	1128.53
128	-2.45	-4.95	8.98	1128.59
129	-2.83	-5.04	8.98	1128.65
130	-2.90	-4.80	8.96	1128.72
131	-3.20	-4.82	8.95	1128.78
132	-3.28	-4.73	8.99	1128.85
133	-3.48	-4.67	9.00	1128.91
134	-3.30	-4.42	9.00	1128.97
135	-2.99	-4.29	8.98	1129.04
136	-2.94	-4.40	9.08	1129.10
137	-2.55	-4.21	9.12	1129.16
138	-2.43	-4.45	9.12	1129.23
139	-2.60	-4.63	9.14	1129.29
140	-2.60	-4.87	9.14	1129.36
141	-2.45	-4.94	9.07	1129.42
142	-2.63	-4.97	8.99	1129.48
143	-2.26	-4.86	8.95	1129.55
144	-2.69	-5.09	8.99	1129.61
145	-2.76	-5.29	8.95	1129.67
146	-3.08	-5.15	8.90	1129.74

147	-3.24	-4.97	8.92	1129.80
148	-3.54	-5.04	8.95	1129.86
149	-3.52	-5.06	8.98	1129.93
150	-3.31	-4.88	8.99	1129.99
151	-2.99	-4.88	8.99	1130.06
152	-3.03	-4.78	9.04	1130.12
153	-2.69	-4.80	9.10	1130.18
154	-2.23	-4.84	9.14	1130.25
155	-1.87	-5.59	9.18	1130.31
156	-2.00	-5.46	9.16	1130.37
157	-2.24	-5.13	9.09	1130.44
158	-2.26	-5.44	9.02	1130.50
159	-2.07	-5.19	9.00	1130.57
160	-1.98	-5.44	9.00	1130.63
161	-2.33	-5.24	8.98	1130.69
162	-2.98	-5.53	8.98	1130.76
163	-2.91	-5.21	8.98	1130.82
164	-3.07	-5.17	8.96	1130.88
165	-3.21	-5.15	8.97	1130.95
166	-3.19	-4.89	9.01	1131.01
167	-3.15	-4.76	9.05	1131.08
168	-2.88	-4.74	9.06	1131.14
169	-2.66	-4.70	9.10	1131.20
170	-2.36	-4.66	9.13	1131.27
171	-2.21	-4.75	9.14	1131.33
172	-2.06	-4.87	9.12	1131.39
173	-2.01	-4.88	9.05	1131.46
174	-1.87	-4.96	9.01	1131.52
175	-2.36	-4.76	8.99	1131.58
176	-2.08	-4.67	8.97	1131.65
177	-2.58	-4.99	8.96	1131.71
178	-3.13	-4.92	8.96	1131.78
179	-2.93	-5.93	8.98	1131.84
180	-3.38	-5.18	9.00	1131.90
181	-4.28	-5.30	9.03	1131.97
182	-4.39	-5.14	9.07	1132.03
183	-3.02	-4.53	9.08	1132.09
184	-3.12	-4.63	9.09	1132.16
185	-3.04	-4.57	9.10	1132.22
186	-2.17	-4.79	9.10	1132.29
187	-3.05	-5.33	9.08	1132.35
188	-3.32	-5.42	9.05	1132.41
189	-2.15	-4.95	9.02	1132.48
190	-2.28	-5.01	9.01	1132.54
191	-2.49	-5.22	8.98	1132.60
192	-2.83	-5.27	8.99	1132.67
193	-3.57	-5.67	8.96	1132.73
194	-4.18	-5.71	9.00	1132.80
195	-3.67	-5.31	9.04	1132.86

196	-4.41	-5.49	9.04	1132.92
197	-4.18	-5.38	9.04	1132.99
198	-3.97	-5.14	9.05	1133.05
199	-3.50	-4.94	9.05	1133.11
200	-3.64	-4.96	9.05	1133.18
201	-3.05	-5.12	9.06	1133.24
202	-2.47	-4.61	9.09	1133.30
203	-3.39	-5.35	9.08	1133.37
204	-3.18	-5.62	9.06	1133.43
205	-2.53	-4.78	9.03	1133.50
206	-2.82	-4.67	8.98	1133.56
207	-1.57	-4.49	8.93	1133.62
208	-1.29	-4.45	8.92	1133.69
209	-2.47	-4.67	8.94	1133.75
210	-2.45	-4.50	8.99	1133.81
211	-1.78	-4.12	8.97	1133.88
212	-1.64	-4.02	8.97	1133.94
213	-3.40	-4.87	8.98	1134.01
214	-3.41	-4.58	8.94	1134.07
215	-3.33	-4.59	8.99	1134.13
216	-2.93	-4.41	9.00	1134.20
217	-2.83	-4.26	9.06	1134.26
218	-2.42	-4.38	9.13	1134.32
219	-2.20	-4.49	9.12	1134.39
220	-2.83	-4.74	nan	1134.45
221	-3.62	-4.97	nan	1134.52
222	-3.37	-4.85	8.99	1134.58
223	-3.35	-5.12	8.99	1134.64
224	-3.20	-5.45	9.00	1134.71
225	-3.80	-5.52	8.97	1134.77
226	-3.80	-5.40	8.99	1134.83
227	-4.40	-5.43	9.06	1134.90
228	-4.62	-5.31	9.06	1134.96
229	-3.93	-5.04	9.10	1135.02
230	-3.69	-5.03	nan	1135.09
231	-3.02	-4.68	nan	1135.15
232	-3.15	-4.85	nan	1135.22
233	-3.19	-5.34	9.19	1135.28
234	-2.47	-4.90	9.21	1135.34
235	-3.30	-5.29	9.17	1135.41
236	-2.79	-5.20	9.08	1135.47
237	-2.86	-5.49	9.04	1135.53
238	-2.48	-5.65	9.02	1135.60
239	-3.19	-5.93	8.98	1135.66
240	-3.68	-5.52	8.94	1135.73
241	-3.16	-5.01	9.06	1135.79
242	-3.19	-4.89	9.05	1135.85
243	-3.09	-4.74	nan	1135.92
244	-3.06	-4.61	nan	1135.98

245	-2.87	-4.69	nan	1136.04
246	-2.65	-4.90	8.95	1136.11
247	-2.16	-4.56	9.08	1136.17
248	-2.27	-4.07	9.02	1136.24
249	-2.19	-4.15	9.17	1136.30
250	-2.10	-4.23	9.17	1136.36
251	-2.30	-4.43	9.14	1136.43
252	-2.42	-4.57	9.09	1136.49
253	-2.66	-4.78	9.04	1136.55
254	-2.56	-4.69	9.04	1136.62
255	-2.85	-4.90	8.99	1136.68
256	-2.97	-4.95	8.93	1136.74
257	-3.07	-5.08	8.96	1136.81
258	-3.19	-4.69	8.98	1136.87
259	-3.22	-4.62	9.00	1136.94
260	-2.94	-4.56	9.02	1137.00
261	-3.08	-4.55	9.04	1137.06
262	-2.85	-4.47	9.06	1137.13
263	-2.32	-4.30	9.09	1137.19
264	-2.16	-4.51	9.13	1137.25
265	-2.22	-4.81	9.16	1137.32
266	-1.97	-4.74	9.13	1137.38
267	-2.59	-4.99	9.07	1137.45
268	-2.44	-4.79	9.02	1137.51
269	-2.27	-4.91	8.99	1137.57
270	-2.60	-5.09	9.01	1137.64
271	-2.99	-4.76	8.92	1137.70
272	-3.13	-4.56	8.91	1137.76
273	-3.29	-4.55	8.94	1137.83
274	-3.26	-4.69	8.98	1137.89
275	-3.29	-4.34	9.00	1137.96
276	-2.92	-4.36	9.01	1138.02
277	nan	nan	9.06	1138.08
278	-2.27	-4.14	9.10	1138.15
279	-2.23	-4.87	9.13	1138.21
280	-2.25	-4.54	9.14	1138.27
281	-2.21	-4.84	9.11	1138.34
282	-2.18	-4.49	9.03	1138.40
283	-1.54	-4.30	8.98	1138.46
284	-2.06	-4.57	8.96	1138.53
285	-2.65	-4.93	8.96	1138.59
286	-2.81	-5.07	9.00	1138.66
287	-2.82	-4.78	8.95	1138.72
288	-2.97	-4.77	8.94	1138.78
289	-3.04	-4.57	8.95	1138.85
290	-3.01	-5.17	8.97	1138.91
291	-2.76	-4.52	8.97	1138.97
292	-2.33	-4.10	8.97	1139.04
293	-1.95	-4.61	8.99	1139.10

294	-1.76	-4.66	9.03	1139.17
295	-2.12	-5.64	9.07	1139.23
296	-1.91	-5.01	9.11	1139.29
297	-1.55	-4.90	9.08	1139.36
298	-2.16	-5.15	9.07	1139.42
299	-2.85	-5.20	8.98	1139.48
300	-3.21	-5.19	8.97	1139.55
301	-3.42	-5.27	9.00	1139.61
302	-3.44	-4.86	8.99	1139.68
303	-3.23	-4.68	8.96	1139.74
304	-2.78	-4.57	9.03	1139.80
305	-2.66	-4.79	9.02	1139.87
306	-2.71	-5.07	9.04	1139.93
307	-2.11	-5.06	9.06	1139.99
308	-2.31	-4.95	9.04	1140.06
309	-2.48	-5.00	9.06	1140.12
310	-1.67	-4.83	9.09	1140.18
311	-2.33	-4.96	9.11	1140.25
312	-2.57	-5.26	9.12	1140.31
313	-2.87	-5.26	9.11	1140.38
314	-3.31	-5.18	9.11	1140.44
315	-3.85	-5.15	9.08	1140.50
316	-3.76	-5.02	9.06	1140.57
317	-3.35	-4.85	9.01	1140.63
318	-3.41	-4.93	8.97	1140.69
319	-3.26	-4.91	8.99	1140.76
320	-2.90	-4.86	8.99	1140.82
321	-2.46	-4.72	nan	1140.89
322	-2.22	-5.02	nan	1140.95
323	-2.21	-5.08	9.02	1141.01
324	-2.53	-4.99	9.05	1141.08
325	-2.83	-4.89	9.06	1141.14
326	-2.25	-5.02	9.10	1141.20
327	-1.89	-4.92	9.13	1141.27
328	-2.19	-5.24	9.13	1141.33
329	-2.71	-5.39	9.12	1141.40
330	-2.92	-5.19	9.07	1141.46
331	-3.34	-5.08	9.06	1141.52
332	-3.65	-5.17	8.98	1141.59
333	-3.68	-5.12	9.02	1141.65
334	-3.55	-4.54	8.97	1141.71
335	-3.49	-4.95	8.99	1141.78
336	-3.25	-4.83	8.98	1141.84
337	-3.24	-4.85	8.99	1141.90
338	-2.83	-4.83	9.01	1141.97
339	-2.30	-4.95	9.04	1142.03
340	-2.30	-4.70	9.08	1142.10
341	-2.69	-5.36	9.05	1142.16
342	-2.35	-4.84	9.06	1142.22

343	-2.50	-5.17	9.08	1142.29
344	-2.78	-5.00	9.06	1142.35
345	-1.99	-4.85	9.04	1142.41
346	-2.55	-5.03	9.01	1142.48
347	-3.07	-5.05	9.02	1142.54
348	-3.28	-4.98	9.00	1142.61
349	-3.66	-5.69	9.00	1142.67
350	-3.69	-5.26	8.92	1142.73
351	-3.50	-4.85	8.94	1142.80
352	-3.56	-4.78	8.96	1142.86
353	-3.38	-4.73	8.97	1142.92
354	-3.05	-4.67	8.98	1142.99
355	-2.75	-4.53	9.00	1143.05
356	-2.38	-4.56	9.03	1143.12
357	-2.26	-4.76	9.06	1143.18
358	-2.45	-4.83	9.08	1143.24
359	-2.10	-5.01	9.10	1143.31
360	-2.45	-4.69	9.07	1143.37
361	-2.50	-5.65	9.04	1143.43
362	-2.56	-5.03	9.05	1143.50
363	-2.89	-4.85	9.00	1143.56
364	-3.32	-4.94	9.02	1143.63
365	-3.53	-4.87	9.03	1143.69
366	-3.82	-5.01	8.98	1143.75
367	-3.45	-5.58	9.01	1143.82
368	-3.26	-4.71	9.04	1143.88
369	-2.75	-4.76	9.06	1143.94
370	-2.54	-4.75	9.05	1144.01
371	-1.97	-4.36	9.08	1144.07
372	-2.24	-4.82	9.11	1144.13
373	-2.37	-5.34	9.15	1144.20
374	-2.62	-4.97	9.18	1144.26
375	-2.79	-4.74	9.18	1144.33
376	-2.09	-4.75	9.14	1144.39
377	-2.66	-5.17	9.08	1144.45
378	-2.98	-5.28	9.02	1144.52
379	-3.27	-4.24	8.99	1144.58
380	-3.33	-4.81	8.98	1144.64
381	-3.15	-4.86	8.99	1144.71
382	-2.90	-5.09	9.01	1144.77
383	-2.92	-4.71	9.00	1144.84
384	-2.58	-4.75	9.00	1144.90
385	-2.64	-4.86	9.02	1144.96
386	-2.03	-4.78	9.01	1145.03
387	-2.05	-4.93	9.08	1145.09
388	-2.05	-4.96	9.15	1145.15
389	-2.46	-5.00	9.17	1145.22
390	-2.41	-4.89	9.18	1145.28
391	-2.68	-5.73	9.18	1145.35

392	-3.04	-5.44	9.12	1145.41
393	-3.34	-6.01	9.08	1145.47
394	-3.38	-5.40	9.05	1145.54
395	-3.21	-5.15	9.07	1145.60
396	-2.89	-5.11	9.02	1145.66
397	-2.45	-4.51	9.01	1145.73
398	-2.06	-5.55	9.06	1145.79
399	-1.93	-4.84	9.06	1145.85
400	-1.68	-4.68	9.11	1145.92
401	-2.44	-4.72	9.10	1145.98
402	-2.36	-5.19	9.13	1146.05
403	-2.35	-4.75	9.10	1146.11
404	-2.72	-5.09	9.08	1146.17
405	-2.95	-5.37	9.10	1146.24
406	-3.13	-5.03	9.14	1146.30
407	-3.34	-5.22	9.09	1146.36
408	-3.39	-5.23	9.09	1146.43
409	-3.57	-4.88	9.03	1146.49
410	-3.03	-4.56	9.05	1146.56
411	-2.69	-4.55	9.06	1146.62
412	-2.73	-4.43	9.01	1146.68
413	-2.17	-4.41	9.00	1146.75
414	-1.93	-5.43	9.04	1146.81
415	-1.91	-4.79	9.05	1146.87
416	-2.44	-5.33	9.04	1146.94
417	-2.14	-5.29	9.06	1147.00
418	-1.96	-5.01	9.09	1147.07
419	-2.44	-5.23	9.07	1147.13
420	-2.67	-4.99	9.05	1147.19
421	-4.66	-4.89	9.08	1147.26
422	-4.50	-4.66	9.10	1147.32
423	-2.99	-4.72	9.09	1147.38
424	-2.18	-4.46	9.08	1147.45
425	-3.61	-4.87	9.08	1147.51
426	-4.43	-4.90	9.02	1147.57
427	-4.81	-4.87	9.00	1147.64
428	-2.11	-4.87	8.99	1147.70
429	-1.51	-4.75	9.01	1147.77
430	-2.12	-4.78	9.03	1147.83
431	-3.16	-4.78	9.05	1147.89
432	-3.13	-4.79	9.07	1147.96
433	-2.17	-4.85	9.04	1148.02
434	-1.84	-5.06	9.03	1148.08
435	-1.92	-4.81	9.07	1148.15
436	-1.95	-4.81	9.10	1148.21
437	-3.60	-5.12	9.11	1148.28
438	-4.41	-5.09	9.11	1148.34
439	-2.49	-4.64	9.09	1148.40
440	-1.92	-4.56	9.06	1148.47

441	-2.43	-4.72	9.05	1148.53
442	-3.28	-4.77	9.05	1148.59
443	-2.77	-4.92	9.00	1148.66
444	-2.77	-4.86	8.97	1148.72
445	-2.80	-4.74	8.99	1148.79
446	-2.53	-4.76	8.99	1148.85
447	-3.42	-4.92	8.97	1148.91
448	-3.87	-4.98	8.98	1148.98
449	-2.71	-4.94	9.01	1149.04
450	-2.27	-4.96	9.06	1149.10
451	-2.69	-5.17	9.10	1149.17
452	-3.14	-4.99	9.12	1149.23
453	-4.39	-4.99	9.13	1149.29
454	-4.42	-5.02	9.10	1149.36
455	-3.70	-5.00	9.08	1149.42
456	-3.94	-4.93	9.03	1149.49
457	-3.88	-4.95	9.01	1149.55
458	-4.19	-4.99	9.02	1149.61
459	-4.56	-5.47	9.02	1149.68
460	-3.46	-5.16	9.01	1149.74
461	-3.49	-5.12	9.02	1149.80
462	-2.90	-4.87	9.03	1149.87
463	-2.87	-5.31	9.02	1149.93
464	-2.28	-5.04	9.04	1150.00
465	-3.09	-5.22	9.07	1150.06
466	-3.39	-4.88	9.10	1150.12
467	-4.53	-5.17	9.13	1150.19
468	-4.94	-5.54	9.16	1150.25
469	-4.14	-5.36	9.16	1150.31
470	-4.20	-5.21	9.14	1150.38
471	-4.28	-5.18	9.06	1150.44
472	-2.16	-4.91	9.02	1150.51
473	-2.49	-5.12	9.01	1150.57
474	-2.62	-5.15	9.01	1150.63
475	-3.07	-5.16	8.95	1150.70
476	-3.70	-5.21	8.97	1150.76
477	-3.06	-5.04	8.98	1150.82
478	-3.01	-4.91	9.08	1150.89
479	-2.92	-4.93	nan	1150.95
480	-3.23	-4.90	nan	1151.01
481	-2.82	-4.40	9.02	1151.08
482	-1.94	-4.29	9.11	1151.14
483	-2.39	-4.63	9.14	1151.21
484	-2.83	-4.75	9.19	1151.27
485	-2.76	-4.93	9.19	1151.33
486	-2.23	-4.82	9.14	1151.40
487	-2.64	-5.12	9.07	1151.46
488	-3.15	-5.12	8.99	1151.52
489	NaN	NaN	8.89	1151.59

490	-2.73	-4.35	8.84	1151.65
491	NaN	NaN	8.83	1151.72
492	NaN	NaN	8.89	1151.78
493	-3.69	-5.02	8.89	1151.84
494	-3.72	-4.87	8.98	1151.91
495	-3.79	-4.96	8.99	1151.97
496	-3.90	-5.00	8.97	1152.03
497	-3.64	-4.40	8.98	1152.10
498	-4.06	-4.96	8.97	1152.16
499	-3.72	-4.79	9.01	1152.23
500	-3.68	-4.96	9.01	1152.29
501	-3.98	-5.07	8.96	1152.35
502	-4.03	-5.25	9.00	1152.42
503	-3.74	-5.33	8.95	1152.48
504	-3.98	-5.40	8.93	1152.54
505	-3.82	-5.01	8.98	1152.61
506	-3.69	-4.92	8.92	1152.67
507	-3.67	-4.94	8.93	1152.73
508	-3.50	-5.00	8.91	1152.80
509	-3.64	-5.01	8.94	1152.86
510	-3.50	-4.90	8.94	1152.93
511	-3.61	-4.75	8.96	1152.99
512	-3.70	-5.84	8.96	1153.05
513	-3.62	-5.00	8.90	1153.12
514	-3.75	-5.00	8.92	1153.18
515	-3.44	-4.73	8.99	1153.24
516	-3.24	-5.20	8.97	1153.31
517	-3.29	-4.90	8.90	1153.37
518	-3.38	-5.30	8.90	1153.44
519	-3.39	-5.36	8.87	1153.50
520	-3.50	-4.80	8.91	1153.56
521	-3.76	-5.66	8.81	1153.63
522	-3.68	-5.06	8.76	1153.69
523	-3.37	-5.08	8.82	1153.75
524	-3.38	-5.15	8.89	1153.82
525	-3.34	-5.21	8.88	1153.88
526	-3.51	-5.43	8.85	1153.95
527	-3.59	-5.17	8.92	1154.01
528	-3.56	-5.05	8.98	1154.07
529	-3.70	-4.86	9.05	1154.14
530	-3.62	-4.70	9.07	1154.20
531	-3.69	-5.37	9.08	1154.26
532	-3.54	-4.89	9.05	1154.33
533	-3.51	-4.92	9.01	1154.39
534	-3.65	-4.86	8.98	1154.45
535	-3.39	-5.23	8.96	1154.52
536	-3.10	-5.21	8.94	1154.58
537	-3.16	-5.41	8.91	1154.65
538	-3.22	-5.51	8.88	1154.71

539	-3.31	-5.57	8.92	1154.77
540	-2.66	-5.54	8.95	1154.84
541	-2.49	-4.88	8.98	1154.90
542	-2.75	-4.51	9.02	1154.96
543	-2.81	-4.76	9.06	1155.03
544	-2.84	-4.92	9.07	1155.09
545	-2.89	-5.09	9.08	1155.16
546	-2.75	-5.26	9.08	1155.22
547	-3.03	-5.30	9.09	1155.28
548	-2.90	-4.93	9.04	1155.35
549	-3.03	-4.78	8.99	1155.41
550	-3.12	-4.54	8.98	1155.47
551	-3.16	-4.70	8.96	1155.54
552	-3.10	-4.69	8.93	1155.60
553	-3.02	-5.03	8.93	1155.67
554	-2.81	-5.10	8.89	1155.73
555	-2.30	-5.61	8.94	1155.79
556	-2.29	-5.15	8.96	1155.86
557	-2.73	-5.11	8.90	1155.92
558	-2.12	-4.96	8.95	1155.98
559	-2.27	-4.93	8.99	1156.05
560	-2.44	-5.00	9.02	1156.11
561	-2.42	-4.73	9.02	1156.17
562	-2.67	-4.67	9.03	1156.24
563	-2.80	-4.50	9.03	1156.30
564	-2.86	-4.93	9.00	1156.37
565	-2.68	-6.30	8.96	1156.43
566	-2.24	-5.25	8.93	1156.49
567	-2.04	-4.71	8.98	1156.56
568	-2.03	-4.88	8.99	1156.62
569	-2.06	-5.59	8.93	1156.68
570	-2.03	-5.79	8.92	1156.75
571	-2.36	-4.89	8.94	1156.81
572	-2.35	-5.22	8.96	1156.88
573	-2.18	-5.85	nan	1156.94
574	-3.07	-5.07	nan	1157.00
575	-3.43	-5.37	nan	1157.07
576	-3.34	-5.11	nan	1157.13
577	-3.37	-5.17	nan	1157.19
578	-3.31	-5.17	nan	1157.26
579	-3.40	-4.98	9.08	1157.32
580	-2.74	-5.15	9.06	1157.39
581	-2.59	-4.99	9.02	1157.45
582	-2.30	-5.16	8.97	1157.51
583	-2.67	-5.12	8.96	1157.58
584	-3.10	-5.03	8.95	1157.64
585	-2.28	-4.95	8.92	1157.70
586	-2.70	-5.09	8.95	1157.77
587	-2.76	-4.94	8.97	1157.83

588	nan	nan	9.01	1157.89
589	-2.65	-4.59	9.04	1157.96
590	-2.35	-4.55	9.07	1158.02
591	-2.06	-5.18	9.09	1158.09
592	-1.75	-4.74	9.11	1158.15
593	-1.90	-4.58	9.11	1158.21
594	-2.10	-4.95	9.11	1158.28
595	-1.91	-4.97	9.08	1158.34
596	-2.20	-5.11	9.10	1158.40
597	-2.55	-5.06	9.07	1158.47
598	-2.79	-4.89	9.02	1158.53
599	-2.76	-4.60	8.99	1158.60
600	-2.55	-4.48	8.95	1158.66
601	-2.50	-4.25	8.94	1158.72
602	-2.15	-4.31	9.00	1158.79
603	-2.02	-4.34	9.01	1158.85
604	-1.95	-4.47	9.00	1158.91
605	-1.90	-4.38	8.97	1158.98
606	-2.17	-4.79	9.01	1159.04
607	-2.62	-4.72	9.06	1159.11
608	-2.53	-4.86	9.13	1159.17
609	-2.15	-4.48	9.19	1159.23
610	-2.50	-4.59	9.21	1159.30
611	-3.09	-4.95	9.18	1159.36
612	-2.88	-4.70	9.12	1159.42
613	-2.78	-4.34	9.08	1159.49
614	-2.50	-4.15	9.05	1159.55
615	-2.25	-4.14	9.02	1159.62
616	-2.14	-4.55	8.93	1159.68
617	-1.97	-4.50	8.94	1159.74
618	-1.79	-4.62	8.97	1159.81
619	-2.48	-5.16	8.97	1159.87
620	-1.86	-4.73	9.05	1159.93
621	-2.55	-4.94	9.06	1160.00
622	-2.82	-4.80	9.08	1160.06
623	-2.97	-4.76	9.13	1160.12
624	-2.87	-4.54	9.11	1160.19
625	-3.05	-4.55	9.16	1160.25
626	-2.45	-4.19	9.18	1160.32
627	-1.97	-4.19	9.16	1160.38
628	-1.75	-4.37	9.09	1160.44
629	-2.03	-4.93	8.98	1160.51
630	-2.13	-4.93	8.92	1160.57
631	-2.30	-4.87	8.93	1160.63
632	-2.43	-5.06	8.88	1160.70
633	-2.70	-5.35	8.91	1160.76
634	-2.85	-5.15	8.96	1160.83
635	-2.86	-5.04	8.98	1160.89
636	-2.73	-4.40	8.95	1160.95

637	-2.61	-4.55	8.92	1161.02
638	-1.93	-4.54	8.96	1161.08
639	-2.09	-4.69	9.04	1161.14
640	-2.06	-4.76	9.11	1161.21
641	-1.98	-5.04	9.14	1161.27
642	-1.87	-5.17	9.09	1161.34
643	-2.15	-5.50	9.05	1161.40
644	-2.55	-5.73	8.98	1161.46
645	-2.57	-5.48	8.96	1161.53
646	-2.72	-5.23	8.96	1161.59
647	-3.04	-5.28	8.93	1161.65
648	-3.08	-4.80	8.91	1161.72
649	-3.02	-4.62	nan	1161.78
650	-2.55	-5.82	nan	1161.84
651	-2.59	-4.54	nan	1161.91
652	-2.54	-4.66	nan	1161.97
653	-2.31	-4.88	nan	1162.04
654	-2.15	-4.77	nan	1162.10
655	-2.12	-5.08	nan	1162.16
656	-2.33	-4.88	nan	1162.23
657	-2.91	-5.10	nan	1162.29
658	-2.85	-5.18	nan	1162.35
659	-3.15	-5.04	nan	1162.42
660	-3.41	-4.86	nan	1162.48
661	-3.54	-4.52	nan	1162.55
662	-3.36	-4.24	nan	1162.61
663	-2.98	-4.91	nan	1162.67
664	-2.55	-4.66	8.93	1162.74
665	-2.71	-4.48	8.99	1162.80
666	-2.61	-4.69	9.05	1162.86
667	-2.53	-4.77	9.09	1162.93
668	-2.73	-4.82	9.12	1162.99
669	-2.30	-4.68	9.12	1163.06
670	-2.67	-4.88	9.12	1163.12
671	-3.13	-5.47	9.13	1163.18
672	-3.29	-5.30	9.14	1163.25
673	-2.98	-4.59	9.10	1163.31
674	-2.50	-4.07	9.05	1163.37
675	-2.46	-4.11	9.02	1163.44
676	-2.50	-4.33	9.00	1163.50
677	-2.68	-4.24	8.98	1163.56
678	-2.89	-4.52	8.91	1163.63
679	-2.75	-4.48	8.87	1163.69
680	-2.93	-4.95	8.88	1163.76
681	-2.96	-4.75	8.89	1163.82
682	-2.76	-4.91	8.94	1163.88
683	-3.10	-5.07	8.99	1163.95
684	-3.29	-4.82	9.03	1164.01
685	-3.26	-4.60	9.07	1164.07

686	-3.00	-4.12	9.12	1164.14
687	-2.88	-4.92	9.15	1164.20
688	-2.71	-4.80	9.19	1164.27
689	-2.69	-4.15	9.16	1164.33
690	-2.66	-5.13	9.16	1164.39
691	-2.77	-4.63	9.10	1164.46
692	-2.73	-4.54	9.04	1164.52
693	-2.89	-4.60	8.97	1164.58
694	-3.25	-4.62	8.97	1164.65
695	-2.86	-4.57	8.97	1164.71
696	-2.58	-4.62	8.98	1164.78
697	-2.77	-4.97	8.98	1164.84
698	-2.50	-4.70	8.97	1164.90
699	-2.16	-4.40	8.98	1164.97
700	-2.07	-4.47	9.00	1165.03
701	-2.48	-4.27	9.04	1165.09
702	-2.46	-4.27	9.08	1165.16
703	-2.29	-4.34	9.11	1165.22
704	-1.90	-4.67	9.12	1165.28
705	-2.91	-4.56	9.06	1165.35
706	-3.05	-4.35	8.97	1165.41
707	-2.81	-4.41	9.02	1165.48
708	-2.77	-4.73	9.02	1165.54
709	nan	nan	8.95	1165.60
710	-3.47	-4.83	8.80	1165.67
711	-3.17	-4.88	8.75	1165.73
712	-3.38	-5.57	nan	1165.79
713	-3.38	-5.76	nan	1165.86
714	-3.48	-4.93	9.07	1165.92
715	-2.98	-4.84	8.99	1165.99
716	-2.97	-4.63	8.94	1166.05
717	-3.54	-4.73	9.02	1166.11
718	-2.93	-4.66	9.04	1166.18
719	-3.14	-4.97	9.12	1166.24
720	-3.27	-5.01	9.15	1166.30
721	-3.46	-5.15	9.15	1166.37
722	-3.34	-5.90	9.07	1166.43
723	-3.50	-5.29	8.98	1166.50
724	-3.33	-5.31	9.02	1166.56
725	-3.41	-5.56	8.98	1166.62
726	-3.61	-5.49	8.89	1166.69
727	-3.46	-4.88	9.01	1166.75

Bibliography

Allen, M. S., New ideas about Late Holocene climate variability in the Central Pacific, *Current Anthropology*, *47*(3), 521–535, 2006.

Allison, N., A. A. Finch, J. M. Webster, and D. A. Clague, Palaeoenvironmental records from fossil corals: The effects of submarine diagenesis on temperature and climate estimates, *Geochem. et Cosmochim. Acta*, *71*, 4693–4703, doi: 10.1016/j.gca.2007.07.026, 2007.

Ammann, C. M., F. Joos, D. S. Schimel, B. L. Otto-Bliesner, and R. A. Tomas, Solar influence on climate during the past millennium: results from transient simulations with the NCAR Climate System Model., *Proceedings of the National Academy of Sciences of the United States of America*, *104*(10), 3713–8, doi:10.1073/pnas.0605064103, 2007.

Ashok, K., S. K. Behera, S. A. Rao, H. Weng, and T. Yamagata, El nio modoki and its possible teleconnection, *Journal of Geophysical Research: Oceans*, *112*(C11), n/a–n/a, doi:10.1029/2006JC003798, c11007, 2007.

Ault, T., C. Deser, M. Newman, and J. Emile-Geay, Characterizing decadal to centennial variabiliy in the equatorial Pacific during the last millennium, *Geophysical Research Letters*, *40*, 3450–3456, doi:10.1002/grl50647, 2013.

Battisti, D. S., and A. C. Hirst, Interannual Variability in a Tropical Atmosphere-Ocean Model: Influence of the Basic State, Ocean Geometry, and Nonlinearity, *Journal of Atmospheric Sciences*, *46*(12), 1687–1712, 1989.

Beck, J. W., R. L. Edwards, E. Ito, F. W. Taylor, J. Recy, F. Rougerie, P. Joannot, and C. Henin, Sea-surface temperature from coral skeletal Strontium/Calcium ratios, *Science*, *257*, 644–647, 1992.

Bellenger, H., E. Guilyardi, J. Leloup, M. Lengaigne, and J. Vialard, ENSO Representation in climate models: from CMIP3 to CMIP5, *Climate Dynamics*, *42*, 1999–2018, 2014.

Bjerknes, J., Atmospheric teleconnections from the equatorial Pacific, *Mon. Wea. Rev.*, *97*, 163–72, 1969.

Braconnot, P., S. P. Harrison, M. Kageyama, P. J. Bartlein, V. Masson-Delmotte, A. Abe-Ouchi, B. Otto-Bliesner, and Y. Zhao, Evaluation of climate models using palaeoclimatic data, *Nature Climate Change*, *2*(6), 417–424, doi:10.1038/nclimate1456, 2012.

Bradley, R. S., *Paleoclimatology: Reconstructing Climates of the Quaternary*, 2nd ed. ed., Academic Press, New York, 1999.

Bradley, R. S., M. K. Hughes, and H. F. Diaz, Climate in Medieval Time, *Science*, *302*(5644), 404–405, 2003.

Brown, J., Moise, and Delage, Changes in the South Pacific Convergence Zone in IPCC AR4 future climate projections, *Climate Dynamics*, *39*(1-2), 1–19, doi:10.1007/s00382-011-1192-0, 2012a.

Brown, J. R., A. F. Moise, and R. A. Colman, The South Pacific Convergence Zone in CMIP5 simulations of historical and future climate, *Climate Dynamics*, *41*(7-8), 2179–2197, doi:10.1007/s00382-012-1591-x, 2012b.

Brown, J. R., A. F. Moise, and R. A. Colman, The South Pacific Convergence Zone in CMIP5 simulations of historical and future climate, *Climate Dynamics*, *41*(7-8), 2179–2197, doi:10.1007/s00382-012-1591-x, 2012c.

Cane, M. A., and S. E. Zebiak, A Theory for El Niño and the Southern Oscillation, *Science*, *228*, 1085–1087, 1985.

Capotondi, A., et al., Understanding enso diversity, *Bulletin of the American Meteorological Society*, *96*(6), 921–938, doi:10.1175/BAMS-D-13-00117.1, 2015.

Clarke, A. J., El Niño Physics and El Niño Predictability, *Annual Review of Marine Science*, *6*, 79–99, doi:10.1146/annurev-marine-010213-135026, 2014.

Clement, A., R. Seager, M. Cane, and S. Zebiak, An Ocean Dynamical Thermostat, *Journal of Climate*, *9*, 1996.

Cobb, K. M., C. D. Charles, H. Cheng, and R. L. Edwards, El Niño/Southern Oscillation and tropical Pacific climate during the last millennium., *Nature*, *424*(6946), 271–6, doi:10.1038/nature01779, 2003a.

Cobb, K. M., C. D. Charles, H. Cheng, M. Kastner, and R. L. Edwards, U/Th-dating living and young fossil corals from the central tropical Pacific, *Earth and Planetary Science Letters*, *210*, 91–103, 2003b.

Cobb, K. M., N. Westphal, H. R. Sayani, J. T. Watson, E. Di Lorenzo, H. Cheng, R. L. Edwards, and C. D. Charles, Highly variable El Niño-Southern Oscillation throughout the Holocene., *Science (New York, N.Y.)*, *339*(6115), 67–70, doi:10.1126/science.1228246, 2013.

Cohen, A. L., G. D. Layne, S. R. Hart, and P. S. Lobel, Kinetic control of skeletal sr/ca in a symbiotic coral: Implications for the paleotemperature proxy, *Paleoceanography*, *16*(1), 20–26, doi:10.1029/1999PA000478, 2001.

Cole, J. E., and R. G. Fairbanks, The Southern Oscillation recorded in the δ^{18}O of corals from Tarawa Atoll, *Paleoceanography*, *5*, 669–683, 1990.

Cole, J. E., R. B. Dunbar, T. R. McClanahan, and N. A. Muthiga, Tropical Pacific Forcing of Decadal SST Variability in the Western Indian Ocean over the Past Two Centuries, *Science*, *287*, 617–619, 2000.

Collins, M., et al., The impact of global warming on the tropical Pacific Ocean and El Niño, *Nature Geoscience*, *3*(6), 391–397, doi:10.1038/ngeo868, 2010.

Comboul, M., J. Emile-Geay, M. N. Evans, N. Mirnateghi, K. M. Cobb, and D. M. Thompson, A probabilistic model of chronological errors in layer-counted climate proxies: applications to annually-banded coral archives, *Clim. Past.*, *10*, 825–841, doi:10.5194/cp-10-825-2014, 2014.

Comboul, M., J. Emile-Geay, G. Hakim, and M. Evans, Paleoclimate Sampling as a Sensor Placement Problem, *Journal of Climate*, *28.19*, 7717–7740, 2015.

Compo, G. P., et al., The Twentieth Century Reanalysis Project, *Quat. J. Royal. Met. Soc.*, *137*(Part A), 1–28, doi:10.1002/qj.776, 2011.

Conroy, J. L., J. T. Overpeck, J. E. Cole, T. M. Shanahan, and M. Steinitz-Kannan, Holocene changes in eastern tropical Pacific climate inferred from a Galápagos lake sediment record, *Quaternary Science Reviews*, *27*(11), 1166–1180, 2008.

Conroy, J. L., A. Restrepo, J. T. Overpeck, M. Steinitz-Kannan, J. E. Cole, M. B. Bush, and P. A. Colinvaux, Unprecedented recent warming of surface temperatures in the eastern tropical Pacific Ocean, *Nature Geoscience*, *2*(1), 46–50, doi:10.1038/ngeo390, 2009.

Conroy, J. L., D. M. Thompson, K. M. Cobb, D. Noone, S. Rea, and A. N. Legrande, Spatiotemporal variability in the 18o-salinity relationship of seawater across the tropical pacific ocean, *Paleoceanography*, *32*(5), 484–497, doi:10.1002/2016PA003073, 2017.

Cook, E. R., and M. N. Evans, Improving estimates of drought variability and extremes from centuries-long tree ring chronologies: A PAGES/CLIVAR example, *PAGES/CLIVAR Newsl.*, *8*, 9–10, 1999.

Cook, E. R., K. R. Briffa, and P. D. Jones, Spatial regression methods in dendroclimatology – A review and comparison of 2 techniques, *Int. J. Clim.*, *14*, 379–402, 1994.

Cook, E. R., D. M. Meko, D. W. Stahle, and M. K. Cleaveland, Drought reconstructions for the continental United States, *J. Clim.*, *12*, 1145–1162, 1999.

Cook, E. R., B. M. Buckley, R. D. D'Arrigo, and M. J. Peterson, Warm-season temperatures since 1600 B.C. reconstructed from Tasmanian tree rings and their relationship to large-scale sea surface temperature anomalies, *Climate Dynamics*, *16*, 79–91, 2000.

Cook, E. R., C. A. Woodhouse, C. M. Eakin, D. M. Meko, and D. W. Stahle, Long-term aridity changes in the western United States., *Science (New York, N.Y.)*, *306*(5698), 1015–8, doi:10.1126/science.1102586, 2004.

Corrége, T., Sea surface temperature and salinity reconstruction from coral geochemical tracers, *Palaeog. Palaeoc. Palaeoecol.*, *232*, 408–428, doi: 10.1016/-j.palaeo.2005.10.014, 2006.

Craig, H., Isotopic standards for carbon and oxygen and correction factors for mass-spectrometric analysis of carbon dioxide, *Geochimica et Cosmochimica Acta*, *12*(1), 133 – 149, doi:https://doi.org/10.1016/0016-7037(57)90024-8, 1957.

De Villiers, S., G. T. Shen, and B. K. Nelson, The Sr/Ca-temperature relationship in coralline aragonite: Influence of variability in (Sr/Ca)seawater and skeletal growth parameters, *Geochimica et Cosmochimica Acta*, *58*, 197–208, 1994.

Dee, S., J. Emile-Geay, M. Evans, A. Allam, E. Steig, and D. Thompson, PRYSM: An open-source framework for PRoxY System Modeling, with applications to yxgen-isotope systems, *Journal of Advances in Modeling Earth System*, *7*, 1220–1247, 2015.

Delcroix, T., G. Alory, S. Cravatte, T. Correge, and M. McPhaden, A gridded sea surface salinity data set for the tropical Pacific with sample applications (1950 - 2008), *Deep Sea Research Part I: Oceanographic Research Papers*, *58*(1), 38–48, doi:10.1016/j.dsr.2010.11.002, 2011.

DeLong, K., T. M. Quinn, F. W. Taylor, K. Lin, and C.-C. Shen, Sea surface temperature variability in the southwest tropical Pacific since AD 1649, *Nature Climate Change*, *2*(11), 799–804, doi:10.1038/nclimate1583, 2012.

DeLong, K. L., T. M. Quinn, and F. W. Taylor, Reconstructing twentieth-century sea surface temperature variability in the southwest Pacific: A replication study using multiple coral Sr/Ca records from New Caledonia, *Paleoceanography*, *22*(4), n/a–n/a, 2007a.

DeLong, K. L., T. M. Quinn, and F. W. Taylor, Reconstructing twentieth-century sea surface temperature variability in the southwest Pacific: A replication study using multiple coral Sr/Ca records from New Caledonia, *Palaeoceanogr.*, *22*, PA4212, doi:10.1029/2007PA001444, 2007b.

DeLong, K. L., T. M. Quinn, F. W. Taylor, C.-C. Shen, and K. Lin, Improving coral-base paleoclimate reconstructions by replicating 350 years of coral Sr/Ca variations, *Palaeog. Palaeoc. Palaeoecol.*, *373*, 6–24, 2013.

Deser, C., M. A. Alexander, S.-P. Xie, and A. S. Phillps, Sea Surface Temperature Variability: Patterns and Mechanisms, *Annual Review of Marine Science*, *2*, 115–143, doi:10.1146/annurev-marine-120408-151453, 2010.

Diaz, H. F., R. Trigo, M. K. Hughes, M. E. Mann, E. Xoplaki, and D. Barriopedro, Spatial and Temporal Characteristics of Climate in Medieval Times Revisited,

Bulletin of the American Meteorological Society, *92*(11), 1487–1500, doi:10.1175/BAMS-D-10-05003.1, 2011.

DiNezio, P. N., A. C. Clement, G. A. Vecchi, B. J. Soden, B. P. Kirtman, and S.-K. Lee, Climate response of the equatorial pacific to global warming, *Journal of Climate*, *22*(18), 4873–4892, doi:10.1175/2009JCLI2982.1, 2009.

DiNezio, P. N., G. A. Vecchi, and A. C. Clement, Detectability of Changes in the Walker Circulation in Response to Global Warming, *Journal of Climate*, *26*, 4038–4048, 2013.

Druffel, E. R., and S. Griffin, Variability of surface ocean radiocarbon and stable isotopes in the southwestern Pacific, *Journal of Geophysical Research*, *104*, 607–623, 1999.

Duke, G., Using simulated $\delta^{18}O$ to characterize ENSO and SPCZ variance during the anthropocene, honors B.S. thesis, Department of Atmospheric and Oceanic Science, University of Maryland, College Park, 2015.

Dunbar, R. B., and J. E. Cole, Annual Records of Tropical Systems (ARTS): Recommendations for Research, *Tech. rep.*, PAGES/CLIVAR, 1996.

Dunbar, R. B., G. M. Wellington, M. W. Colgan, and P. W. Glynn, Eastern Pacific sea surface temperature since 1600 A.D.: The δ^{18}O record of climate variability in Galápagos corals, *Paleoceanography*, *9*, 291–315, 1994.

Edwards, R. L., J. H. Chen, and G. J. Wasserburg, $^{238}U -^{234} -U -^{230} Th -^{232} Th$ systematics and the precise measurement of time over the past 500,000 years, *Earth and Planetary Science Letters*, *81*, 175–192, 1987.

Emile-Geay, J., R. Seager, M. A. Cane, E. R. Cook, and G. H. Haug, Volcanoes and ENSO over the past millennium, *J. Clim.*, *21(13)*, 3134–3148, doi: 10.1175/2007JCLI1884.1, 2008.

Emile-Geay, J., K. M. Cobb, M. E. Mann, and A. T. Wittenberg, Estimating Central Equatorial Pacific SST Variability over the Past Millennium. Part I: Methodology and Validation, *Journal of Climate*, *26*(7), 2302–2328, doi:10.1175/JCLI-D-11-00510.1, 2013a.

Emile-Geay, J., K. M. Cobb, M. E. Mann, and A. T. Wittenberg, Estimating Central Equatorial Pacific SST Variability over the Past Millennium. Part II: Reconstructions and Implications, *Journal of Climate*, *26*(7), 2329–2352, doi:10.1175/JCLI-D-11-005100.1, 2013b.

Enmar, R., M. Stein, M. Bar-Matthews, E. Sass, A. Katz, and B. Lazar, Diagenesis in live corals from the Gulf of Aqaba. I. The effect on paleo-oceanography tracers, *Geochem. et Cosmochim. Acta*, *64(18)*, 3123–3132, 2000.

Epstein, S., R. Buchsbaum, H. Lowenstam, and H. C. Urey, Carbonate-Water Isotopic Temperature Scale, *Geological Society of America Bulletin*, *62*, 417–426, doi:10.1130/0016-7606(1951)62, 1951.

Epstein, S., R. Buchsbaum, H. Lowenstam, and H. C. Urey, Revised Carbonate-Water Isotopic Temperature Scale, *Geological Society of America Bulletin*, *64*, 1315–1325, doi:10.1130/0016-7606(1953)64, 1953.

Evans, M., A. Kaplan, and M. Cane, Optimal sites for coral-based reconstruction of global sea surface temperature, *Paleoceanography*, *13.5*, 502–516, 1998.

Evans, M. N., R. G. Fairbanks, and J. L. Rubenstone, The thermal oceanographic signal of El Nino reconstructed from a Kiritimati Island coral, *Journal of Geophysical Research*, *104*, 1999.

Evans, M. N., A. Kaplan, and M. A. Cane, Intercomparison of coral oxygen isotope data and historical sea surface temperature (SST): Potential for coral-based SST field reconstruction, *Paleoceanography*, *15*(5), 551–563, 2000.

Evans, M. N., M. A. Cane, D. P. Schrag, A. Kaplan, B. K. Linsley, R. Villalba, and G. M. Wellington, Support for tropically-driven Pacific decadal variability based on paleoproxy evidence, *Geophys. Res. Lett.*, *28*, 3689–3692, 2001.

Evans, M. N., A. Kaplan, and M. A. Cane, Pacific sea surface temperature field reconsotruction from coral $\delta^{18}O$ data using reduced space objective analysis, *Paleoceanography*, *17*(1), 1–13, 2002.

Evans, M. N., S. Tolwinski-Ward, D. M. Thompson, and K. J. Anchukaitis, Applications of proxy system modeling in high resolution paleoclimatology, *Quaternary Science Reviews*, *76*, 16–28, 2013.

Evans, M. N., K. J. Selmer, B. T. Breeden III, A. S. Lopatka, and R. E. Plummer, Correction algorithm for on-line continuous flow $\delta^{13}C$ and $\delta^{18}O$ carbonate and cellulose stable isotope analyses, *Geochemistry, Geophysics, Geosystems*, *17*, 2016.

Fedorov, A., and S. G. Philander, Is El Niño Changing?, *Science*, *288*(5473), 1997–2002, 2000.

Felis, T., J. Pätzold, and Y. Loya, Mean oxygen-isotope signatures in porites spp. corals: inter-colony variability and correction for extension-rate effects, *Coral Reefs*, *22*(4), 328–336, doi:10.1007/s00338-003-0324-3, 2003.

Fernández-Donado, L., et al., Large-scale temperature response to external forcing in simulations and reconstructions of the last millennium, *Climate of the Past*, *9*(1), 393–421, doi:10.5194/cp-9-393-2013, 2013.

Fogt, R. L., and D. H. Bromwich, Decadal Variability of the ENSO Teleconnection to the High-Latitude South Pacific Governed by Coupling with the Southern Annual Mode, *Journal of Climate*, *19*, 979–997, doi:10.1175/JCLI3671.1, 2006.

Folland, C., J. Renwick, M. Salinger, and A. Mullan, Relative influences of the Interdecadal Pacific Oscillation and ENSO on the South Pacific Convergence Zone, *Geophysical Research Letters*, *29*(13), 2–5, 2002.

Gao, C., A. Robock, and C. Ammann, Volcanic forcing of climate over the past 1500 years: An improved ice core-based index for climate models, *Journal of Geophysical Research: Atmospheres*, *113*(D23), n/a–n/a, doi:10.1029/2008JD010239, d23111, 2008.

Garreaud, R. D., and D. S. Battisti, Interannual (ENSO) and interdecadal (ENSO-like) variability in the Southern Hemisphere tropospheric circulation, *J. Climate*, *12*, 2113–2122, 1999.

Gershunov, A., and T. P. Barnett, Interdecadal Modulation of ENSO Teleconnections, *Bulletin of the American Meteorlogical Society*, *79*(12), 2715–2725, 1998.

Ghil, M., and K. Mo, Intraseasonal oscillations in the global atmosphere. part i: Northern hemisphere and tropics, *Journal of the Atmospheric Sciences*, *48*(5), 752–779, doi:10.1175/1520-0469(1991)048⟨0752:IOITGA⟩2.0.CO;2, 1991.

Ghil, M., et al., Advanced spectral methods for climatic time series, *Rev. Geophys.*, *40*(1), 2002.

Glantz, M. H., R. W. Katz, and N. Nicholls, *Teleconnections Linking Worldwide Climate Anomalies*, Cambridge University Press, 1991.

Gomez, B., L. Carter, A. R. Orpin, K. M. Cobb, M. J. Page, N. A. Trustrum, and A. S. Palmer, ENSO/SAM interactions during the middle and late Holocene, *The Holocene*, *22*, 23–30, 2011.

Goodwin, I., et al., A reconstruction of extratropical Indo-Pacific sea-level pressure patterns during the Medieval Climate Anomaly, *Climate Dynamics*, doi:10.1007/s00382-013-1899-1, 2014.

Gouriou, Y., and T. Delcroix, Seasonal and ENSO variations of sea surface salinity and temperature in the South Pacific Convergence Zone during 1976-2000, *Journal of Geophysical Research*, *107*(C12), 1–14, 2002.

Graham, N., C. Ammann, D. Fleitmann, K. M. Cobb, and J. Luterbacher, Support for global climate reorganization during the Medieval Climate Anomaly, *Climate Dynamics*, *37*(5-6), 1217–1245, doi:10.1007/s00382-010-0914-z, 2011.

Graham, N. E., et al., Tropical Pacific–mid-latitude teleconnections in medieval times, *Clim. Change*, *83*(1), 241–285, 2007.

Grossman, E. L., and T.-L. Ku, Oxygen and carbon isotopic fractionation in biogenic aragonite: Temperature effects, *Chem. Geol.*, *59*, 59–74, 1986.

Grottoli, A. G., and C. M. Eakin, A review of modern coral 18o and 14c proxy records, *Earth-Science Reviews*, *81*(1), 67 – 91, doi:https://doi.org/10.1016/j.earscirev.2006.10.001, 2007.

Guilderson, T. P., and D. P. Schrag, Reliability of coral isotope records from the western Pacific warm pool: A comparison using age-optimized records, *Paleoceanography*, *14*, 457–464, 1999.

Guilyardi, E., A. T. Wittenberg, A. Fedorov, M. Collins, C. Wang, A. Capotondi, G. Jan van Oldenborgh, and T. Stockdale, Understanding El Niño in OceanAtmosphere General Circulation Models: Progress and Challenges, *Bulletin of the American Meteorological Society*, *90*(3), 325–340, doi:10.1175/2008BAMS2387.1, 2009.

Hasson, A. E., T. Delcroix, and D. Raphael, An Assessment of the mixed layer salinity budget in the tropical Pacific Ocean. Observations and modelling (1990-2009), *Ocean Dynamics*, *63*, 179–194, 2013.

Held, I., and B. Soden, Robust Responses of the Hydrological Cycle to Global Warming, *Journal of Climate*, pp. 5686–5699, 2006.

Hendy, E. J., M. K. Gagan, C. A. Alibert, M. T. McCulloch, J. M. Lough, and P. J. Isdale, Abrupt decrease in tropical Pacific sea surface salinity at end of Little Ice Age., *Science (New York, N.Y.)*, *295*(5559), 1511–4, doi:10.1126/science.1067693, 2002.

Hendy, E. J., M. K. Gagan, J. M. Lough, M. McCulloch, and P. B. deMenocal, Impact of skeletal disolution and secondary aragonite on trace element and isotopic climate proxies in *Porites* corals, *Paleoc.*, *22*, PA4101, doi: 10.1029/2007PA001462, 2007.

Henke, L., F. Lambert, and D. Charman, Was the Little Ice Age more or less El Niño-like than the Mediaeval Climate Anomaly? Evidence from hydrological and temperature proxy data, *Climate of the Past: Discussions*, *11*, 5549–5604, 2015.

Hereid, K. A., T. M. Quinn, and Y. M. Okumura, Assessing spatial variability in El Niño-Southern Oscillation event detection skill using coral geochemistry, *Paleoceanography*, *28*(1), 14–23, doi:10.1029/2012PA002352, 2013.

Hoerling, M. P., J. W. Hurrell, and T. Xu, Tropical origins for recent North Atlantic climate change, *Science*, *292*, 90–92, 2001.

Holton, J. R., and G. J. Hakim, *An Introduction to Dynamic Meteorology, Fifth Edition*, Academic Press, Inc., 2013.

Huang, B., et al., Extended reconstructed sea surface temperature version 4 (ersst.v4). part i: Upgrades and intercomparisons, *Journal of Climate*, *28*(3), 911–930, doi:10.1175/JCLI-D-14-00006.1, 2015.

IPCC Working Group 1, I., et al., IPCC, 2013: Climate Change 2013: The Physical Science Basis. Contribution of Working Group I to the Fifth Assessment Report of the Intergovernmental Panel on Climate Change, *IPCC*, *AR5*, 1535, 2013.

Jin, F.-F., An Equatorial Ocean Recharge Paradigm for ENSO . Part I : Conceptual Model Pacific from his analysis of the empirical relations of, *Journal of the Atmospheric Sciences*, *54*, 811–829, 1997.

Jin, F.-F., and J. D. Neelin, Modes of Interannual Tropical Ocean-Atmosphere Interaction - A Unified View. Part I: Numerical Results, *Journal of the Atmospheric Sciences*, *50*(21), 3477–3503, 1993.

Jochum, M., and R. Murtugudde, Internal variability of the tropical pacific ocean, *Geophysical research letters*, *31*(14), 2004.

Jones, P., et al., High-resolution palaeoclimatology of the last millennium: a review of current status and future prospects, *The Holocene*, *1*, 3–49, 2009.

Jungclaus, J. H., et al., Climate and carbon-cycle variability over the last millennium, *Climate of the Past*, *6*(5), 723–737, doi:10.5194/cp-6-723-2010, 2010.

Kaplan, A., M. A. Cane, Y. Kushnir, A. C. Clement, M. B. Blumenthal, and B. Rajagopalan, Analyses of global sea surface temperature 18561991, *Journal of Geophysical Research: Oceans*, *103*(C9), 18,567–18,589, doi:10.1029/97JC01736, 1998.

Kennedy, J. J., N. A. Rayner, R. O. Smith, D. E. Parker, and M. Saunby, Reassessing biases and other uncertainties in sea surface temperature observations measured in situ since 1850: 1. measurement and sampling uncertainties, *Journal of Geophysical Research: Atmospheres*, *116*(D14), n/a–n/a, doi:10.1029/2010JD015218, d14103, 2011.

Kiladis, G. N., H. von Storch, and H. van Loon, Origin of the south pacific convergence zone, *Journal of Climate*, *2*, 1185–1195, 1989.

Kilbourne, K. H., T. M. Quinn, F. W. Taylor, T. Delcroix, and Y. Gouriou, El niosouthern oscillationrelated salinity variations recorded in the skeletal geochemistry of a porites coral from espiritu santo, vanuatu, *Paleoceanography*, *19*(4), n/a–n/a, doi: 10.1029/2004PA001033, pA4002, 2004.

Kim, S.-T., and J. R. O'Neil, Equilibrium and nonequilibrium oxygen isotope effects in synthetic carbonates, *Geochimica et Cosmochimica Acta*, *61*(16), 3461–3475, 1997.

Kinsman, D. J. J., and H. D. Holland, The co-precipitation of cations with $caco_3$ – IV. The co-precipitation of Sr^{2+} with aragonite between 16^o and 96^oc, *Geochem. et Cosmochim. Acta*, *33*, 1–17, 1969.

Knutson, D., R. Buddemeiser, and S. Smith, Coral chronometers: seasonal growth bands in reef corals, *Science*, *177*(4045), 270–272, 1972.

Lamb, H., The Early Medieval Warm Epoch and Its Sequel, *Palaegeography, Palaeoclimatology, Palaeoecology*, *1*, 13–37, 1965.

Le Bec, N., A. Juillet-LeClerc, T. Corrège, D. Blamart, and T. Delcroix, A coral δ^{18}O record of ENSO driven sea surface salinity variability in Fiji (south-western tropical Pacific, *Geophys. Res. Lett.*, *27(23)*, 3897–3900, 2000.

LeGrande, A. N., and G. A. Schmidt, Global gridded data set of the oxygen isotopic composition in seawater, *Geophys. Res. Lett.*, *33*, L12,604, doi:10.1029/2006GL026011, 2006.

L'Heureux, M. L., L. Sukyoung, and B. Lyon, Recent multidecadal strengthening the Walker circulation across the tropical Pacific, *Nature Climate Change*, pp. 1–6, 2013.

Li, J., S.-P. Xie, E. R. Cook, G. Huang, R. D'Arrigo, F. Liu, J. Ma, and X.-T. Zheng, Interdecadal modulation of El Niño amplitude during the past millennium, *Nature Clim. Change*, *1*, 114–118, doi: 10.1038/nclimate1086, 2011.

Li, J., et al., El Niño modulations over the past seven centuries, *Nature Clim. Change*, *3*, 822–826, doi: 10.1038/nclimate1936, 2013.

Linsley, B., R. Messier, and R. Dunbar, Assessing between-colony oxygen isotope variability in the coral porites lobata at clipperton atoll, *Coral Reefs*, *18*(1), 13–27, doi: 10.1007/s003380050148, 1999.

Linsley, B. K., R. B. Dunbar, G. M. Wellington, and D. A. Mucciarone, A coral-based reconstruction of Intertropical Convergence Zone variability over Central America since 1707, *J. Geophys. Res.*, *99*(C5), 9977–9994, 1994.

Linsley, B. K., G. M. Wellington, and D. P. Schrag, Decadal sea surface temperature variability in the subtropical South Pacific from 1726 to 1997 A.D., *Science (New York, N.Y.)*, *290*(5494), 1145–8, 2000.

Linsley, B. K., G. M. Wellington, D. P. Schrag, L. Ren, M. J. Salinger, and A. W. Tudhope, Geochemical evidence from corals for changes in the amplitude and spatial pattern of south pacific interdecadal climate variability over the last 300 years, *Climate Dynamics*, *22*(1), 1–11, doi:10.1007/s00382-003-0364-y, 2004.

Linsley, B. K., A. Kaplan, Y. Gouriou, J. Salinger, P. B. DeMenocal, G. M. Wellington, and S. S. Howe, Tracking the extent of the South Pacific Convergence Zone since the early 1600s, *Geochemistry, Geophysics, Geosystems*, *7*(4), 1–15, 2006.

Linsley, B. K., P. Zhang, A. Kaplan, S. S. Howe, and G. M. Wellington, Interdecadal-decadal climate variability from multicoral oxygen isotope records in the South Pacific Convergence Zone region since 1650 A.D., *Paleoceanography*, *23*(2), n/a–n/a, doi: 10.1029/2007PA001539, 2008.

Lopatka, A., M. Evans, A. Lorrey, H. K. Kilbourne, H. McGregor, M. Allen, and A. Morrison, Detecting enso from modern southern cook island corals, *Climate of the Past*, in prep.

Lopatka, A. S., G. Duke, C. Hyde, and A. Lorrey, Diagenetic testing in porites coral, National Institute of Water and Atmospheric Research, unpublished white paper, 2015.

Lorrey, A., personal communication, 2018.

Lorrey, A., G. Dalu, J. Renwick, H. Diamond, and M. Gaetani, Reconstructing the South Pacific Convergence Zone Position During the Presatellite Era: A La Nina Case Study, *Monthly Weather Review*, *140*, doi:10.1175/MWR-D-11-00228.1, 2012.

Lorrey, A., N. Fauchereau, C. Stanton, P. Chappell, S. Phipps, A. Mackintosh, J. Renwick, I. Goodwin, and A. Fowler, The Little Ice Age climate of New Zealand reconstructed from Southern Alps cirque glaciers: a synoptic type approach, *Climate Dynamics*, doi: 10.1007/s00382-013-1876-8, 2014.

Lough, J., and D. Barnes, Environmental controls on growth of the massive coral Porites., *Journal of experimental marine biology and ecology*, *245*(2), 225–243, 2000.

Lough, J. M., A strategy to improve the contribution of coral data to high-resolution paleoclimatology, *Palaeogeog., Palaeoclim., Palaeoecol.*, *204(1-2)*, 115–143, 2004.

Lough, J. M., Climate records from corals, *WIRES Clim. Change*, *1(3)*, 318–331, doi: 10.1002/wcc.39, 2010.

Lough, J. M., and D. J. Barnes, Several centuries of variation in skeletal extension, density, and calcification in massive *porites* colonies from the Great Barrier Reef: A proxy for seawater temperature and a background of variability against which to identify unnatural change, *J. Exper. Mar. Biol. Ecol.*, *211*, 29–67, 1997.

Mann, M. E., Z. Zhang, S. Rutherford, R. S. Bradley, M. K. Hughes, D. Shindell, C. Ammann, G. Faluvegi, and F. Ni, Global signatures and dynamical origins of the Little Ice Age and Medieval Climate Anomaly., *Science (New York, N.Y.)*, *326*(5957), 1256–60, doi:10.1126/science.1177303, 2009.

Mantua, N. J., S. R. Hare, Y. Zhang, J. M. Wallace, and R. C. Francis, A Pacific Interdecadal Climate Oscillation with Impacts on Salmon Production *, *Bulletin of the American Meteorological Society*, *78*, 1069–1079, 1997.

Marshall, J., A. Donohue, D. Ferreira, and D. McGee, The ocean's role in setting the mean position of the inter-tropical convergence zone, *Climate Dynamics*, *42*, 1967 – 1979, 2014.

McConnaughey, T., 13C and 180 isotopic disequilibrium in biological carbonates : II . In vitro simulation of kinetic isotope effects, *Geochimica et Cosmochimica Acta*, 1989a.

McConnaughey, T., ^{13}C and ^{18}O isotopic disequilibrium in biological carbonates: I. Patterns, *Geochim. Cosmochim. Acta*, *53*, 151–162, 1989b.

McCrea, J. M., On the isotopic chemistry of carbonates and a paleotemperature scale, *J. Chem. Phys.*, *18(6)*, 849–857, 1950.

McCulloch, M. T., M. K. Gagan, G. E. Mortimer, A. R. Chivas, and P. J. Isdale, A high-resolution Sr / Ca and d18O coral record from the Great Barrier Reef , Australia , and the 1982-1983 El Nino, *Geochimica et Cosmochimica Acta*, *58*(12), 2747–2754, 1994.

McGregor, H., M. Fischer, M. Gagan, D. Fink, and C. Woodroffe, Environmental control of the oxygen isotope composition of Porites coral microatolls, *Geochimica et Cosmochimica Acta*, *75*(14), 3930–3944, doi:10.1016/j.gca.2011.04.017, 2011.

McGregor, H. V., and M. Gagan, Diagenesis and geochemistry of *Porites* corals from Papua New Guinea: Implications for paleoclimate reconstruction, *Geochimica et Cosmochimica Acta*, *67*(12), 2147–2156, 2003.

McGregor, H. V., and M. K. Gagan, Western Pacific coral δ 18 O records of anomalous Holocene variability in the El NiñoSouthern Oscillation, *Geophysical Research Letters*, *31*(11), L11,204, doi:10.1029/2004GL019972, 2004.

McGregor, H. V., et al., Robust global ocean cooling trend for the pre-industrial Common Era, *Nature Geoscience*, 2015.

McGregor, S., and A. Timmermann, The effect of explosive tropical volcanism on enso, *Journal of Climate*, *24*(8), 2178–2191, doi:10.1175/2010JCLI3990.1, 2011.

Neukom, R., and J. Gergis, Southern Hemisphere high-resolution palaeoclimate records of the last 2000 years, *The Holocene*, *22*(5), 501–524, doi:10.1177/0959683611427335, 2011.

Newman, M., G. P. Compo, and M. A. Alexander, ENSO-forced variability of the Pacific Decadal Oscillation, *J. Clim.*, *16(23)*, 3853–3857, 2003.

NOAA, Niño 3.4 SST Index, `https://www.esrl.noaa.gov/psd/gcos_wgsp/Timeseries/Nino34/`, accessed: Dec 2017, 2018a.

NOAA, Southern Oscillation Index, `https://www.ncdc.noaa.gov/teleconnections/enso/indicators/soi/`, accessed: Dec 2017, 2018b.

Oppo, D. W., Y. Rosenthal, and B. K. Linsley, 2,000-year-long temperature and hydrology reconstructions from the Indo-Pacific warm pool., *Nature*, *460*(7259), 1113–6, doi:10.1038/nature08233, 2009.

Otto-Bliesner, B. L., E. C. Brady, J. Fasullo, A. Jahn, L. Landrum, S. Stevenson, N. Rosenbloom, A. Mai, and G. Strand, Climate variability and change since 850 ce: An ensemble approach with the community earth system model, *Bulletin of the American Meteorological Society*, *97*(5), 735–754, doi:10.1175/BAMS-D-14-00233.1, 2016.

Pereira, N., A. Sial, R. Frei, C. Ullmann, C. Korte, R. Kikuchi, V. Ferreira, and K. Kilbourne, The potential of the coral species porites astreoides as a paleoclimate archive for the tropical south atlantic ocean, *Journal of South American Earth Sciences*, *77*, 276 – 285, doi:https://doi.org/10.1016/j.jsames.2017.05.008, 2017.

Philander, S. G. H., *El Niño, La Niña, and the Southern Oscillation.*, 293 pp., Academic Press, San Diego, 1990.

Phipps, S. J., et al., Paleoclimate Data-Model Comparison and the Role of Climate Forcings over the Past 1500 Years, *Journal of Climate*, *26*, 6915–6936, 2013.

Picaut, J., M. Ioualalen, C. Menkes, T. Delcroix, and M. J. McPhaden, Mechanism of the zonal displacements of the Pacific Warm Pool: Implications for ENSO, *Science*, *274*, 1486–1489, 1996.

Pierce, D. W., Distinguishing coupled ocean-atmosphere interactions from background noise in the North Pacific, *Prog. Oceanog.*, *49*, 331–352, 2001.

Power, S., F. Delage, C. Chung, G. Kociuba, and K. Keay, Robust twenty-first-century projections of El Niño and related precipitation variability., *Nature*, *502*(7472), 541–5, doi:10.1038/nature12580, 2013.

Ramesh, N., and R. Murtugudde, All flavours of El Niño have similar early subsurface origins, *Nature Climate Change*, *3*, 42–46, doi:10.1038/NCLIMATE1600, 2012.

Ren, L., B. K. Linsley, G. M. Wellington, D. P. Schrag, and O. Hoegh-Guldberg, Deconvolving the δ^{18}O seawater component from subseasonal coral δ^{18}o and Sr/Ca at Rarotonga in the southwestern subtropical Pacific for the period 1726 to 1997, *Geochem. et Cosmochim. Acta*, *67(9)*, 1609–1621, doi: 10.1016/S0016-7037(02)00917-1, 2002.

Russon, T., A. Tudhope, G. Hegerl, and A. Schurer, Assessing the significance of changes in enso amplitude using variance metrics, *Journal of Climate*, *27*, 4911–4922, doi: 10.1175/JCLI-D-13-00077.1, 2014.

Russon, T., A. Tudhope, M. Collins, and G. Hegerl, Inferring changes in enso amplitude from the variance of proxy records, *Geophysical Research Letters*, *42*, doi:10.1002/2014GL062331, 2015.

Sachs, J., D. Sachse, R. Smittenber, Z. Zhang, D. Battisti, and S. Golubic, Southward movement of the Pacific intertropical convergence zone AD14001850, *Nature Geoscience*, *2*(7), 519–525, doi:10.1038/ngeo554, 2009.

Salinger, M., J. Renwick, and A. Mullan, Interdecadal Pacific Oscillation and South Pacific climate, *International Journal of Climatology*, *21*(14), 1705–1721, doi:10.1002/joc.691, 2001.

Salinger, M. J., R. E. Basher, B. B. Fitzharris, J. E. Hay, P. D. Jones, J. P. MacVeigh, and I. Schmidely-Leleu, Climate trends in the South-west Pacific, *Int. J. Clim.*, *15*, 285–302, 1995.

Sayani, H. R., K. M. Cobb, A. L. Cohen, W. C. Elliot, I. S. Nurhati, R. B. Dunbar, K. A. Rose, and L. K. Zaunbrecher, Effects of diagenesis on paleoclimate reconstructions from modern and young fossil corals, *Geochimica et Cosmochimica Acta*, *75*, 6361–6373, 2011.

Schmidt, G. A., Enhancing the relevance of palaeoclimate model/data comparisons for assessments of future climate change, *J. Quat. Sci.*, *25*(1), 79–87, doi: 10.1002/jqs.1314, 2010.

Schmidt, G. A., et al., Climate forcing reconstructions for use in PMIP simulations of the Last Millennium (v1.0), *Geosci. Mod. Devel.*, *4*(4), 33–45, doi: 10.5194/gmd-4-33-2011, 2011.

Schmidt, G. A., et al., Climate forcing reconstructions for use in PMIP simulations of the Last Millennium (v1.1), *Geosci. Mod. Devel.*, *5*(1), 185–191, doi: 10.5194/gmd-5-185-2012, 2012.

Schmidt, G. A., et al., Using palaeo-climate comparisons to constrain future projections in cmip5, *Climate of the Past*, *10*, 221–250, doi:10.5194/cp-10-221-2014, 2014.

Schneider, T., T. Bischoff, and G. H. Haug, Migrations and dynamics of the intertropical convergence zone, *Nature*, *513*, 45 – 53, doi:10.1038/nature13636, 2014.

Schrag, D. P., Rapid analysis of high-precision sr/ca ratios in corals and other marine carbonates, *Paleoceanography*, *14(2)*, 97–102, 1999.

Schurer, A. P., G. C. Hegerl, M. E. Mann, S. F. B. Tett, and S. J. Phipps, Separating forced from chaotic climate variability over the past millennium, *Journal of Climate*, *26*(18), 6954–6973, doi:10.1175/JCLI-D-12-00826.1, 2013.

Shen, C.-C., T. Lee, C.-Y. Chen, C.-H. Wang, and C.-F. Dai, The calibration of D[Sr/Ca] versus sea surface temperature relationship for *Porites* corals, *Geochim. Cosmochim. Acta*, *60*(20), 3849–3858, 1996.

Sigl, M., et al., Timing and climate forcing of volcanic eruptions for the past 2,500 years, *Nature*, *523*(7562), 543, 2015.

Singh, A., and T. Delcroix, Estimating the effects of ENSO upon the observed freshening trends of the western tropical Pacific Ocean, *Geophysical Research Letters*, *38*(21), n/a–n/a, doi:10.1029/2011GL049636, 2011.

Smerdon, J. E., Climate models as a test bed for climate reconstruction methods: pseudo-proxy experiments, *WIRES Climate Change*, *3*, 63–77, doi: 10.1002/wcc.149, 2012.

Smerdon, J. E., A. Kaplan, D. Chang, and M. N. Evans, A pseudoproxy evaluation of the CCA and RegEM methods for reconstructing climate fields of the last millennium, *J. Clim.*, *24*, 1284–1309, doi: 10.1175/2010JCLI4110.1, 2011.

Smerdon, J. E., et al., Comparing proxy and model estimates of hydroclimate variability and change over the common era, *Climate of the Past Discussions*, *2017*, 1–70, doi: 10.5194/cp-2017-37, 2017.

Stevenson, S., H. V. McGregor, S. V. Phipps, and B. Fox-Kemper, Quantifying errors in coral-based ENSO estimates: Toward improved forward modeling of δ^{18}O, *Paleoceanography*, *28*, 1–17, doi: 10.1002/palo.20059, 2013.

Stevenson, S., B. Otto-Bliesner, Fasullo, and E. Brady, el nio like hydroclimate responses to last millennium volcanic eruptions, *Journal of Climate*, *29*(8), 2907–2921, doi:10.1175/JCLI-D-15-0239.1, 2016.

Stevenson, S., A. Capotondi, J. Fasullo, and B. Otto-Bliesner, Forced changes to twentieth century enso diversity in a last millennium context, *Climate Dynamics*, 2017.

Stevenson, S. L., Significant changes to ENSO strength and impacts in the twenty-first century: Results from CMIP5, *Geophys. Res. Lett.*, *39*, L17,703, doi: 10.1029/2012GL052759, 2012.

Stoddart, D. R., and P. E. Gibbs, Almost-atoll of aitutaki: Reef studies in the cook islands, south pacific, *Tech. rep.*, Smithsonian National Museum of Natural History, atoll Research Bulletin, 1975.

Suarez, M. J., and P. S. Schopf, A Delayed Action Oscillator for ENSO, *Journal of Atmospheric Sciences*, *45*(21), 3283–3287, 1988.

Taylor, J., *Introduction to error analysis, the study of uncertainties in physical measurements*, University Science Books, 1997.

Taylor, K. E., R. J. Stouffer, and G. A. Meehl, An Overview of CMIP5 and the Experiment Design, *Bulletin of the American Meteorological Society*, *93*(4), 485–498, doi:10.1175/BAMS-D-11-00094.1, 2012.

Thompson, D., T. Ault, M. Evans, J. Cole, and J. Emile-Geay, Comparison of observed and simulated tropical climate trends using a forward model of coral δ 18 O, *Geophysical Research Letters*, *38*(14), n/a–n/a, doi:10.1029/2011GL048224, 2011.

Thompson, D. M., T. R. Ault, M. N. Evans, J. E. Cole, J. Emile-Geay, and A. LeGrande, Coral-CGCM comparison highlights role of salinity in long-term trends, *PAGES News*, *21(2)*, 2013a.

Thompson, J. F., *A survey of composite grid generation for general three-dimensional regions*, AIAA, 1986.

Thompson, L. G., E. Mosley-Thompson, M. E. Davis, V. S. Zagorodnov, I. M. Howat, V. N. Mikhalenko, and P.-N. Lin, Annually resolved ice core records of tropical climate variability over the past $\sim$1800 years, *Science*, *340*, 945–950, 2013b.

Thomson, D. J., et al., Multitaper analysis of nonstationary and nonlinear time series data, *Nonlinear and nonstationary signal processing*, pp. 317–394, 2000.

Tierney, J. E., N. J. Abram, K. J. Anchukaitis, M. N. Evans, C. Giry, K. H. Kilbourne, C. P. Saenger, H. C. Wu, and J. Zinke, Tropical sea surface temperatures for the past four centuries reconstructed from coral archives, *Paleoceanography*, *30*(3), 226–252, 2015.

Trenberth, K. E., Signal vs. noise in the Southern Oscillation, *Mon. Wea. Rev.*, *112*, 326–332, 1984.

Trenberth, K. E., The definition of El Niño, *Bull. Amer. Met. Soc.*, *78*, 2771–2777, 1997.

Vallis, G. K., *Atmospheric and Oceanic Fluid Dynamics*, Cambridge University Press, 2006.

Vautard, R., P. Yiou, and M. Ghil, Singular-spectrum analysis: A toolkit for short, noisy chaotic signals, *Physica D: Nonlinear Phenomena*, *58*(1), 95–126, 1992.

Vazey, R. S., Preliminary investigations into the use of modern and fossil coral reef-flat microatolls (*Porites lutea*) as reliable indicators of sub-tropical sea surface temperature and sea surface salinity in the southern Cook Islands, Honours B.S. thesis, discipline of Earth Sciences, School of Environmental and Life Sciences, University of Newcastle, 2008.

Vecchi, G. A., Examining the Tropical Pacific's Response to Global Warming, *Eos, Transactions American Geophysical Union*, *89*(9), 81–83, doi:10.1029/2008EO090002, 2008.

Vecchi, G. A., and A. T. Wittenberg, El Niño and our future climate: where do we stand?, *WIREs Climate Change*, *1*, 260–270, 2010.

Vecchi, G. A., B. J. Soden, A. T. Wittenberg, I. M. Held, A. Leetmaa, and M. J. Harrison, Weakening of tropical Pacific atmospheric circulation due to anthropogenic forcing., *Nature*, *441*(7089), 73–6, doi:10.1038/nature04744, 2006.

Vincent, D. G., The south pacific convergence zone (spcz): A review, *Monthly Weather Review*, *122*, 1949–1970, 1994.

Wallace, J. M., Observed Climatic Variability: Time Dependence, in *Decadal Climate Variability: Dynamics and Predictability*, *NATO ASI Series I: Global environmental change*, vol. 44, pp. 1–30, Springer-Verlag, 1996a.

Wallace, J. M., Observed Climatic Variability: Spatial Structure, in *Decadal Climate Variability: Dynamics and Predictability*, *NATO ASI Series I: Global environmental change*, vol. 44, pp. 31–81, Springer-Verlag, 1996b.

Wallace, J. M., and P. V. Hobbs, *Atmospheric Science: An Introductory Survey*, Academic Press, Inc., 2006.

Wang, J., J. Emile-Geay, J. E. Smerdon, and B. Rajartatnam, Evaluating climate field reconstruction techniques using improved emulations of real-world conditions, *Climate of the Past*, *10*, 1–19, 2014.

Weber, J. N., and P. M. J. Woodhead, Temperature dependence of Oxygen-18 concentration in reef coral carbonates, *J. Geophys. Res.*, *77*(3), 463–473, 1972.

Widlansky, M. J., P. J. Webster, and C. D. Hoyos, On the location and orientation of the South Pacific Convergence Zone, *Clim. Dyn.*, *36*, 561–578, doi: 10.1001/s00382-010-0871-6, 2011.

Widlansky, M. J., A. Timmermann, K. Stein, S. McGregor, N. Schneider, M. H. England, M. Lengaigne, and W. Cai, Changes in South Pacific rainfall bands in a warming climate, *Nature Climate Change*, *3*(4), 417–423, doi:10.1038/nclimate1726, 2012.

Wilks, D. S., *Statistical methods in the atmospheric sciences*, vol. 100, second ed., Academic press, 2006.

Wittenberg, A. T., Are historical records sufficient to constrain ENSO simulations?, *Geophys. Res. Lett.*, *36*, L12,702, doi: 10.1029/2009GL038710, 2009.

Woodroffe, C. D., and M. K. Gagan, Coral microatolls from the central Pacific record late Holocene El Niño, *Geophys. Res. Lett.*, *27(10)*, 1511–1514, 2000.

Wyrtki, K., El Niño – The dynamic response of the equatorial Pacific Ocean to atmospheric forcing, *J. Phys. Oceanog.*, *5*, 572–84, 1975.

Yan, H., L. Sun, D. W. Oppo, Y. Wang, L. Zhonghui, Z. Xie, X. Liu, and W. Cheng, South China Sea hydrological changes and Pacific Walker Circulation variations over the last millennium., *Nature communications*, *2*, 293, doi:10.1038/ncomms1297, 2011a.

Yan, H., L. Sun, Y. Wang, W. Huang, S. Qiu, and C. Yang, A record of the Southern Oscillation Index for the past 2,000 years from precipitation proxies, *Nature Geoscience*, *4*(9), 611–614, doi:10.1038/ngeo1231, 2011b.

Yeh, S.-W., J.-S. Kug, B. Dewitte, M.-H. Kwon, B. P. Kirtman, and F.-F. Jin, El niño in a changing climate, *Nature*, *461*(7263), 511–514, 2009.

Zebiak, S. E., and M. A. Cane, A Model EI Nino-Southern Oscillation *, *Monthly Weather Review*, *115*(1987), 2262–2278, 1987.